

**MOLECULAR DYNAMICS SIMULATION OF COMPLEX MOLECULES AT
INTERFACES: DENDRITIC SURFACTANTS IN CLAY AND AMYLOID
PEPTIDES NEAR LIPID BILAYERS**

A Dissertation

by

KUNWOO HAN

Submitted to the Office of Graduate Studies of
Texas A&M University
in partial fulfillment of the requirements for the degree of

DOCTOR OF PHILOSOPHY

August 2006

Major Subject: Chemical Engineering

**MOLECULAR DYNAMICS SIMULATION OF COMPLEX MOLECULES AT
INTERFACES: DENDRITIC SURFACTANTS IN CLAY AND AMYLOID
PEPTIDES NEAR LIPID BILAYERS**

A Dissertation

by

KUNWOO HAN

Submitted to the Office of Graduate Studies of
Texas A&M University
in partial fulfillment of the requirements for the degree of

DOCTOR OF PHILOSOPHY

Approved by:

Chair of Committee, David M. Ford
Committee Members, Daniel F. Shantz
Perla B. Balbuena
Ali Beskok
Head of Department, Kenneth R. Hall

August 2006

Major Subject: Chemical Engineering

ABSTRACT

Molecular Dynamics Simulation of Complex Molecules at Interfaces: Dendritic Surfactants in Clay and Amyloid Peptides near Lipid Bilayers. (August 2006)

Kunwoo Han, B.S.; M.S, Pohang University of Science and Technology

Chair of Advisory Committee: Dr. David M. Ford

We apply a molecular dynamics (MD) simulation technique to complex molecules at interfaces. Partitioning of dendritic surfactants into clay gallery and A β protein behavior near hydrated lipids are chosen for the purpose. Using a full atomistic model of dendritic surfactants, the confinement force profiles featuring oscillatory fashion at moderate layer separation of 10 to 25 Å were observed. Integration of the confinement forces led to free energy profiles, which, in turn, were used to determine the final morphology of the nanocomposite. From the free energy profiles, smaller and linear surfactants (G1 and G2L) are expected to intercalate into the clay comfortably, while larger surfactants (G2 and G3) are expected to form frustrated intercalated structures due to the location and depth of the free energy minima. This would agree with the previous observations.

As primary steps to understand the A β protein behavior under biological conditions, simulations of bulk water and hydrated lipids were performed and the results were compared with the literature. Hydrated lipids were simulated using a full atomistic model of lipids (dipalmitoylphosphatidylcholine) and water with a cvff force-field and it was found that structural properties such as the molecular head group area and membrane thickness were accurately produced with MD simulation. Systems of the protein A β (1-42) in bulk water were simulated and some secondary structural change, with loss of part of the α -helical structure, occurred during the 1 ns of simulation time at 323K. The fragment A β (31-42) with β -sheet conformation was also simulated in bulk water, and the extended β -sheet structure became a bent structure. Simulations of A β (1-42) or A β (31-42) near lipid bilayers have been performed to investigate the structural

property changes under biological conditions. The different nature of structural change was observed from the simulations of the protein or fragment in water and near lipid bilayers due to the different solvent environment. The protein has close contacts with the membrane surface. It was impossible to observe the conformational change to β -sheet and protein entrance into the lipid bilayer within 1 ns simulations.

To my family

ACKNOWLEDGMENTS

I can hardly thank my advisor and the committee chair, Prof. Ford enough. He truly has been my role model and guided me in the right track of research and life too. I sincerely thank my committee members, Prof. Shantz, Prof. Balbuena and Prof. Beskok for their fruitful comments and suggestions throughout the course of this research. I acknowledge Sandia National Laboratories for the support of the bio-research (Molecular Simulations of Beta-Amyloid Protein near Hydrated Lipids (PECASE), Sandia Report SAND2005-7497).

Prof. Cagin has been willingly helping me a lot since we first met in 2005. Dr. Pérez at Laboratory for Molecular Simulation of the Chemistry Department has been a tremendous help to my research. I've been delighted to have such wonderful professors, colleagues, and friends here in College Station. Mr. Polasek's help regarding computer issues was truly invaluable.

I especially thank my parents, Songhag Han and Insoon Lee, parents-in-law Dongwoo Lee and Jaegi Kim, my sister and brother, and my sisters-in-law and brother-in-law in South Korea for their concern and encouragement. My heartfelt thanks are attributed to friends in South Korea and the U.S., too.

Finally, I would like to thank my wife, Yun Ja, for her everlasting love, sacrifice, and support and our kids, Woongbin and Seojin, with all my heart. They are the reason for my existence and this would be valueless without them.

TABLE OF CONTENTS

	Page
ABSTRACT	iii
DEDICATION	v
ACKNOWLEDGMENTS.....	vi
TABLE OF CONTENTS	vii
LIST OF FIGURES.....	x
LIST OF TABLES	xv
CHAPTER	
I INTRODUCTION.....	1
1.1 Introduction to Molecular Simulation	1
1.2 Research Overview	2
1.3 Nano-Research	3
1.3.1 Polymer-Clay Nanocomposite	3
1.3.2 Experiments.....	3
1.3.3 Simulations.....	4
1.3.4 Work Scope	5
1.4 Bio-Research	6
1.4.1 Alzheimer's Disease and A β Protein	6
1.4.2 Hydrated Lipids.....	6
1.4.3 A β Protein Research.....	9
1.4.4 Work Scope	10
II THEORY.....	12
2.1 Molecular Dynamics Simulation.....	12
2.1.1 Introduction	12
2.1.2 Ensemble	13
2.1.3 Treatment of Long-Range Electrostatics.....	17
2.1.4 Long-Range Correction for van der Waals Energy.....	24
2.2 Nano-Research	25
2.2.1 Overall Process of Ion Exchange	25
2.2.2 Thermodynamic Quantities from Simulation.....	29
2.3 Bio-Research	31
2.3.1 Phase of Hydrated Lipids	32
2.3.2 Order Parameter	33
2.3.3 Hydrocarbon Chain Conformations	36

CHAPTER	Page
2.3.4 Other Structural Properties	40
III SYSTEM AND METHOD	44
3.1 Nano-Research	44
3.1.1 Model and Simulation Details	44
3.1.2 Data Analysis	49
3.2 Bio-Research	50
3.2.1 Model and Simulation Details	50
3.2.2 Data Analysis	59
IV RESULTS AND DISCUSSION OF NANO-RESEARCH	61
4.1 Overview	61
4.2 Confinement Force	63
4.3 Free Energy Profiles	66
4.4 Comparison with Experiments	67
4.5 Energy-Entropy Interplay	72
V RESULTS AND DISCUSSION OF BIO-RESEARCH	78
5.1 Bulk Water Simulation	78
5.1.1 Thermodynamic Properties	78
5.1.2 Structural Properties	84
5.2 Simulation of Hydrated Lipids	96
5.2.1 Thermodynamic Properties	96
5.2.2 Structural Properties	101
5.3 Simulation of A β (1-42) in Water	111
5.3.1 Thermodynamic Properties	111
5.3.2 Structural Properties	115
5.4 Simulation of A β (31-42) β -Sheet Conformation in Water	121
5.4.1 Thermodynamic Properties	121
5.4.2 Structural Properties	123
5.5 Simulation of A β (1-42) near Hydrated Lipids	127
5.5.1 Simulation of A β (1-42) – A β Series	127
5.5.2 Simulation of A β (1-42) – A β -E Series	134
5.6 Simulation of A β (31-42) β -Sheet Conformation near Hydrated Lipids	151
5.6.1 Thermodynamic Properties	151
5.6.2 Structural Properties	153
VI SUMMARY AND CONCLUSIONS	161
6.1 Summary and Conclusions	161
6.1.1 Nano-Research	161
6.1.2 Bio-Research	162

CHAPTER	Page
6.2 Suggestions and Future Directions.....	163
6.2.1 Nano-Research	163
6.2.2 Bio-Research	164
REFERENCES	166
APPENDICES.....	181
VITA	207

LIST OF FIGURES

		Page
Figure II-1	Representation of canonical and microcanonical ensembles.	15
Figure II-2	Conceptual figure of the potential at point charge q_i : The solid rod represents point charges, U- or cup-type curves the Gaussian charge cloud or the compensating charge cloud in Fourier space, the dotted large ovals the complementary error functions which are the potentials due to the short-ranged interaction, the dotted small ovals the potentials due to the long-range interaction.	20
Figure II-3	Simplified ion exchange process.	26
Figure II-4	Graphs representing different types of partitioning.	28
Figure II-5	Schematic of lipid phase transitions; $L\beta'$ is one dimensional lamella lattice in tilted gel phase, $P\beta'$ is a ripple phase, $L\alpha$ is liquid crystalline phase; Adapted from Pasini and Zannoni, 2000.	32
Figure II-6	Schematic of vectors associated with order parameter calculation. ...	34
Figure II-7	Defining the angle for the trans/gauche conformation differentiation.	37
Figure II-8	Defining the ζ vector.	39
Figure III-1	Schematics of dendritic surfactants.	44
Figure III-2	Linear density profile of a G3 molecule between clay layers; 10 ns, 10.0 Å separation.	47
Figure III-3	Linear density profile of a G3 molecule between clay layers; 50 ns, 70.0 Å separation.	49
Figure III-4	Structure of DPPC molecule.	51
Figure III-5	Structure of $A\beta$ protein with conformational information. Adapted from Serpell, 2000.	53
Figure III-6	Construction of a DPPC lipid bilayer.	54
Figure III-7	$A\beta(1-42)$ protein in fully hydrated lipids; hydrogen atoms are intentionally hidden.	56
Figure III-8	Conceptual figure of $A\beta$ protein in hydrated lipid bilayer.	59

	Page	
Figure IV-1	Snapshots of a G3 molecule between clay layers; 10.0 Å separation. The red balls of the top and bottom planes represent the oxygen atoms of the model clay.....	62
Figure IV-2	Snapshots of a G3 molecule between clay layers; 50.0 Å separation. The red balls of the top and bottom planes represent the oxygen atoms of the model clay.....	62
Figure IV-3	Total confinement force profiles of single dendrimers between clay layers.	64
Figure IV-4	Confinement force profiles of a G2L molecule between clay layers.	65
Figure IV-5	Free energy profiles of different types of a dendrimers; reference point of infinite separation is 70 Å; medium dash line represents the bare clay interlayer spacing of 14.7 Å, long dash line represents 15.7 Å.	67
Figure IV-6	Wall-atom potential energy profiles of different types of dendrimers.	73
Figure IV-7	Energetic contribution profiles to the free energy difference of different types of dendrimers; the total potential is considered as the potential energy.	74
Figure IV-8	Entropic contribution profiles to the free energy difference of different types of dendrimers; the total potential is considered as the potential energy.	75
Figure IV-9	Energy-entropy interplay for a G1 molecule between clay layers.	77
Figure V-1	Sketch of a water model	79
Figure V-2	Total energy profiles for the cvff and SPC water models with a target pressure of 75 atm and at 323K.....	81
Figure V-3	MSD of O-atoms for two different water models; the external pressure of 75 atm at 323K.	84
Figure V-4	Self-diffusion coefficients of water molecules at 323K.....	86
Figure V-5	Pressure-volume relationship from bulk water simulations.....	88
Figure V-6	Radial distribution functions using cvff water model with different bulk pressures.....	89
Figure V-7	Radial distribution functions using SPC water model with different bulk pressures	90

	Page	
Figure V-8	Comparison of radial distribution functions for different water models with an experimental result; the external pressure of 75 atm at 323K; Data points were generated from Narten et al., 1967.	91
Figure V-9	Radial distribution functions using the cvff water model with bulk pressure of 75 atm; W-e_2 case.	92
Figure V-10	Radial distribution functions using the SPC water model with bulk pressure of 75 atm; W-j_2 case.	93
Figure V-11	Oxygen-hydrogen radial distribution functions for different water models with bulk pressure of 75 atm.	94
Figure V-12	Energy profiles for hydrated lipids simulation; HD-j.	98
Figure V-13	Structural properties for hydrated lipids; HD-j case	102
Figure V-14	Comparison of head group areas for different lateral pressures; P_N is maintained at 1atm, data from this study is obtained from the last 500 ps simulations, experimental data are from de Young and Dill, 1988; Lewis and Engelman, 1983; Lis et al., 1982; Nagle, 1993; Nagle et al., 1996; Pace and Chan, 1982; Petrache et al., 2000; Schindler and Seelig, 1975; Thurmond et al., 1991, the P_L for the experimental data is set to 0.	103
Figure V-15	Regression plots to obtain the lateral compressibility.	107
Figure V-16	Comparison of bilayer thickness from literature and current study; Simulation data from Lee et al., 2004; Shinoda et al., 1997; Sum, 2005; Tieleman and Berendsen, 1996; Tu et al., 1995, Experimental data from Inoko and Mitsui, 1978; Lewis and Engelman, 1983; Lis et al., 1982; Nagle et al., 1996.	108
Figure V-17	Order parameters for hydrated lipids; HD-j case.	109
Figure V-18	Comparison of order parameters; This study simulation represents HD-j case study. Curves are generated from data of Doxastakis et al., 2005; Lee et al., 2004; Seelig and Seelig, 1974; Tieleman and Berendsen, 1996; Tu et al., 1995.	110
Figure V-19	Energy profiles for A β (1-42) in water simulation; A β _W-A	113
Figure V-20	Box length profiles for A β (1-42) in water simulation; A β _W-A case.	115
Figure V-21	Profile of the number of H bonds for A β (1-42) in water simulation; A β _W-A case.	117

	Page
Figure V-23 Comparison of RMS deviations for A β (1-42) in water simulation; A β _W-A (at 323K) and A β _W-B (at 310K) cases.....	119
Figure V-24 Snapshots for A β (1-42) in water; 2 frames, red ribbon represents the initial structure, cyan ribbon is the last structure, A β _W-A case.....	120
Figure V-25 Energy profiles for A β (31-42) β -sheet conformation in water simulation; A β _W- β a.....	122
Figure V-26 Profiles of end-to-end distance and R _G for A β (31-42) β -sheet conformation in water simulation; A β _W- β a.....	125
Figure V-27 Snapshots for A β (31-42) β -sheet conformation in water; 2 frames, red ribbon represents the initial structure, cyan ribbon is the last structure, A β _W- β a case.....	126
Figure V-28 Energy profiles for A β (1-42) near hydrated lipids; A β -E case.....	128
Figure V-29 Profiles of DPPC structural properties for A β (1-42) near hydrated lipids; A β -E case.....	129
Figure V-30 Profiles of structural properties for A β (1-42) near hydrated lipids; A β -E case.....	130
Figure V-31 Profile of the number of H bonds for A β (1-42) near hydrated lipids; A β -E case.....	131
Figure V-32 Structural properties of A β (1-42) in hydrated lipids; A β -E case.....	132
Figure V-33 Snapshots for A β (1-42) near hydrated lipids; configurations of start and after 1000000 steps or 2ns, red ribbon represents the initial structure, cyan ribbon is the final structure, A β -E case.....	133
Figure V-34 Generating the starting configurations for A β -E series from the simulation of A β -E case.....	135
Figure V-35 Potential energy profiles for A β (1-42) near hydrated lipids; A β -E series.....	137
Figure V-36 Profiles of structural properties for A β (1-42) near hydrated lipids; A β -E_01 case.....	140
Figure V-37 Comparison of structural properties at different A β (1-42) locations; A β -E series.....	141

	Page
Figure V-38 Comparison of the number of H bonds at different A β (1-42) locations; A β -E series.	142
Figure V-39 A snapshot of initial configuration of A β (1-42) near hydrated lipids; A β -E_01 case.	143
Figure V-40 A snapshot of final configuration of A β (1-42) near hydrated lipids; A β -E_01 case.	144
Figure V-41 R_G data as a function of instantaneous D ; A β -E_01 case, first 500ps.	145
Figure V-42 R_G data as a function of instantaneous D ; A β -E_01 case, last 500ps.	146
Figure V-43 Comparison of RMS deviation for various simulation case studies of A β (1-42) near hydrated lipids.	147
Figure V-44 Snapshots for A β (1-42) near hydrated lipids; 11 frames, red ribbon represents the initial structure, cyan ribbon is the last structure, A β -E_init case.	149
Figure V-45 Snapshots for A β (1-42) near hydrated lipids; 11 frames, red ribbon represents the initial structure, cyan ribbon is the last structure, A β -E_04 case.	150
Figure V-46 A snapshot of A β (31-42) β -conformation near hydrated lipids; the protein is in close proximity to the interface, hydrogen atoms are intentionally hidden.	152
Figure V-47 Total and potential energy profiles for A β (31-42) β -sheet conformation in hydrated lipids; A β -n_01 case.	153
Figure V-48 Profiles of structural properties for A β (31-42) in hydrated lipids; A β -n_01 case.	154
Figure V-49 R_G profile as a function of D ; 0 to 500ps, A β -n_01 case.	155
Figure V-50 R_G profile as a function of D ; 500ps to 1ns, A β -n_01 case.	156
Figure V-51 Comparison of RMS deviation for A β (31-42) in water and near hydrated lipids; A β -n_01 and A β _W- β a cases.	158
Figure V-52 Snapshots for A β (31-42) near hydrated lipids; 2 frames, red ribbon represents the initial structure, cyan ribbon is the last structure, A β _n-01 case.	159

LIST OF TABLES

		Page
Table II-1	Thermodynamic properties and computing time comparison for different long-range electrostatic treatment methods; the second row of the first column represents the method and the number of cpus is shown in the parenthesis, the second row of the last column is the speedup relative to choice_01 simulation case, NVE, 1000 steps with $\Delta t = 2.0$ fs, $r_c = 10.0$ Å, accuracy = 1.0×10^{-4} , whole_run01_070105.10000 as the starting configuration.	23
Table II-2	Characteristic angles and the corresponding cosine values for determining the conformation.	39
Table IV-1	Free energy and the relative probability of finding the particular states at different layer separation	69
Table IV-2	Comparison of intercalation process of melamine-based dendritic surfactants into clay; experiment vs simulation; reference state = infinite separation.	72
Table V-1	Several water models for biomolecular research.	79
Table V-2	Summary of simulation parameters for bulk water; P_tar means the target pressure.	80
Table V-3	Thermodynamic properties from bulk water simulations; V is the specific volume, E_pair includes the pair short-range interaction energy, E_bond is the total intra-molecular interaction energy, E_total is the total energy, KE is the kinetic energy, and PE is the potential energy.	83
Table V-4	Diffusion coefficient from bulk water simulations.	85
Table V-5	Comparison of bulk water properties from this study and published results; Data for this study were obtained at 75 atm and 323K.	95
Table V-6	Summary of simulation parameters for hydrated lipids; the data file for all simulations is data.H2O_DPPC_110805_min_1_10k except HD-j_2(H2O_DPPC_113005_1.500000), HD-k_2 and HD-l_2(H2O_DPPC_120505_1.500000), HD-k case started with $P_z = -1$ atm.	97
Table V-7	Thermodynamic properties measured from simulations for hydrated lipids with different case studies; second row values are the standard deviations.	99

	Page	
Table V-8	Comparison of MD results for hydrated lipids; second row values are the standard deviations; A is the molecular head group area, D_z the z-dimension box length, D_{mem} is the membrane thickness or P-P atom distance.....	101
Table V-9	Summary of simulation parameters for A β (1-42) in water; the starting data file for all simulations is Ab_H2O_100505_min_1_10k, CAT cluster with 8 cpus.....	112
Table V-10	Thermodynamic properties measured from simulations for A β (1-42) in water with different case studies; second row values are the standard deviations.....	114
Table V-11	Summary of simulation parameters for A β (31-42) β -conformation in water; the three pressure components are coupled.....	122
Table V-12	Thermodynamic properties measured from simulations for A β (31-42) in water with different case studies; second row values are the standard deviations.....	124
Table V-13	Summary of simulation parameters for A β (1-42) in hydrated lipids; A β -E series, CAT cluster with 8 cpus except A β -E_08_COS where COSMOS with 16 cpus used, the lateral pressure is set to 75 atm and the normal pressure is 1 atm, time span of 1ns used, and the last 500 ps data were used for analysis. ...	136
Table V-14	Thermodynamic properties measured from simulations for A β (1-42) in hydrated lipids with different case studies; A β -E series, second row values are the standard deviations.....	138
Table V-15	Structural properties measured from simulations for A β (1-42) in hydrated lipids with different case studies; A β -E series, AVG(average) and STEDV(standard deviation) values are obtained from the last 500 ps data.....	139

CHAPTER I

INTRODUCTION

1.1 Introduction to Molecular Simulation

Since the Second World War simulations using electronic computers have emerged as a new field to perform high load scientific calculations (Allen and Tildesley, 1987; Frenkel and Smit, 2002). Magnificent advancement has been made in the technological development of computers. Computers can carry out numerous tasks ranging from quantum level calculations to chemical plant design. In this study, we focus our attention on the atomic or molecular scale simulations, which covers the time scale up to a few tens of nano-seconds and the length scale up to a few tens of nanometers.

Molecular simulation plays two pivotal roles in the current nano-scale research (Allen and Tildesley, 1987; Frenkel and Smit, 2002). First, it can serve to test molecular models by comparing the properties from simulations with experimental results. We can improve our expression of intermolecular and intra-molecular interactions, the force-field, by validating the simulations results against the experiments. Molecular simulation, therefore, gives aid to guide the physical experiments. On the other hand, it can be used to test theories developed by theoreticians. In this case simulations can screen the theories and play the role of experiment. So some researchers call the process as *computer experiment* (Frenkel and Smit, 2002).

Molecular simulations calculate macroscopic properties such as pressure, internal energy, and so on using the microscopic level information (Allen and Tildesley, 1987). Macroscopic properties can be classified as the equilibrium and transport properties. Equilibrium properties can be obtained from either the average of ensembles or the time-averages, while dynamic properties can be measured during the simulation time span. Molecular dynamics (MD) simulation and Monte Carlo (MC) simulation are the two basic techniques in the molecular simulation world.

This dissertation follows the style of *Biophysical Journal*.

Monte Carlo simulation is called so because it uses computer-generated random numbers (Frenkel and Smit, 2002). Since it is a probabilistic way of calculating macroscopic properties, the use of MC is limited to the calculation of equilibrium properties. Quite differently from MC, MD method measures both the equilibrium and dynamic properties (Frenkel and Smit, 2002), for it is a deterministic way of obtaining the properties. In other words, it measures properties along the time evolution. One of the postulates of statistical mechanics states that the properties averaged over time are equivalent to ensemble-averaged properties (Hill, 1986). Therefore, the two methods can be complementary each other to check the simulation results for the equilibrium property predictions.

Even though it is possible to study the macroscopic properties of classical many-body system via molecular simulation, we need a bridge between the measurement from the experiment and the simulation, because what we measure from the experiment does not necessarily correspond to what we predict from the molecular simulation. Statistical mechanics, which deals with macroscopic systems from microscopic or molecular point of view, can serve for this purpose. We leave the details of statistical mechanics to the readers' option (Hill, 1986; McQuarrie, 2003).

1.2 Research Overview

Complex molecules such as polymers and proteins at interface play an important role in the nano-scale science characterizing the macroscopic behaviors. We, therefore, have been seeking to apply the powerful molecular simulation tools to study complex molecules at interfaces and selected two applications which are of importance in both industrial and academic point of view. As a first part of this work, we study the fabrication process of polymer-clay nanocomposite. Specifically, we intend to apply molecular dynamics simulation to the partitioning process of single freely-moving dendritic surfactants into clay gallery. Our second field of study is beta-amyloid or A β protein behavior near hydrated lipids. We pay special attention to the thermodynamic

and structural properties of lipid bilayer and A β protein along both the simulation time and distance from the lipid bilayer interface.

After the construction of model systems, we will perform molecular dynamics simulation to obtain both the thermodynamic and structural properties of the system. We will then analyze and compare the simulation results with experiments and literature available. Finally, we will draw conclusions and propose future work.

1.3 Nano-Research

1.3.1 Polymer-Clay Nanocomposite

Advantages of polymer-clay nanocomposites over traditional polymers such as greater mechanical strength and higher heat resistance have led to research interest for a variety of applications (Carrado, 2000; Jacob et al., 2003; Kojima et al., 1993; Krishnamoorti et al., 1996; Manias et al., 2001; Nam et al., 2002; Zhu et al., 2001). Two common morphologies are found for miscible polymer-clay mixture, known as intercalated and exfoliated (or delaminated) structures. As polymer-clay miscibility or interaction strongly depends on the polymer-clay interface, in many cases the clay is first treated with surfactants using cation exchange with organo-functionalized ammonium ions (Burnside and Giannelis, 1995; Vaia et al., 1993; Vaia et al., 1995). Experiment on hyperbranched polymer (HBP)-montmorillonite nanocomposite, where HBP is a dendrimer analogue, revealed significantly advanced mechanical properties including stiffness reinforcement in the presence of exfoliated silicate layers (Plummer et al., 2002), while preventing the re-aggregation problem on drying which is common in the preparation of polymer-clay nanocomposites (Levy and Francis, 1975; Ogata et al., 1997).

1.3.2 Experiments

As mentioned in the previous sub-section, interest has been paid to dendrimers, because they exhibit quite different morphological characteristics despite of the similar

chemistry. Recently, experiments of mixing bentonite clay with melamine-based dendritic surfactants and characterization of the materials were performed in Simanek's group at Chemistry Department of Texas A&M University (Acosta et al., 2003). It was hypothesized that there exists "frustrated intercalation", where the dendritic portion is anchored between clay layers and the rest of the molecule is extended into the solvent, for the surfactant intercalation into the clay. The previous experimental work clearly demonstrated that the key factors determining the intercalation structure are the size and shape of the surfactant molecule.

We intend to rationally explain why we observe the different morphological properties depending on the nature of dendrimers. Experimentally we are limited to achieve the goal, since it is hard to measure the key thermodynamic properties such as the free energy. Therefore, we switch the gear toward molecular simulation to study the phenomena from the fundamental view.

1.3.3 Simulations

One way of examining the intercalation problem of polymer-clay nanocomposite from the simulation viewpoint is to study the confinement of molecules in a slit, which models the clay gallery. Most simulation works on a polymer in confinement are limited to a linear polymer in a repulsive tube or slit with emphasis on scaling concepts (de Joannis et al., 2000; Livadaru and Kreuzer, 2003; Milchev and Binder, 1998). One research group reported Monte-Carlo simulation works on the confinement of isolated polymers with different topology (Chen and Escobedo, 2001; Chen and Escobedo, 2004). They found that the molecular topology affects the partitioning of the polymer and the interaction between the polymer and confining surface. Polymer melt intercalation in organically-modified layered silicates (OLS) has been studied exploiting experiment and simulations (Hackett et al., 1998; Hackett et al., 2000; Lee et al., 1998; Vaia and Giannelis, 1997a; Vaia and Giannelis, 1997b; Vaia et al., 1996). A study on the simulations of the layered silicate modified with alkyl-ammonium surfactant showed layered structure of the surfactant in confined geometry featuring oscillating density

profiles (Hackett et al., 1998). From the free energy analyses, Vaia and coworkers categorized four different types of nanocomposite structures which can be expressed as immiscible, intercalated, ill-defined intercalated, and exfoliated structures, respectively (Vaia and Giannelis, 1997a). Molecular modeling study on the binding energies among nylon-ammonium salt, ammonium salt-clay, clay-nylon was reported, determining which quaternary ammonium salt is most effective in providing a high interfacial strength between the clay sheets and the dispersed nylon (Tanaka and Goettler, 2002). The effect of polymer architecture on the miscibility of the polymer-surfactant modified clay was investigated using self-consistent field theory (Singh and Balazs, 2000), and experimental results substantiating the theoretical prediction was recently reported (Robello et al., 2004).

Much attention has been paid to thermodynamic analyses for the interaction between polymer and clay. However, no special concern has been paid to analyzing the partitioning of a dendritic surfactant from the combined standpoint of thermodynamics and confinement force. In particular the previous modeling works mainly focused on the *polymer* intercalation into surfactant-modified silicates, but to the authors' knowledge the simulation research on the surfactant-clay interaction or the partitioning of a *surfactant molecule* into clay layers has not been much investigated. Thus, it is desirable to theoretically and thermodynamically understand the partitioning or intercalation phenomena of dendritic surfactant into clay. With those motivations we intend to explore the interactions among dendritic surfactant and clay.

1.3.4 Work Scope

We will simulate systems of single freely-moving or untethered dendrimers partitioning into a clay gallery. Confinement forces will be directly measured from simulations and the corresponding free energy profiles are obtained by integrating them at different clay layer separations. Final morphology of the nanocomposite will be predicted from the free energy profiles.

1.4 Bio-Research

1.4.1 Alzheimer's Disease and A β Protein

Alzheimer's disease, characterized as a progressive, degenerative disorder, affects the functionality of human brain. It is widely accepted that the deposition or aggregation of β -amyloid(A β) is related to AD (Hardy and Pastor, 1994; Sisodia and Price, 1995). The peptide structure and aggregation are critical in neurotoxicity of AD. In spite of the importance of the problem, accurate information of the toxic structure and mechanism associated with the toxicity still remains unclear.

To address the problem via molecular simulations we explore fundamental studies on bulk water, hydrated lipids, and finally systems of A β in hydrated lipids. In the later sections, we discuss the previous studies on the hydrated lipids which are model membranes of biological systems and the A β protein research in detail.

1.4.2 Hydrated Lipids

To correctly describe the physical phenomena at the interface of water-lipids we need to have an accurate model lipid. DPPC or dipalmitoylphosphatidylcholine was chosen as our model lipid due to its abundance in biological system and experimental and simulation data availability. Discussions of the previous studies on lipids in this section are limited to the material, unless otherwise noted.

Starting from early 70's there has been considerable amount of work on hydrated lipids which consist of biological membranes. Studies of DPPC bilayers using neutron magnetic resonance (NMR) and X-ray diffraction (XRD) experiments have been reported. Before explaining the previous experimental work, it should be stressed that the head group area itself is not directly measured, rather it is calculated from measured and assumed properties. The lowest limit of the DPPC head group area was obtained as 56.0 \AA^2 by Pace and Chan (Pace and Chan, 1982). NMR results for head group area measurement ranges from 56.0 to 71.7 \AA^2 (de Young and Dill, 1988; Nagle, 1993; Pace

and Chan, 1982; Petrache et al., 2000; Thurmond et al., 1991). 69 \AA^2 of the molecular area at $50 \text{ }^\circ\text{C}$ was reported from NMR experiment by de Young and Dill (1988). The area was found to be increased slightly with increased temperature. XRD data exhibited the similarly scattered pattern for head group areas such as 62.9 \AA^2 (Nagle et al., 1996), 66.5 \AA^2 (Lewis and Engelman, 1983) and 71.2 \AA^2 (Lis et al., 1982).

Sudden change in the head group area between the gel and liquid crystalline phase was observed for various lipid bilayers (Mouritsen, 1991). Average segmental acy-chain order parameter of 0.9 in the gel phase has been reduced to 0.3 above 314K of the melting temperature for DPPC bilayer from computer simulation (Mouritsen and Jorgensen, 1994).

Hydrated lipids have been studied extensively via molecular simulations to produce reliable structural properties (Chiu et al., 1995, 1999a, b; Egberts and Berendsen, 1988; Marrink et al., 1993, 1996; Mori et al., 2004; Niemela et al., 2004; Patra et al., 2003, 2004; Robinson et al., 1994; Tieleman and Berendsen, 1996; Ulander and Haymet, 2003; van Buuren et al., 1995; van der Ploeg and Berendsen, 1982). Various kinds of lipids such as dimyristoylphosphatidylcholine (DMPC) (Chiu et al., 1995; Damodaran and Merz, 1994; Robinson et al., 1994; Takaoka et al., 1998) and dioleoylphosphatidylcholine (DOPC) (Chiu et al., 1999b; Mashl et al., 2001) have been studied computationally, however, one of the best studied model lipid has been DPPC. Yet the lipid molecules have been represented as united-atom models in most cases (Egberts et al., 1994; Essmann et al., 1995; Marrink et al., 1996; Mashl et al., 2001; Shinoda et al., 1995, 1997; Smondyrev and Berkowitz, 1999a, 1999b). Recently, simulation works of hydrated lipids with all-atom force-field have been reported with the increased computer power (Takaoka et al., 1998; Tu et al., 1995, 1996). The lipid head group area, together with order parameter of a hydrocarbon chain and the membrane thickness, is one of the key structural properties to be investigated during the simulation. Shinoda and colleagues obtained one of the lowest equilibrium head group areas of 53.4 \AA^2 irrespective of initial conditions, at 353K (Shinoda et al., 1997). Some reported values of head group area are 61 \AA^2 at 325K (Chiu et al., 1999a), 64.5 \AA^2 at 323K (Patra

et al., 2003), and 69 \AA^2 at 323K (Leontiadou et al., 2004) for DPPC bilayers. Most of the molecular area was found to be from 60 to 69 \AA^2 at temperatures around 323K.

Bilayer membrane thickness, which is quite similar to the phosphorous-phosphorous atom distance between the upper and lower layers or the head-head separation distance has been measured experimentally (Inoko and Mitsui, 1978; Lewis and Engelman, 1983; Lis et al., 1982; Nagle et al., 1996). Reported bilayer thickness value reaches to 43.1 \AA at $45 \text{ }^\circ\text{C}$ (Inoko and Mitsui, 1978). Sometimes it is represented as the thickness of hydrocarbon chains (Douliez et al., 1995; Lewis and Engelman, 1983; Petrache et al., 2000; Schindler and Seelig, 1975). It has been found to be 35 to 40 \AA from the previous simulation studies (Doxastakis et al., 2005; Lee et al., 2004; Shinoda et al., 1997; Sum, 2005; Tieleman and Berendsen, 1996; Tu et al., 1995).

The order parameter which characterizes the fluidity of lipid membrane features drastic change from gel phase to liquid crystalline phase (Mouritsen and Jorgensen, 1994). The absolute plateau value of averaged order parameters from order parameter profile, usually from 4th carbon to 8th carbon, is known to be 0.2. The order parameter tails off as the chain number increases, i.e. in the middle of the bilayer. Doxastakis and coworkers predicted the order parameter well in the bilayer middle, but slightly overestimated near the water-lipid interface (Doxastakis et al., 2005). Lee and colleagues (Lee et al., 2004) overestimated the order parameter by 40% in the head of the lipids, while well predicted the last segmental order parameter of 0.08 close to the experimental result by Seelig et al. (Seelig and Seelig, 1974).

Tu and coworkers published several studies on the hydrated DPPC using molecular dynamics simulations with all-atom models (Tu et al., 1995, 1996, 1998). One of them deals with DPPC bilayer in liquid crystalline phase at $50 \text{ }^\circ\text{C}$ with constant pressure and temperature MD (Tu et al., 1995). The distance between phosphate groups was found to be 39.8 \AA^2 and the lipid molecular area was 61.8 \AA^2 from the simulations. Excellent reviews on the computer simulations of hydrated lipids are found elsewhere (Tieleman et al., 1997; Tobias et al., 1997).

1.4.3 A β Protein Research

Research has been done on the structure and aggregation of A β experimentally (Lee et al., 1999; Mansfield et al., 1998; Mason et al., 1996; Pallitto et al., 1999; Terzi et al., 1997; Wang et al., 2003). Researchers pointed out that A β (17-21) fragment is critical in the aggregation of A β peptide (Mansfield et al., 1998; Pallitto et al., 1999). Good and coworkers reported important data on the fibril formation of A β .(Lee et al., 2005; Wang et al., 2003) Hydrogen exchange-mass spectrometry(HX-MS) experiment revealing the distribution of species suggests that the N-terminus of the peptide does not participate in fibril formation, while the C-terminus is found to be important in fibril formation (Wang et al., 2003). Moreover, Hsp20, a novel α -crystalline protein, was found to drastically reduce A β toxicity to two different cells and the prevention of A β fibril formation was confirmed by electron microscopy in recent publication (Lee et al., 2005).

Considerable research interest has been paid to the interaction of A β with lipid membranes (Ariga and Yu, 1999; Choo-Smith et al., 1997; Mason et al., 1996; McLaurin et al., 1998; Terzi et al., 1997; Yoo, 2002). Result of small angle X-ray diffraction analysis of the A β (25-35) with liposomes implies that the peptide has strong lipophilicity and inserts into the membrane hydrocarbon core (Mason et al., 1996). It was insisted that A β binding occurs electrostatically to the outer envelope of polar head group region from the study on interaction of A β (1-40) with lipid membranes (Terzi et al., 1997). Studies show that membrane containing those molecules significantly affects the aggregation of A β , although the roles of both cholesterol and gangliosides are not clearly understood (Ariga and Yu, 1999; ChooSmith et al., 1997; McLaurin et al., 1998; Yoo, 2002). Experiments using membranes with gangliosides showed that gangliosides might be the A β binding site on the cell membrane (Yoo, 2002) and reduction in cholesterol and sialic acid content protected cells from toxic effect (Wang et al., 2001).

Molecular simulations with A β as the target protein have been studied, but the system has not been resolved since then. Considerable amount of molecular dynamics studies mainly focused on the conformations and the structures of A β (1-42) has been

done by Mager and coworkers (Mager, 1998a; Mager, 1998b; Mager, 2001; Mager and Fischer, 2001; Mager et al., 2002; Mager et al., 2001). Conformations of A β (1-28) peptide fragment depending on pH have been investigated at 298K using molecular dynamics without lipid bilayers (Kirshenbaum and Daggett, 1995). MD simulation study of A β peptide (25-35), another important fragment of A β , has been reported in aqueous trifluoroethanol (TFE) solution and it was found that TFE plays an important role in the formation of α -helix (Lee and Kim, 2004). The structure and dynamics of A β (10-35)-NH₂ peptide in aqueous solution has been studied via molecular dynamics simulations (Massi et al., 2001; Massi and Straub, 2003) and it was insisted that the central LVFFA hydrophobic cluster (17-21) and the VGSN turn (24-27) regions are strongly correlated with the preservation of the structure (Massi et al., 2001). MC simulation of A β insertion into cell membranes at amino acid level has been investigated and it was shown that most familial AD (FAD) mutations have a central effect on the insertion of A β peptide (Mobley et al., 2004).

As a summary, we intend to provide a full-atomistic model of hydrated lipids reliably and use it for further study. Regardless of the huge amount of research on the A β peptides, to the best of our knowledge studies on the A β peptides near hydrated lipid bilayer with full atomistic models have not been reported. Therefore, we intend to apply MD technique to study the interaction behavior of A β with cell membranes.

1.4.4 Work Scope

In this work, several sets of simulations including the bulk water with different water models such as the SPC and cvff water models, hydrated lipids (DPPC bilayer in water), and the A β peptides (A β (1-42) and A β (31-42)), in water will be followed by the simulations of the A β peptides near hydrated lipids. After building the hydrated lipids the structural properties such as the average molecular head group area, membrane thickness, and order parameters are studied to ensure the quality of work. Then, the model bilayer will be used to simulate the peptides near hydrated lipids. Finally, we will

examine the thermodynamic and structural properties associated with the insertion or partitioning of the A β peptides with different starting structure and its relative location to the membrane interface.

CHAPTER II

THEORY

2.1 Molecular Dynamics Simulation

2.1.1 Introduction

The discussion in this section is largely based on the book of Frenkel and Smit (2002). Interesting phenomena happen at the interfaces while we might observe changes in thermodynamic properties such as the free energy profile, which may be intractable from experiments only. Free energy profiles can be captured using molecular simulations, since it provides meaningful thermodynamic quantities even less than Å scale differences.

Integrating Equation of Motion

As mentioned in the previous chapter, molecular dynamics simulation can compute the equilibrium and transport properties of a classical system. The idea is that we measure certain macroscopic properties by monitoring the atomic or molecular movement along the simulation. The positions and velocities of atoms are determined from the Newton's equation of motion or $f = ma$. The fundamental underlying principle is that once we know the position and velocity of each atom at current time step, we can predict the position and velocity at the next time step by integrating the equation of motion.

The two first-order ordinary differential equations can be solved simultaneous by several integration methods.

$$\frac{dr_i}{dt} = v_i \quad (\text{II-1})$$

$$\frac{dv_i}{dt} = \frac{f_i}{m_i} \quad (\text{II-2})$$

where the subscript i is the atom identifier, \mathbf{r} , \mathbf{v} , and \mathbf{f} are the position, velocity and force vectors, respectively. \mathbf{f} is calculated from the force-field, and depends on $\{\mathbf{r}_i\}$.

One of the most efficient algorithms for solving the equations is known as Verlet algorithm. Since LAMMPS (Large-scale Atomic/Molecular Massively Parallel Simulator) (Plimpton, 1995) employs the standard velocity Verlet we briefly discuss the idea of the scheme.

This algorithm looks like a Taylor series expansion

$$\mathbf{r}(t + \Delta t) = \mathbf{r}(t) + \mathbf{v}(t)\Delta t + \frac{\dot{\mathbf{f}}(t)}{2m} \Delta t^2 \quad (\text{II-3})$$

And the velocity is updated from

$$\mathbf{v}(t + \Delta t) = \mathbf{v}(t) + \frac{\dot{\mathbf{f}}(t + \Delta t) + \dot{\mathbf{f}}(t)}{2m} \Delta t \quad (\text{II-4})$$

Since this method stores the position, velocity, and force all at the same time, it minimizes the round-off error and provides numerical stability, convenience, and simplicity (Allen and Tildesley, 1987).

2.1.2 Ensemble

A statistical mechanical ensemble is a collection of microstates (e.g. atomic positions, velocities) that are consistent with a set of macroscopic constraints. There are a number of ensembles for specific purposes. Most popular ensembles are microcanonical (NVE), canonical (NVT), isothermal-isobaric (NPT), and grand-canonical (μ VT) ensembles.

Microcanonical Ensemble

This ensemble is the basic ensemble which is characterized by constant number of particles(N), volume(V), and total energy(E). Since basic MD is simply to solve the

Newton's equation of motion, the natural MD simulation is known to be microcanonical. This ensemble can be used to check the correctness of an algorithm. Also it can serve to test the adequacy of a time step by checking conservation of total energy.

Canonical Ensemble

In this ensemble the fixed variables are N , V , and T (temperature). Since temperature is not a specified property in the microcanonical system and many experiments have been performed at constant temperature, most of current molecular simulations take advantage of this ensemble.

Several methods have been developed to serve the purpose; stochastic method, constraint methods (velocity-scaling and isokinetic method), and extended system method. The extended system method has been widely used because it produces a canonical distribution of microstates (Frenkel and Smit, 2002).

Nosé-Hoover Thermostat

Nosé-Hoover thermostat is the best known extended system method and we explain its basic idea, which is implemented in LAMMPS, in this subsection. The whole system is composed of two sub-systems or the system of interest and a thermostat as shown in Figure II-1. Energy can be transferred to and from the system to maintain the same temperature.

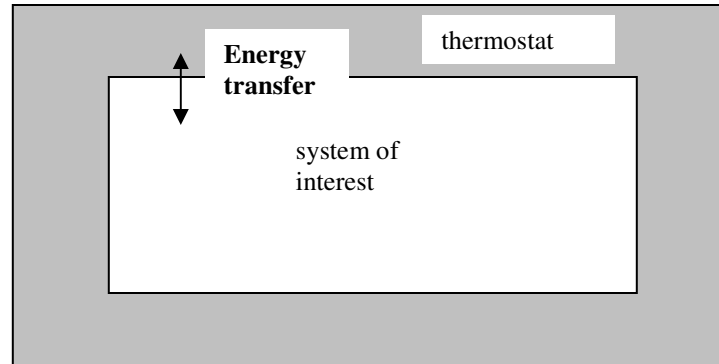


Figure II-1 Representation of canonical and microcanonical ensembles.

The equations of motion in the Nosé-Hoover thermostat are given by

$$\dot{\mathbf{r}}_i = \frac{\mathbf{p}_i}{m_i} \quad (\text{II-5})$$

$$\dot{\mathbf{p}}_i = -\frac{\partial U(\mathbf{r}^N)}{\partial \mathbf{r}_i} - \xi \mathbf{p}_i \quad (\text{II-6})$$

$$\dot{\xi} = \left(\sum_i \frac{p_i^2}{m_i} - \frac{L}{\beta} \right) / Q \quad (\text{II-7})$$

$$\frac{\dot{s}}{s} = \frac{d \ln s}{dt} = \xi \quad (\text{II-8})$$

where $\beta = 1/kT$, \mathbf{p} is the momentum, s is an additional coordinate, the prime indicates the real variable, p_s is the momentum associated to s , Q is an effective mass, $\xi = \frac{sp_s}{Q}$ is the thermodynamic friction coefficient. The conserved total energy is correspondingly expressed as

$$H_{Nose} = \sum_{i=1}^N \frac{p_i^2}{2m_i} + U(r^N) + \frac{\xi^2 Q}{2} + L \frac{\ln s}{\beta} \quad (\text{II-9})$$

with $L = 3N$.

Isothermal-Isobaric Ensemble

We will perform our production simulations for biomolecular research using isothermal-isobaric ensemble or *constant pressure ensemble* which specifically means NP_NP_LT. We can refer this ensemble to constant surface-tension ensemble or N γ T. This choice of ensemble has been made, since constant volume ensemble is not suitable for bilayer simulations because of the fluidity (Tieleman and Berendsen, 1996).

The proposed equations of motion by Martyna et al. for isotropic cell fluctuations in the isothermal-isobaric ensemble are as follows (Martyna et al., 1996).

$$\dot{\mathbf{r}}_i = \frac{\mathbf{p}_i}{m_i} + \frac{p_\epsilon}{W} \mathbf{r}_i \quad (\text{II-10})$$

$$\dot{\mathbf{p}}_i = \mathbf{F}_i - \left(1 + \frac{d}{dN}\right) \frac{p_\epsilon}{W} \mathbf{p}_i - \frac{p_\xi}{Q} \mathbf{p}_i \quad (\text{II-11})$$

$$\dot{V} = \frac{dV p_\varepsilon}{W} \quad (\text{II-12})$$

$$\dot{p}_\varepsilon = dV(P_{\text{int}} - P_{\text{ext}}) + \frac{d}{dN} \sum_{i=1}^N \frac{\mathbf{p}_i^2}{m_i} - \frac{p_\varepsilon p_\xi}{Q} \quad (\text{II-13})$$

$$\dot{\xi} = \frac{p_\xi}{Q} \quad (\text{II-14})$$

$$\dot{p}_\xi = \sum_{i=1}^N \frac{\mathbf{p}_i^2}{m_i} + \frac{p_\varepsilon^2}{W} - (dN + 1)kT \quad (\text{II-15})$$

where P_{ext} is the external pressure, and the internal pressure is given by

$$P_{\text{int}} = \frac{1}{dV} \left[\sum_{i=1}^N \frac{\mathbf{p}_i^2}{m_i} + \sum_{i=1}^N \mathbf{r}_i \cdot \mathbf{f}_i - (dV) \frac{\partial U(V)}{\partial V} \right] \quad (\text{II-16})$$

d is the dimension, V is the simulation volume, W is the mass of the barostat, p_ε is the momentum associated with the logarithm of the volume.

The conserved quantity is

$$H = \sum_{i=1}^N \frac{\mathbf{p}_i^2}{2m_i} + \frac{p_\varepsilon^2}{2W} + \frac{p_\xi^2}{2Q} + U(V) + (dN + 1)kT\xi + P_{\text{ext}}V \quad (\text{II-17})$$

2.1.3 Treatment of Long-Range Electrostatics

The systems we are to study are 2-D periodic nanocomposite materials and 3-D periodic biomolecular systems. Nano-composite system consists of dendritic surfactant(s) and MMT (montmorillonite) clay while the biomolecular system is composed of a protein

(A β), water molecules and phospholipids. The intra-molecular forces are easily and quickly obtainable during the simulations, while the intermolecular forces such as the van der Waals interaction and Coulomb interaction requires some computational effort, especially for large systems. Since the largest contribution to the intermolecular potential and forces are due to the short-range neighbor atoms, we normally apply a spherical truncation method for the van der Waals energy calculation, where the potential energy is treated as zero at distances larger than the cutoff radius. For nano-composite research the model system is 2000 Å long in x - and y -dimensions and only one molecule occupies the whole simulation box. Our choice of relatively large cutoff radius of 50 Å can be justified, since the sizes of dendrimers (2.4 nm for G1 and 3.6 nm for G2L (Acosta et al., 2003)) are quite smaller than the cutoff radius and the forces at distances larger than the cutoff radius are essentially zero in that case.

Long-range force can be defined as an electrostatic interaction in which the spatial interaction falls off no faster than r^{-d} where d is the system dimensionality. This includes the charge-charge interaction and dipole-dipole interaction. Since inaccuracy from the simulations is involved with a truncation of the long-range forces, we need a method to handle the electrostatic force within a reasonable amount of time and effort.

Among many useful methods of long-range treatment we cast our focus on the lattice methods, especially the Ewald sum and PPPM (particle-particle/particle-mesh) methods. CPU time scales with the number of particle as $O(N^{3/2})$ in the fully optimized Ewald sum method. But, it should be noticed that the reciprocal or Fourier space part of the Ewald sum scales as $O(N^2)$. To improve the efficiency of calculation in Fourier part several schemes using the fact that the Poisson's equation can be much more efficiently solved if the charges are distributed on a mesh point were developed. The fast Fourier transform (FFT)-accelerated methods scales as $O(N \log N)$ where N represents the number of points of discrete Fourier transform.

The earliest attempt to use particle-mesh approach has been attributed to Hockney and Eastwood (Hockney and Eastwood, 1981). The technique has been greatly improved by splitting the calculation into a short-range and a long-range part. The short-range

contribution can be calculated directly from the particle-particle interactions and the long-range contribution can be solved with particle-mesh technique. There are several methods sharing the same spirit, which rely on the use of Ewald sum with widespread research-attention: PPPM, particle-mesh Ewald (PME), and smooth PME.

Ewald Summation Method

The fundamental idea is as follows. Since the total sum of the electrostatic potential is conditionally convergent, by adding a set of screened charges(real space) and compensating potential(Fourier space), we can obtain the electrostatic potential energy correctly. The screening charge distribution is Gaussian distribution in this method and there are three contributions to the electrostatic potential due to the point charge q_i , the (Gaussian) screening charge cloud $-q_i$, the compensating charge cloud q_i . Total potential is the sum of the real space and Fourier space components and the self-interaction term is removed from it. Here is the summary of the calculation method.

- Short-ranged direct summation of the point charge q_i and the (Gaussian) screening charge cloud $-q_i$ within a cutoff
- Long-ranged summation of the compensating potentials
- Self-interaction term(q_i and compensating potential q_i) is subtracted

A conceptual figure representing different contributions to the total potential was drawn in Figure II-2. The Coulomb potential energy for a charge-neutral system is given by

$$U_{Coul} = \frac{1}{2} \sum_{i=1}^N q_i \phi_i(r_i) \quad (\text{II-18})$$

where $\phi_i(r_i) = \sum'_{j,n} \frac{q_j}{|\mathbf{r}_{ij} + \mathbf{n}L|}$ and the prime in the summation notation means the sum is performed over all the periodic images \mathbf{n} and over all particles j , except $j = i$ if $\mathbf{n} = \mathbf{0}$,

so we only need to calculate the potential at each charge point i . In this equation the electrostatic potential does not depend on the point charge i , but depends on the charge distribution except the point charge i . To obtain ϕ_i is to solve the Poisson's equation.

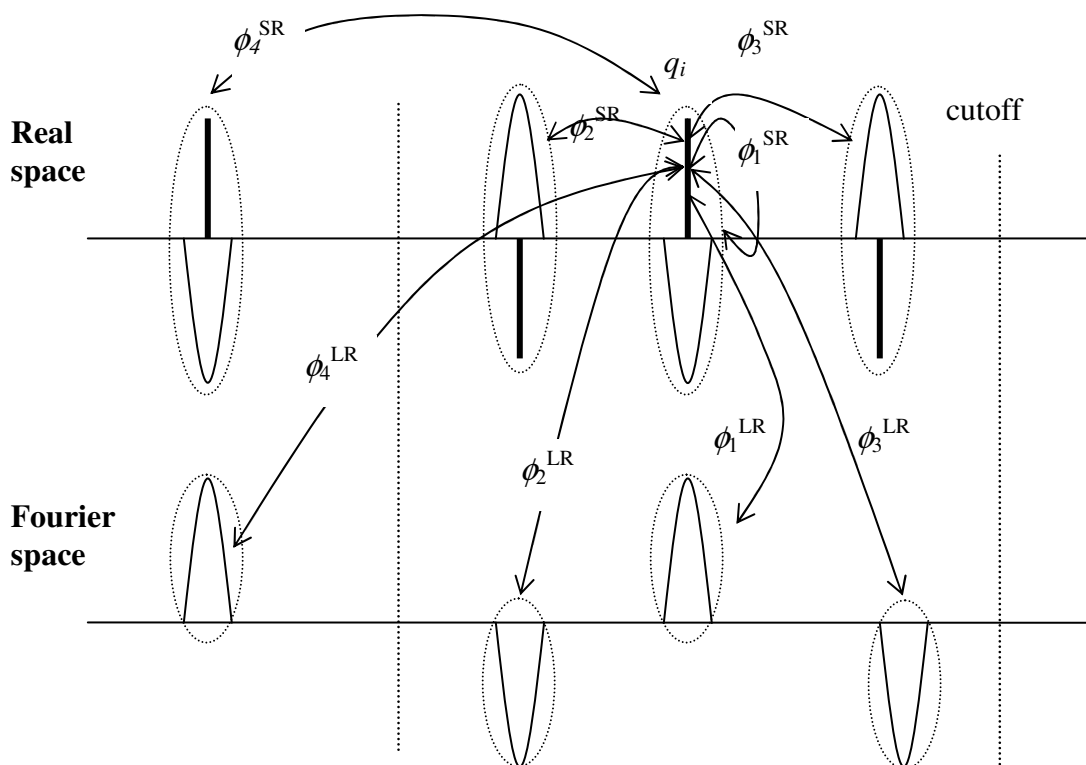


Figure II-2 Conceptual figure of the potential at point charge q_i : The solid rod represents point charges, U- or cup-type curves the Gaussian charge cloud or the compensating charge cloud in Fourier space, the dotted large ovals the complementary error functions which are the potentials due to the short-ranged interaction, the dotted small ovals the potentials due to the long-range interaction.

If we separate the potential in the following way, then the problem becomes to solve the potential for the two parts and get the sum of them.

$$\phi_i(r_i) = \phi_i^{SR}(r_i) + \phi_i^{LR}(r_i) \quad (\text{II-19})$$

For a point charge q_i , the total potential is

$$\begin{aligned} \phi_1 &= (\phi_1^{SR} - \phi_1^{SR}) + (\phi_1^{LR} - \phi_1^{LR}) + \phi_2^{SR} + \phi_2^{LR} + \phi_3^{SR} + \phi_3^{LR} + \phi_4^{SR} + \phi_4^{LR} + \dots \\ &= (\phi_2^{SR} + \phi_3^{SR}) + (\phi_4^{SR} + \dots) + (\phi_1^{LR} + \phi_2^{LR} + \phi_3^{LR} + \phi_4^{LR} + \dots) - \phi_1^{LR} \quad (\text{II-20}) \\ &= \sum_{j \neq 1} \phi_j^{SR} + \sum_j \phi_j^{LR} - \phi_1^{Self} \end{aligned}$$

The first summation is performed in real space within the cutoff, since terms larger than the cutoff rapidly go to zero. For example, $\phi_i^{SR} = \frac{q_i \operatorname{erfc}(\sqrt{\alpha} r_i)}{r_i} \approx 0.00008 q_i$ when the typical value of $\sqrt{\alpha} r_c = 2.6$ is chosen from $\operatorname{erf}(2.6) = 0.9998$. The last term, self-interaction term which is generated by the potential of the compensating charge cloud in Fourier space, is intrinsically given by the choice of splitting parameter and point charges. In Ewald summation method the second summation term is obtained in Fourier space analytically. This method scales as $O(N^{3/2})$ as mentioned earlier.

Particle-Particle/Particle-Mesh (PPPM) Method

The motivation of development of this technique stems from the fact that fully optimized Ewald scales as $O(N^{3/2})$, but for a fixed cutoff the Fourier part scales as $O(N^2)$. Therefore, the Ewald sum method is inefficient for large systems. On the other hand compared to the Ewald method, PPPM scales as $O(N \log N)$, which is particularly useful

for large systems. It is a faster way for an approximate computation of the reciprocal or long-range contribution to the total force calculation derived from the Ewald summation method.

The method to deal with the second term in eq II-20 differentiates PPPM technique, a numerical method, from the original Ewald summation method. We summary the steps to evaluation of the long-range force using PPPM method as follows.

- 1) Charge assignment on the grid point using charge assignment function
- 2) Solving Poisson's equation via a FFT technique
- 3) Differentiation of the electrostatic energy to obtain the forces at mesh points
- 4) Backinterpolation via the assignment function to obtain the force at each particle

Since it features the hybrid of PP and PM methods, it is as accurate as PP method and as fast as PM method.

Summary and Conclusions for Bio-Research

In LAMMPS several styles for Coulomb interactions are implemented such as “cutoff”, “smooth”, “ewald”, “pppm”, “charm/switch”, “eam”, and “debye”, but Ewald summation method and PPPM method are found to be the best approaches for most simulation studies for our biomolecular systems. Therefore, we tested the two methods available in LAMMPS and we need to make selection between the two.

Results using different methods of long-range electrostatics showed that PPPM can be the best choice from the computation time and accuracy (Deserno and Holm, 1998; Pollock and Glosli, 1996). We tested the two different methods with short runs on CAT cluster with the total number of atoms over 40,000 and part of results is shown in Table II-1. Comparing PPPM with Ewald method, we found a huge speedup of approximately 10 for single and 2-cpu jobs maintaining the same accuracy.

Table II-1 Thermodynamic properties and computing time comparison for different long-range electrostatic treatment methods; the second row of the first column represents the method and the number of cpus is shown in the parenthesis, the second row of the last column is the speedup relative to choice_01 simulation case, NVE, 1000 steps with $\Delta t = 2.0$ fs, $r_c = 10.0$ Å, accuracy = 1.0×10^{-4} , whole_run01_070105.10000 as the starting configuration.

Index	Total E [kcal/mol]	KE [kcal/mol]	Temp [K]	PE [kcal/mol]	E_bond [kcal/mol]	E_anlge [kcal/mol]	E_dihed [kcal/mol]	E_impr [kcal/mol]	E_vdw [kcal/mol]	E_coul [kcal/mol]	E_long [kcal/mol]	Press [atm]	Time [s]
choice_01	-60819.6	21459.1	189.6	-82278.7	4554.9	11854.7	2183.2	78.5	12760.3	393673.7	-507384.1	-41.0	40415.7
Ewald(1)	2.2	19.1	0.2	20.0	6.1	19.9	15.8	1.2	52.5	59.7	2.0	43.5	
choice_02	-60815.3	21462.3	189.6	-82277.6	4547.9	11854.4	2199.4	77.1	12708.2	355624.9	-469289.5	-100.9	3591.5
PPPM(1)	2.8	13.6	0.1	12.6	10.9	17.2	8.4	1.3	119.5	129.8	3.3	90.3	11.3
choice_05	-60819.7	21455.5	189.5	-82275.1	4554.6	11853.2	2183.3	78.5	12752.8	393686.6	-507384.1	-43.5	32382.9
Ewald(2)	2.2	19.9	0.2	20.1	6.1	19.4	15.8	1.2	68.8	83.6	2.2	47.3	1.2
choice_06	-60815.2	21465.2	189.6	-82280.4	4547.7	11852.8	2199.0	77.1	12707.4	355624.5	-469288.8	-100.6	2087.7
PPPM(2)	2.8	12.2	0.1	11.7	11.3	16.1	7.9	1.3	121.2	130.8	2.7	89.9	19.4

As a conclusion, the PPPM method is the clear choice for the large systems such as protein in hydrated lipids. Since the PPPM method itself is intrinsically approximate to the true solution of the Poisson's equation, we may need optimization of some tuning parameters. This difficulty might be avoided, since LAMMPS developers already set the default parameters for the number of meshes and the order of the charge assignment function.

2.1.4 Long-Range Correction for van der Waals Energy

This part of theory was based on the discussion of McQuarrie's book (McQuarrie, 2003). Since we have applied a truncation method for the van der Waals interaction, we may need to correct the long-range interaction. The expression for multi-component energy is given by

$$E = K + U = \frac{3}{2} NkT + 2\pi N\rho \sum_{i,j} x_i x_j \int_0^{\infty} g_{ij}(r) u_{ij}(r) dr \quad (\text{II-21})$$

Where $g_{ij}(r)$ is the radial distribution function (RDF, will be discussed in section 2.3) and x is the mole fraction. The potential energy part can be split into two parts and the second term,

$$U = 2\pi N\rho \sum_{i,j} x_i x_j \int_0^{r_c} g_{ij}(r) u_{ij}(r) dr + 2\pi N\rho \sum_{i,j} x_i x_j \int_{r_c}^{\infty} g_{ij}(r) u_{ij}(r) dr \quad (\text{II-22})$$

where r_c represents the cutoff radius. The first term is directly obtained from the simulation and the second term, the long-range correction, can be simplified by reasonably assuming $g_{ij}(r) \cong 1$.

$$U^{LR} = \frac{8\pi}{3\rho} N \sum_{i,j} \rho_i \rho_j \varepsilon_{ij} \sigma_{ij}^3 \left[\frac{1}{3} \left(\frac{\sigma_{ij}}{r_c} \right)^9 - \left(\frac{\sigma_{ij}}{r_c} \right)^3 \right] \quad (\text{II-23})$$

where $\rho_i = \frac{N_i}{\langle V \rangle}$ is the number density of species i , and ε and σ represent the Lennard-Jones parameters. We used Lorentz-Bertholet mixing rule for the mixture LJ parameters.

2.2 Nano-Research

2.2.1 Overall Process of Ion Exchange

Figure II-3 shows a conceptual picture of the ion exchange process. The overall picture of partitioning of the surfactant is quite complicated and many processes are involved. Simply speaking, the dendritic surfactant will enter the clay gallery to perform the cation exchange with the large cations in the clay units. Detailed description is given below. As a solution containing the dendritic surfactant is introduced to the clay solution, the confinement of surfactants happens. Then, the ionic bonds of cation-clay break and the surfactants are tethered to the clay surface. Solvent molecules are rearranged throughout the overall process. The total free energy change associated with the overall process can be divided into several terms as shown below.

$$\Delta A = \Delta A_{ib} + \Delta A_{cs} + \Delta A_{ts} + \Delta A_{sr} \quad (\text{II-24})$$

ΔA_{ib} is the free energy change due to the ionic bond change, ΔA_{cs} represents the free energy change due to the confinement of surfactants, ΔA_{ts} is the free energy change associated with the tethering of surfactants and ΔA_{sr} is the free energy change due to the solvent rearrangement. The first and fourth terms can be reasonably obtained from literature. The second term is of our interest in this work and can be measured from

molecular simulation. The third term is quite relevant to the present work, but is out of work scope.

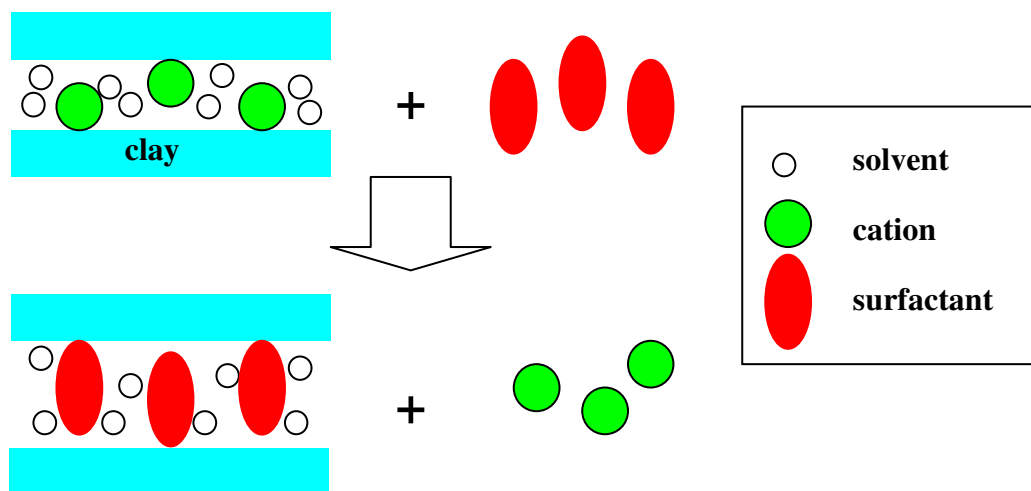


Figure II-3 Simplified ion exchange process.

As described in Chapter I, the free energy is fundamentally associated with the process of intercalation/exfoliation. From the previous works on the simulations of polymer-silicate or confined polymer systems we know that the free energy profile, the relative free energy change at different layer separation distance, is the ultimate thermodynamic criterion for determining the physical process of intercalation. We can classify the type of partitioning based on the free energy profiles, which has been discussed by Vaia and Giannelis (Vaia and Giannelis, 1997a). Before the discussion of theories associated with this work, we intend to mention the difference between their study and ours. They studied the intercalation of a polymer in an organically modified

silicate, while we modeled the partitioning of single surfactants into bare clay. Another intrinsic difference of result analysis is the characteristics of free energy profile associated with forming the nanocomposite structures, which will be discussed in the following paragraph.

Let us start the discussion of free energy profiles by briefly describing their classification of free energy profiles. The reference state or the location where the free energy difference is zero refers to the unintercalated gallery height (h_0) in their study. The abscissa represents the difference between the gallery height (h) after intercalation and the unintercalated gallery height, i.e. $h - h_0$ and the ordinate shows the free energy change per unit area. If a system is immiscible, the profile will be an increasing function along the layer separation (type I). If a system has a minimum or minima of the free energy profiles at finite layer separation, it is considered to form an intercalated structure (types IIa, IIb). But if the free energy profile doesn't exhibit a local minimum and monotonically decreases, the structure can be explained as an exfoliated one (type III).

We provide a conceptual figure of the different types of free energy profiles for miscible nanocomposite based on our model system and reference state in Figure II-4. If we set the reference state as infinite separation or $\Delta A = 0$ at infinity, we will observe several different types of free energy profiles. Note that this choice of reference state is different from Vaia and Giannelis for polymer intercalation. We can classify the type of intercalation following their discussion.

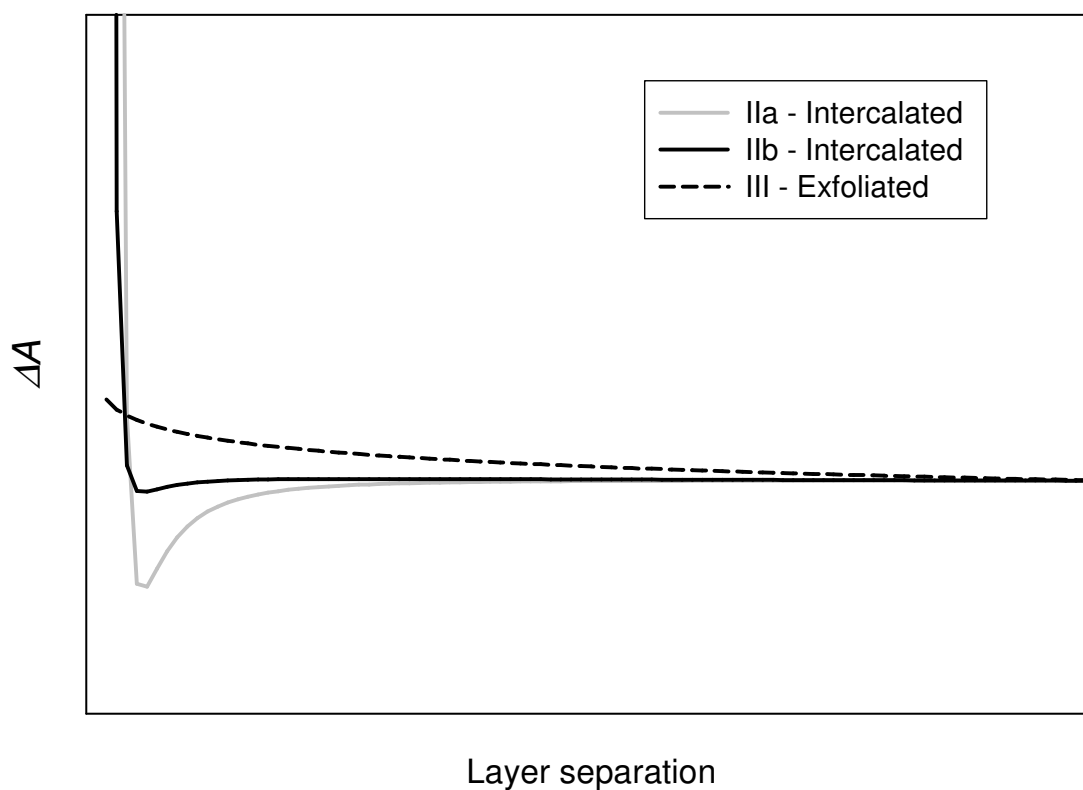


Figure II-4 Graphs representing different types of partitioning.

The free energy profile will be an increasing function of the layer separation if the system is immiscible (type I, not shown in Figure II-4). The favorable intercalation (type IIa) which exhibits only one minimum in their publication corresponds to the frustrated intercalation or complete intercalation at finite separation from our viewpoint. Type IIb system with multiple minima, termed as ill-defined intercalated structures or intermediate intercalated structures before complete layered exfoliation, features an intercalated structure at finite separation and/or the exfoliated structure which follows the intercalation (frustrated or complete intercalation) in our analyses. The relative depth of minimum at finite separation determines whether the final morphology will be

intercalated or exfoliated. If the depth of minimum(a) at finite separation(s) is lower than that of infinite separation, the intercalated structure will be favorable. However, it is less stable than type IIa intercalation. In the case of exfoliation (type III), the free energy profile will be a decreasing function of layer separation.

2.2.2 Thermodynamic Quantities from Simulation

The confinement forces can be physically defined as the forces exerted by the surfaces on the surfactant molecule confined between them. So the mathematical expression for the confinement force of our system is obtained by

$$\mathbf{f}_{conf} = -\nabla U^{sd}(r) \quad (\text{II-25})$$

where \mathbf{f}_{conf} is the confinement force and the U^{sd} is the surface-dendritic surfactant (dendrimer) interaction potential energy.

The total confinement force, due to the presence of top and bottom surfaces, can be expressed as the sum of two force components, \mathbf{f}_{bottom} and \mathbf{f}_{top} , and measured from the simulations using eq II-25 for a given distance between clay surface and surfactant site and both forces have the same average magnitude due to the symmetry but with opposite directions. The average total confinement force is defined as

$$\langle \mathbf{f}_{conf} \rangle = \langle \mathbf{f}_{bottom} \rangle - \langle \mathbf{f}_{top} \rangle \quad (\text{II-26})$$

where the quantity inside the bracket represents the its average value (e.g. over an MD trajectory) and the subscripts bottom and top are the bottom surface and top surface, respectively. The confinement force due to the bottom surface is positive if it is repulsive, while it is negative if attractive. The confinement force due to the top surface has reverse sign.

We consider surface-dendrimer interaction for the free energy calculation only, so the interaction between clay surfaces is neglected. The free energy change associated with the partitioning is obtained by integrating the measured confinement force as will be explained below. Since we are interested in simulating an infinite dilution case, we are restricted to considering a system where the xy -plane has literally infinite dimension of length while the z -direction does not, so the only meaningful component of forces is the z -component. Therefore, we obtain the z -component of f_{conf} or f_{conf}^z from the general definition of a force from a free energy, i.e. the partial derivative of a free energy with minus sign,

$$\langle f_{conf}^z \rangle = \langle f_{bottom}^z \rangle - \langle f_{top}^z \rangle = - \left. \frac{\partial A^{ex}}{\partial D'} \right|_D \text{ at surface separation of } D \quad (\text{II-27})$$

where A^{ex} is the excess Helmholtz free energy and it is termed as the free energy subsequently throughout this paper. As the only extra potential that is related to the excess Helmholtz free energy is the surface-dendrimer interaction or more precisely the confinement force, the free energy, potential energy, and entropy are excess properties.

We have the relative free energy defined as the difference between the free energy at the separation of D and that of at infinite separation.

$$\Delta A^{ex} = - \int_{\infty}^D \langle f_{conf}^z(D') \rangle dD' \quad (\text{II-28})$$

We assume that the free energy at infinite separation goes to zero, i.e. $A^{ex}(\text{reference}) = A^{ex}(\infty) = 0$, which makes sense because at large separation there is little free energy change associated with placing a molecule into a slit.

So the final expression for A^{ex} becomes

$$\Delta A^{ex} = A^{ex}(D) - A^{ex}(\infty) \cong A(D) = -\int_{\infty}^D \langle f_{bottom}^z(D') \rangle dD' + \int_{\infty}^D \langle f_{top}^z(D') \rangle dD' \quad (\text{II-29})$$

From thermodynamics we can analyze a free energy as the combination of energetic and entropic parts, i.e.,

$$\Delta A = \Delta E - T\Delta S \quad (\text{II-30})$$

where E is the total internal energy and S is the entropy. By comparing the relative magnitude of each contribution with another component, one can say which component dominates in a process associated with free energy change. This argument applies to the analysis of free energy associated with the partitioning of a dendrimer into the clay. For our study we are interested in the free energy change with the partitioning or confinement, so the excess Helmholtz free energy is simplified as

$$\Delta A^{ex} = \Delta U - T\Delta S^{ex} \quad (\text{II-31})$$

where S^{ex} is the excess entropy. From the simulations we directly measure the total potential energy and we obtain the excess Helmholtz free energy from eq II-29. Finally, the difference of the excess entropy, ΔS^{ex} , is calculated from eq II-31.

2.3 Bio-Research

There are many structural and thermodynamic properties that characterize protein behavior in hydrated lipids. Though our ultimate simulation goal is to determine the free energy profiles along the separation distance between the protein and the lipid bilayer interface, we need to study bulk water and hydrated lipids without a protein. Putting aside the thermodynamic properties, which will be discussed in Chapter III of Method

and System, we describe structural properties to be compared with experiment during the simulation works.

2.3.1 Phase of Hydrated Lipids

We need to simulate the bio-system as found under physiological conditions. The main phase of the lipid bilayer can be classified as a gel phase or a liquid crystalline phase. The gel phase is well ordered, while the liquid crystalline phase exhibits less order.

Three major phases of lipid bilayer have been depicted in Figure II-5. The main transition can be considered as a disordering process by which the lipid bilayer turns into a liquid from a solid gel losing its translational order or from $L\beta$ (untilted gel) or $L\beta'$ (tilted gel) to $L\alpha$. Depending on the water concentration at 323K Lecithin-water system can have the tilted gel phase $L\beta'$ or liquid crystalline phase $L\alpha$. Ripple phase $P\beta'$ might appear at different water concentration and/or temperature. The transition from $P\beta'$ to $L\alpha$ is considered as the main transition in the lipid bilayer (Pasini and Zannoni, 2000).

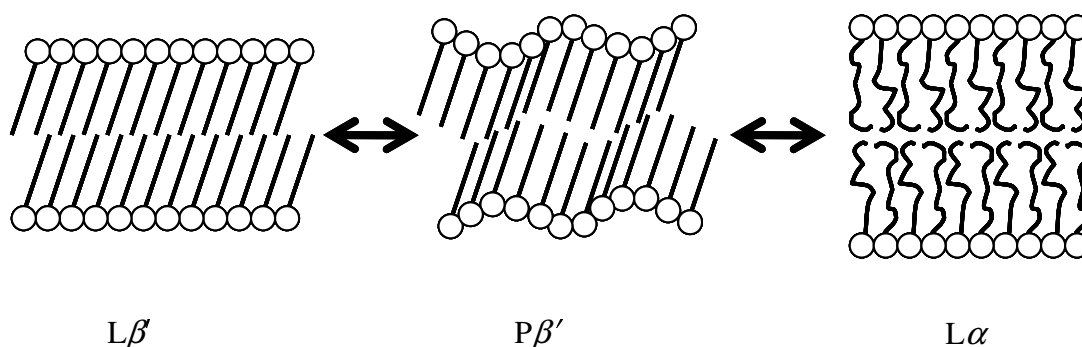


Figure II-5 Schematic of lipid phase transitions; $L\beta'$ is one dimensional lamella lattice in tilted gel phase, $P\beta'$ is a ripple phase, $L\alpha$ is liquid crystalline phase; Adapted from Pasini and Zannoni, 2000.

We need to determine if our model DPPC bilayer is in the $L\alpha$ phase at the target temperature of 323K. At temperatures above T_m (melting temperature, 314K for DPPC),

it is known that the bilayer is in the liquid crystalline phase (Mouritsen and Jorgensen, 1994). Most simulation studies of lipid bilayers have been performed at well above T_m , and even higher than body temperature, since the liquid crystalline phase resembles physiological conditions (Abe et al., 2002; Shinoda et al., 1995; Tieleman and Berendsen, 1996; Tu et al., 1995). There are various kinds of lipids and other biomolecules, which biological membranes consist of such as cholesterol. Consequently, if we just simulate hydrated lipid systems composed of DPPC only at 310K, we are not truly studying real biological membranes, since the hydrated lipid is not in liquid crystalline phase. Therefore, we need to perform simulations at higher temperature than T_m .

2.3.2 Order Parameter

The segmental order parameter or the tensor of hydrocarbon chains is defined as

$$S_{ij} = \frac{1}{2} \langle 3 \cos \theta_i \cos \theta_j - \delta_{ij} \rangle \quad (\text{II-32})$$

where the bracket represents the time average. Usually S_{yz} is small and the trace is 0, if the molecular motion is such that the isotropic rotation around the molecular z axis occurs then $S_{zz} = -2S_{xx} = -2S_{yy}$. S_{zz} is often referred to as S_{chain} . S_{ij} is a second-order tensor and θ_i is the angle between the i -th molecular axis and bilayer normal.

$$S_{xx} = \frac{1}{2} \langle 3 \cos^2 \theta_x - 1 \rangle \quad (\text{II-33})$$

$$S_{yy} = \frac{1}{2} \langle 3 \cos^2 \theta_y - 1 \rangle \quad (\text{II-34})$$

$$S_{zz} = \frac{1}{2} \langle 3 \cos^2 \theta_z - 1 \rangle \quad (\text{II-35})$$

where $\cos \theta_x = \frac{\mathbf{n} \cdot \mathbf{x}}{|\mathbf{n}| |\mathbf{x}|}$, $\cos \theta_y = \frac{\mathbf{n} \cdot \mathbf{y}}{|\mathbf{n}| |\mathbf{y}|}$, and $\cos \theta_z = \frac{\mathbf{n} \cdot \mathbf{z}}{|\mathbf{n}| |\mathbf{z}|}$.

The molecular axes for the n -th CH_2 unit are defined as: z -vector from C_{n-1} to C_{n+1} , y -vector perpendicular to z and in the plane through C_{n-1} , C_n , and C_{n+1} , and x -vector perpendicular to z and y . A simplified figure showing the bilayer normal and the corresponding axes vectors are drawn in Figure II-6.

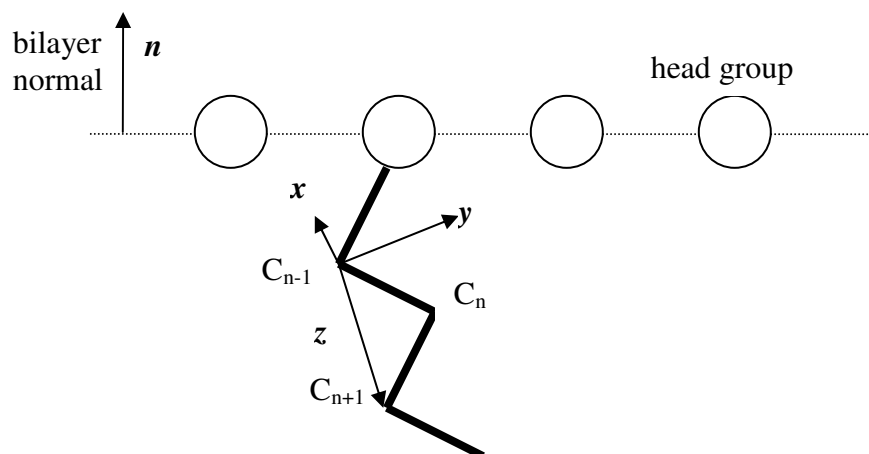


Figure II-6 Schematic of vectors associated with order parameter calculation.

We define the normal vector to the bilayer interface as $(0,0,1)$ or $\mathbf{n} = (0,0,1)$. Now, the z -vector can be directly obtained from the position vectors.

$$\mathbf{z} = C_{n+1} - C_{n-1} = (x_{n+1} - x_{n-1}, y_{n+1} - y_{n-1}, z_{n+1} - z_{n-1}) = (a, c, e) \quad (\text{II-36})$$

Let us define the \mathbf{y} -vector, which is perpendicular to \mathbf{z} and in the plane through C_{n-1} , C_n , and C_{n+1} , as (x_Y, y_Y, z_Y) . From the orthogonality between \mathbf{y} and \mathbf{z} , we have

$$\mathbf{y} \cdot \mathbf{z} = x_Y a + y_Y c + z_Y e \equiv 0 \quad (\text{II-37})$$

Since \mathbf{y} is perpendicular to \mathbf{p} (A, B, C), the normal vector of the plane, we know

$$\mathbf{y} \cdot \mathbf{p} = x_Y A + y_Y B + z_Y C \equiv 0 \quad (\text{II-38})$$

Solving the two equations we have the following for a given x_Y , i.e. x_Y can be chosen arbitrarily. One simple choice is to select the x component of C_n or x_n as x_Y .

$$y_Y = \frac{aC - eA}{eB - cC} x_Y \quad (\text{II-39})$$

$$z_Y = -\frac{x_Y a + y_Y c}{e} \quad (\text{II-40})$$

The only remaining independent vector \mathbf{x} , perpendicular to both \mathbf{y} and \mathbf{z} , is obtained from the definition of a cross product.

$$\mathbf{x} = \mathbf{y} \times \mathbf{z} \quad (\text{II-41})$$

$$\mathbf{x} = (ey_Y - cz_Y, az_Y - ex_Y, cx_Y - ay_Y) \quad (\text{II-42})$$

Numerically, if the value of e is too small (~ 0.0), z_Y can diverge and we will have to define the y -vector in a different way. We first choose z_Y by applying the z -component of C_n . Then by solving the two equations, we finally arrive at

$$y_Y = \frac{aC - eA}{cA - aB} z_Y \quad (\text{II-43})$$

$$x_Y = -\frac{cy_Y + ez_Y}{a} \quad (\text{II-44})$$

Deuterium order parameter is defined as

$$-S_{CD} = \frac{2}{3}S_{xx} + \frac{1}{3}S_{yy} \quad (\text{II-45})$$

A dramatic change in the average segmental order parameter $\langle S \rangle$ is found at 314K, which is known to be the liquid-crystalline to gel phase transition temperature, for hydrated DPPC from 0.9 to 0.3 (Mouritsen and Jorgensen, 1994). Usually the segmental order parameter ($-S_{CD}$) value of DPPC/water is from 0.05 to 0.25 at 335K (Essmann et al., 1995; Tieleman and Berendsen, 1996). Another definition related to the segmental order parameter is the molecular order parameter which is defined as $S_{mol} = -2S_{CD}$ (Seelig and Niederbe, 1974).

2.3.3 Hydrocarbon Chain Conformations

The fraction of trans/gauche conformation can be used to determine the phase of the hydrated lipids we are simulating. The conformation is determined from the dihedral angle between the two projected vectors on the same plane. A representative figure defining the vectors and dihedral angle is drawn in Figure II-7. We define vectors associated with the analysis as follows.

$$\mathbf{a}' = \mathbf{B} - \mathbf{A} \quad (\text{II-46})$$

$$\mathbf{b}' = \mathbf{D} - \mathbf{C} \quad (\text{II-47})$$

$$\mathbf{n} = \mathbf{C} - \mathbf{B} \quad (\text{II-48})$$

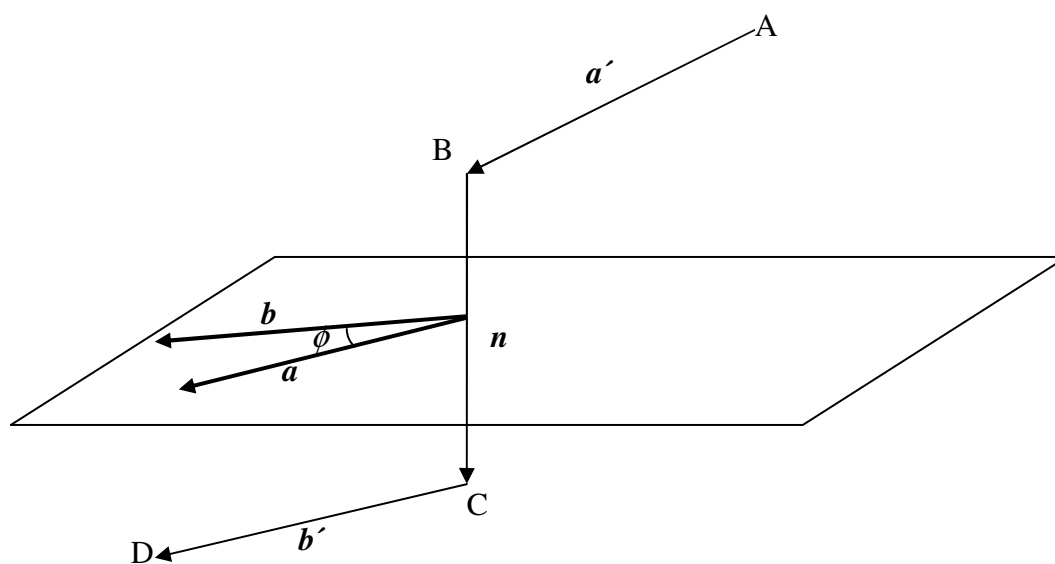


Figure II-7 Defining the angle for the trans/gauche conformation differentiation.

The torsion angle ϕ is defined as the angle about \mathbf{n} -vector from $-\mathbf{Pa}'$ to \mathbf{Pb}' , where P indicates the vector projection onto the plane whose normal vector is \mathbf{n} . The projection of a vector \mathbf{v} onto the plane perpendicular to \mathbf{n} is given by (http://www.math.fsu.edu/~quine/IntroMathBio_04/torsion_pdb/torsion_pdb.pdf, accessed on 5/18/2006)

$$P\mathbf{v} = \mathbf{v} - \left(\frac{\mathbf{v} \cdot \mathbf{n}}{|\mathbf{n}|^2} \right) \mathbf{n} \quad (\text{II-49})$$

Therefore, the two projected vectors are

$$\mathbf{a} = -P\mathbf{a}' = -\mathbf{a}' + \left(\frac{\mathbf{a}' \cdot \mathbf{n}}{|\mathbf{n}|^2} \right) \mathbf{n} \quad (\text{II-50})$$

$$\mathbf{b} = P\mathbf{b}' = \mathbf{b}' - \left(\frac{\mathbf{b}' \cdot \mathbf{n}}{|\mathbf{n}|^2} \right) \mathbf{n} \quad (\text{II-51})$$

The angle between the two projected vectors \mathbf{a} and \mathbf{b} on the plane whose normal vector is \mathbf{n} , one of the criteria determining the conformation of the lipids as discussed before, can be obtained from the following equation.

$$\cos \phi = \frac{\mathbf{a} \cdot \mathbf{b}}{|\mathbf{a}| |\mathbf{b}|} \quad (\text{II-52})$$

The angle value to determine the conformation of chains is tabulated in Table II-2. From the cosine value we can differentiate between the trans conformation and the gauche or gauche conformation. However, by just looking at the $\cos \phi$ it is impossible to tell the gauche conformation from gauche conformation, since the cosine function is symmetric with respect to π . This ambiguity can be solved by defining the cross product of the two vectors \mathbf{a} and \mathbf{b} and comparing the angle between the new vector and \mathbf{n} .

Table II-2 Characteristic angles and the corresponding cosine values for determining the conformation.

Conformation	ϕ	$\cos\phi$	$\cos\zeta$
trans	$2\pi/3$ to $4\pi/3$	-1 to -1/2	1 or -1
gauche(gauche-)	0 to $2\pi/3$	-1/2 to 1	1
gauché(gauche+)	$4\pi/3$ to 2π	-1/2 to 1	-1

Let us define \mathbf{c} as the cross product of \mathbf{a} and \mathbf{b} . We also define the angle ζ between \mathbf{c} and \mathbf{n} which has either zero or π by definition as shown in Figure II-8.

$$\mathbf{c} = \mathbf{a} \times \mathbf{b} \quad (\text{II-53})$$

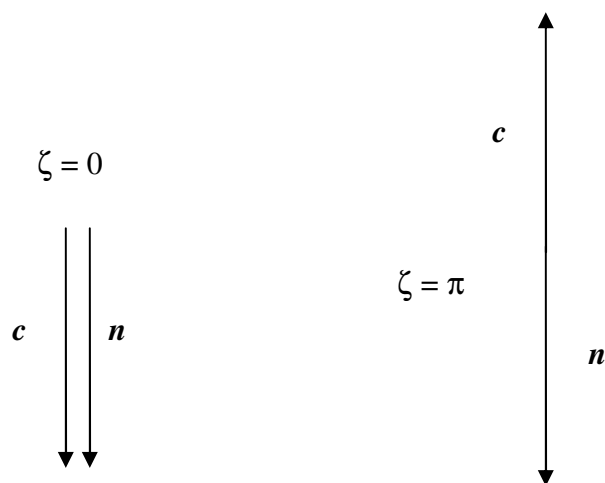


Figure II-8 Defining the ζ vector.

If $0 \leq \phi \leq \frac{2\pi}{3}$ and \mathbf{c} is parallel to \mathbf{n} with opposite direction ($\zeta=0$), then the conformation is considered to be gauche. If ϕ lies in $\frac{4\pi}{3}$ to 2π and \mathbf{c} has the same direction of \mathbf{n} ($\zeta=\pi$), the conformation is called gauché.

$$\cos \zeta = \frac{\mathbf{c} \cdot \mathbf{n}}{|\mathbf{c}| |\mathbf{n}|} \quad (\text{II-54})$$

2.3.4 Other Structural Properties

Center-Of-Mass (COM)

The center of mass is defined as follows:

$$x_{COM} = \frac{1}{M} \sum_{i=1}^N m_i x_i \quad (\text{II-55})$$

$$y_{COM} = \frac{1}{M} \sum_{i=1}^N m_i y_i \quad (\text{II-56})$$

$$z_{COM} = \frac{1}{M} \sum_{i=1}^N m_i z_i \quad (\text{II-57})$$

Radius of Gyration

The radius of gyration (R_G), a measure of the size of a molecule, is defined as

$$\langle R_G^2 \rangle = \frac{1}{M} \left\langle \left[\sum_{i=1}^N m_i |r_i - r_{COM}|^2 \right] \right\rangle \quad (\text{II-58})$$

The shape of the protein can be analyzed from the radius of gyration in a difference sense, i.e. based on the radius of gyration without mass weighting (R_g).

$$x_{com} = \sum_{i=1}^N x_i \quad (\text{II-59})$$

$$y_{com} = \sum_{i=1}^N y_i \quad (\text{II-60})$$

$$z_{com} = \sum_{i=1}^N z_i \quad (\text{II-61})$$

$$\langle R_g^2 \rangle = \frac{1}{N} \left\langle \left[\sum_{i=1}^N |r_i - r_{com}|^2 \right] \right\rangle \quad (\text{II-62})$$

Head Group Area

From the simulations we obtain the average head group area A per DPPC molecule. This quantity is obtained by the xy rectangular area divided by the number of DPPC molecule in a layer. In this study the total number of DPPC molecules in one simulation box is 128. Since it has two layers, each leaflet has 64 DPPC molecules.

Bilayer Thickness

We define the upper interface z -distance as the average z value of the phosphorous (P) atoms, $\langle z_P \rangle_{up}$ in the upper layer. The corresponding lower interface $\langle z_P \rangle_{lo}$ is defined as the average z value of the P atoms in the lower layer. The membrane thickness or P-P atom distance (D_{mem}) is simply the difference between the two quantities, which is

$$D_{mem} = \langle z_P \rangle_{up} - \langle z_P \rangle_{lo} \quad (\text{II-63})$$

Distance between the Protein and Lipid Bilayer Interface

We define the distance D between the protein and the interface by the distance between the center-of-mass of the protein or protein fragment and the upper layer interface. The upper layer interface is defined as the average z-position of the phosphorous atoms in DPPC molecules, so the distance can be positive even though the protein is contact with the DPPC molecules.

Diffusion Coefficients

From the Einstein relationship we obtain the diffusion coefficient of the water molecules. We expect some difference between the normal and lateral direction diffusivities of water molecules in hydrated lipid systems. The diffusivity of water molecules in one-dimension is obtained from the relationship between the mean-square displacement and time by

$$\lim_{t \rightarrow \infty} \langle |x(t) - x(0)|^2 \rangle = 2D_{x,H_2O}t \quad (\text{II-64})$$

and in three dimensions by

$$\lim_{t \rightarrow \infty} \langle |r(t) - r(0)|^2 \rangle = 6D_{H_2O}t \quad (\text{II-65})$$

The mean squared displacement or MSD can be obtained from either the direct simulations or from the position data saved. In canonical ensemble the MSD calculation is straightforward, but it seems to be problematic in constant pressure ensemble, since the box dimension changes at each time step. LAMMPS provides MSD calculation data even in NPT ensemble simulation. Instantaneous fluctuations in box size approximately “average out” if the system is in equilibrium, so the NPT and NVT MSD data are typically the same within statistical error.

Now, let us explain the method used in this work for the diffusivity calculations. First, from the raw data of MSD we take the logarithm of eq II-64.

$$\log(MSD_x) = \log 2 + \log D_x + \log t \quad (\text{II-66})$$

where $MSD_x = \lim_{t \rightarrow \infty} \langle |x(t) - x(0)|^2 \rangle$. We observe the x -range where slope of eq II-66 is equal or very close to 1. We then take the region as our x -range and fit the data to obtain $2D_x$ in eq II-64. Finally, by dividing the slope by 2, the diffusivity of the system is obtained from eq II-64.

RMSD

To examine the structural changes of the protein or protein fragment, RMS (root-mean squared) deviation is often used. It can be obtained by measuring the displacement of heavy atoms, such as C, O, N, S, from the starting conformation.

Radial Distribution Function

A structure of material can be characterized by distribution function and the most commonly used distribution function is $g_2(\mathbf{r}_i, \mathbf{r}_j)$ or $g_2(r_{ij})$ or $g(r)$. It is called the pair correlation function or the radial distribution function (RDF). It gives the probability of finding a pair of atoms at distance r , relative to the bulk average density. In the canonical ensemble it is represented as the following (Allen and Tildesley, 1987).

$$g(\mathbf{r}_1, \mathbf{r}_2) = \frac{N(N-1)}{\rho^2 Z_{NVT}} \int d\mathbf{r}_1 d\mathbf{r}_2 \cdots d\mathbf{r}_N \exp[-\beta U(\mathbf{r}_i)] \quad (\text{II-67})$$

where N is the number of atoms, ρ is the density, and Z_{NVT} is the canonical partition function, and $U(\mathbf{r}_i)$ is the potential energy.

CHAPTER III SYSTEM AND METHOD

3.1 Nano-Research

3.1.1 Model and Simulation Details

Materials and Model

The clay material of this study is montmorillonite whose chemical formula is $\text{Al}_4\text{Si}_8\text{O}_{20}(\text{OH})_4$. Four different types of dendritic surfactant, namely G1, G2, G2L (linear analog of G2), and G3, are used for this study. The structures of dendrimers are shown in Figure III-1. G1, the smallest one, has a molecular weight of 525.8 g/mol. G2 is a 2nd generation of melamine-based dendrimer with molecular weight of 1110.6 g/mol, while G2L is a linear analog of G2 with the same molecular weight. The largest dendrimer in this work is G3 whose molecular weight is 2280.4 g/mol. The fully extended size of G1 dendrimer is 2.4 nm and that of G2L is 3.6 nm (Acosta et al., 2003). Chemistry, synthesis, and characterization details are found in the same publication. The interlayer spacing (ILS) of bare clay was found to be 1.47 nm in the experiments.

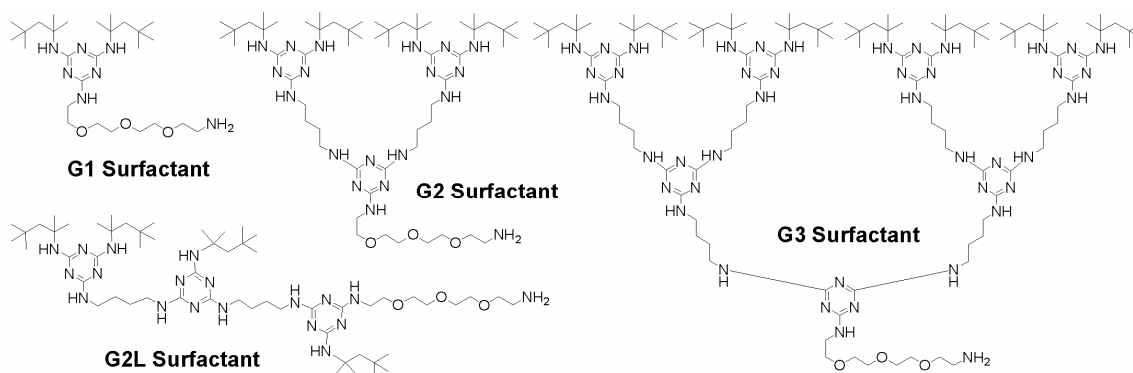


Figure III-1 Schematics of dendritic surfactants (Acosta et al., 2003).

Montmorillonite clay surface was modeled as charge-neutral oxygen-only surface with uniform density. A smoothed clay surface composed of oxygen (O) only was considered as a “first approximation” to effectively interpret the interaction between a dendrimer and clay surface. However, full atomistic models for dendrimers were employed for the study. We considered a system consisting of a dendritic surfactant molecule and two parallel clay layers encompassing it, which are separated in z -direction only. In this study, we focus on the confinement of single dendrimers partitioning into clay surfaces, i.e. partitioning at infinite dilution conditions only.

The simulation box was periodic in x - and y -directions, but nonperiodic in z -direction. The clay layer had dimension of 2000 Å each in x - and y -directions, but the layer separation varied in z -direction. The separation distance changed from 6 to 500 Å, and 70 Å was chosen as the infinite separation reference, since simulation at higher separation than 70 Å leads to negligible force values. Since we were interested in the infinite dilution case, a relatively large value of x - and y -dimension was taken as the reference distance.

Dendritic surfactant molecules were created using Cerius² (Accelrys Software Inc.). Then, we ran Discover Cerius² 4.8 with the “No Cross No Morse” cvff force-field. It generated automatic parameters such as the quadratic angle parameters for c-n-cp and c2-n-cp and the out-of-plane parameters for c-n-cp-hn, c2-n-cp-hn and n-cp-np-np. We took the automatic parameters and added them to the cvff force-field with χ_0 values of 0.0° for the above out-of-plane parameters. The improper torsion term of c2-n3-hn-hn was deleted to remove the redundancy. Otherwise, the default parameters of cvff were used. Finally, the data file was converted to assign force-field values for LAMMPS runs.

The van der Waals interaction was employed with a cutoff radius of 50 Å, and the cutoff radius of 50 Å was taken for the Coulomb electrostatic interaction. The size of dendrimers for G2L (3.6nm) was quite smaller than the cutoff radius, so our choice of cutoff radius is justified as discussed in Chapter II. In addition to the intramolecular and intermolecular potential energies, a surface-dendrimer interaction based on the Lennard-Jones 10-4 equation, shown in eq III-1, was added. One sheet of two-dimensional

uniform clay surface was assumed and eq III-1 was obtained for the interaction between O atom on the clay surface and each atom within surfactant molecule.

$$U^{sd}(z) = 4\pi\rho\varepsilon\sigma^2 \left[\frac{1}{5} \left(\frac{\sigma}{z} \right)^{10} - \frac{1}{2} \left(\frac{\sigma}{z} \right)^4 \right] \quad (\text{III-1})$$

where σ and ε are the oxygen-dendrimer atom LJ interaction parameters and ρ is the 2-D oxygen density of 0.06216 atoms/Å² for our model clay. The LJ parameters for O atom were $\varepsilon = 0.2280$ kcal/mol and $\sigma = 2.8598$ Å, and Lorentz-Bertholet mixing rules for the interaction between surfactant site and the surface O atom were applied.

Simulation Details

All the simulations were carried out using LAMMPS with modifications, such as incorporating the subroutine which calculates the confinement forces at each time step, into the program. Canonical ensemble was chosen for the production runs. The time step of 0.5 fs and frequency constant of 0.05 fs⁻¹ were chosen for the canonical production runs based on time-step tests using microcanonical simulations. The total simulation time was at least 10.0 ns, and the thermodynamic properties were measured for the last 5.0 ns. The confinement forces and surface-atom interaction potentials were recorded every 2000 time steps. Also, the thermodynamic properties including the kinetic and potential energies were recorded every 4000 time step. Longer simulation time (~ 45 ns) was used to measure the quantities for larger clay layer separations (30 to 70 Å).

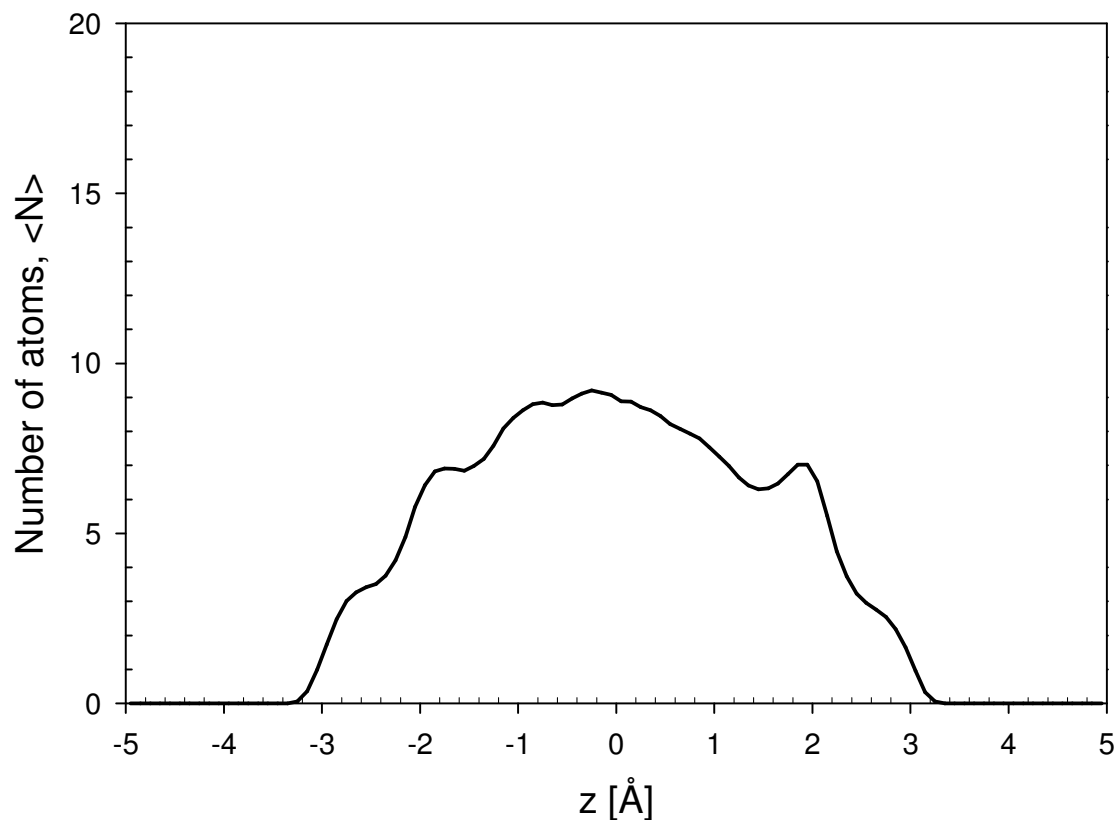


Figure III-2 Linear density profile of a G3 molecule between clay layers; 10 ns, 10.0 Å separation.

The data files created by Cerius² were converted to LAMMPS data files using a converter program. We put the molecule between two layers with the layer separation distance of 50 Å and performed the energy minimization, then gradually squeezed the box by moving the clay sheets in the z -direction after small amount of simulation such as 100000 steps. If the box length reaches 6 Å the process of generating initial configuration ends. We used that configuration file as a starting point of canonical simulations. We calculated the confinement forces and other thermodynamics properties along the simulation time. Simulations were repeated changing the layer separation in z -

direction and for 5 ns simulations the thermodynamic properties were measured and averaged for the last half of simulation time.

To check the reliability of sampling we examined the COM profile of dendrimers. One indicator of adequate sampling would be that the COM of each dendrimer moves from one surface to the other, without being permanently trapped near one surface. This was observed in all cases, thus verifying that the molecule is freely moving and also the algorithm samples the system correctly. Linear density profiles for the molecules were also checked for symmetry to confirm the soundness of sampling, and examples are shown in Figure III-2 and Figure III-3. Linear density profiles were obtained by counting each atom within a molecule in a bin which has 1/100 of the total simulation volume and averaged over the simulation time. The confined molecule doesn't have much freedom to move for narrow separation distance, which was confirmed in Figure III-2. So the local density of the molecule is highest at the center position. But as the layer separation becomes larger, the molecule moves from the top surface to the bottom surface or vice versa as shown in Figure III-3. The profile is symmetric and the density near the surface is higher than that of the center, which proves that the sampling process is acceptable.

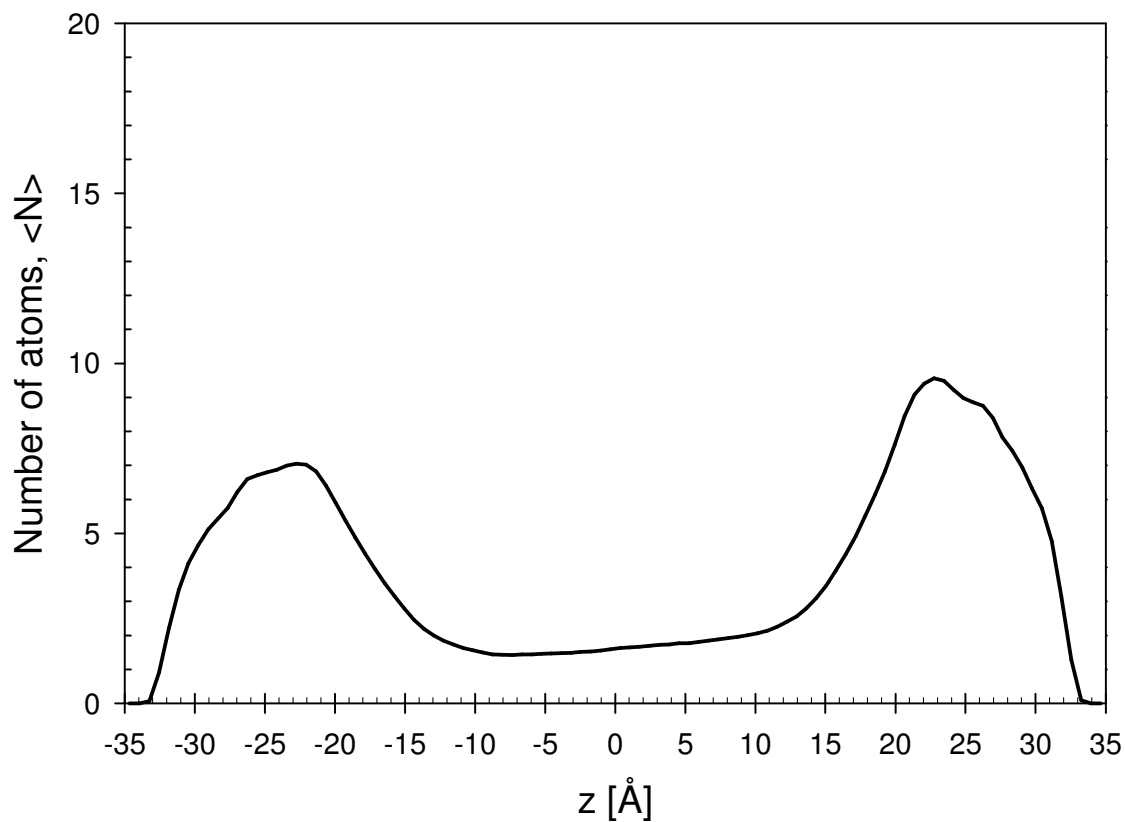


Figure III-3 Linear density profile of a G3 molecule between clay layers; 50 ns, 70.0 Å separation.

3.1.2 Data Analysis

Free Energy Analysis

The potential due to the presence of clay surfaces, which is only a function of the z -direction separation distance $U^{sd}(z)$, is obtained from eq II-27 or

$$f_{conf}^z = -\frac{dU^{sd}}{dz} \quad (\text{III-2})$$

FE profiles are obtained by numerically integrating the forces according to eq II-30 and the individual contributions of energetic and entropic factors are analyzed based on eq II-31.

3.2 Bio-Research

3.2.1 Model and Simulation Details

We intend to investigate the relationship between the properties of the system and the protein position, which can be examined using different starting structure. We construct a model system consisting of the protein, lipids and water molecules after building a model membrane of a fully hydrated DPPC bilayer.

The protein itself is very large (~ 50 Å), which requires a high computing load, therefore, we mainly focus on the simulations of important fragments of the protein, or A β (31-42), which is highly hydrophobic and the whole protein A β (1-42) with a moderately sized of simulation box.

First, we simulate pure water to check the applicability of our simulation tool, LAMMPS. We also perform simulations of hydrated lipids without the protein to check the performance of our lipid bilayer model.

Considering the system size, including the number of atoms and the dimension of simulation box and the computing power we have, the maximum real time will be on the order of several ns at best, and we are not able to observe the full folding/unfolding of A β during our simulations. However, we can look for indicators of structural changes such as the radius of gyration and root-mean-square distance. We also measure thermodynamic properties, such as the kinetic and potential energies, including each intramolecular interaction term. We calculate structural properties such as the box dimensions, head group area, and order parameters of DPPC phase for hydrated lipid systems. Properties, such as the radius of gyration of the protein and the distance between the protein and the lipid interface, are obtained from post-simulation data processing.

Figure III-5 shows the amino acid sequence of the full A β protein structure. A β (1-42) has a molecular weight of 4514.2g/mol (630 atoms) and the chemical formula is C₂₀₃H₃₁₁N₅₅O₆₀S₁. The molecular weight of the protein fragment A β (31-42) is 1141.5g/mol and the number of atoms and the formula are 175 and C₅₃H₉₆N₁₂O₁₃S₁, respectively.

The pdb file (1iyt), downloaded from the PDB site, is negatively charged (-3.0). We have carefully reviewed the charge values and determined that the total charge of 0.0 (or neutrality) is the correct choice under physiological conditions based on Herrera-Valdez table data (from Table 3 of <http://math.arizona.edu/~herrera/biochem/proteins.pdf>, accessed on 2/23/2006). Referring to the following statements we have more detailed description of the formal charge values for the amino acids which are not neutral. “Note that 8 of the 20 amino acids *have ionizable sidechains*. Arginine, lysine and histidine can have a *positive charge*, while aspartic acid and glutamic acid can possess a *negative charge* under physiological conditions. It is also possible for serine, tyrosine and cysteine to *ionize to a negatively charged species* during certain biological processes (excerpt from <http://wiz2.pharm.wayne.edu/biochem/prot.html>, accessed on 2/23/2006)”.

Summarized data representing the charge values of the full protein A β (1-42) are

- positively charged residues: ⁵Arg, ⁶His, ¹³His, ¹⁴His, ¹⁶Lys, ²⁸Lys, N-terminal
- negatively charged residues: ¹Asp, ³Glu, ⁷Asp, ¹¹Glu, ²²Glu, ²³Asp, C-terminal

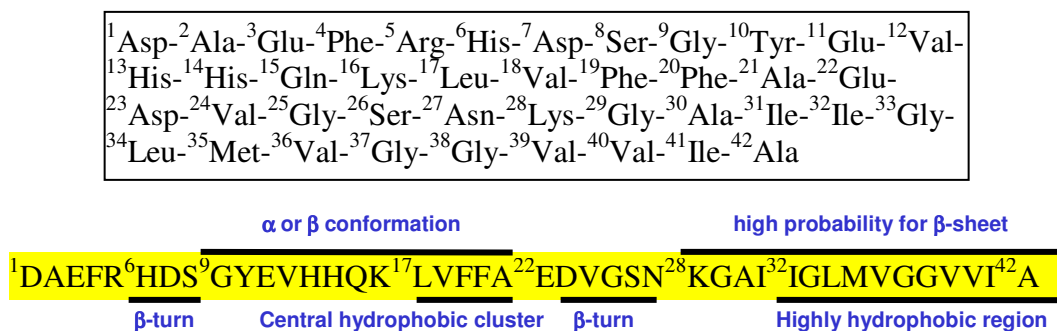


Figure III-5 Structure of Aβ protein with conformational information. Adapted from Serpell, 2000.

The total number of atoms in the system for a typical data file is 43892 with 16640 atoms for the DPPC molecules (130 atoms/molecule × 128 molecules), 26622 atoms for the water molecules (3 atoms/molecule × 8874 molecules), and 630 atoms for the Aβ molecule (630 atoms/molecule × 1 molecules).

Construction of Model Systems

Similar steps have been taken to generate the initial configurations of model systems as described in 3.1.1 section. The overall procedure involves the construction of the model lipid bilayer, insertion of protein, and hydration. Right after the construction of the lipid bilayer, hydration has been performed for the hydrated lipid simulations. For the simulations of protein in water, addition of water was performed after placing the protein in the center of the simulation box.

Simulation box of water was constructed with 500 water molecules for bulk water simulation. Lipid bilayer was constructed as described in the following paragraph, and using soak function in Insight II the system was hydrated. For peptides in water systems, Aβ(1-42) in water and Aβ(31-42) in water, a peptide was first located in a simulation

box manually and the system was hydrated following the same procedure of lipid hydration.

Now, let us start the description of the model construction containing peptides in hydrated lipid by explaining the bilayer formation procedure. We first construct a DPPC molecule and then form an 8 by 8 monolayer by placing the lipids at a certain distance. Finally, copying the “leaflet” and adjusting the position of the layers, we can construct the whole bilayer with 128(8×8×2) DPPC molecules. The energy minimization should be performed from the beginning at each increment of DPPC molecules. Figure III-6 shows the DPPC bilayer model without the water molecules. Addition of the water molecules completes the model construction of hydrated lipids and can be performed using the soak function in Insight II.

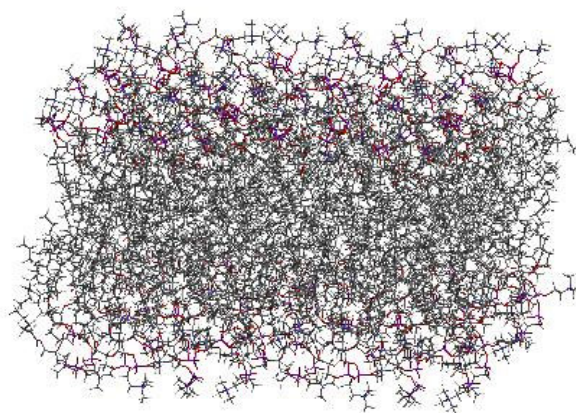


Figure III-6 Construction of a DPPC lipid bilayer.

After constructing the DPPC box we add the sub-boxes, the water box and the A β -hydrated box, on top of the head groups of each lipid layer avoiding bad overlaps to build a system with A β (1-42) or A β (31-42) in hydrated lipids. Water molecules are then added to the simulation box to finish up the model construction using the soak function in Insight II or by adding two water phases as discussed in the following paragraph.

Two water phases are generated separately, where one of the phases encompasses the target protein or protein fragment or the protein is intercalated between the water phase and DPPC bilayer phase. A simulation box containing A β protein with the proper dimensions, for example 63.4 \times 63.4 \times 33.6 Å for one side of hydrated A β protein, is created using Crystal Builder in Cerius². We load the file(.car) using Insight II and hydrate it with PBC option. The saved configuration is energy-minimized using Cerius². Combining the three phases including the lipid bilayer, we form a starting structure of a protein in hydrated lipids. At this time the head group area is slightly larger than the experimental value (62.9 Å, (Nagle et al., 1996)) to avoid overlap of atoms. We then perform a short molecular dynamics simulation in the isothermal-isobaric ensemble with higher external pressure to slightly squeeze the simulation box, especially in *x*- and *y*-directions. We then perform the energy-minimization with fixed cell parameters (63.4 Å, 63.4 Å, and 107.2 Å for box lengths of *x*, *y* and *z*, respectively) and the final structural properties are; head group area 62.9 Å, total bilayer thickness 39.3 Å, cell angles 90 degrees. Figure III-7 shows a starting configuration of A β (1-42) protein in hydrated lipids.

Conversion of Cerius² car and mdf files into LAMMPS data file follows the model construction. Since Cerius² cannot save such a large file with more than 10,000 hydrogen atoms, a program which converts an msi file to a modified msi file that Cerius² is then able to save as a car file and mdf file has been developed at the Laboratory for Molecular Simulation (LMS) and used.

End configurations can be used as starting configurations for simulations when locating the protein in different position. To accomplish this we run a simulation with expansion in x - and y -directions, for example by applying highly negative pressure $P_x = P_y = -100$ atm, and save configurations frequently. Then, we take the restart files from the simulation and use them as our starting points for new simulations. By doing this, we perform simulations at different starting positions and conformations of the protein.

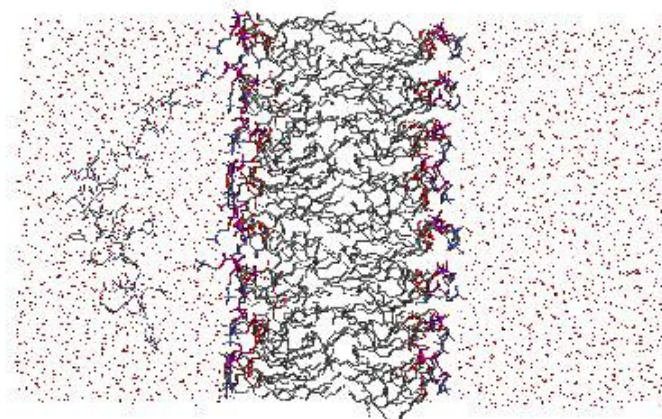


Figure III-7 A β (1-42) protein in fully hydrated lipids; hydrogen atoms are intentionally hidden.

Simulation Details

We need a DPPC head group area that is consistent with the experimental value and it is reasonable to allow the bilayer freedom to move, therefore we decided to use the NPT ensemble for the protein in hydrated lipid systems. The boundary condition remains periodic with constant pressure. Choices have been made for the pressure components, and the lateral pressure of the system or $P_x = P_y$ varied from -100 atm to 100 atm, while the normal pressure was set to 1 atm for most simulation cases. The experimental pressure to cause a phase change for hydrated DPPC at 314 K is about 40 dynes/cm (Albrecht et al., 1978), which corresponds to the difference between the surface tensions of water-air and water-lipid interfaces (Chiu et al., 1995). We obtain the water-lipid surface tension γ_{WL} of 28 dynes/cm using the water-air surface tension γ_{WA} of 68 dynes/cm (Chiu et al., 1995). The boundary surface tension γ is obtained from the following formula.

$$\gamma = \int_{Z_1}^{Z_2} [P_N(Z) - P_L(Z)] dZ = (Z_2 - Z_1) - \int_{Z_1}^{Z_2} P_L(Z) dZ \quad (\text{III-3})$$

where P_N is the normal pressure which exerts perpendicular to membrane interface and P_L is the lateral pressure, P_x or P_y . Assuming the normal pressure to be 1 atm, the above equation is simplified as

$$\frac{\int_{Z_1}^{Z_2} P_L(Z) dZ}{(Z_2 - Z_1)} = 1 - \frac{\gamma}{(Z_2 - Z_1)} \quad (\text{III-4})$$

By rearranging eq III-4 we obtain the mean lateral pressure as

$$\langle P_L \rangle = 1 - \frac{\gamma}{\langle L_z \rangle} \quad (\text{III-5})$$

Substitution of γ with $56 \text{ dynes/cm} = 5527 \text{ atm}\text{\AA}$, due to the two interfaces, reduces to the average lateral pressure of -50.6 atm , assuming the z -dimensional box length of 107.2 \AA . Relevant discussions on the constant surface tension simulations are found elsewhere (Chiu et al., 1995; Leontiadou et al., 2004; Teleman et al., 1987).

We chose the cvff force-field without cross terms as our simulation force-field (Dauber-Osguthorpe et al., 1988). The detailed atom information of simulations of A β (1-42) or A β (31-42) in water or near hydrated lipids is shown in Appendix A. The SHAKE algorithm (Ryckaert et al., 1977) has been applied to c1-h, c2-h, and c3-h bonds in the protein and o*-h* bond of water molecules to save computing time, which made it possible to use a large time step of 2.0 fs. The water model used in this work is cvff with $r_e = 0.96 \text{ \AA}$ and $\theta_e = 104.5^\circ$ and the charge values of H and O atoms are $+0.41e$ and $-0.82e$ respectively (section 5.1). The simulation box has a slab geometry and periodic boundary condition is employed. The temperature and pressure damping parameters were determined from short simulations of 0.1 ps and 1.0 ps, respectively. Since the majority of experimental and previously reported computational studies have been performed around $T = 323 \text{ K}$, most of the simulations were carried out at that temperature. Two different methods of long-range electrostatics treatment were tested and PPPM (with precision of 1.0×10^{-3}) showed much faster simulation times without losing accuracy. Therefore, the production runs are being performed using PPPM for long-range electrostatics.

SGI machines at LMS and the department of chemistry at Texas A&M University have been used for the model construction using Cerius² and Insight II. Energy-minimizations were performed using either SGI machines or an Apple 2.3 GHz Xserve G5 cluster (CAT) of the Department of Chemical Engineering or SGI Altix 3700 (COSMOS) at Texas A&M University Supercomputing Facility. Production runs have been performed on CAT cluster and COSMOS with multiple cpus, typically 8 to 16 cpus.

3.2.2 Data Analysis

Thermodynamic Properties

MD simulations provide the thermodynamic properties of the model systems such as, the kinetic and potential energies (bond energy, angle energy, etc.). The shortest simulation time span is 1 ns, but some simulations were run for 2 ns. The thermodynamic properties were measured every 1 or 2 ps depending on the length of the simulation. Average thermodynamic properties were obtained from block averages, where each block has a 50 ps average or longer. The number of blocks used ranged from 10 to 20. For a 1 ns simulation we took the last 500 ps to provide the statistical averages. A conceptual figure for the whole system is shown in Figure III-8. Thermodynamic and structural properties can be analyzed according to the distance D between the protein and the lipid bilayer interface as discussed in Section 2.3.4.

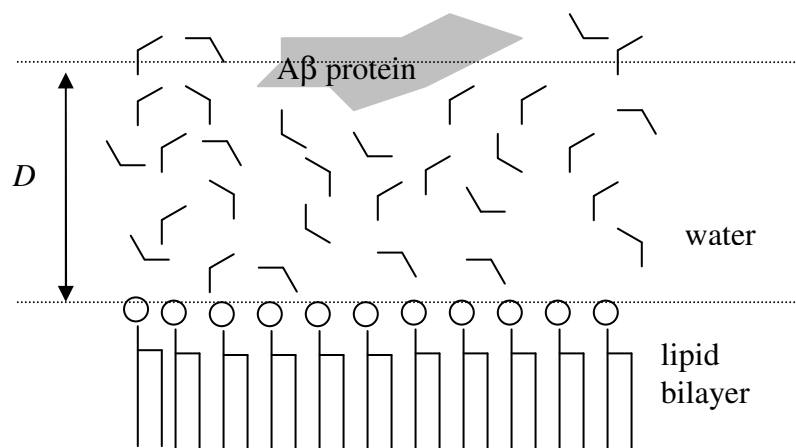


Figure III-8 Conceptual figure of A β protein in hydrated lipid bilayer.

Structural Properties

From the MD simulations we collected the position data of each atom at fixed time interval, i.e. 1 ps. We developed Fortran programs to calculate the structural properties, such as the protein-interface distance and the radius of gyration of the protein from the position data as described in Section 2.3. We modified and used converter program to generate animations using the position data using VMD (Humphrey et al., 1996) and VideoMach as described for the nano-composite research.

CHAPTER IV

RESULTS AND DISCUSSION OF NANO-RESEARCH

4.1 Overview

In this chapter we report the simulation results and discuss them using the several important thermodynamic properties. First, the shape and magnitude of confinement force profiles, which are direct outputs of simulations, for different dendritic surfactants will be discussed. We will then briefly review the experimental observations of Simanek's group which initiated this study. The free energy profiles, obtained from the integration of the confinement force, will be presented and the characteristics will be analyzed with the corresponding experimental results. The partitioning type of each dendrimer into clay gallery will be determined from the location and depth of free energy minimum(a). Detailed descriptions of limitations of this modeling work will follow. The contributions of energy and entropy to the free energy profiles will suffice the discussion.

In order to visualize the simulation output, frames with the positions of each atom within a dendrimer have been written to an output file. Then, the position data have been converted to pdb-formatted files. Finally, a movie generating software VideoMach was used to create an animation with each frame file. Snapshots of the systems of interest are shown in Figure IV-1 and Figure IV-2 using VMD. It shows two figures of a confined G3 molecule between clay layers at the separation of 10 and 50 Å.

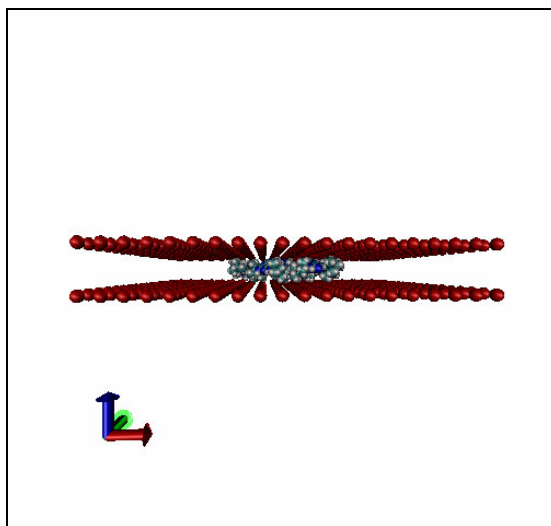


Figure IV-1 Snapshots of a G3 molecule between clay layers; 10.0 Å separation. The red balls of the top and bottom planes represent the oxygen atoms of the model clay.

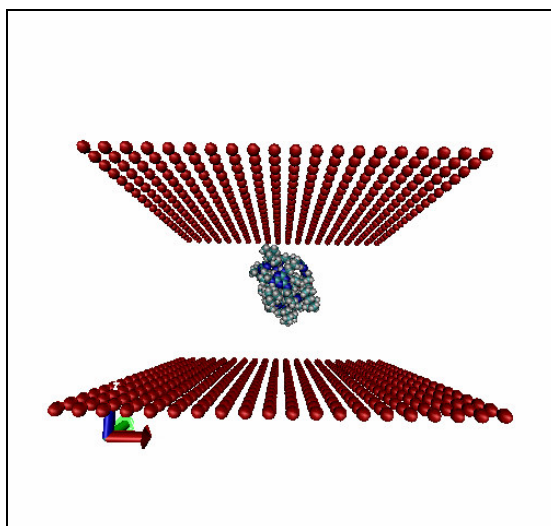


Figure IV-2 Snapshots of a G3 molecule between clay layers; 50.0 Å separation. The red balls of the top and bottom planes represent the oxygen atoms of the model clay.

4.2 Confinement Force

The confinement force profiles as a function of separation for the four different molecules are shown in Figure IV-3. At very narrow separations (less than 10 Å), the confinement force value due to the presence of surfaces goes to positive infinity. In other words, repulsive force dominates at very narrow region. As the separation gets larger, the repulsion becomes weaker in a fluctuating manner. This region can be considered as the moderate separation region where the confinement force value changes non-monotonically because of the changes in molecular configuration of the surfactant. At these moderate separations (~ 25 Å) the force can be either repulsive or slightly attractive, i.e. the sign might change. At very large separations the force becomes negligible, i.e. its value goes to zero. The overall trend in force reveals that there is highly repulsive interaction at very short layer separation, but the magnitude of repulsion fluctuates with the repulsive force turning into a slightly attractive one or vice versa at moderate separations, and it exhibits negligible interaction with the surfaces at large separation.

The oscillatory phenomenon observed in the moderate separation region is a unique feature of this work as compared to previous nanoclay modeling studies. Some researchers reported the oscillatory solvation force of molecules under confined geometry (Ayappa and Ghatak, 2002; Chan and Horn, 1985; Christenson, 1983; Gee et al., 1990; Ghatak and Ayappa, 2001; Ghatak and Ayappa, 2004; Horn and Israelachvili, 1981; Israelachvili and Kott, 1988), but to the authors' knowledge no publication on the oscillatory force in the confinement of a dendritic surfactant has been found. The forces associated with the confinement of molecules are studied in various systems. Oscillating solvation force behaviors have been observed for fluids and polymers from experiments and molecular simulations (Chan and Horn, 1985; Christenson, 1983; Gee et al., 1990; Horn and Israelachvili, 1981; Israelachvili and Kott, 1988). Simulations of confined Lennard-Jones fluids also exhibited oscillating solvation behaviors (Ayappa and Ghatak, 2002; Ghatak and Ayappa, 2001; Ghatak and Ayappa, 2004).

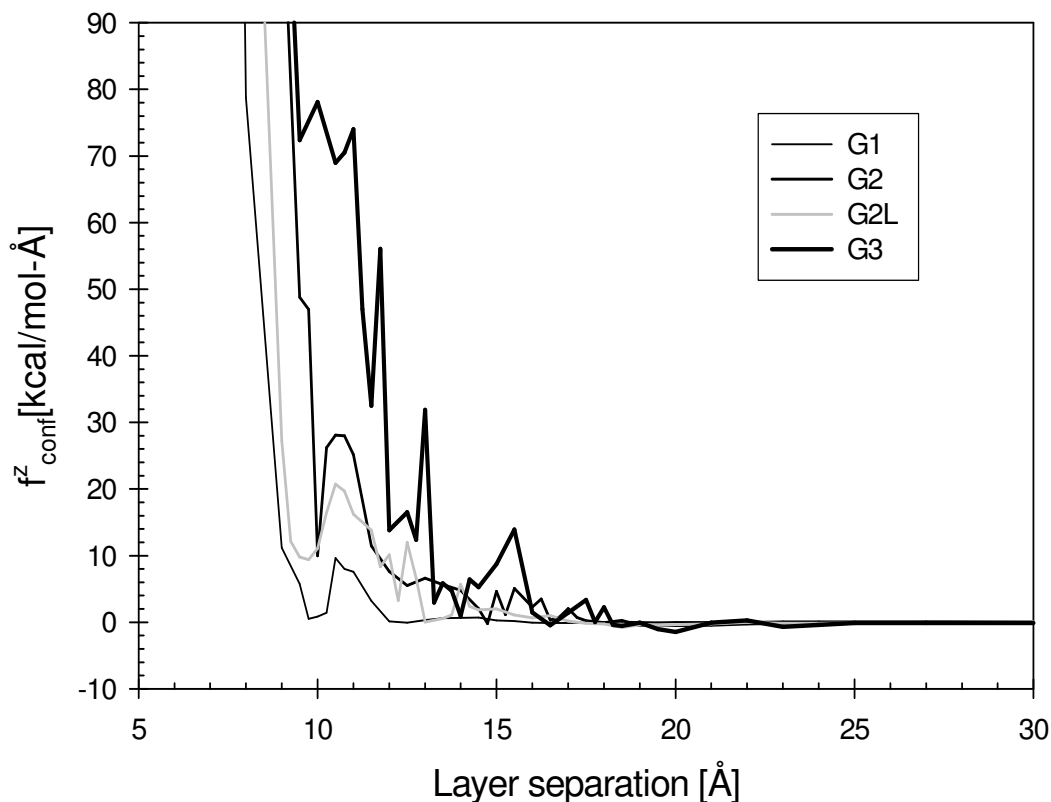


Figure IV-3 Total confinement force profiles of single dendrimers between clay layers.

Density profiles in oscillatory fashion as in the solvation force behaviors have been reported for confined fluids or solid-liquid interface via molecular simulations (Bitsanis and Pan, 1993; Gupta et al., 1994; Manias et al., 1996; Padilla and Toxvaerd, 1994; Ribarsky and Landman, 1992; Xia et al., 1992). Another feature of confinement force behavior is that the profile fluctuates much more as the molecule becomes large. As found in Figure IV-3, the number of confinement force peaks of G1 is 2, while those of larger molecules are larger than 4 (~ 25 Å separation). This phenomenon can be explained as the entropic feature of a dendritic surfactant. As the molecule gets larger, it has more possibility of changing its configuration between the clay surfaces. Another finding in this figure is that the larger molecule has higher peak value than that of the

smaller molecule. Since the large and complex molecule has more atoms, G3 exhibits higher peak values than that of G1.

To support the reliability of the confinement force profiles, the individual component (top and bottom) force profiles of G2L molecule are provided in Figure IV-4. The average magnitude of confinement forces should be identical for those two forces, i.e. $\langle f_{bottom} \rangle = -\langle f_{top} \rangle$. As one can see, the confinement force due to the bottom surface has the same magnitude with opposite sign of the confinement force due to the top surface. Therefore, it can be insisted that the total confinement force profile represent the true physical phenomena of a dendrimer partitioning.

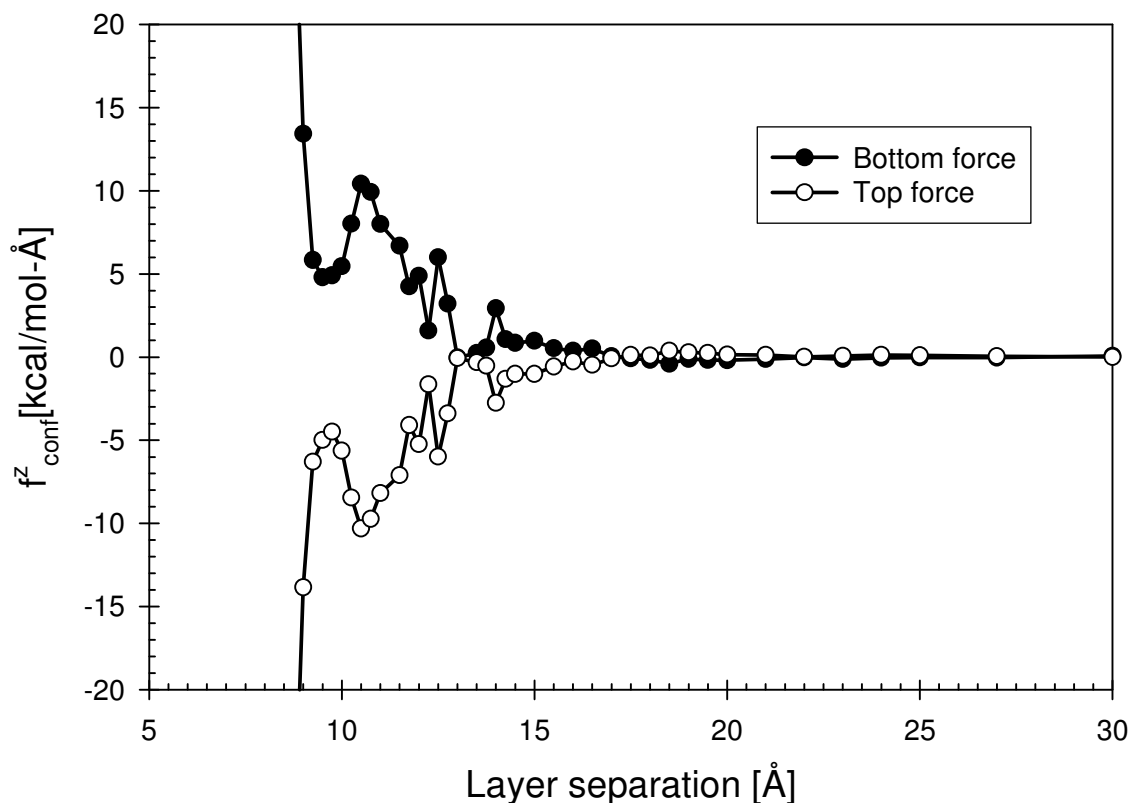


Figure IV-4 Confinement force profiles of a G2L molecule between clay layers.

4.3 Free Energy Profiles

The free energy profiles based on the numerical integration of confinement force were shown in Figure IV-5. It contains the free energy profiles for the four different types of surfactant molecule between clay surfaces, where 70 Å is the reference separation. The medium dash line represents the bare clay ILS (14.7 Å), while the long dash line represents 15.7 Å, which is the increased ILS of G2 and G3 in the experiment (Acosta et al., 2003). We notice that the free energy profile shifts toward the larger separation as the dendrimer becomes larger because of the size of the molecule. Also, we observe that the relative depth(s) of minimum becomes deeper as the dendrimer becomes larger. A local minimum of free energy profile at 15.5 Å with very small depth was found for G1, followed by monotonic decrease at larger clay layer separations. Simulations of G2L molecule revealed a local minimum of free energy at layer separation of 17 Å. In the free energy profile of G2 we observed a global minimum at layer separation of 18 Å. Two free energy minima at finite separations for G3 occur at the layer separations of 18 and 22 Å, which represent potential intercalated states of the surfactant partitioning.

From the comparison of free energy profiles we found that they are different due to the molecular size of the confined dendritic surfactants. Furthermore, surfactants with different geometry, G2 and G2L, exhibit different profiles. Combined analysis of energetic and entropic contributions, which will be discussed in the later section, together with the free energy profiles will clarify the above arguments.

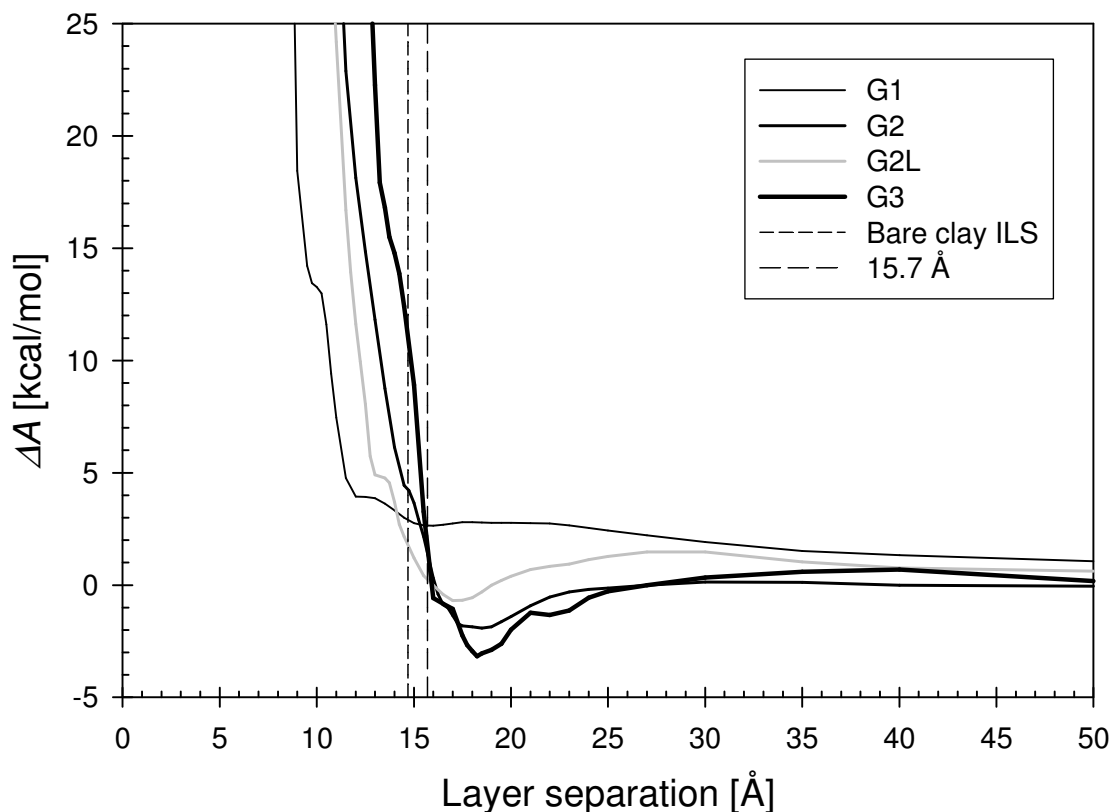


Figure IV-5 Free energy profiles of different types of a dendrimers; reference point of infinite separation is 70 Å; medium dash line represents the bare clay interlayer spacing of 14.7 Å, long dash line represents 15.7 Å.

4.4 Comparison with Experiments

According to Simanek's group, smaller and linear molecules (G1 and G2L) were found to exhibit completely intercalated structures, while frustrated intercalation were observed for larger surfactants, G2 and G3 (Acosta et al., 2003). One characteristics of the frustrated intercalation is the nominal increase of interlayer spacing between clay layers.

From the free energy profiles (Figure IV-5) we observe that the position where the local minimum of free energy occurs for G1 is quite smaller than its fully extended molecular size (24 Å), but comparable to the ILS of bare clay, 14.7 Å from the

experimental work (Acosta et al., 2003). The relative depth of the local minimum is quite shallow compared with that of other surfactants, therefore we conclude that there exists an intercalated structure whose state is not very stable, and it is much more comfortable at infinite separation. We speculate that the higher loading of untethered surfactants (driven by a favorable energy change in ionic bonding, See Figure II-3 in Chapter III) may lead to a free energy profile that is a monotonically decreasing function as the separation gets larger due to the repulsion between surfactants or exfoliated structure is favorable for the surfactant with higher loadings. We would need more experimental data for the verification of the “possible” intercalated structure.

The free energy values at different clay layer separations are reported and their relative probabilities with the reference separation of 70 Å are calculated in Table IV-1 accordingly. The relative probability is obtained using the following equation;

$$\frac{P_{s1}}{P_{s2}} = \exp\left(-\frac{\Delta A_{s1-s2}}{RT}\right) \quad (\text{IV-1})$$

where subscripts s1 and s2 represent the states 1 and 2 and R is the gas constant, 8.3145 J/mol-K. The relative probabilities of finding intercalated structures at 14.5 to 15.5 Å for G1 are extremely low (less than 0.02 for all separations) compared to that at infinite separation. Therefore, it would not be easy to find them at finite separations or the exfoliated structure is dominant morphology of the system. To verify this hypothesis we need supplementary experimental results in the future.

Table IV-1 Free energy and the relative probability of finding the particular states at different layer separation.

	D [Å]	G1	G2	G2L	G3
A [kcal/mol]	14.50	2.995	4.429	2.159	12.411
	15.00	2.75	3.65	1.20	8.92
	15.50	2.653	2.154	0.422	3.262
	16.00	2.636	0.314	-0.014	-0.586
	18.50		-1.918		
	17.00			-0.694	
	18.25				-3.174
	70.00	0.000	0.000	0.000	0.000
Probability	14.50	0.006	0.001	0.026	0.000
	15.00	0.010	0.002	0.133	0.000
	15.50	0.011	0.026	0.490	0.004
	16.00	0.012	0.588	1.023	2.689
	18.50		25.500		
	17.00			3.231	
	18.25				212.874
	70.00	1.000	1.000	1.000	1.000

It is not clear from the free energy profile of G2L whether the depth of minimum at finite separation of 17 Å is greater than that of the reference separation 70 Å. But it will also form an intercalated structure, since it has a local minimum of the free energy profile. Unlike the case of G1 surfactant, the relative probability at 15.0 Å becomes quite comparable to that at infinite separation (0.49). It is 3.2 at local minimum of 17 Å, which means that we will find the structure at that separation three times more than that at infinite separation. However, the difference between the two probabilities is not big enough, which makes us reasonably conclude that it is unclear to determine the final morphology of G2L nanocomposite by just looking at the free energy profile.

The larger surfactants, G2 and G3, do not fit comfortably into the clay gallery at the bare clay ILS. Their local minima, which are deep, occur near 18 Å of separation, implying that there exists intercalated structure at that separation. Therefore, we speculate that these two surfactants will form frustrated intercalated structure with the most common gallery separation being 18 Å.

Note that we observe the drastic decrease of the free energy difference for G2 and G3 surfactants from 14.7 Å to 15.7 Å, where their clay gallery spacing was found to be in the experiments. Since we found that the moderate increase in the clay gallery is one of the characteristics of frustrated intercalation, we would expect frustrated intercalated structures for the larger surfactants. Following our model predictions, we expect that G2 and G3 are very unlikely to intercalate at 14.7 Å. However, experiments showed that we should see some intercalated structure at 15.7 Å. Figure IV-5 shows that for 15.7 Å separation, ΔA is predicted to be very close to zero and thus we expect to observe intercalated structure at that separation. We obtain the relative probabilities of 0.004 and 2.7 at separations of 15.5 and 16.0 Å. The relative probability obtained from assuming the interpolation between the two data points is 1.1, which tells that we see almost equally probable to observe the intercalated structures. This analysis lies in the same experimental finding of observed intercalated structure at 15.7 Å.

Our collaborators hypothesized that the reason for the relatively low amount of larger surfactants for the nanocomposite fabrication was because of the inability of molecules to access the interlayer. However, based on the free energy profiles of the two larger surfactants we construct an alternative hypothesis. As pointed out in the previous paragraph, the single surfactants are predicted to fit comfortably into the gallery above 15.7 Å, but they may entropically exclude others from entering. Therefore, we cannot observe nanocomposites of G2 and G3 with higher surfactant content in the experiment. The validity of our hypothesis can be tested from the simulations of multiple dendrimers into clay gallery. As a part of future work, we plan to perform simulations with higher loadings of dendrimers and perform the similar analysis as in this work. If the free energy profile looks like a monotonic decreasing function of layer separation, we can conclude that our alternative hypothesis is valid for the partitioning, since the free energy profile changes due to the interaction between dendrimers.

We could successfully predict the intercalation behavior from simulations, however, it is not easy to quantitatively predict the intercalation behavior, since we used a simplified model. There are several limitations of our model clay for the accurate

prediction of intercalation phenomena; i) anchoring effect is excluded during the simulations, ii) interactions between dendrimers are excluded, iii) portion of dendrimer is not extended into the solvent, iv) effects of water and organic content are ignored, v) interaction between the clay surfaces are neglected. One major reason of this discrepancy stems from the restriction of molecule's movement. In the experimental works, the cationic exchange is one of the key parts in the fabrication of the dendrimer-clay nanocomposite. The cation-exchanged surfactant can be considered as a tethered molecule to one of the clay surfaces. But in the simulations we used a model molecule with free movement, in other words the molecule is not attached or tethered to either side of the surfaces, and finally the simulations results do not lead to the full understanding of the experiments performed. Another major reason for the difference relies on the fact that we simulated the system of interest at extremely low density, i.e. one dendritic surfactant in 2000 by 2000 Å clay surface. Since we modeled a low density system, the interaction between dendrimers within clay layers is automatically ignored. However, in real experiments it is very important to understand the physics of the intercalation of multiple molecules into the clay or higher loading cases. The other reason is the negligence of partial extension of dendrimer outside the clay surfaces. As we studied on the partitioning of the dendrimers, we are limited to simulate the dendrimers between clay surfaces and we did not study a system where some portion of dendrimer is extended outside of the clay surfaces as in the frustrated intercalation. We also neglected other electrostatic interactions in retaining water and other organic solvents. The free energy analyses we performed in this study are associated with the partitioning of dendritic surfactants only. We cannot extend the results from this finding to the study of interaction between polymers and clay surface. A summary of comparison between the experimental and simulation results is tabulated in Table IV-2.

Table IV-2 Comparison of intercalation process of melamine-based dendritic surfactants into clay; experiment vs simulation; reference state = infinite separation.

		G1	G2	G2L	G3
Experiment		Complete Intercalation	Frustrated Intercalation	Complete Intercalation	Frustrated Intercalation
	Characteristics of local minima	Very shallow; higher than reference state	Deep; lower than reference state	Moderate; comparable to reference state	Deepest; lower than reference state
Simulation - Free energy profiles	Location of local minimum(a)	Near bare clay ILS	Above bare clay ILS	Well above bare clay ILS	Well above bare clay ILS
	At reference state	Global minimum	Local minimum	Not obvious	Local minimum

4.5 Energy-Entropy Interplay

The partitioning process can be addressed as the competition between favorable energetic contribution due to the surfactant-surface interaction (we simplified the model by neglecting contributions from other sources such as surfactant-surfactant and surfactant-solvent interaction, etc.) and entropic loss mainly due to the confined nature of the surfactant within the clay layers. The only extra potential energy, which contributes to the excess Helmholtz free energy, taken into consideration in this model is the surface-dendrimer interaction. The surface-dendrimer potential energy curves obtained from the simulations are plotted against the layer separation in Figure IV-6. As one can expect from the surface-dendrimer potential interaction formula, the observed potential energy profile looks quite similar to LJ type interaction potential. The slit distances where the minimum of the surface-atom potential energy occurred for different dendrimers are the same, i.e. 9 Å. As the molecular size becomes larger, the well of ΔU^{sd} becomes deeper because of the number of attractive interaction sites within a molecule. For example, the well depth of G1 is 15 kcal/mol, and that of G3 is approximately 50 kcal/mol.

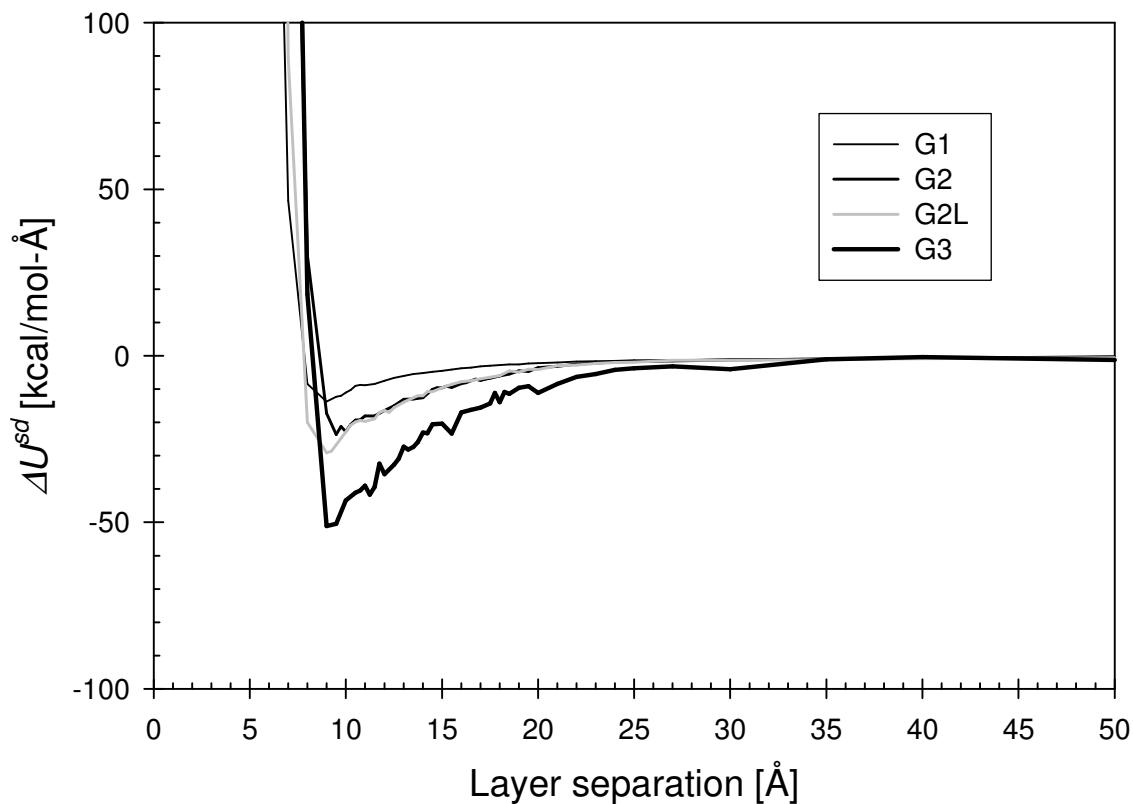


Figure IV-6 Wall-atom potential energy profiles of different types of dendrimers.

The energy-entropy interplay based on eq II-31 can be analyzed for the dendrimer partitioning. The total potential energy profiles for the energy-entropy analysis were drawn in Figure IV-7. It turns out that the size of dendrimer affects the potential energy behaviors as well as free energy behaviors. The total potential energy profiles for the four surfactants are quite different due to the difference in the size and shape of surfactants. Moreover, the two surfactants with the same number of generation, G2 and G2L, behave quite differently from the energetic point of view. Therefore, it can be concluded that both the molecular size and shape affect the energetic contribution to the free energy profiles.

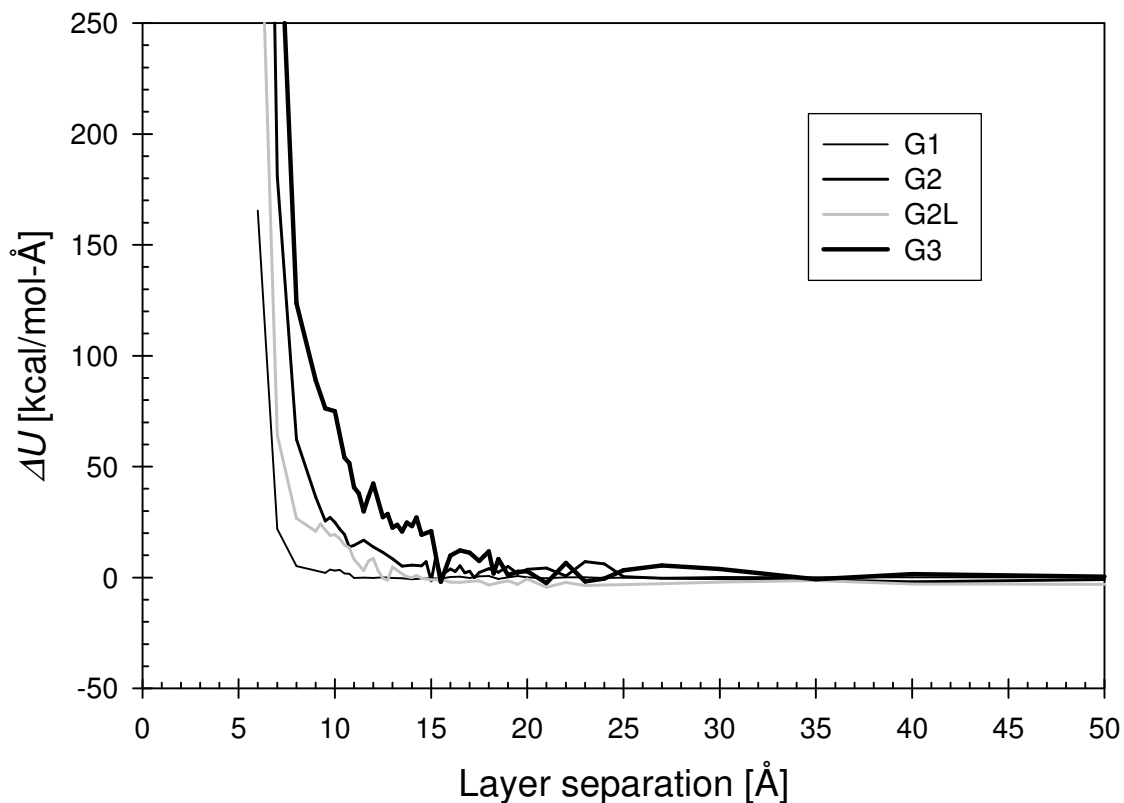


Figure IV-7 Energetic contribution profiles to the free energy difference of different types of dendrimers; the total potential is considered as the potential energy.

The relative entropy profiles for the four different dendrimers are drawn in Figure IV-8. The relative entropy was obtained by using eq II-31. It is clear that the uprising point of entropy for each dendrimer is different, moreover the larger the molecule, the righter the uprising point of entropy. This finding is in accordance with the fact that the largest molecule(G3) has little degree of freedom than that of G1 at a given narrow layer

separation (~ 10 Å), or there is huge entropic penalty of partitioning G3 into clay at narrow separations than that of G1.

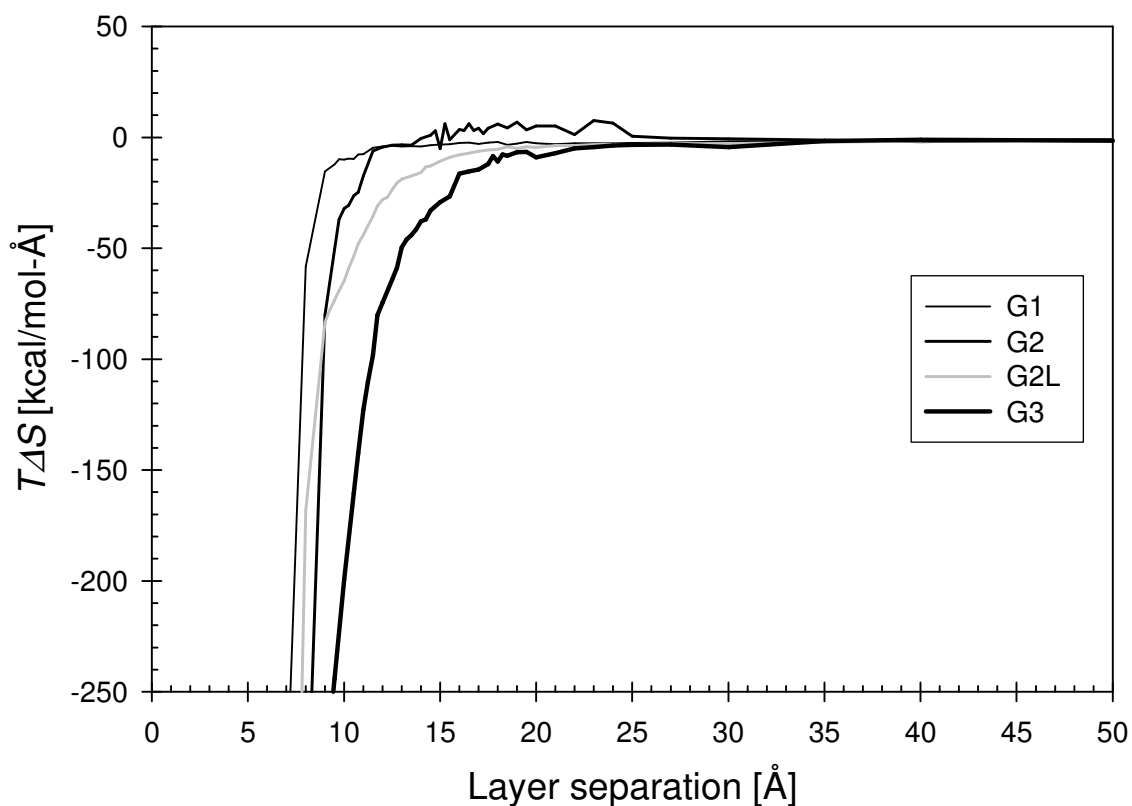


Figure IV-8 Entropic contribution profiles to the free energy difference of different types of dendrimers; the total potential is considered as the potential energy.

From this observation it can be concluded that the size of each dendrimer is one of the critical factors for determining the free energy behavior. Combined explanation of the partitioning process with confinement force clarifies our understanding of the partitioning process. The larger molecule, for instance G3, has larger value of

confinement force than that of the smaller one (G1). Since G3 has higher repulsive forces at narrow and moderate layer separation, the relative entropy of G3 is smaller than that of G1. Therefore, we reach a conclusion that the size difference leads to the different partitioning characteristics.

We have already figured out in the previous section that the free energy profiles are different, given that they have different size and geometry. We observed that the partitioning of G2L is more favorable than G2 in the relative energy profiles. Even though it is entropically favorable to put G2 than G2L, the entropic penalty is overcome by the energetic favorability for G2L. As a summary of entropic contribution profile curves, the entropic contributions of G2 and G2L are quite different leading to the different free energy behavior or phenomenologically different intercalation behavior due to the difference in molecular shape. In brief, the intercalation behavior is strongly dependent on the shape of the dendrimer. From the energy-entropy analyses we found that the final outcome of free energy profile is explained by the competition of the energetic and entropic factors. We report the energy-entropy interplay graph of G1 showing the relative energy, entropy, and free energy profiles in Figure IV-9 as an example. As a concluding remark, both the confinement force and free energy profiles strongly support the argument that the size and shape determining the energy and entropy contributions are the critical factors for the partitioning process of the dendrimers into the clay gallery.

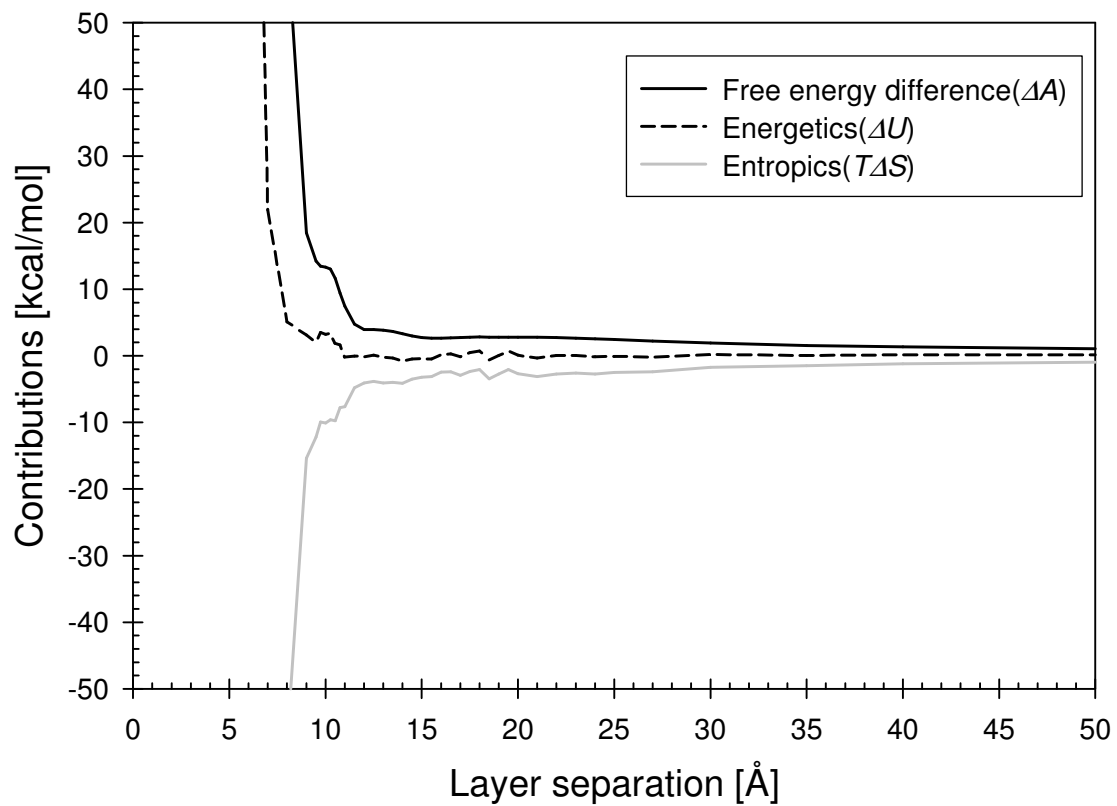


Figure IV-9 Energy-entropy interplay for a G1 molecule between clay layers.

CHAPTER V

RESULTS AND DISCUSSION OF BIO-RESEARCH

Several sets of preliminary simulation studies, such as the machine reliability, determination of temperature and damping parameters, and speedup, have been performed and the results with tables and figures discussed in Appendix B.

5.1 Bulk Water Simulation

5.1.1 Thermodynamic Properties

Water is a key material for all bio-systems, but a broadly applicable and accurate molecular model remains elusive despite its necessity and popularity. This work is a part of the bio-molecular research on A β -lipid bilayer-water system. As a first and fundamental step toward the A β research, a reliable model of water must be chosen. In this section we investigate the thermodynamic and structural properties of bulk water such as the potential energy, diffusion coefficient, bulk density, isothermal compressibility, and the radial distribution function with two different water models, i.e. SPC (Simple Point Charge) and cvff models. Moreover, we intend to examine the applicability of cvff model as our water model for biomolecular system, since little research has been performed using cvff water model. The thermodynamic and structural properties such as the potential energy, the diffusion coefficient, and the radial distribution function are to be investigated from simulations with different bulk pressure using the two different models. Special attention will be cast to the isothermal compressibility, which is of importance to describe the membrane fluidity for biomolecular systems.

A sketch of water model is drawn in Figure V-1. The variable q_i designates the partial charge on atom i , and r and θ designate the O-H bond distance and H-O-H angle, respectively. Several model parameters are tabulated in Table V-1.

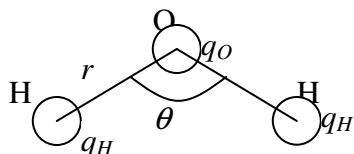


Figure V-1 Sketch of a water model

Table V-1 Several water models for biomolecular research.

Model	q_O [e]	q_H [e]	σ [Å]	ϵ [kcal/mol]	k_r [kcal/mol]	r_0 [Å]	k_θ [kcal/mol]	θ_0 [°]
cvff	-0.82	0.41	3.16552	0.155416	540.6336	0.96	50.00	104.50
SPC	-0.82	0.41	3.166	0.1554	554.14	1	45.77	109.47
SPC/E	-0.8476	0.4238	3.166	0.1554	554.14	1	45.77	109.47

The SPC model is a widely used water model, which assumes there is a point charge located at each atom of a water molecule. The SPC model parameters were chosen from Teleman and colleagues (Teleman et al., 1987). Extended simple point charge or SPC/E model assumes the same force-field parameters, except for the point charge values (Berendsen et al., 1987). The main difference between cvff and SPC models comes from the intra-molecular potential energy parameters.

The nonbond interaction includes both the 6-12 Lennard-Jones interaction and Coulomb charge-charge interactions:

$$U^{LJ}(r) = 4\epsilon \left[\left(\frac{\sigma}{r} \right)^{12} - \left(\frac{\sigma}{r} \right)^6 \right] \quad (\text{V-1})$$

$$U^{Coul}(r) = \frac{z_i z_j}{4\pi\epsilon_0 r} \quad (V-2)$$

where σ and ϵ are the LJ parameters, z_i and z_j are the charge values, and ϵ_0 is the permittivity of free space. The intra-molecular interactions for bond stretching and angle bending are given by

$$U^r(r) = k_r (r - r_0)^2 \quad (V-3)$$

$$U^\theta(r) = k_\theta (\theta - \theta_0)^2 \quad (V-4)$$

where r_0 and θ_0 are the equilibrium bond distance and angle respectively.

The total number of water molecules in these simulations was 500. Simulation details for bulk water are summarized in Table V-2.

Table V-2 Summary of simulation parameters for bulk water; P_tar means the target pressure.

Index	Original Index	Model	P_tar [atm]	Span [ps]	Average [ps]	Data file
W-a	H2O_030606_7	cvff	-75.00	200	last 100	data.H2O_111005_1
W-b	H2O_030606_9	cvff	-50.00	200	last 100	data.H2O_111005_1
W-c	H2O_030606_6	cvff	1.00	200	last 100	data.H2O_111005_1
W-d	H2O_030606_10	cvff	50.00	200	last 100	data.H2O_111005_1
W-e	H2O_030606_8	cvff	75.00	200	last 100	data.H2O_111005_1
W-e_2	H2O_042006_1	cvff	75.00	200	last 100	data.H2O_111005_1
W-f	H2O_030706_1	SPC	-75.00	200	last 100	data.H2O_030706_spc
W-g	H2O_030706_4	SPC	-50.00	200	last 100	data.H2O_030706_spc
W-h	H2O_030706_2	SPC	1.00	200	last 100	data.H2O_030706_spc
W-i	H2O_030706_5	SPC	50.00	200	last 100	data.H2O_030706_spc
W-e	H2O_030606_8	SPC	75.00	200	last 100	data.H2O_030706_spc
W-j_2	H2O_042006_2	SPC	75.00	200	last 100	data.H2O_030706_spc

Since it is reasonable to simulate the biomolecular system using the NPT ensemble, our main variable is the pressure which is varied from -75 to 75 atm (Table V-2). Simulations were performed at 323K with Nosé-Hoover thermostat, a time step of 2 fs and the SHAKE algorithm (Ryckaert et al., 1977). The long-range electrostatics was treated with PPPM as described in section 2.1.3. The production run time was 200 ps and the average properties of the last 100 ps were used for analysis.

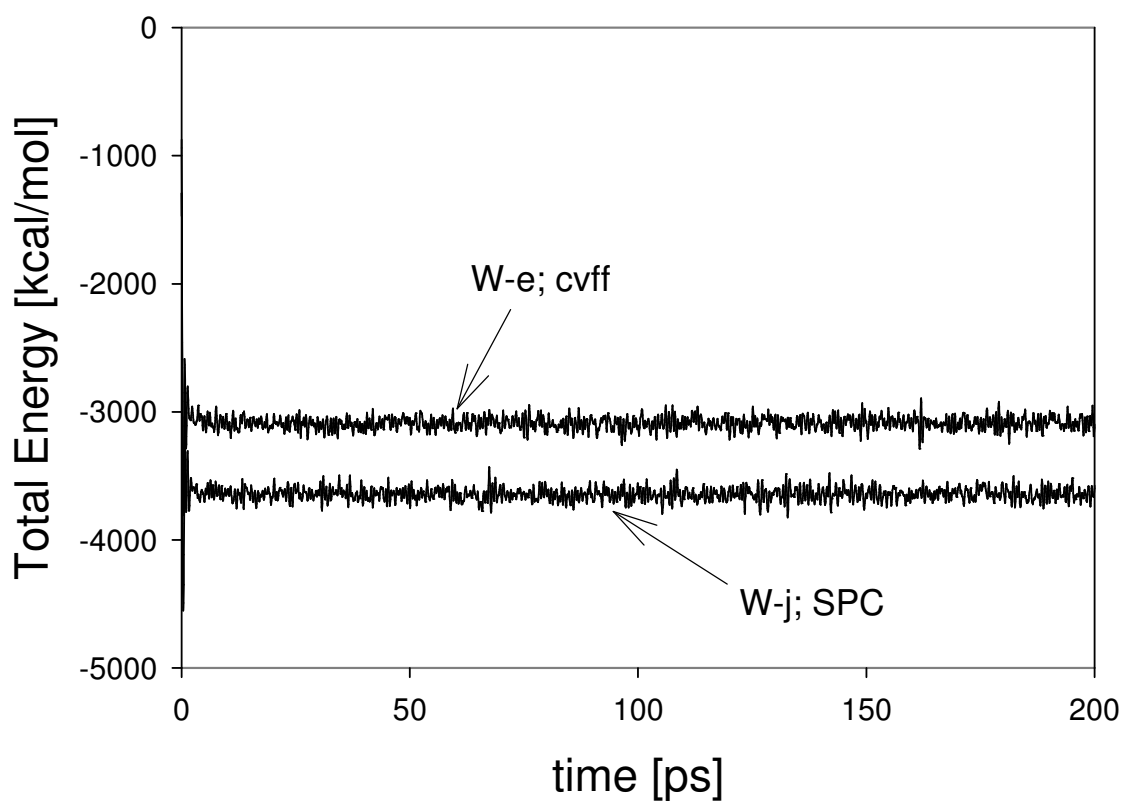


Figure V-2 Total energy profiles for the cvff and SPC water models with a target pressure of 75 atm and at 323K.

Total energy profiles for the two case studies are drawn in Figure V-2. After 20 to 30 ps of equilibration time, the kinetic, potential and the total energy fluctuate around an average value, for example the total energy of -3086 and -3643 kcal/mol for W-e case and W-j case, respectively. Similar energy profiles were obtained from the other simulation cases.

Thermodynamic properties with different pressures are obtained and reported in Table V-3. In this table each column from the 2nd stands for the energy value term by term, and the 2nd row of each production run lists the standard deviation. We observe that the average measured pressure is quite similar to the target pressure applied. The analysis of term-by-term energy contribution to the total energy led to the conclusion that the pressure doesn't change the potential energy contribution much if the same water model is used. The potential energy differed significantly between the two water models. Different water models led to different potential energy evaluation (Berendsen et al., 1987; Teleman et al., 1987).

We observed that the potential energy of the system at 75 atm is -35.2 kJ/mol using cvff model. SPC model predicted it as -39.9 kJ/mol. One of the earlier studies of SPC model showed that the potential energy from water simulation is -42.2 kJ/mol at 300K and that from the experiment was found to be -41.5 kJ/mol (Berendsen et al., 1987). Slightly different results were reported at different conditions; -37.7 kJ/mol of SPC model at 308K and -1 bar and -41.4 kJ/mol at 306K and 6 bar for SPC/E model (Berendsen et al., 1987). The difference between the two models is approximately 12% based on SPC model and the degree of difference is quite comparable to the difference between SPC and SPC/E models as shown in the above information.

Table V-3 Thermodynamic properties from bulk water simulations; V is the specific volume, E_{pair} includes the pair short-range interaction energy, E_{bond} is the total intra-molecular interaction energy, E_{total} is the total energy, KE is the kinetic energy, and PE is the potential energy.

Index	Model	Temp [K]	E _{pair} [kcal/mol]	E _{angle} [kcal/mol]	E _{total} [kcal/mol]	P _{tar} [atm]	P [atm]	Volume [Å ³]	Density [g/cc]	V [cm ³ /mol]	KE [kcal/mol]	PE [kcal/mol]	PE/N [kJ/mol]
W-a	cvff	322.95	-4480.22	282.83	-3075.28	-75.00	-68.87	16172.27	0.92	19.47	1123.09	-4198.30	-35.13
		0.24	9.13	3.27	6.72		10.02	63.28			0.84	6.17	
W-b	cvff	323.07	-4480.65	283.40	-3074.70	-50.00	-46.48	16155.73	0.93	19.45	1123.54	-4198.24	-35.13
		0.24	9.35	3.75	7.08		7.46	71.09			0.83	6.26	
W-c	cvff	323.01	-4491.80	285.84	-3083.64	0.00	2.56	16054.64	0.93	19.33	1123.30	-4206.52	-35.20
		0.38	6.76	2.85	5.60		13.06	50.29			1.32	6.05	
W-d	cvff	322.97	-4489.45	283.75	-3083.50	50.00	54.06	16065.02	0.93	19.34	1123.18	-4206.69	-35.20
		0.34	10.08	3.28	7.88		13.33	68.51			1.17	6.71	
W-e	cvff	322.91	-4492.72	284.66	-3086.07	75.00	78.55	16028.37	0.93	19.30	1122.98	-4209.19	-35.22
		0.30	5.76	3.16	4.83		12.29	24.45			1.04	4.16	
W-e ₂	cvff	322.88	-4494.82	285.12	-3087.83	75.00	78.88	16025.13	0.93	19.29	1121.87	-4209.70	-35.23
		0.23		4.61	5.94		8.93	71.07			0.79	6.23	
W-f	SPC	323.24	-5060.86	305.66	-3632.06	-75.00	-78.03	15617.92	0.96	18.80	1124.13	-4755.99	-39.80
		0.30	7.23	2.52	5.81		9.56	53.07			1.04	5.96	
W-g	SPC	322.95	-5063.56	305.99	-3635.45	-50.00	-48.13	15578.18	0.96	18.76	1123.10	-4758.35	-39.82
		0.41	9.42	2.40	8.59		6.35	52.71			1.43	8.21	
W-h	SPC	322.93	-5064.59	306.42	-3636.10	0.00	3.74	15548.62	0.96	18.72	1123.05	-4759.30	-39.83
		0.33	9.28	2.47	7.28		16.20	64.77			1.16	7.29	
W-i	SPC	323.24	-5070.00	306.67	-3640.21	50.00	45.85	15507.03	0.96	18.67	1124.11	-4764.12	-39.87
		0.31	8.18	2.75	8.10		9.90	46.39			1.08	8.04	
W-j	SPC	323.10	-5071.79	306.27	-3642.89	75.00	74.85	15479.82	0.97	18.64	1123.61	-4766.32	-39.88
		0.30	8.53	3.06	6.62		11.67	51.57			1.05	5.73	
W-j ₂	SPC	323.06	-5067.86	306.71	-3638.64	75.00	74.86	15473.88	0.97	18.63	1122.51	-4761.14	-39.84
		0.29		2.81	9.38		12.23	69.47			1.02	9.68	

5.1.2 Structural Properties

In this section we present the structural and physical properties from bulk water simulations. One example plot of the mean-squared displacements of oxygen atoms in water molecules from the cvff and SPC water models is shown in Figure V-3. The MSD of the cvff model is approximately 1.5 times larger than that of SPC model, which in turn implies that the diffusion coefficient of water molecules using cvff will be larger than that of SPC model, since the diffusion coefficient is proportional to the slope of MSD curve in the large time limit (Refer to eq II-66).

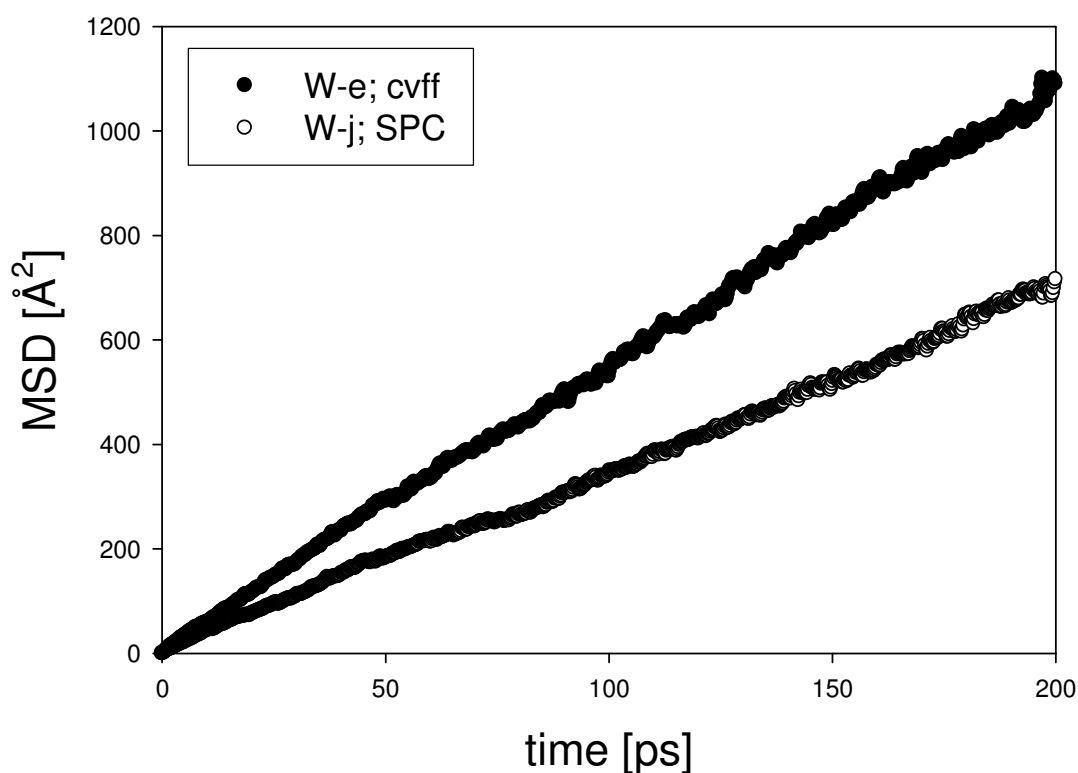


Figure V-3 MSD of O-atoms for two different water models; the external pressure of 75 atm at 323K.

Simulation results of self-diffusion coefficients using different water models and pressures are shown in Table V-4 and Figure V-4. The MSDs were obtained from an intrinsic function of LAMMPS (fix msd).

Table V-4 Diffusion coefficient from bulk water simulations.

Model	cvff		SPC	
p [atm]	Index	D×10 ⁵ [cm ² /s]	Index	D×10 ⁵ [cm ² /s]
-75.0	W-a	9.05	W-f	6.13
-50.0	W-b	8.61	W-g	6.12
1.0	W-c	9.54	W-h	5.72
50.0	W-d	9.34	W-i	5.62
75.0	W-e	9.85	W-j	5.89
average		9.28		5.90

We note that the diffusion coefficients of the two water models show approximately a 60% difference. According to Tieleman and Berendsen, the estimated water diffusion coefficient is 6.2×10^{-5} cm²/sec at 325K using the SPC model, which is quite close to our simulation result using our SPC model (Tieleman and Berendsen, 1996). The diffusion coefficient of water using cvff model (9.85×10^{-5} cm²/sec at 75 atm) was overestimated compared to the SPC model (5.89×10^{-5} cm²/sec at 75 atm) and the experimental values of 3.90×10^{-5} cm²/sec at 10MPa and 323.2K, which is nearly constant over the wide range of bulk pressure (Krynicky et al., 1978). Based on the diffusion coefficient from each model, we expect that the water molecules represented by cvff model will move faster than those of SPC model. Therefore, we may observe some structural property differences due to the employment of cvff water model.

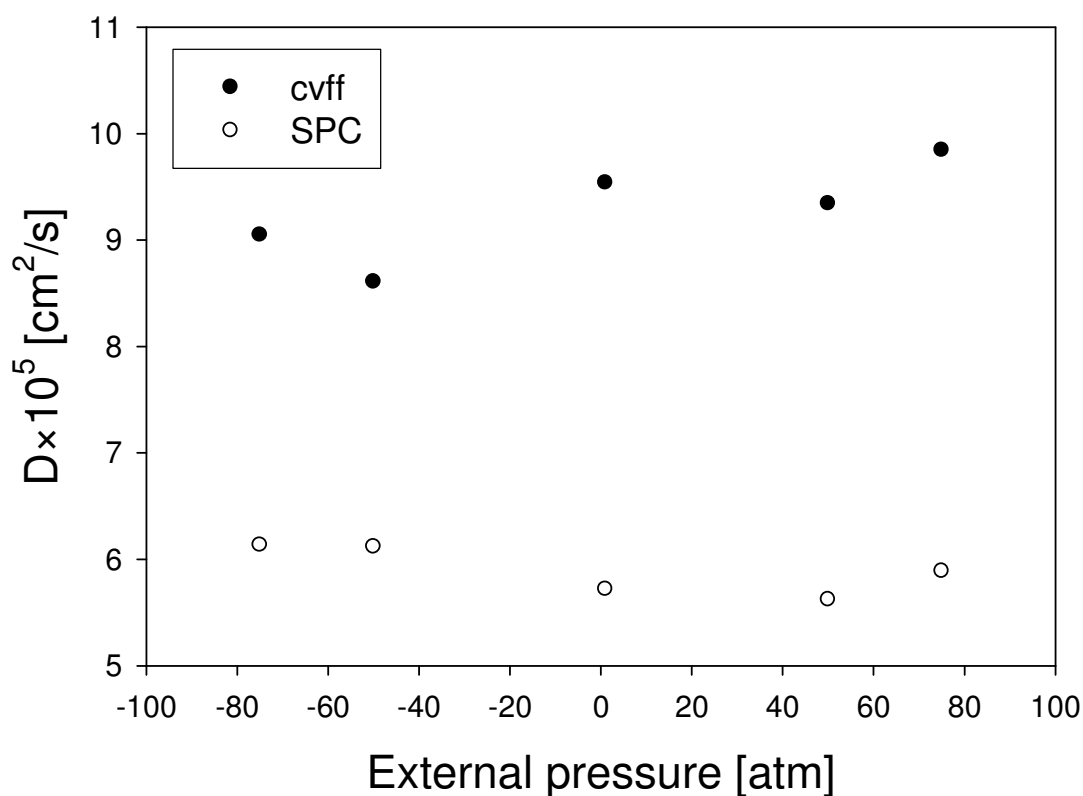


Figure V-4 Self-diffusion coefficients of water molecules at 323K.

Considering the cvff and SPC water models we can reasonably conclude that we observe higher self-diffusion coefficient in the cvff model. Since water molecules from the cvff model have shorter equilibrium distance and a smaller equilibrium angle compared to the SPC model, the molecules have smaller effective radius than those of SPC. Therefore, smaller water molecules from cvff diffuse faster than bulky SPC water molecules. We have already seen that the density of the cvff model is lower than that of SPC (Table V-3), which also explains the higher diffusion coefficient by the cvff model. In other words, the water molecules represented by cvff are less packed and have greater room to diffuse throughout other molecules.

We observed that the water model difference led to the different simulated self-diffusion coefficient. To determine if the cvff will provide meaningful results for biomolecular systems, we would like to measure the isothermal compressibility and the result is to be compared with literature.

In general, the isothermal compressibility is expressed as

$$\beta = -\frac{1}{V} \left(\frac{\partial V}{\partial p} \right)_T \quad (\text{V-5})$$

where V is the system volume and usually the specific volume, V_s , is used. From the simulation data from Table V-3, we can draw a relationship between the pressure and specific volume or molar volume for two different water models. The relationship is shown graphically in Figure V-5. The slopes were calculated to be $-0.0011 \text{ cm}^3/\text{mol-atm}$ for the cvff model and $-0.0010 \text{ cm}^3/\text{mol-atm}$ for the SPC model. The relative difference is approximately 10 %, which is quite small compared to the difference in diffusion coefficients. Substituting the specific volumes of each simulation result in eq V-5 (at 75 atm $V_s = 19.3 \text{ cm}^3/\text{mol}$ for cvff and $18.6 \text{ cm}^3/\text{mol}$ for SPC), we obtain compressibility of $5.70 \times 10^{-5}/\text{atm}$ for cvff and $5.46 \times 10^{-5}/\text{atm}$ for SPC models at 323K, respectively. The two models predicted slightly different compressibilities ($\sim 4\%$ difference based on cvff model), which will have little effect on the membrane fluidity.

Referring to Kell's review on density, thermal expansivity, and compressibility of liquid water at different temperatures, we see $44.1732 \times 10^{-6}/\text{bar}$ of compressibility at 50 °C (1975). Conversion to common experimental units, we obtain $4.48 \times 10^{-5}/\text{atm}$. Compressibility using cvff overestimates the compressibility 21% at that temperature.

We end the discussion of compressibility concluding that the isothermal compressibilities using two water models are very similar, therefore the choice of cvff model is justified, even though simulation results slightly overestimate the compressibility when compared to the experimental result.

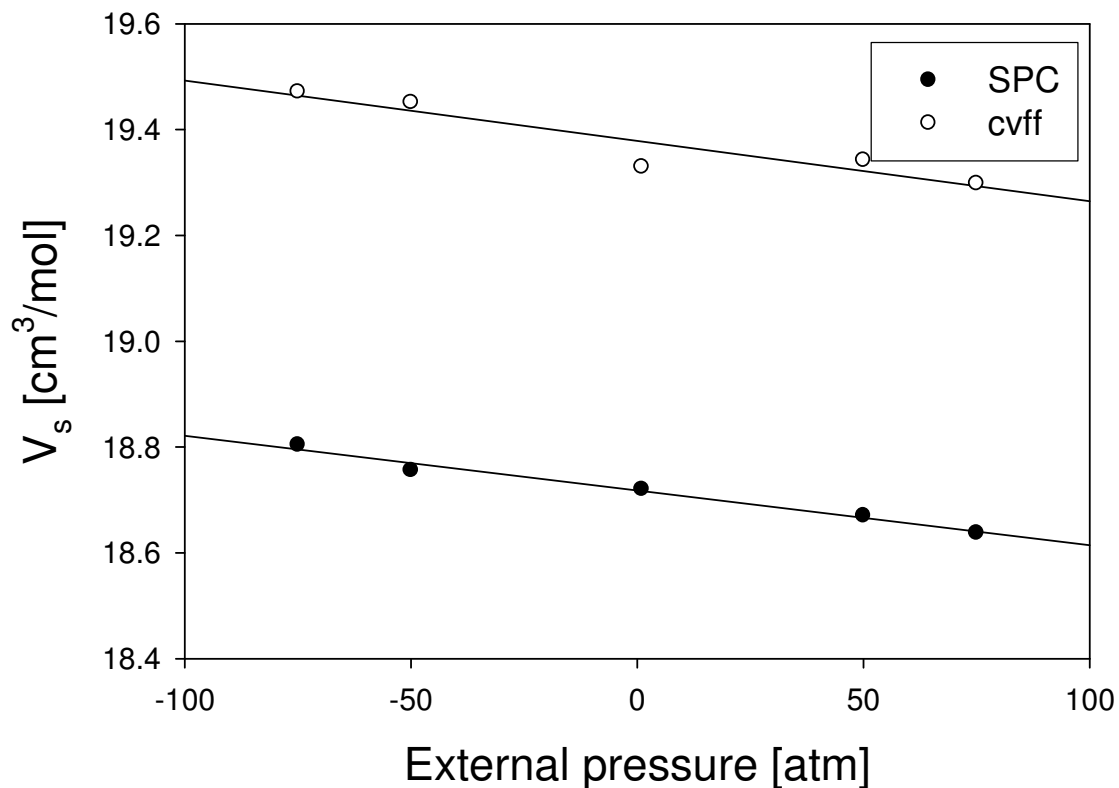


Figure V-5 Pressure-volume relationship from bulk water simulations.

The radial distribution function is a measure of structural properties. The O-O atom radial distribution functions are drawn at different pressures for the two water models in Figure V-6 and Figure V-7. Very little difference was found among the radial distribution functions at different pressures.

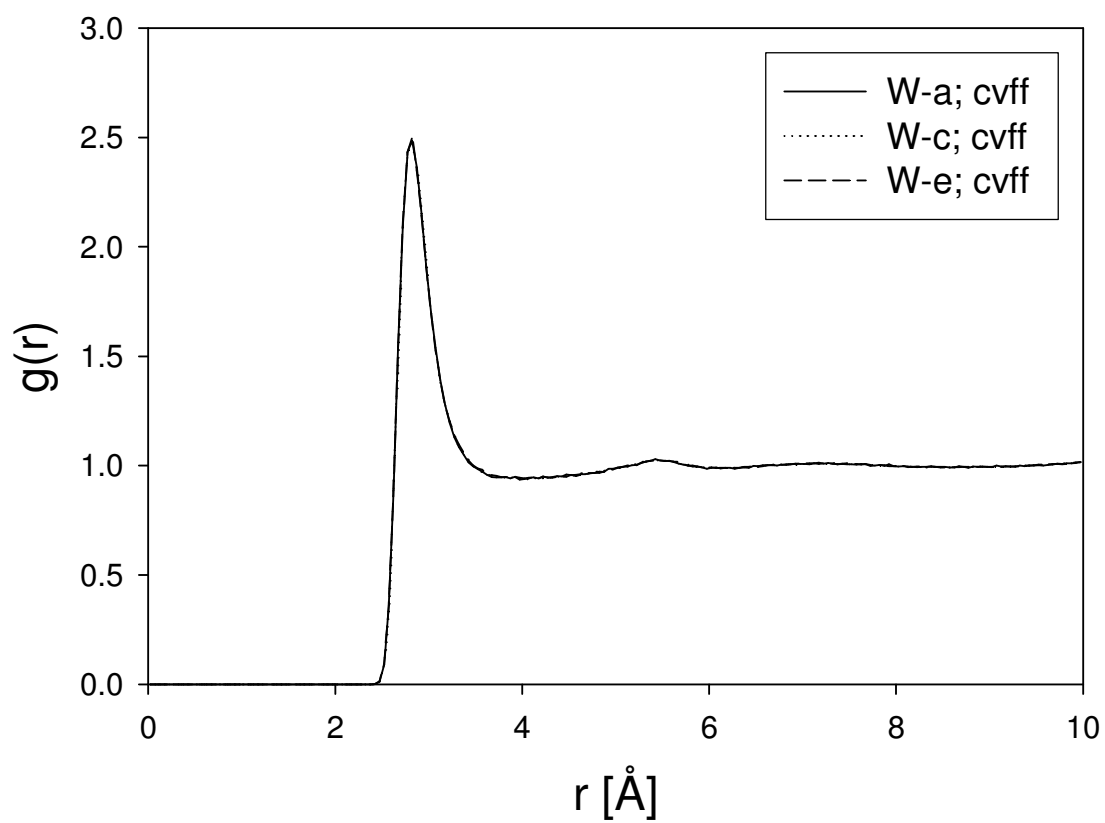


Figure V-6 Radial distribution functions using cvff water model with different bulk pressures.

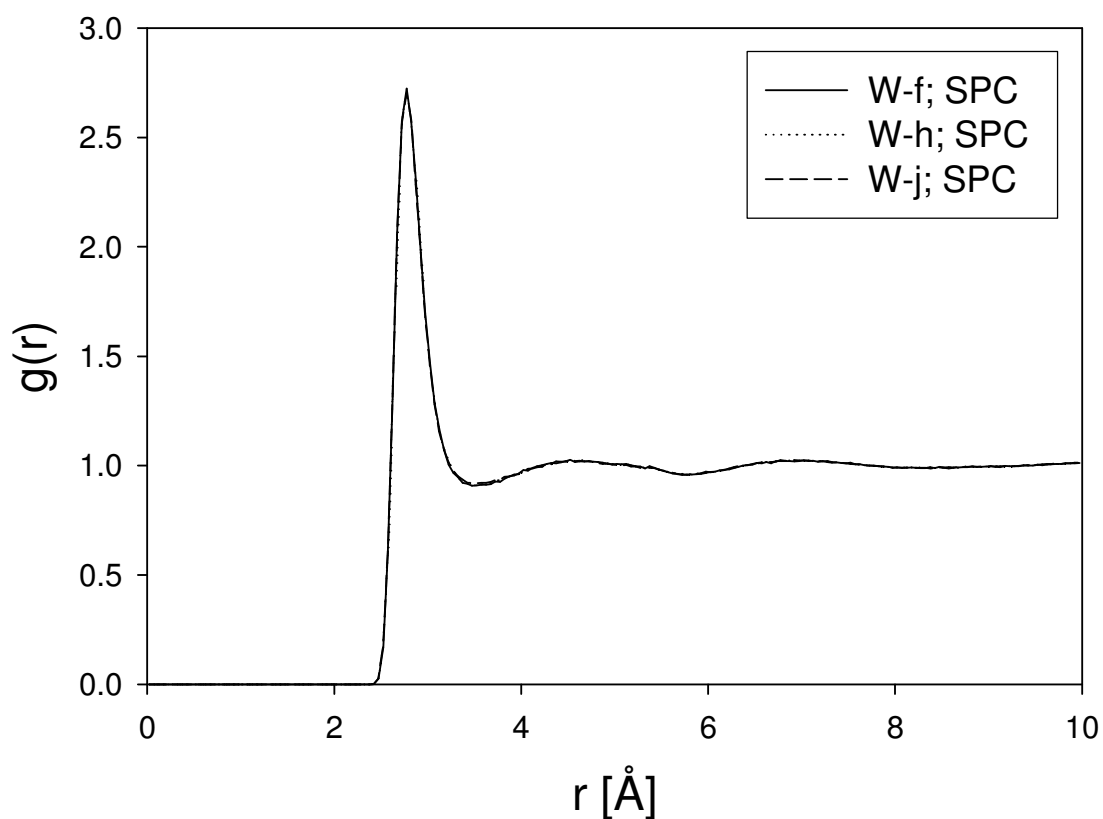


Figure V-7 Radial distribution functions using SPC water model with different bulk pressures

We compare the radial distribution functions with an experimental result by Narten et al. (1967) in Figure V-8. The absolute value of the first peak from cvff is closer to the experiment than that of SPC. The first peak of radial distribution function using SPC has slightly higher value and the distance where the second peak appears is shifted toward the lower position than that of cvff. Since more dense materials or solid-like materials exhibit sharper peak, SPC model describes water molecules more dense compared to cvff. This argument reaches to the same conclusion that cvff model of water is expressed more repulsively as suggested in the diffusivity discussion paragraphs.

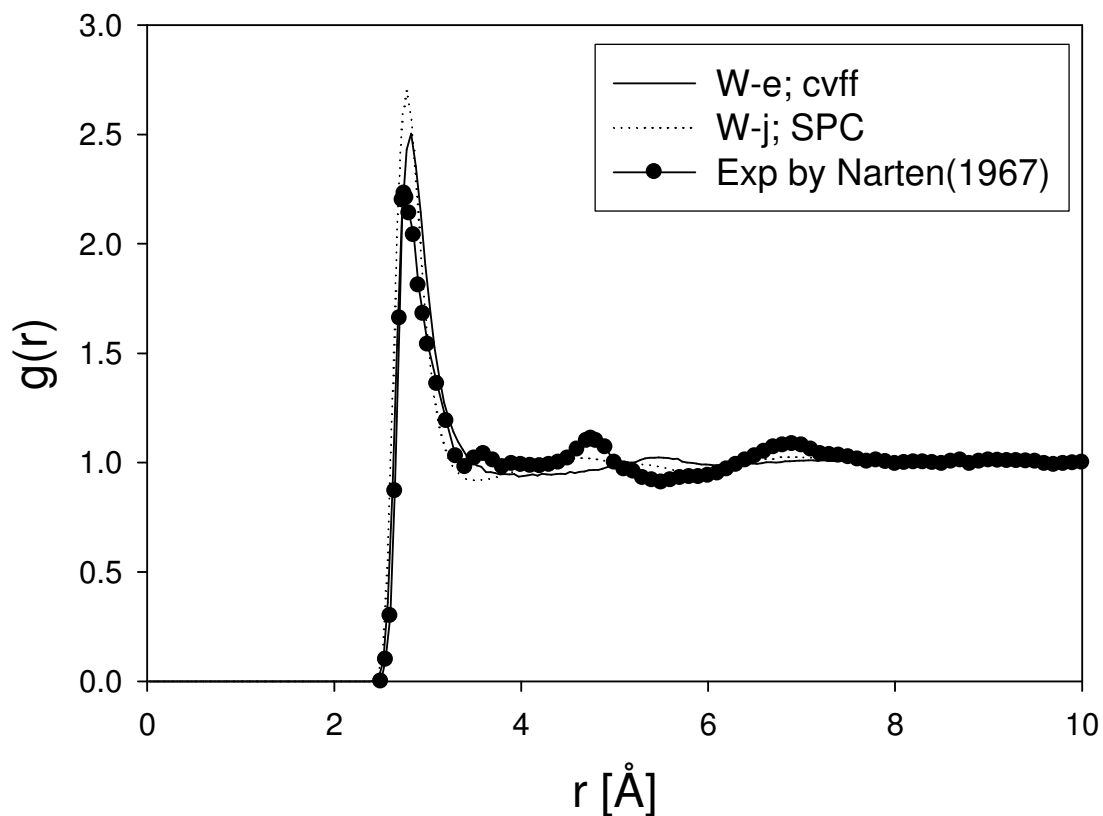


Figure V-8 Comparison of radial distribution functions for different water models with an experimental result; the external pressure of 75 atm at 323K; Data points were generated from Narten et al., 1967.

Different structural properties are obtained from the radial distribution functions of O-H (g_{OH}) and H-H (g_{HH}) atoms at a pressure of 75 atm as shown in Figure V-9 and Figure V-10. The O-H RDF shows that oxygen and hydrogen atoms are in close proximity featuring hydrogen bonding (around 2 Å) for both models.

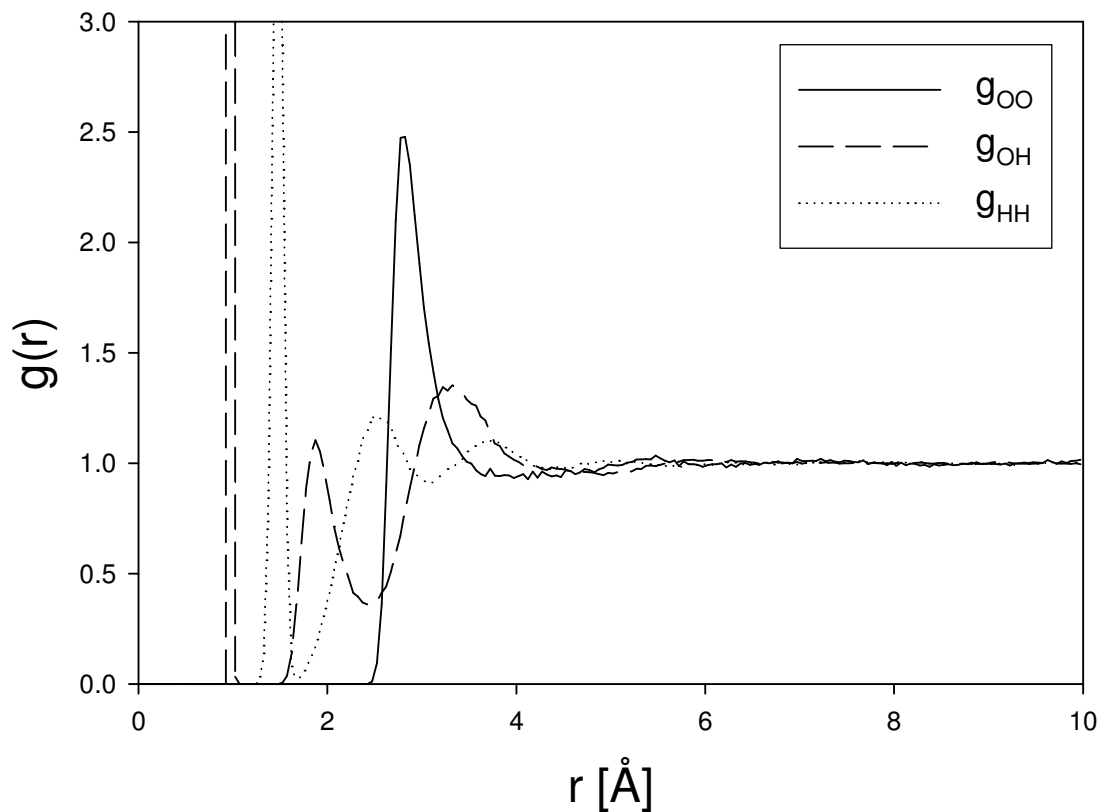


Figure V-9 Radial distribution functions using the cvff water model with bulk pressure of 75 atm; W-e_2 case.

RDFs are strongly dependent on the choice of atoms as confirmed by Figure V-10. RDFs using the SPC model exhibit a similar pattern as the cvff RDFs, but the O-H RDF is slightly different compared to the cvff model. The SPC model predicts higher RDF at the first peak of O-H RDF than that of cvff model.

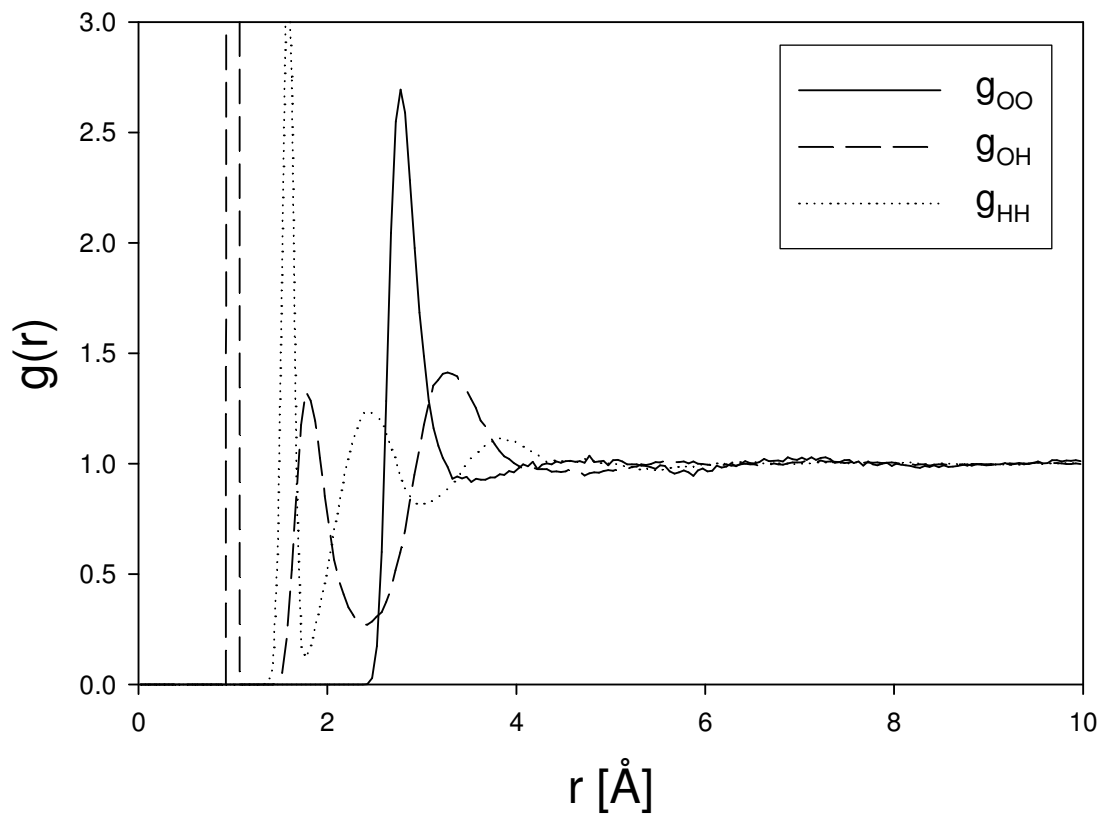


Figure V-10 Radial distribution functions using the SPC water model with bulk pressure of 75 atm; W-j_2 case.

The comparison of oxygen-hydrogen radial distribution functions from cvff and SPC is shown in Figure V-11. They exhibit the same peak behaviour with slightly different peak values. The SPC model features a more structured profile, which is also the case in the comparison of the g_{OO} profile.

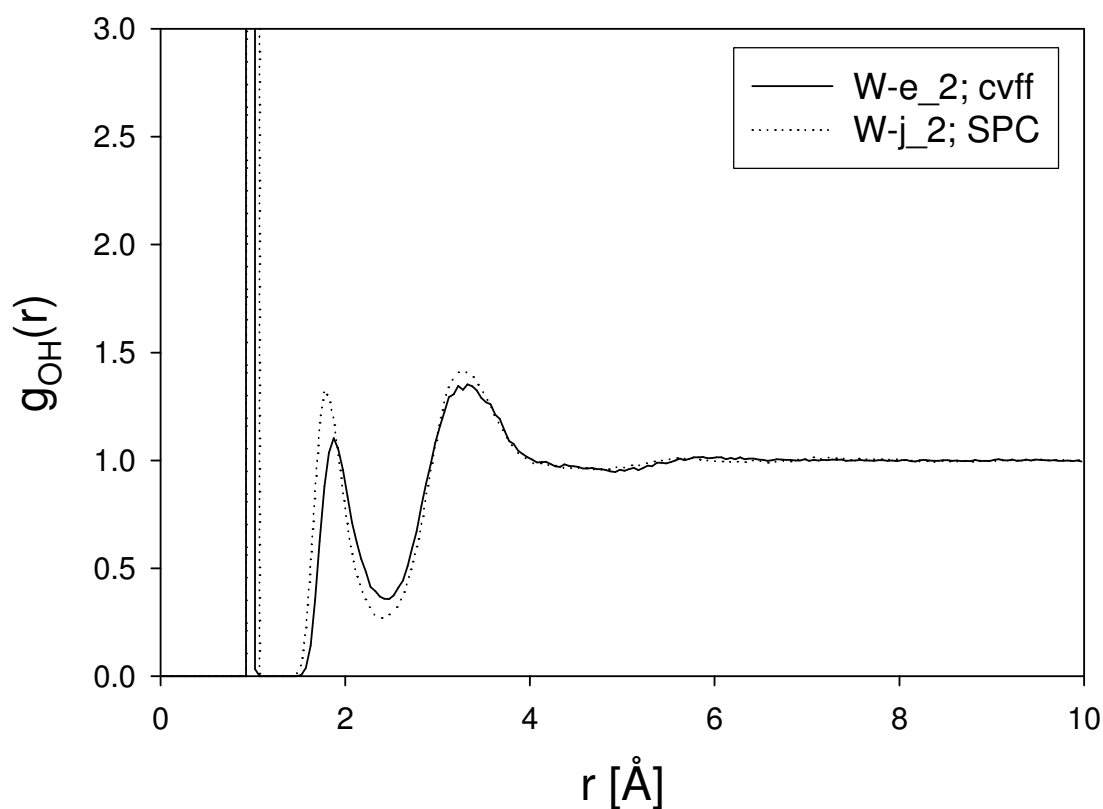


Figure V-11 Oxygen-hydrogen radial distribution functions for different water models with bulk pressure of 75 atm.

Starting from a structure with different model parameters as the SPC model, we thoroughly investigated the adequacy of cvff water model for biomolecular simulations. A summary table for the comparison of this study and other literature is presented in Table V-5. We have observed some difference predicted by the two water models studied. The bulk density is underestimated using the cvff model compared to the experimental result, while the other properties such as the diffusion coefficient and the isothermal compressibility are overestimated compared to the experiment. The radial distribution function using cvff water model represents the first peak better than that of the SPC model compared to the experiment as discussed previously.

Table V-5 Comparison of bulk water properties from this study and published results; Data for this study were obtained at 75 atm and 323K.

Properties	This study		Simulation		Experiment
	cvff	SPC	SPC	SPC/E	
PE [kJ/mol]	-35.2	-39.9	-37.7 ^a	-41.4 ^b	-41.5 ^a
ρ [g/cm ³]	0.93	0.97	0.97 ^a	0.998 ^b	0.99 ^d
Diffusivity $\times 10^5$ [cm ² /s]	9.85	5.89	4.3 ^a , 6.2 ^c	2.5 ^b	3.9 ^e
$\beta \times 10^5$ [atm ⁻¹]	5.70	5.46			4.48 ^d
$g_{OO}(r)$	cvff model predicts the first peak of $g_{OO}(r)$ better than SPC model compared to the experimental result ^f .				

^a (Berendsen et al., 1987); at -1atm and 308K, Original data for PE comes from Postma, J.P.M. Ph.D.

Thesis, University of Groningen, 1985

^b (Berendsen et al., 1987); at 6atm and 306K

^c (Tieleman and Berendsen, 1996); at 323K

^d (Kell, 1975); at 1atm

^e (Krynicky et al., 1978); at 100atm and 323.2K

^f (Narten et al., 1967); at 323K

Based on the simulation data on the several property predictions such as the bulk density and diffusivity, we see that the SPC model predicts the properties better than the cvff model. But note that there is little consensus which model is the best for lipid bilayer simulations, because different research groups have used different water models: SPC (Doxastakis et al., 2005), SPC/E (Chiu et al., 1995; Shinoda et al., 1995), TIP3P (Smondyrev and Berkowitz, 1999b) and TIP4P (Shinoda et al., 1997) with different force-fields or parameter sets. Moreover, we have solid reasoning to use the cvff water model instead of the commonly used SPC model for our further research, since the difference of isothermal compressibilities from the two models, which characterizes the biological membrane fluidity, is of no significance. Also, the radial distribution function using the cvff model, a character of structure, at very short distances matches with the experimental result better than the SPC model as pointed out earlier. As concluding

remarks, our observations of the thermodynamic and structural properties show that bulk water simulations with different models lead to some discrepancy in measured properties, but adding the fact that the cvff water model for biomolecular system has never been reported by any other research group to the best of the authors' knowledge to the reasoning for using the cvff model for further research, we explore biomolecular systems with cvff water model. We may observe differences in thermodynamic and structural properties due to the use of cvff compared to the literature for the simulations of hydrated lipids, A β protein in water and near lipid Bilayers. However, we leave the improvement of the water model as one of our future works.

5.2 Simulation of Hydrated Lipids

5.2.1 Thermodynamic Properties

We prepared initial models of hydrated lipids using the method described in Section 3.2. We then ran MD simulations with the prepared models. A summary for the simulation parameters is tabulated in Table V-6. The major variable of this study is the lateral pressure or $P_L = P_x = P_y$ as described in Section 3.2.

The thermodynamic properties for different case simulations are summarized in Table V-7. The major contribution to the potential energy is found to be the long-range electrostatics, therefore, short truncation method for large systems, such as a protein in hydrated lipids, will fail to describe detailed characteristics. As an example of the thermodynamic properties, total and potential energy profiles for the HD-j case simulation are shown in Figure V-12. The potential energy profile clearly shows that the system is equilibrated after 500 ps of simulation time.

Table V-6 Summary of simulation parameters for hydrated lipids; the data file for all simulations is data.H2O_DPPC_110805_min_1_10k except HD-j_2(H2O_DPPC_113005_1.500000), HD-k_2 and HD-l_2(H2O_DPPC_120505_1.500000), HD-k case started with $P_z = -1$ atm.

Index	Original Index	Machine	$P_x = P_y$ [atm]	P_z [atm]	Time span [ps]	Average [ps]	Data file	Remark
HD-a	H2O_DPPC_112105_3	COSMOS/8cpus	1.0	1.0	567.4	last 300	data.H2O_DPPC_110805_min_1_10k	
HD-b	H2O_DPPC_112605_1	COSMOS/16cpus	50.0	1.0	1000	last 500	data.H2O_DPPC_110805_min_1_10k	
HD-c	H2O_DPPC_112205_1	COSMOS/16cpus	100.0	1.0	1000	last 500	data.H2O_DPPC_110805_min_1_10k	
HD-d	H2O_DPPC_112705_1	CAT/8cpus	1.0	1.0	1000	last 500	data.H2O_DPPC_110805_min_1_10k	
HD-e	H2O_DPPC_112705_2	CAT/8cpus	-1.0	1.0	1000	last 500	data.H2O_DPPC_110805_min_1_10k	
HD-f	H2O_DPPC_112905_1	COSMOS/8cpus	1.0	1.0	1000	last 500	data.H2O_DPPC_110805_min_1_10k	
HD-g	H2O_DPPC_112905_2	CAT/8cpus	-10.0	1.0	1000	last 500	data.H2O_DPPC_110805_min_1_10k	
HD-h	H2O_DPPC_112705_3	CAT/8cpus	-51.6	1.0	1000	last 500	data.H2O_DPPC_110805_min_1_10k	
HD-i	H2O_DPPC_112805_1	CAT/8cpus	15.0	1.0	1000	last 500	data.H2O_DPPC_110805_min_1_10k	
HD-j	H2O_DPPC_113005_1	CAT/8cpus	75.0	1.0	1000	last 500	data.H2O_DPPC_110805_min_1_10k	
HD-j_2	H2O_DPPC_013106_1	CAT/8cpus	75.0	1.0	843.6	all 843.6	H2O_DPPC_113005_1.500000	
HD-k	H2O_DPPC_120505_1	CAT/8cpus	51.6	1.0	1000	last 500	data.H2O_DPPC_110805_min_1_10k	
HD-k_2	H2O_DPPC_020106_1	CAT/8cpus	51.6	1.0	2000	all 2000	H2O_DPPC_120505_1.500000	
HD-l	H2O_DPPC_120905_1	CAT/8cpus	51.6	-1.0	1000	last 500	data.H2O_DPPC_110805_min_1_10k	
HD-l_2	H2O_DPPC_012606_1	CAT/10cpus	51.6	-1.0	2000	all 2000	H2O_DPPC_120505_1.500000	
HD-m	H2O_DPPC_022806_1	COSMOS/16cpus	75.0	1.0	2000	last 1000	data.H2O_DPPC_110805_min_1_10k	T = 292K
HD-n	H2O_DPPC_022406_1	COSMOS/16cpus	1.0	1.0	2000	last 1000	data.H2O_DPPC_110805_min_1_10k	$P_x = P_y = P_z$
HD-o	H2O_DPPC_021706_1	COSMOS/16cpus	-1.0	-1.0	2000	last 1000	data.H2O_DPPC_110805_min_1_10k	
HD-p	H2O_DPPC_021706_2	COSMOS/16cpus	60.0	-1.0	2000	last 1000	data.H2O_DPPC_110805_min_1_10k	
HD-q	H2O_DPPC_031206_1	CAT/8cpus	60.0	1.0	2000	last 1000	data.H2O_DPPC_110805_min_1_10k	
HD-r	H2O_DPPC_031206_2	CAT/8cpus	1.0	1.0	2000	last 1000	data.H2O_DPPC_110805_min_1_10k	$P_x = P_y = P_z$

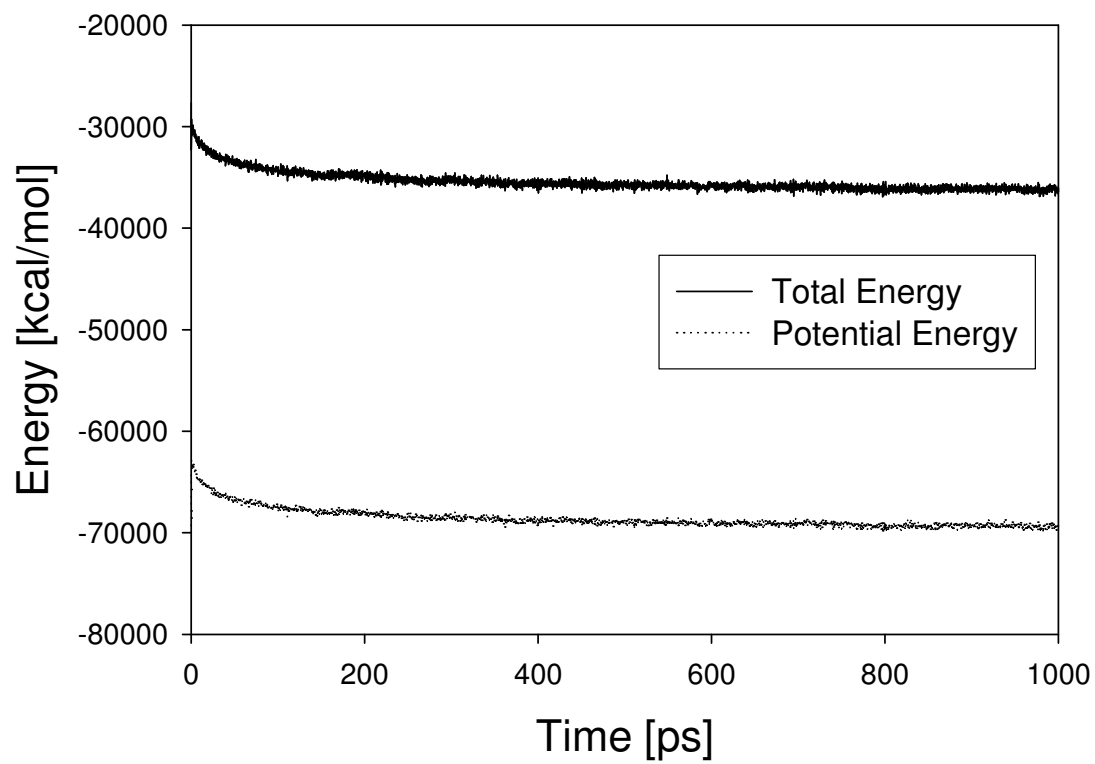


Figure V-12 Energy profiles for hydrated lipids simulation; HD-j.

Table V-7 Thermodynamic properties measured from simulations for hydrated lipids with different case studies; second row values are the standard deviations.

Index	Total E [kcal/mol]	KE [kcal/mol]	Temp [K]	PE [kcal/mol]	E_bond [kcal/mol]	E_anlge [kcal/mol]	E_dihed [kcal/mol]	E_impr [kcal/mol]	E_vdw [kcal/mol]	E_coul [kcal/mol]	E_long [kcal/mol]	Press [atm]	Volume [Å ³]
HD-a	-34817.7 255.3	33183.0 145.1	323.0 1.4	-68000.8 211.1	3039.6 48.8	14944.6 102.4	1660.8 28.2	87.3 7.8	9148.3 164.8	283306.2 246.9	-380187.5 7.8	-4.9 168.5	458505.9 1329.9
HD-b	-35635.9 123.6	33185.6 6.1	323.0 0.1	-68821.5 124.7	3014.6 8.2	14824.7 39.1	1580.7 14.6	87.2 0.5	8715.9 75.1	283149.7 97.9	-380194.4 1.6	34.7 10.8	453440.9 647.3
HD-c	-35602.0 130.6	33182.8 2.9	323.0 0.0	-68784.8 131.3	3008.2 7.2	14840.1 29.6	1589.9 17.4	87.2 0.3	8705.3 85.9	283182.2 95.0	-380197.5 0.9	69.6 5.4	453567.7 666.6
HD-d	-35243.6 145.3	33182.3 3.2	323.0 0.0	-68425.9 142.9	3026.2 1.4	14862.7 14.5	1608.4 16.7	87.2 0.5	8879.5 65.7	283296.4 68.0	-380186.2 1.3	4.9 5.0	455400.8 848.9
HD-e	-35053.9 157.4	33179.9 3.2	323.0 0.0	-68233.8 159.8	3029.2 3.7	14882.4 14.2	1633.8 20.4	87.2 0.4	9004.9 66.9	283313.7 67.4	-380185.0 1.0	-2.1 8.5	457074.2 884.8
HD-f	-35062.9 60.3	33184.5 3.5	323.0 0.0	-68247.4 59.7	3029.8 4.0	14885.4 17.1	1627.7 9.3	87.2 0.3	8980.8 30.5	283328.0 14.4	-380186.4 0.8	1.0 6.8	456732.7 434.3
HD-g	-35136.6 69.6	33182.9 6.7	323.0 0.1	-68319.5 75.6	3029.7 6.9	14883.5 27.9	1615.8 14.3	87.3 0.3	8931.6 69.5	283319.1 52.2	-380186.3 1.0	-2.0 6.0	456273.3 443.7
HD-h	-34862.1 115.7	33182.2 3.6	323.0 0.0	-68044.3 116.3	3028.0 8.6	14859.8 42.2	1622.2 16.8	86.7 0.5	8968.0 76.0	283573.6 55.3	-380182.7 1.5	-36.7 6.8	458313.6 725.4
HD-i	-35305.8 106.5	33184.3 4.7	323.0 0.0	-68490.1 102.5	3029.1 3.4	14878.8 19.7	1606.0 11.5	87.4 0.5	8893.5 43.9	283203.2 60.5	-380188.0 2.3	11.5 3.1	455902.2 561.3
HD-j	-36001.8 152.4	33183.3 7.6	323.0 0.1	-69185.1 150.3	3005.5 7.8	14796.6 25.0	1555.9 18.2	87.5 0.6	8495.5 85.8	283070.7 64.8	-380196.8 1.7	50.0 6.1	450916.5 741.5
HD-j_2	-36399.9 267.2	33182.8 145.6	323.0 1.4	-69582.7 218.7	2994.3 49.7	14727.1 108.9	1496.0 26.1	87.1 7.5	8247.6 164.2	279757.9 263.2	-376892.7 7.4	48.5 172.9	448757.1 1261.5
HD-k	-35580.7 128.4	33182.9 8.0	323.0 0.1	-68763.6 128.7	3023.6 4.6	14864.2 24.1	1598.4 14.8	87.8 1.0	8760.7 54.2	283094.7 84.7	-380192.9 0.8	35.5 5.5	453539.9 578.2
HD-k_2	-36143.6 64.6	33193.5 11.7	323.1 0.1	-69337.1 65.6	3002.2 6.7	14758.6 14.5	1536.5 8.4	87.2 0.7	8352.7 51.6	280737.8 53.0	-377812.1 1.5	28.5 11.6	449696.9 420.2
HD-l	-35670.0 114.2	33181.7 7.3	323.0 0.1	-68851.8 115.4	3017.9 6.0	14836.9 26.1	1584.0 11.7	87.5 0.6	8768.8 45.6	283047.0 57.9	-380193.8 2.0	38.3 6.7	453563.1 476.9
HD-l_2	-36267.9 56.7	33181.8 8.8	323.0 0.1	-69449.7 50.1	3004.9 7.4	14755.9 27.5	1512.1 10.5	87.8 0.4	8285.4 35.7	280712.2 73.6	-377808.1 0.8	37.0 15.9	449050.8 243.2

Table V-7 (Continued).

Index	Total E [kcal/mol]	KE [kcal/mol]	Temp [K]	PE [kcal/mol]	E_bond [kcal/mol]	E_anlge [kcal/mol]	E_dihed [kcal/mol]	E_impr [kcal/mol]	E_vdw [kcal/mol]	E_coul [kcal/mol]	E_long [kcal/mol]	Press [atm]	Volume [Å ³]
HD-m	-44743.4	29993.6	291.9	-74737.0	2783.5	13827.8	1424.9	79.3	9067.3	278301.8	-380221.6	50.2	438817.4
	121.4	5.1	0.0	124.6	6.6	23.0	17.4	0.4	57.0	78.7	1.8	14.1	628.1
HD-n	-35939.2	33183.9	323.0	-69123.1	3009.7	14777.8	1543.6	87.4	8498.1	283153.1	-380192.8	-3.5	452154.3
	78.6	5.4	0.1	78.1	7.7	21.3	11.2	0.7	60.7	58.2	1.1	7.9	628.4
HD-o	-35817.9	33191.9	323.1	-69009.9	3013.1	14785.4	1547.3	87.5	8562.3	283183.5	-380189.0	1.7	452484.6
	186.8	7.4	0.1	189.7	5.9	26.4	16.8	0.5	86.8	83.0	1.6	9.2	1100.2
HD-p	-36358.9	33184.7	323.0	-69543.6	2996.4	14726.4	1505.8	87.3	8280.8	283057.5	-380197.8	33.6	448954.3
	173.9	5.8	0.1	175.0	8.5	33.5	17.4	0.6	112.0	72.5	0.9	11.9	983.8
HD-q	-36055.0	33182.1	323.0	-69237.1	2997.4	14757.0	1529.8	87.1	8489.5	283095.6	-380193.4	41.4	451827.9
	152.2	5.4	0.1	153.3	7.9	18.7	11.6	0.6	69.5	85.7	1.5	12.0	1008.8
HD-r	-35858.1	33183.3	323.0	-69041.5	3010.7	14771.5	1547.7	87.6	8538.6	283193.6	-380191.2	-3.8	452965.2
	104.0	5.4	0.1	108.0	7.1	22.2	9.7	0.4	68.3	51.5	1.5	9.2	803.7

5.2.2 Structural Properties

A summary table of selected data showing the different lateral pressures and some of the structural properties appears in Table V-8. Changes in the lateral pressure resulted in a change of the structural properties. The general trend is that by applying higher lateral pressure, i.e. compressing the simulation box, we get a smaller head group area and larger P-P atom distance, which is consistent with physical intuition. Highly negative lateral pressures (surface tensions) led to abnormally high molecular areas. We found that lateral pressures of 50 to 75 atm were optimum when considering the head group area and membrane thickness compared with the previous reported results; as explained in more detail below.

Table V-8 Comparison of MD results for hydrated lipids; second row values are the standard deviations; A is the molecular head group area, D_z the z-dimension box length, D_{mem} is the membrane thickness or P-P atom distance.

Index	P_L [atm]	A [\AA^2]	D_z [\AA]	D_{mem} [\AA]	trans/gauche		
					trans	g(+)	g(-)
HD-b	50.0	66.40	106.70	38.49	0.91	0.04	0.05
		0.51	0.79	0.26	0.008	0.004	0.004
HD-d	1.0	79.28	89.78	33.86	0.90	0.05	0.05
		1.20	1.50	0.54	0.008	0.003	0.005
HD-e	-1.0	82.25	86.86	33.17	0.89	0.06	0.06
		1.23	1.40	0.60	0.009	0.005	0.005
HD-g	-10.0	81.06	87.97	32.83	0.89	0.05	0.06
		1.10	1.27	0.40	0.007	0.001	0.005
HD-h	-51.6	98.51	72.70	29.10	0.89	0.06	0.05
		1.02	0.83	0.29	0.010	0.005	0.005
HD-i	15.0	73.64	96.77	35.98	0.89	0.06	0.05
		1.54	2.13	0.62	0.008	0.003	0.005
HD-j	75.0	61.13	115.26	40.28	0.93	0.04	0.03
		0.81	1.35	0.24	0.008	0.004	0.004
HD-k	51.6	65.21	108.67	38.87	0.90	0.05	0.05
		0.55	0.83	0.19	0.008	0.006	0.003
HD-q	60.0	62.45	113.07	40.52	0.93	0.03	0.04
		0.44	0.70	0.25	0.008	0.004	0.004

The percentage of trans configuration is approximately 90% for most cases, which is approximately 10% higher than that found in other studies; DMPC at 325K by Chiu et al. (1995), and DPPC at 333K by Essmann et al. (1995). The ratio of configurations (trans vs. the rest) is a weak function of pressure and we observe slightly higher percentage of trans configuration at higher lateral pressure, for example, the HD-b case ($P_L = 50$ atm) shows a trans configuration of 91%, while the HD-g case ($P_L = -10$ atm) shows 89%.

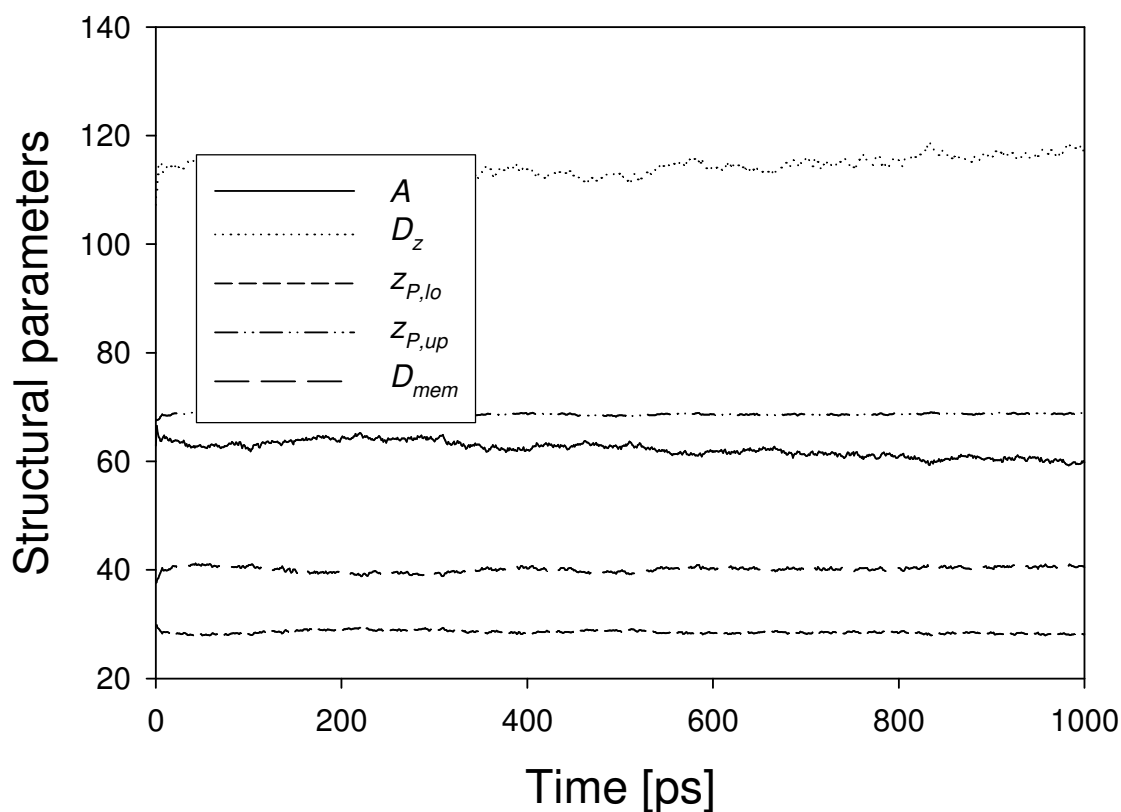


Figure V-13 Structural properties for hydrated lipids; HD-j case.

Several structural properties are plotted against the simulation time in Figure V-13. The properties are equilibrated after 500 ps, including the P-P atom distance, which is a typical amount of time to reach equilibrium in all of our simulations.

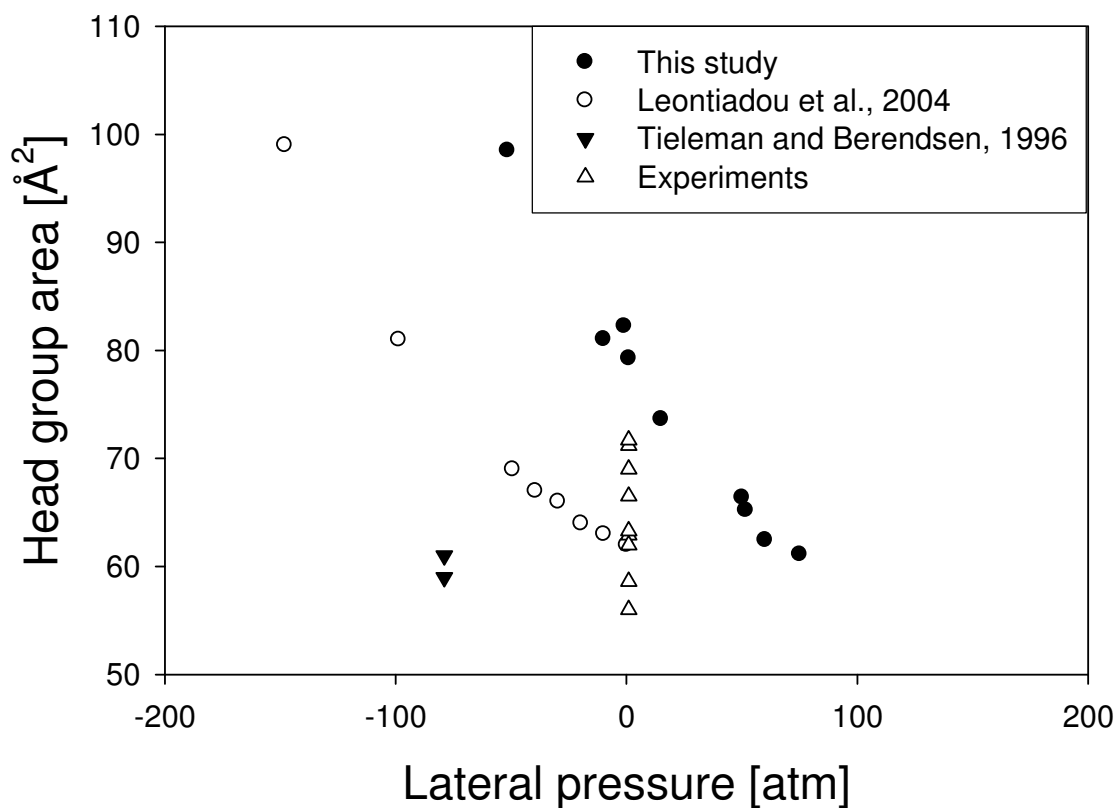


Figure V-14 Comparison of head group areas for different lateral pressures; P_N is maintained at 1atm, data from this study is obtained from the last 500 ps simulations, experimental data are from de Young and Dill, 1988; Lewis and Engelman, 1983; Lis et al., 1982; Nagle, 1993; Nagle et al., 1996; Pace and Chan, 1982; Petrache et al., 2000; Schindler and Seelig, 1975; Thurmond et al., 1991, the P_L for the experimental data is set to 0.

We will now return to the issue of head group area prediction, since we believe this to be a key factor in the validity of our model. We have collected the previous literature

results on the head group area and report a figure showing our simulation data and other researchers' data in Figure V-14. Note that the data of Tieleman and Berendsen are the molecular areas with two different water models (SPC and SPC/E) (1996). Despite the big difference in the lateral pressure, the average head group area doesn't change very much, and this is attributed to the fact that the membrane has relatively small compressibility.

There are several reasons as to why we have to use different lateral pressure to obtain similar values for the head group areas compared to other researchers. First, we used the cvff as our force-field, while others have used different simulation tools such as the GROMOS force-field or GROMACS package. Moreover, they have chosen the SPC or SPC/E water models which were developed to fit the experimental water data, while cvff is a general force-field for peptides and proteins which doesn't necessarily have the best parameters for water. Remembering that Tu and coworker obtained a head group area of 61.8 Å with the CHARMM force-field and an external lateral pressure of 0 atm, based on these results we reach the conclusion that the force-field and/or simulation tool has a huge impact on the choice of simulation details (Tu et al., 1995). Since cvff was not developed for simulations for condensed phase, we recognize that simulations with cvff may not be consistent with other force-field such as GROMOS. Remembering the difference in the diffusion coefficients of water, we arrive at the conclusion that the cvff force-field clearly exhibit greater repulsive forces compared with other force-fields as discussed previously. In other words, the mobility or displacement of water molecules with cvff is overestimated, therefore the hydrated lipid bilayer models require relatively high lateral pressure to obtain similar head group area.

Second, we have to mention that the long-range treatment method characterizes the behavior of the system. Truncation methods for long-range treatments have been widely used in other research groups (Leontiadou et al., 2004; Marrink et al., 1993; Mashl et al., 2001; Tieleman and Berendsen, 1996), while we have employed PPPM to treat the electrostatics. Third, one of the possible reasons for the discrepancy comes from

different algorithm for generating the constant pressure ensemble. We have used the Nosé-Hoover thermostat and barostat, while others have adopted different schemes.

Accepting those possible reasons for the lateral pressure difference, we put an emphasis on the membrane compressibility to understand our results. To explain the argument in detail we recall the concepts related to membrane fluidity. Extending the concept of isothermal compressibility to two dimensional systems, the isothermal lateral compressibility can be defined from the following equation.

$$\kappa_T = -\frac{1}{A} \left(\frac{\partial A}{\partial \pi} \right)_T \quad (\text{V-6})$$

where A is the surface area of a molecule and π is the surface pressure. For a given surface it is known that the sum of the instantaneous surface tension and surface pressure is constant, i.e. $\gamma + \pi = \text{constant}$ (<http://www.nima.co.uk/equipment/ps/wilhelmy.htm>, NIMA Technology, accessed on 5/26/2006).

We are interested in getting an expression of the derivative of the molecular area with respect to the lateral pressure to see how much the area will change when the lateral pressure changes, since we perform simulations in the constant pressure ensemble. Starting from the definition of surface tension (Leontiadou et al., 2004), we obtain an expression of the $\left(\frac{\partial \gamma}{\partial A} \right)_T$ as shown below.

$$\left(\frac{\partial \gamma}{\partial A} \right)_T = \frac{\partial}{\partial A} (L_z (P_N - P_L)) = (P_N - P_L) \left(\frac{\partial L_z}{\partial A} \right)_T - L_z \left(\frac{\partial P_L}{\partial A} \right)_T \quad (\text{V-7})$$

Solving the equation for $\left(\frac{\partial A}{\partial P_L} \right)_T$, we get

$$\left(\frac{\partial A}{\partial P_L}\right)_T = \frac{L_z}{(P_N - P_L)\left(\frac{\partial L_z}{\partial A}\right)_T - \left(\frac{\partial \gamma}{\partial A}\right)_T} \quad (\text{V-8})$$

Jensen and coworkers obtained the mean bilayer area compressibility modulus as $K_A = A_0 \left(\frac{\partial \gamma}{\partial A}\right)_T = 134 \text{ dyn/cm}$ with $A_0 = 62.9 \text{ \AA}^2$ from the regression plot of A vs. γ for DPPC bilayers, which corresponds to $\kappa_T = 0.00746 \text{ cm/dyn}$ (Jensen et al., 2004). From their data, we found that the $\left(\frac{\partial A}{\partial \gamma}\right)_T$ value was $0.469 \text{ \AA}^2/(\text{dyn/cm})$. The calculated slope of $\left(\frac{\partial A}{\partial P_L}\right)_T$ from Leontiadou's data of Table 1 (Leontiadou et al., 2004) was $-0.2488 \text{ \AA}^2/\text{atm}$. The $\left(\frac{\partial A}{\partial \gamma}\right)_T$ from their work was found to be $0.4153 \text{ \AA}^2/(\text{dyn/cm})$, which is quite close to that of Jensen and coworkers as discussed previously ($0.469 \text{ \AA}^2/(\text{dyn/cm})$). The linear regression figures for $\left(\frac{\partial A}{\partial P_L}\right)_T$ from this study and Leontiadou and colleagues are drawn in Figure V-15. From the regression of the simulation data we obtain $\left(\frac{\partial A}{\partial P_L}\right)_T$ as $-0.2931 \text{ \AA}^2/\text{atm}$, which is approximately 20% higher than that of Leontiadou and colleagues.

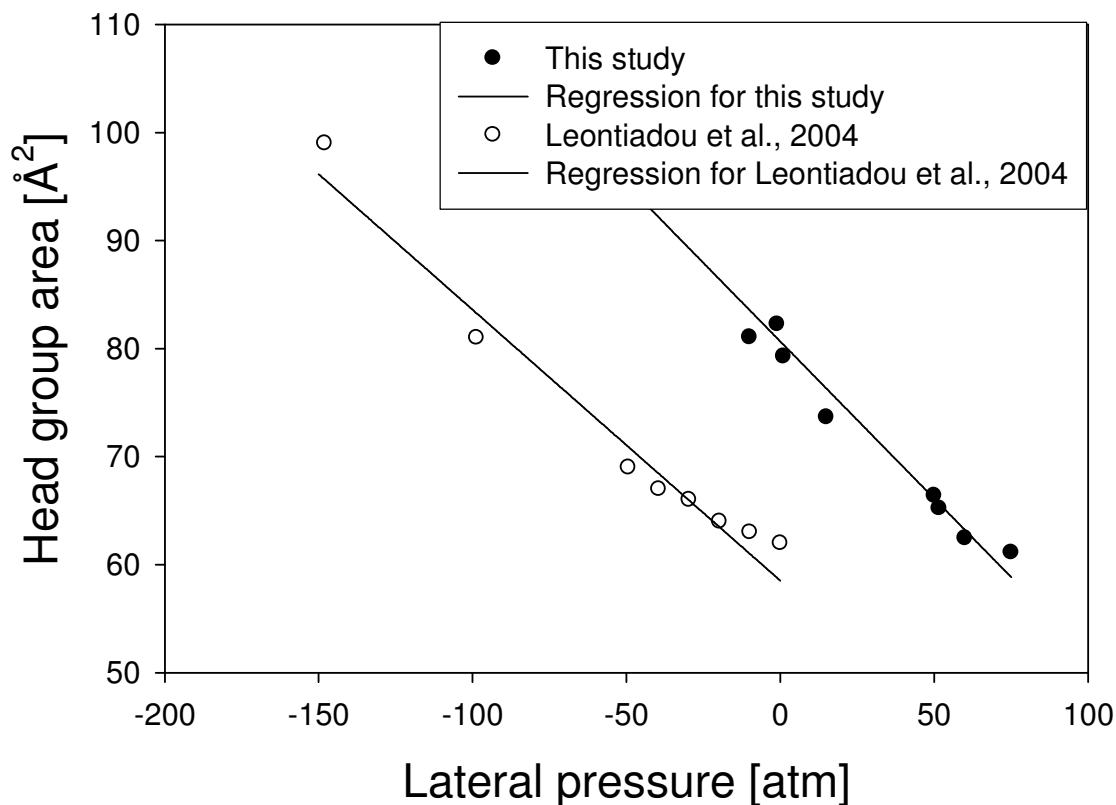


Figure V-15 Regression plots to obtain the lateral compressibility.

Scarлата reported the compressibility results of DMPC at 40 °C as -0.057 to $-0.088/\text{kbar}$, or -5.8×10^{-5} to $-8.9 \times 10^{-5}/\text{atm}$ (1991). Braganza and Worcester estimated the isothermal compressibility to be -0.1 to $-0.6 \times 10^{-4}/\text{atm}$ for DMPC at 19 °C (1986). Comparing the compressibility of bulk water using cvff water model of approximately $6 \times 10^{-5}/\text{atm}$, the cvff water model will predict the structural properties of lipid bilayer without serious artifacts; we think that the literature values are mistakenly using minus sign for the isothermal compressibility values.

A comparison figure for the membrane thickness appears in Figure V-16. Experimental and simulation data from the literature are scattered from 34 to 43 Å. We designate the phosphorous-phosphorous atom distance as the membrane thickness, and report our results with different lateral pressure. The results clearly show that our simulation data are in the same range of other researchers'.

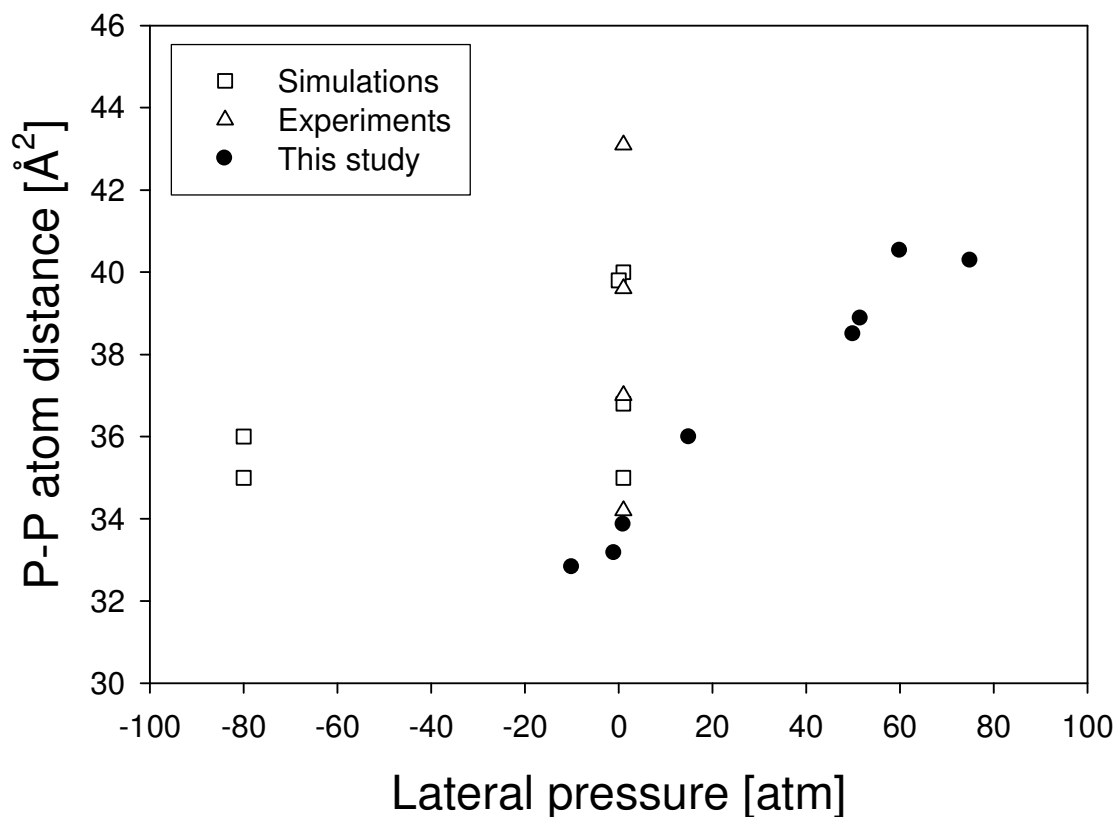


Figure V-16 Comparison of bilayer thickness from literature and current study; Simulation data from Lee et al., 2004; Shinoda et al., 1997; Sum, 2005; Tieleman and Berendsen, 1996; Tu et al., 1995, Experimental data from Inoko and Mitsui, 1978; Lewis and Engelman, 1983; Lis et al., 1982; Nagle et al., 1996.

As mentioned in Chapter I, the order parameter is one of the important parameters to be compared against experiment. The bulky head group is relatively ordered compared to the “floppy” hydrocarbon tails. A 1-ns average order parameters for each carbon chain are shown in Figure V-17. The general trend is that the absolute value of the order parameter decreases along increasing hydrocarbon number for the sn-1 chain, while there is significant difference between the two chains in the water-lipid interface or the region of lower chain numbers. Researchers insist that there be a plateau region, middle of the hydrocarbon (Tieleman and Berendsen, 1996). The average order parameter for the CH₂-groups 4-8 is 0.21 and 0.20 for sn-1 and sn-2 chains respectively.

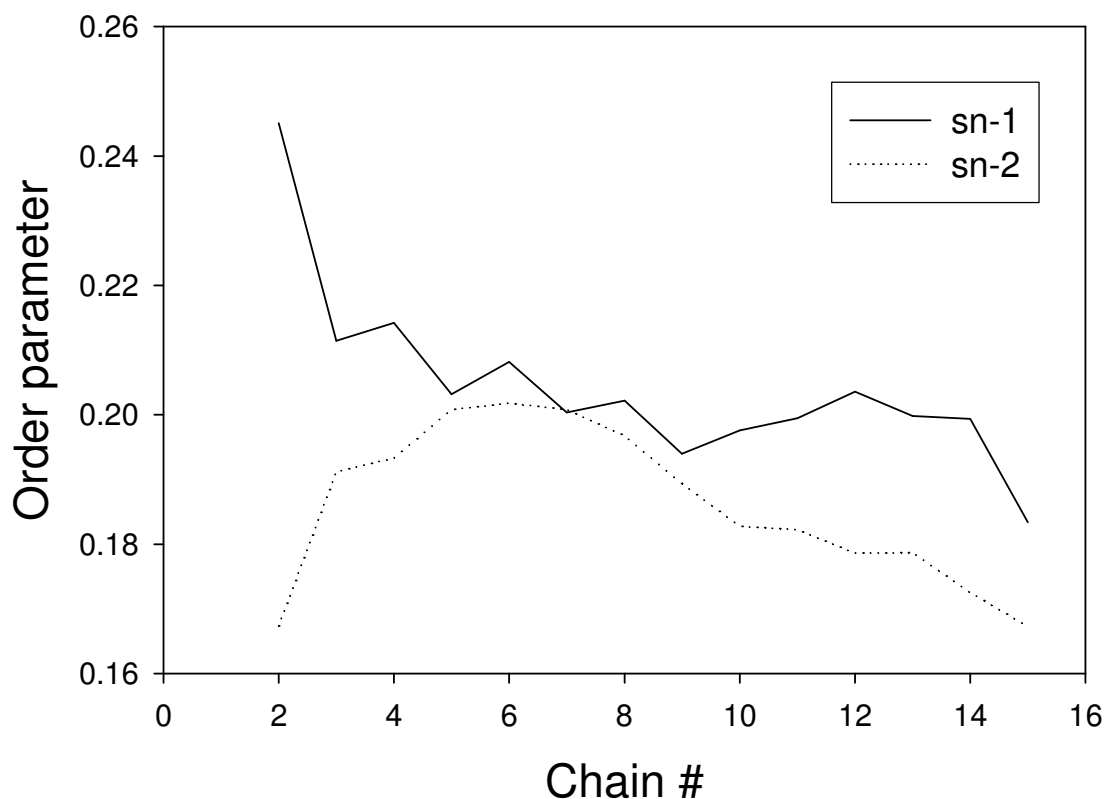


Figure V-17 Order parameters for hydrated lipids; HD-j case.

Figure V-18 compares the order parameters from literature and this work. In general, the order parameter profile can be characterized as a decreasing function of hydrocarbon chain number increase and the tail of the chain loses order. Our simulation results are consistent with previously reported data from the head to middle of the chain, but they don't predict the order in the tail or middle of the bilayer very well. Even some of the published works on the order parameters poorly predict the order parameter profile compared to the experimental results as shown. This is probably because of the choice of the force-field.

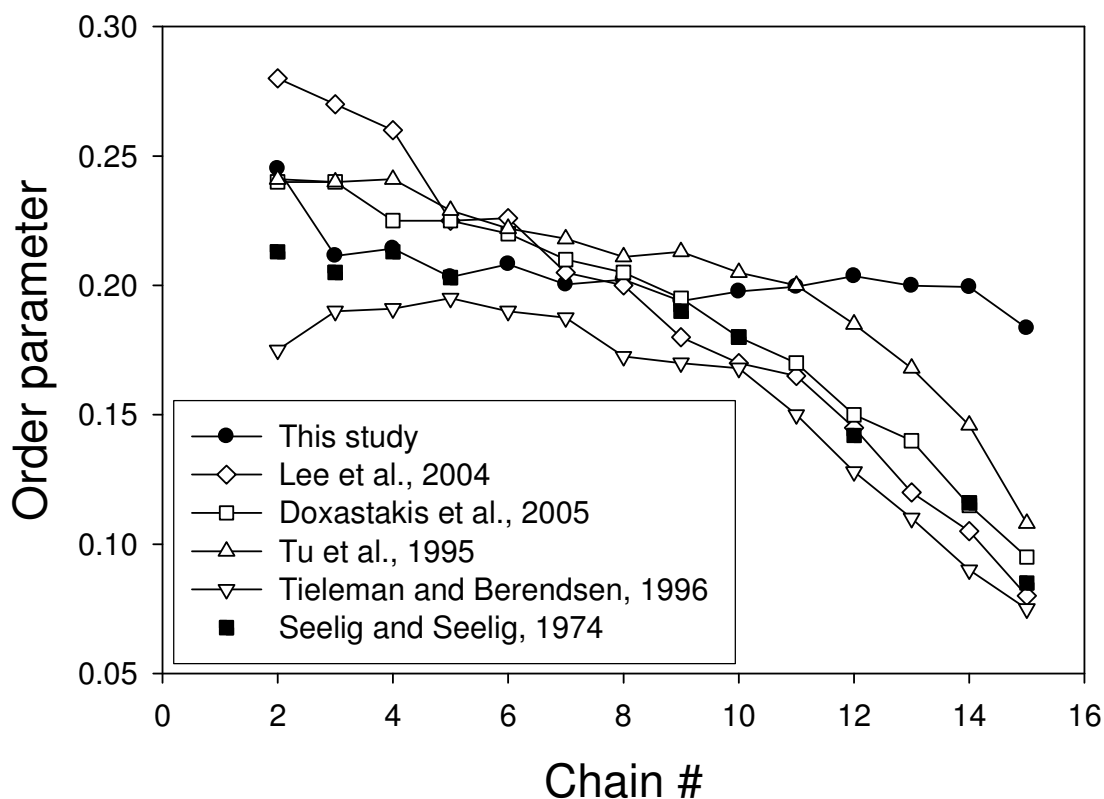


Figure V-18 Comparison of order parameters; This study simulation represents HD-j case study. Curves are generated from data of Doxastakis et al., 2005; Lee et al., 2004; Seelig and Seelig, 1974; Tieleman and Berendsen, 1996; Tu et al., 1995.

Summarizing the discussions in the simulation of hydrated lipids, the optimal pressure to predict the structural properties such as the head group area of approximately 61-66 Å, the membrane thickness of approximately 38-41 Å, and the order parameters of approximately 0.2 for the plateau value was 50 to 75 atm. Considering the structural properties we obtained, we decided to use the lateral pressure as 75 atm to simulate the biomolecular systems consisting of the A β (1-42) or A β (31-42) in hydrated lipid system. Our choice of lateral pressure is somewhat higher than the other research groups due to the choice of force-field and the algorithms employed and this may lead to some differences in the property calculations for the biomolecular systems. We end the discussion in this section with the conclusion that the structural properties such as the molecular head group area and order parameter are largely dependent on the choice of force-field. Therefore, to correctly describe the system we need to check the structural data carefully, even though the simulation parameters, such as the lateral pressure, are unphysical.

5.3 Simulation of A β (1-42) in Water

Before simulating A β (1-42) in hydrated lipids per se, it would be valuable to study A β (1-42) in water, since the system is relatively simple but similar to the case where A β (1-42) is far from the interface with the lipid bilayer. In this section we will discuss the simulation results of A β (1-42) in water at different temperatures and pressures to investigate the protein behavior. The detailed description of the protein model (α -helices with a kink) was described in section 3.2.

5.3.1 Thermodynamic Properties

A simulation box 65 Å which is long in each dimension was constructed. The whole protein was hydrated with the soak function in Insight II. The total number of atoms in the protein/water system is 27396, where 8922 water molecules are present. The system was energy-minimized and a 5 ps MD run without fixing the bonds was performed. The

time step of the system was 0.5 fs and the total potential energy of the system was calculated to be -72714 kcal/mol.

Production simulations were performed with different pressure and temperature to investigate the protein behavior under different physical conditions. The simulation details are tabulated in Table V-9.

Table V-9 Summary of simulation parameters for A β (1-42) in water; the starting data file for all simulations is Ab_H2O_100505_min_1_10k, CAT cluster with 8 cpus.

Index	Original Index	$P_x=P_y=P_z$ [atm]	Time span [ps]	Averages [ps]	Remark
A β _W-A	Ab_H2O_121105_1	1.0	1000	last 500	T = 323K
A β _W-B	Ab_H2O_121105_2	1.0	1000	last 500	T = 310K
A β _W-C	Ab_H2O_121105_3	1.0	77.6	last 47.6	T = 298K
A β _W-D	Ab_H2O_121205_1	1.0	1000	last 500	PPPM $\epsilon = 1.0 \times 10^{-4}$
A β _W-E	Ab_H2O_121205_2	75.0	237	last 137	T = 298K

Profiles of the total and potential energies show that the fluctuations are relatively small compared to the absolute values as shown in Figure V-19. An equilibration period of 100 ps would be sufficient for the A β (1-42) in water system, based on potential energy considerations only.

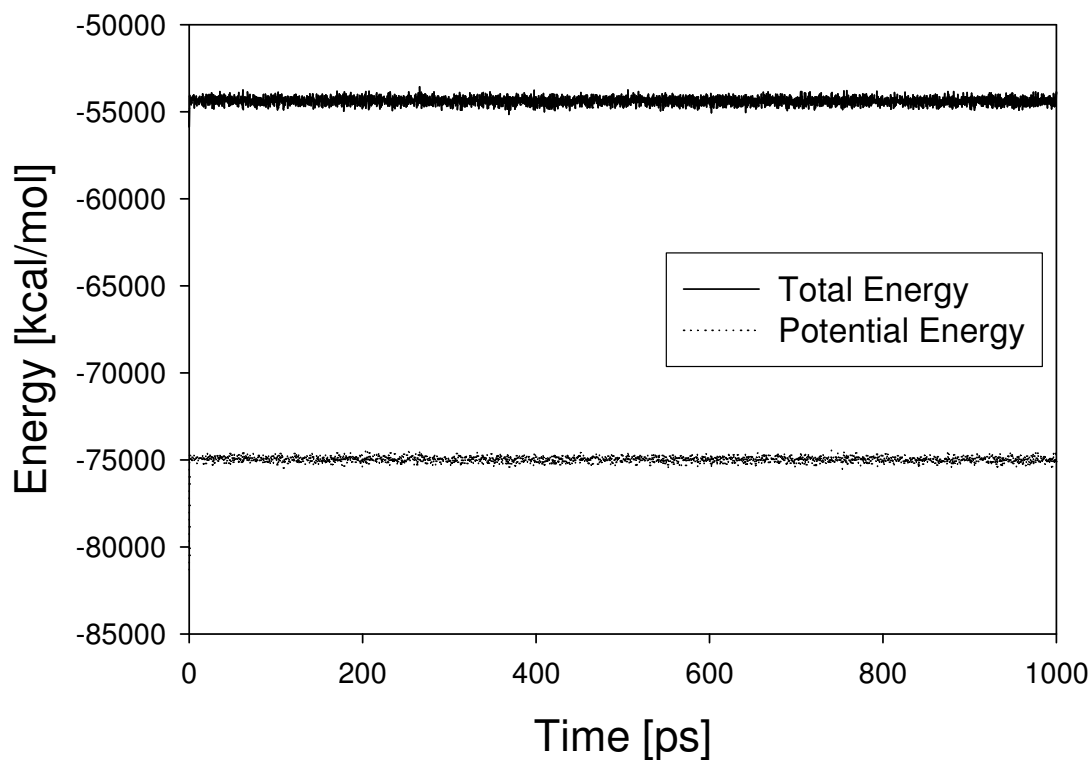


Figure V-19 Energy profiles for A β (1-42) in water simulation; A β _W-A.

The thermodynamic properties of A β (1-42) in water are summarized in Table V-10. By changing the system temperature we observed appreciable differences in the energy terms. For example, the potential energies of A β _W-B (at 310K) and A β _W-C (at 298K) are lower than that of A β _W-A (at 323K). The largest contribution to the difference comes from the nonbonding interactions (the van der Waals and Coulomb energies). The pressure change from 1 atm to 75 atm doesn't affect the thermodynamic properties at all, based on the comparison of A β _W-C and A β _W-E at 298K.

Table V-10 Thermodynamic properties measured from simulations for A β (1-42) in water with different case studies; second row values are the standard deviations.

Index	Total E [kcal/mol]	KE [kcal/mol]	Temp [K]	PE [kcal/mol]	E_bond [kcal/mol]	E_anlge [kcal/mol]	E_dihed [kcal/mol]	E_impr [kcal/mol]	E_vdw [kcal/mol]	E_coul [kcal/mol]	E_long [kcal/mol]	Press [atm]	Volumn [Å ³]
A β _W-A	-54386.6 13.6	20596.3 3.6	323.0 0.1	-74982.9 15.5	287.1 2.2	5539.6 4.8	72.4 0.9	25.1 0.3	10820.8 5.7	264984.0 11.0	-356711.8 0.2	-2.8 3.5	293205.1 104.9
A β _W-B	-56834.8 17.7	19766.7 3.6	310.0 0.1	-76601.5 19.2	277.9 2.6	5438.5 7.2	71.8 0.4	24.2 0.2	11205.1 11.3	263102.4 24.1	-356721.3 0.3	-2.7 1.7	288961.3 139.9
A β _W-C	-59090.4 171.9	19006.8 107.3	298.1 1.7	-78097.2 139.7	273.4 14.3	5367.5 65.8	71.3 5.8	23.9 3.3	11589.7 132.1	261306.9 216.0	-356729.9 6.0	3.7 120.9	285197.6 858.9
A β _W-D	-54369.4 14.5	20593.2 1.8	323.0 0.0	-74962.6 14.6	289.2 2.9	5530.4 4.2	74.1 0.5	25.5 0.1	10830.4 4.8	351198.3 14.5	-442910.6 0.7	0.0 3.7	293275.1 75.1
A β _W-E	-59178.5 201.4	19006.6 187.9	298.1 2.9	-78185.1 179.5	274.0 14.5	5361.3 73.9	71.6 6.4	23.7 3.5	11630.8 145.8	261183.8 271.0	-356730.3 6.1	51.7 807.6	283897.9 945.0

5.3.2 Structural Properties

The standard deviation of the simulation box length for all cases studied cases is less than 0.5% of the total simulation box volume. A profile of the box length is plotted in Figure V-20 for A β _W-A, where the pressure is 1atm.

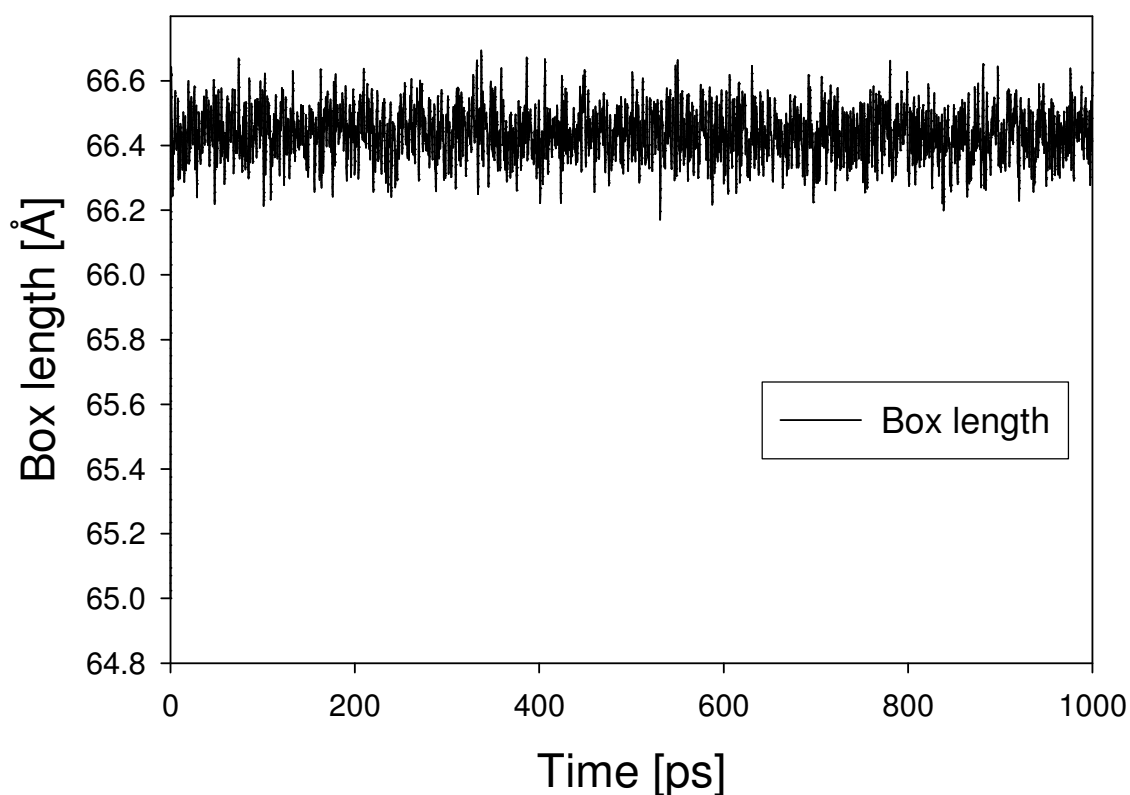


Figure V-20 Box length profiles for A β (1-42) in water simulation; A β _W-A case.

The profile of the number of hydrogen bonds is shown in Figure V-21 for the A β _W-A case. A hydrogen bond breaking environment is necessary for the transition of α -helix to β -sheet (Mager, 1998a), we examine the number of H bonds during the

simulation. It is known that the hydrogen-donor-accepter distance is generally between 2.7 and 3.4 Å (http://web.chemistry.gatech.edu/class/peek/4581/labs/pdb_tutorial.pdf, accessed on 5/24/2006). The number of hydrogen bonds was obtained by counting the cases when the distance between the oxygen atom of *i*-th CO and the nitrogen atom of (*i*+4)-th NH is less than 3.4 Å to check the stability of α -helix. We measured the number of hydrogen bonds starting from the residue 1 to residue 38. We clearly see that the protein changes its conformation as the system evolves. After 600 ps of simulation time, we observe that the total number of hydrogen bonds fluctuates around 4. From the profile of the number of hydrogen bonds we reach the conclusion that some parts of A β (1-42) lose its α -helical structure in bulk water within 1 ns simulation time.

The profiles of end-to-end distance, the distance between N-terminal and C-terminal atoms or H₃N...COO, and the radius of gyration of the protein are plotted in Figure V-22. The end-to-end distance is reduced to approximately 28 Å at the end of the simulation compared to the starting value of approximately 50 Å, which indicates that the protein changes its conformations from a helical structure to a more globular structure. The radius of gyration of the protein has similar trend, showing approximately a 4.5 Å decrease in its value. The difference between R_G and R_g is negligible for the model simulations, for example at the final configuration R_G of 11.76 Å and R_g of 11.88 Å are found. Therefore, from now on the radius of gyration refers to R_G .

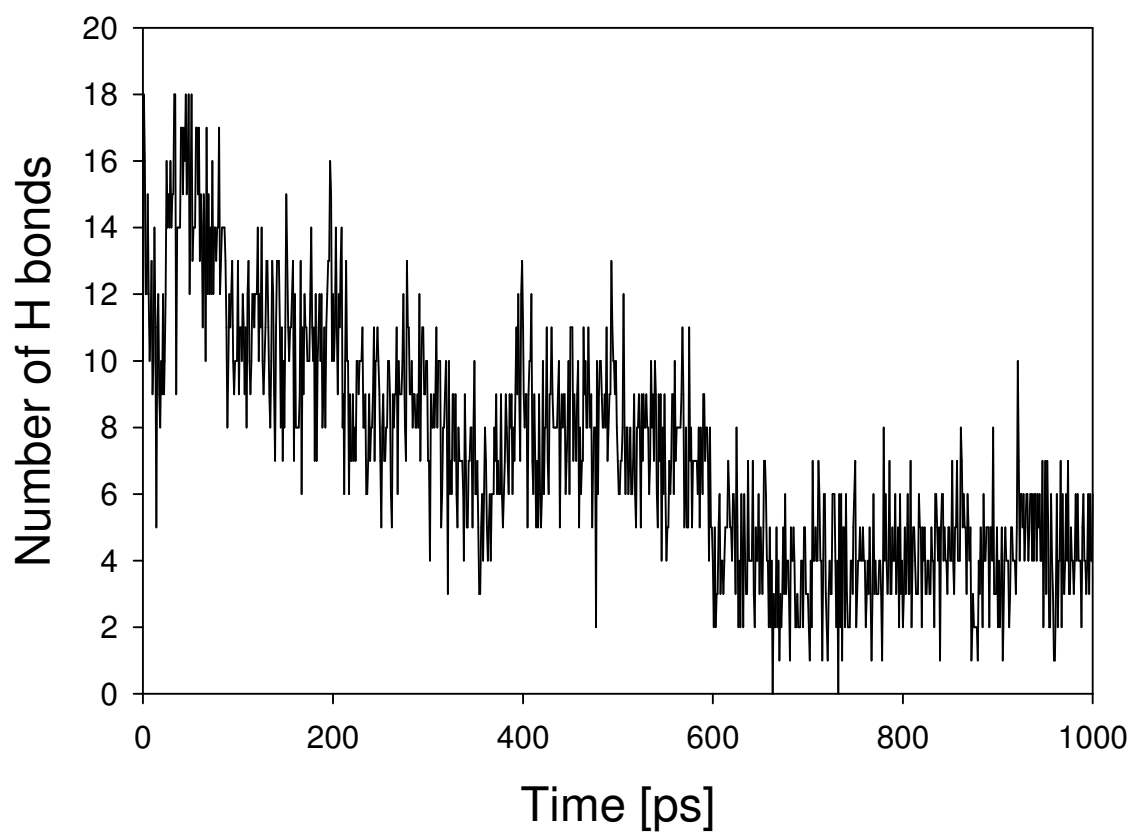


Figure V-21 Profile of the number of H bonds for A β (1-42) in water simulation; A β _W-A case.

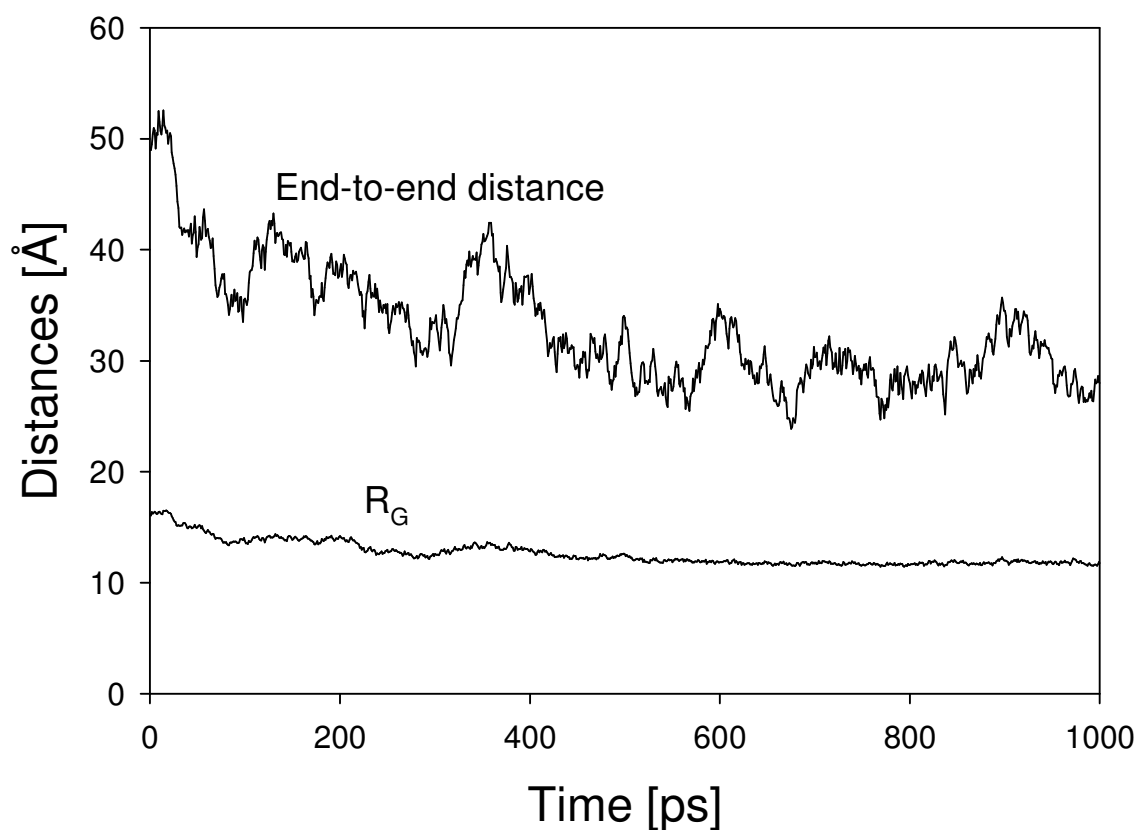


Figure V-22 Profiles of end-to-end distance and R_G for $A\beta(1-42)$ in water simulation; $A\beta_W-A$ case.

The RMS deviations of the heavy atoms in $A\beta(1-42)$ at two different temperatures are plotted in Figure V-23. During the simulation 101 frames were saved and 3-D structures were generated to create animations. In Figure V-23, the RMS deviation profiles show that at the beginning of the simulations, the protein has a characteristic change in its conformation and after 500ps of simulation time, there is little conformational change. At 323K ($A\beta_W_A$) the protein changes its conformation relatively faster than at 310K ($A\beta_W_B$).

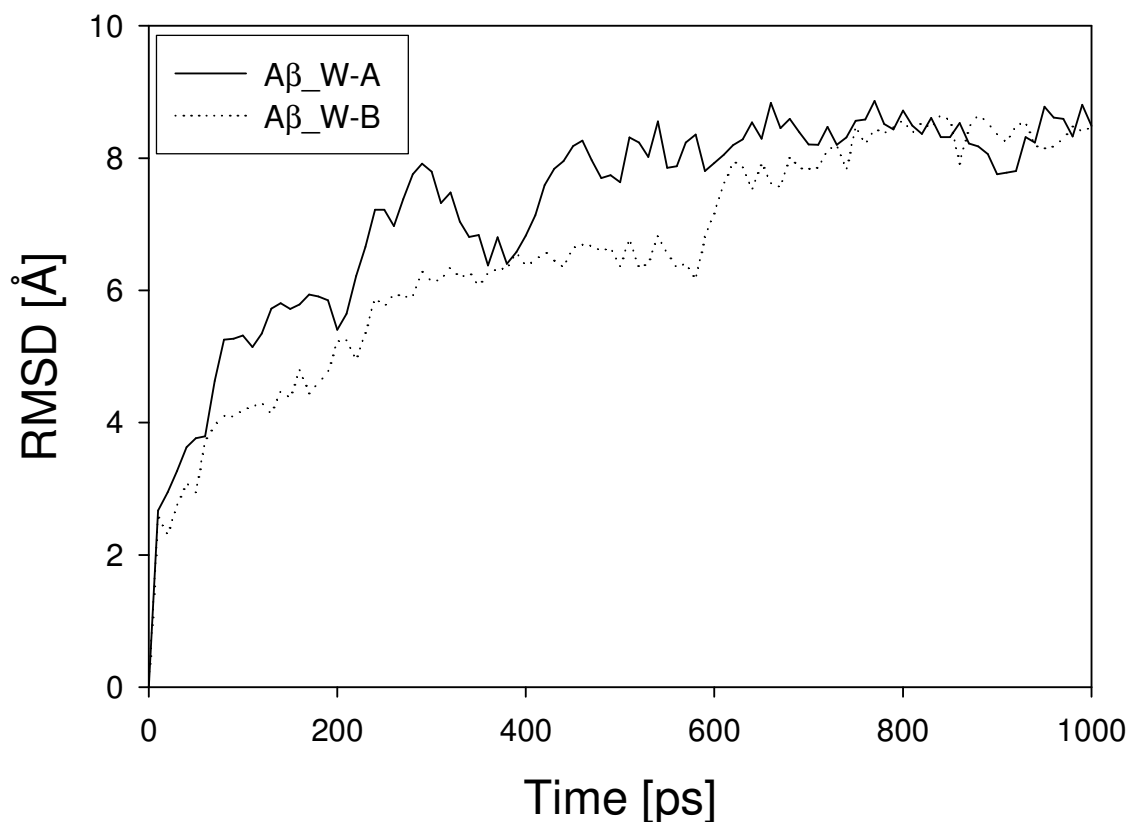


Figure V-23 Comparison of RMS deviations for A β (1-42) in water simulation; A β _W-A (at 323K) and A β _W-B (at 310K) cases.

From the animations we found that the protein maintains some helical structure throughout the simulations, however, the residues near the kink change their structure conformation, as will be discussed in the later paragraphs.

Snapshots of A β (1-42) in water are shown in Figure V-24, where water molecules are intentionally hidden for clarity. Figure V-24 shows both the starting configuration (red ribbon) and the last snapshot (cyan ribbon) after 1ns simulation time. We observe well constructed helical structure with a kink at the beginning of the simulation for A β (1-42) in the figure. The ending configuration shows that the protein has lost a small

portion of its helical structure near kink itself, and the kink became much looser. Lee and Kim have pointed out that loss of helical character can be prevented by adding TFE, an agent that induces the helical structure in the A β protein, though their study was limited to a fragment of A β (25-35) at 300K (Lee and Kim, 2004). Also, the conformation data (Table V) dependent on the peptide concentration and the concentration of the solvents such as TFE and HFIP(Hexafluoro-2-propanol) showed that the percentage of β -sheet conformation is greatly reduced due to the solvents (Mager, 1998b). We also see that the distance between the N- and C-terminus became shorter after the simulation from Figure V-24, which matches what we concluded from the end-to-end distance profile.

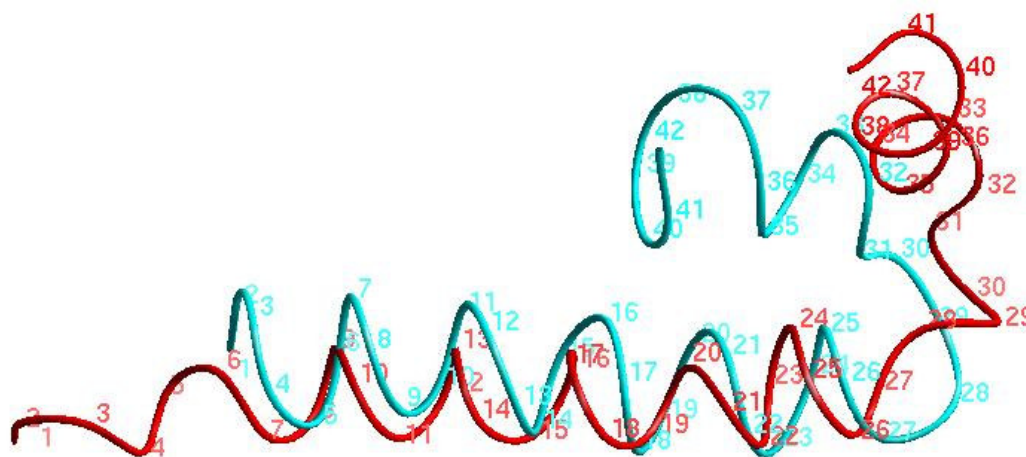


Figure V-24 Snapshots for A β (1-42) in water; 2 frames, red ribbon represents the initial structure, cyan ribbon is the last structure, A β _W-A case.

As a short summary on the results and discussion in this section, combining the analysis of the structural properties for A β (1-42) in water simulations, we observed that the protein experiences a secondary structure change near the kink, losing some helical conformation within 1 ns of simulation and becoming more compact than the starting configuration. We also observed that the structural change occurs faster at higher temperature.

5.4 Simulation of A β (31-42) β -Sheet Conformation in Water

As discussed in previous research, it is widely accepted that β -sheet conformation plays a pivotal role in the formation of A β aggregates. Our simulations are not long enough to observe the conformation change from an α -helical structure to a β -sheet structure. Therefore, we will carry out the simulations with a β -sheet conformation for this study. In this section of study we discuss the simulation results of protein fragment of A β (31-42) in water. The A β (31-42) fragment was chosen for study since it is highly hydrophobic and has a high probability of forming a β -sheet structure. The protein fragment with β -sheet conformation was hydrated and the system was energy-minimized. The starting configuration of the protein fragment A β (31-42) was obtained as described in section 3.2 and the total number of atoms in the systems is 27544 including 9123 water molecules.

5.4.1 Thermodynamic Properties

Simulations with different temperatures and pressures were performed. Table V-11 describes the simulation conditions for the set of simulations. The total and potential energy profiles are plotted in Figure V-25 for the A β _W- β a case study. Considering the energy profiles only, we see that the system is equilibrated within 100 ps of simulation time as observed in the simulations of A β (1-42) in water.

Table V-11 Summary of simulation parameters for A β (31-42) β -conformation in water; the three pressure components are coupled.

Index	Original Index	Machine	P _x = P _y [atm]	P _z [atm]	Span [ps]	Average [ps]	Remark
A β _W- β a	Ab_frag_B_H2O_120505_1	CAT/8cpus	1.0	1.0	1000	last 500	
A β _W- β b	Ab_frag_B_H2O_120505_2	CAT/8cpus			1000	last 500	NVT
A β _W- β c	Ab_frag_B_H2O_120505_3	CAT/8cpus	1.0	1.0	1000	last 500	T=310K
A β _W- β d	Ab_frag_B_H2O_120505_4	CAT/8cpus	1.0	1.0	1000	last 500	T=298K
A β _W- β e	Ab_frag_B_H2O_120705_1	CAT/8cpus	100.0	100.0	1000	last 500	

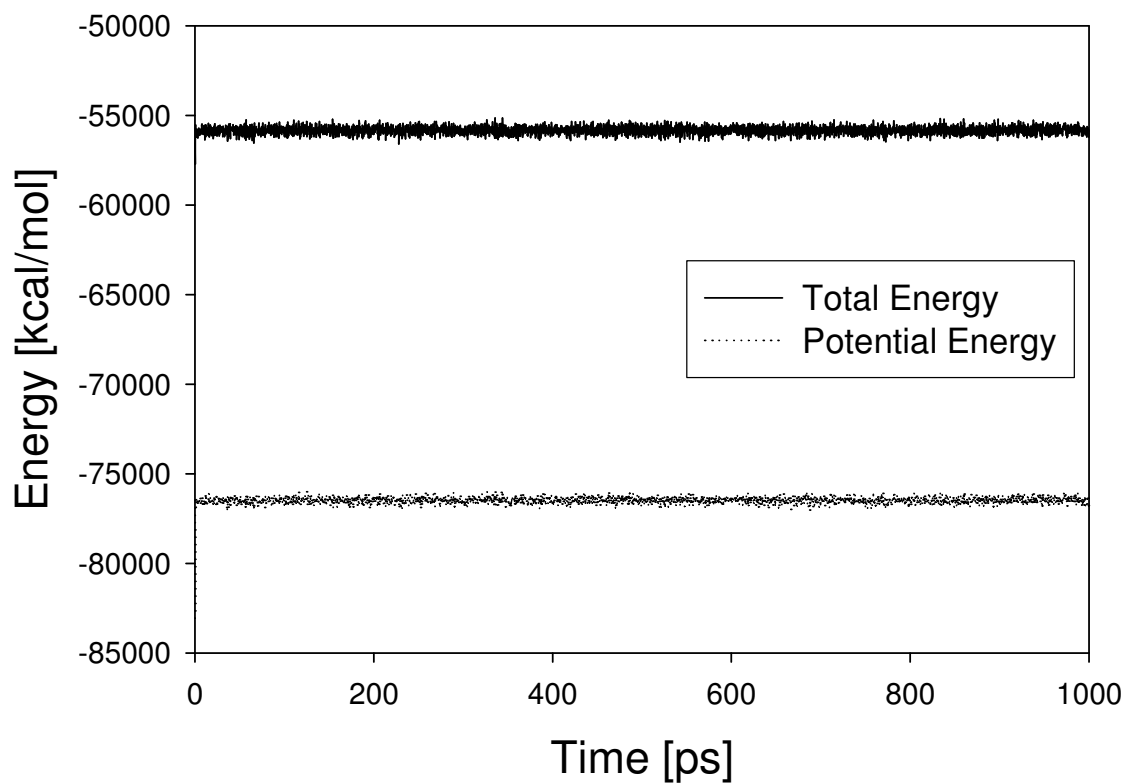


Figure V-25 Energy profiles for A β (31-42) β -sheet conformation in water simulation; A β _W- β a.

We report the thermodynamic properties from the simulation in Table V-12 for A β (31-42) β -sheet conformations. The difference in temperature resulted in the differences in the potential and total energies maintaining the same density of water; the difference in box dimension is negligible for cases A β _W- β a (323K), A β _W- β c (310K), and A β _W- β d (298K).

5.4.2 Structural Properties

Several structural properties of the protein fragment are discussed in this section. We checked the number of hydrogen bonds along the simulation time using the same criterion discussed in section 5.3.2. The maximum number of hydrogen bonds to identify the α -helical structure for this system within the protein fragment is 8, since it consists of 12 residues. The profile of the A β _W- β a case shows mostly 0 for the number of hydrogen bonds with some exceptions (figure not shown in this dissertation). Only 1 H bond is observed during the simulation starting from a β -sheet, thus indicating little change to form a helical structure. However, we need to investigate other indicators such as a Ramachandran plot, which shows the dihedral angles between different backbone atoms as supporting materials. This task remains as one of our future plans.

The profiles of R_G and the end-to-end distance between the N-terminus (residue 31, Ile), and C-terminus (residue 42, Ala) are drawn in Figure V-26. Even though the number of hydrogen bonds doesn't vary much, the protein fragment changes its conformation. It starts with an extended structure and became more compact as indicated by the distance between the two ends becoming shorter. The radius of gyration decreases during the simulation time, which also supports that it becomes more compact or globular.

Table V-12 Thermodynamic properties measured from simulations for A β (31-42) in water with different case studies; second row values are the standard deviations.

Index	Total E [kcal/mol]	KE [kcal/mol]	Temp [K]	PE [kcal/mol]	E_bond [kcal/mol]	E_anlge [kcal/mol]	E_dihed [kcal/mol]	E_impr [kcal/mol]	E_vdw [kcal/mol]	E_coul [kcal/mol]	E_long [kcal/mol]	Press [atm]	D _x [Å]
A β _W- β a	-55834.0 20.6	20641.0 3.7	323.0 0.1	-76475.0 21.5	65.2 0.9	5288.4 13.5	16.5 0.5	5.3 0.1	11008.0 12.6	270487.6 42.4	-363346.0 0.5	-0.3 5.2	66.6 0.0
A β _W- β b	-57401.6 11.3	20639.0 3.6	323.0 0.1	-78040.6 13.5	62.0 1.9	5371.1 6.3	16.9 0.4	5.5 0.2	11805.4 9.3	268057.0 25.5	-363358.5 0.3	1300.2 8.0	
A β _W- β c	-58316.8 10.5	19811.7 6.1	310.0 0.1	-78128.5 8.5	63.4 0.8	5197.0 5.0	16.3 0.4	5.3 0.2	11404.8 6.3	268540.2 14.0	-363355.6 0.6	-0.3 3.9	66.3 0.0
A β _W- β d	-60607.1 9.3	19043.2 3.5	298.0 0.1	-79650.3 8.0	59.3 1.1	5114.7 4.9	14.5 0.3	4.8 0.1	11789.4 8.4	266730.9 14.5	-363363.9 0.4	2.3 3.0	66.0 0.0
A β _W- β e	-55995.2 8.3	20639.5 3.4	323.0 0.1	-76634.7 11.3	62.2 1.1	5297.1 6.7	15.8 0.2	5.3 0.0	11072.5 10.3	270259.5 23.7	-363347.1 0.4	102.0 6.1	66.4 0.0

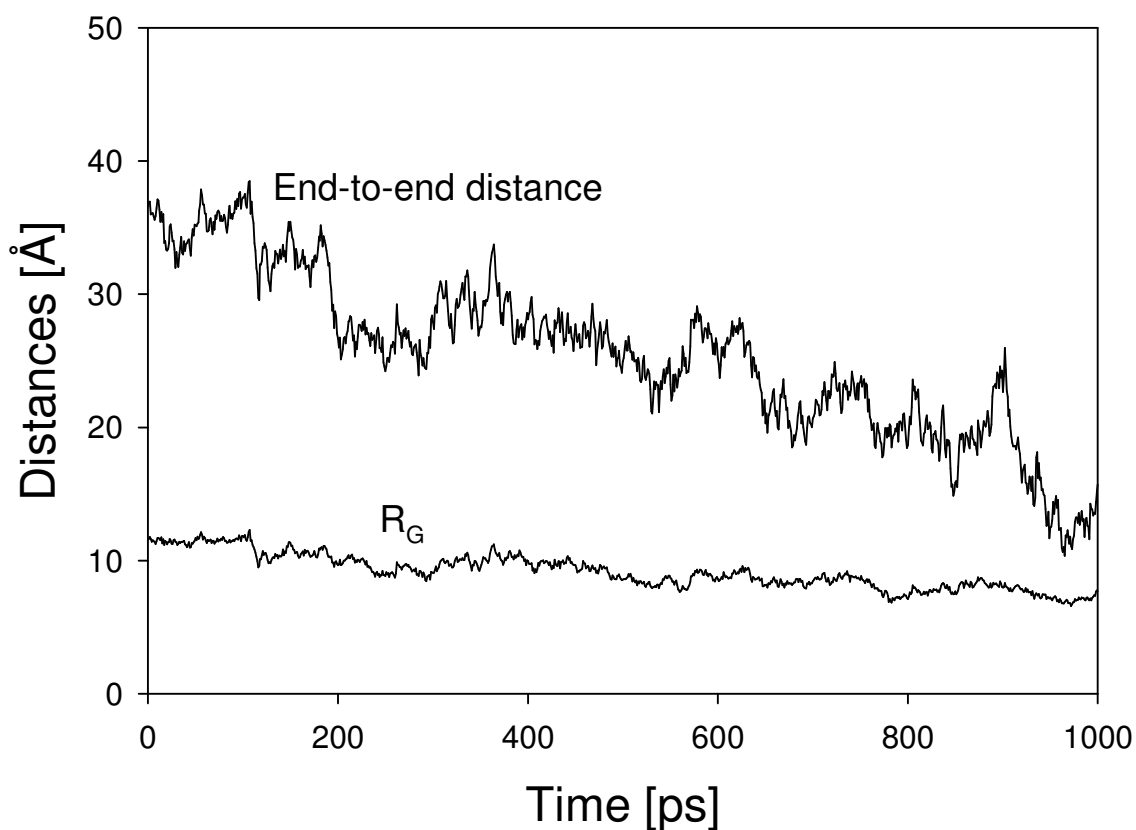


Figure V-26 Profiles of end-to-end distance and R_G for $A\beta(31-42)$ β -sheet conformation in water simulation; $A\beta_W$ - β_a .

The starting and ending configurations of $A\beta(31-42)$ β -sheet in water are shown in Figure V-27. The protein fragment starts with a long extended conformation and the final configuration shows a bent conformation, especially residues 35 (Met) to 38 (Gly). According to a web resource of hydrophobicity index (<http://www.web-books.com/moBio/Free/Ch2A2.htm>, accessed on 6/1/2006), the terminal residues such as Ile(31,32) and Val(39,40), Ile(41), and Ala(42) have higher hydrophobic indices than those of the middle of the fragment (4.5 for Ile (residues 31,32, and 41), -0.4 for Gly (residues 33,37,38), 3.8 for Leu (residue 34), 1.9 for Met (residue 35), 4.2 for

Val(residues 36,39,40), 1.8 for Ala(residue 42)), therefore, it is hypothesized that the hydrophobic interaction between the terminal residues dominate and lead to a bent structure in the middle. Mager also provided the hydrophobicity index profiles showing that residues 28 (Lys) to 40 (Val) form a hydrophobic core with relatively low hydrophobicity in residues 32(Ile) to 36(Val) (Figure 2 and Figure 3), which supports our hypothesis (1998b) from their study of A β (1-42). It is clear that the protein fragment becomes bent during the simulation matching the fact that the end-to-end distance reduces to a half of the starting distance. The radius of gyration plot also confirms that the fragment becomes compact or bent along the time evolution. This is probably because of the fact that there is strong hydrophobic interaction between the fragment A β (31-42) which is highly hydrophobic.

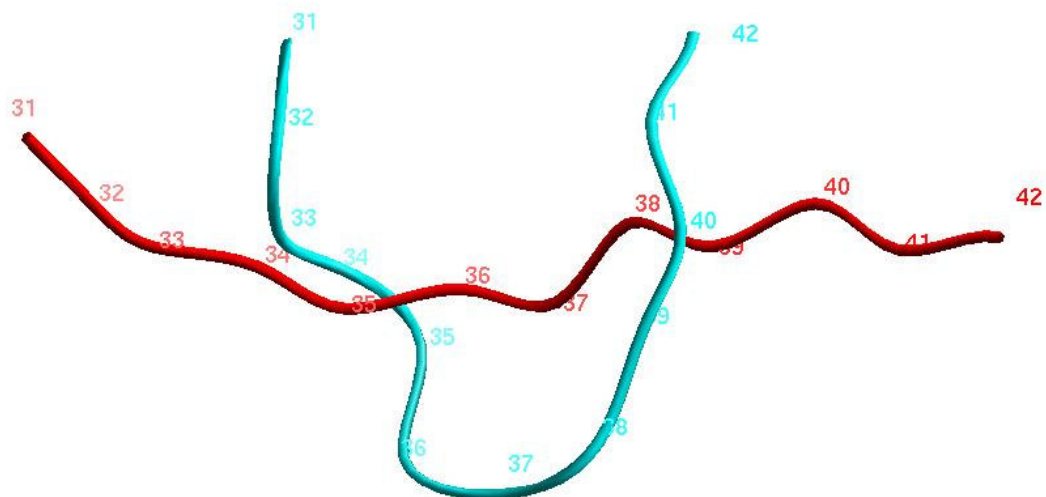


Figure V-27 Snapshots for A β (31-42) β -sheet conformation in water; 2 frames, red ribbon represents the initial structure, cyan ribbon is the last structure, A β _W- β a case.

Consequently, based on the simulation results of A β (31-42) with β -sheet conformation in water we found that the protein fragment changes its conformation to a bent structure, probably because of the hydrophobicity of the fragment. The profiles of R_G and end-to-end distance support the observation of the structural change of the protein fragment.

5.5 Simulation of A β (1-42) near Hydrated Lipids

Since we have studied simulations of the full protein or the fragment in water, we move on to the more complicated but realistic problems, where the protein or the fragment interacts with the lipid bilayer for the following two sections 5.5 and 5.6. In this section we focus on the A β (1-42) behaviour near hydrated lipids. This part of dissertation is not completely finished and the analysis process is under progress. However, we present some of the results and discussions we have done so far.

5.5.1 Simulation of A β (1-42) – A β Series

As described in section 3.2, three sub-boxes, i.e., bulk water, A β (1-42) in water, and DPPC bilayer, were merged and formed a simulation box with dimensions 63.4 \times 63.4 \times 107.2 \AA^3 . Since the protein itself is very large it is not feasible to manually place A β at different locations and perform simulations. Simulations with different ensemble, lateral pressure, and PPPM accuracy criterion have been performed. The simulation conditions and results of thermodynamic properties are shown in Appendix C. In this section we discuss one representative simulation result (A β -E case), where the lateral pressure was set to -100 atm, while the normal pressure was 1 atm.

Figure V-28 shows the energy profiles as functions of the simulation time for case A β -E. We can conclude that 200 ps (or 100000 steps) is sufficient to equilibrate this system. Moreover, 500 ps simulations will provide reasonable estimates of thermodynamic properties (These statements are based on the total potential energy

only; this quantity is not likely to be sensitive to subtle changes in peptide or membrane structure).

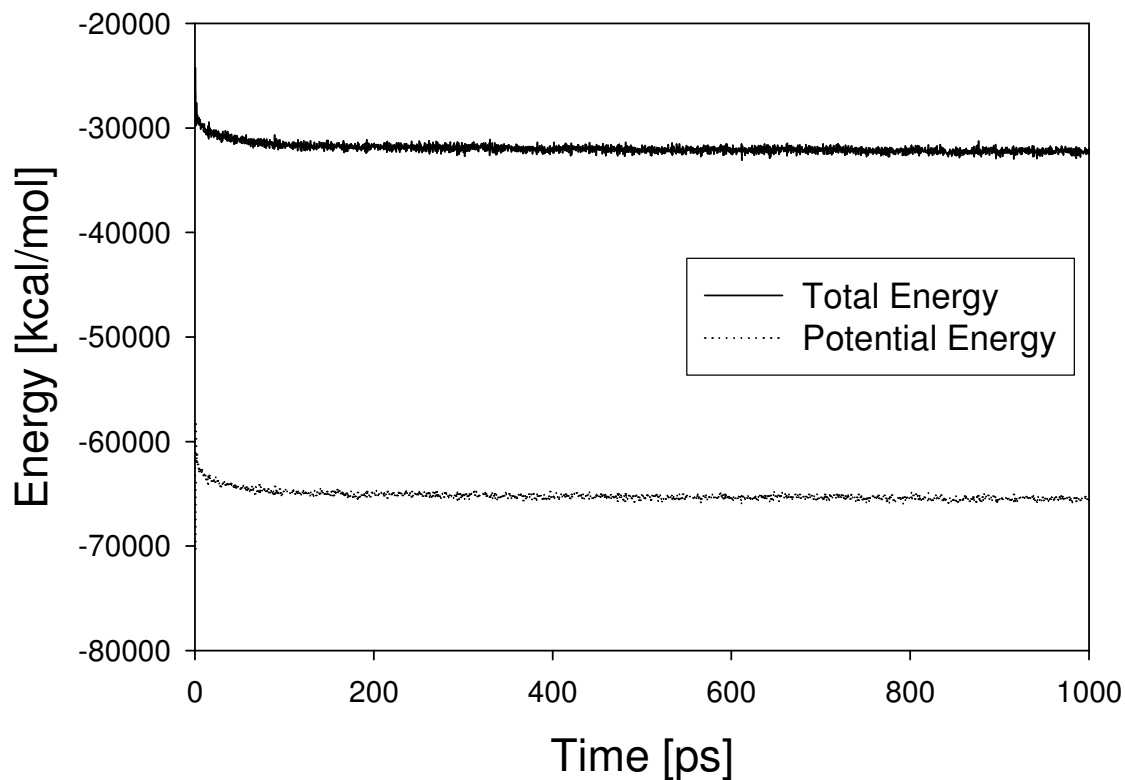


Figure V-28 Energy profiles for A β (1-42) near hydrated lipids; A β -E case.

We next investigate the structural property changes with simulation time. Some of the structural properties of DPPC for the A β -E case simulation are plotted in Figure V-29. We observe that the average P-P atom distance becomes smaller as the system evolves, implying that the membrane is compressed in the z -direction (thickness).

Conversely, the average head group area per DPPC molecule expands with simulation time.

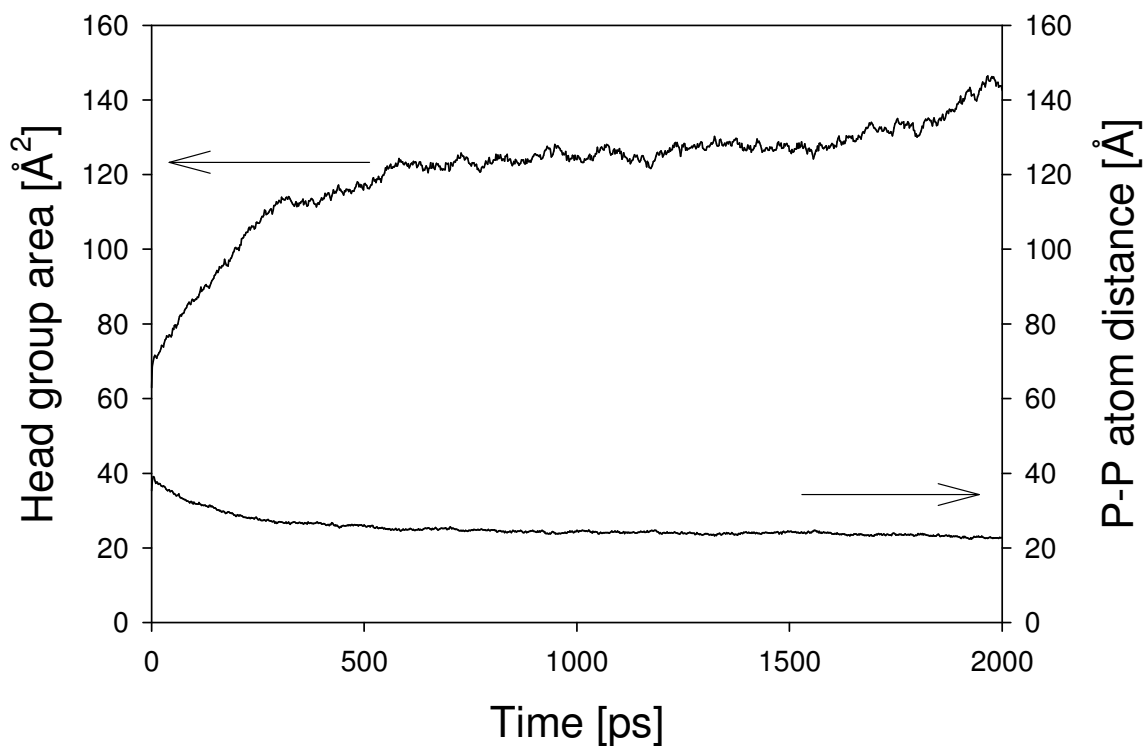


Figure V-29 Profiles of DPPC structural properties for A β (1-42) near hydrated lipids; A β -E case.

Next, we examine the protein behavior with simulation time. The profiles of some structural properties of A β (1-42) are shown in Figure V-30. The z-component of COM of A β protein moves toward the middle of the simulation box. The movement is significant from the beginning of the simulation up to 500 ps. The end-to-end distance exhibits a sudden increase, then decreases initially, becomes smaller at the end of the simulation. The radius of gyration changes very little, decreasing from 16 to 14 Å.

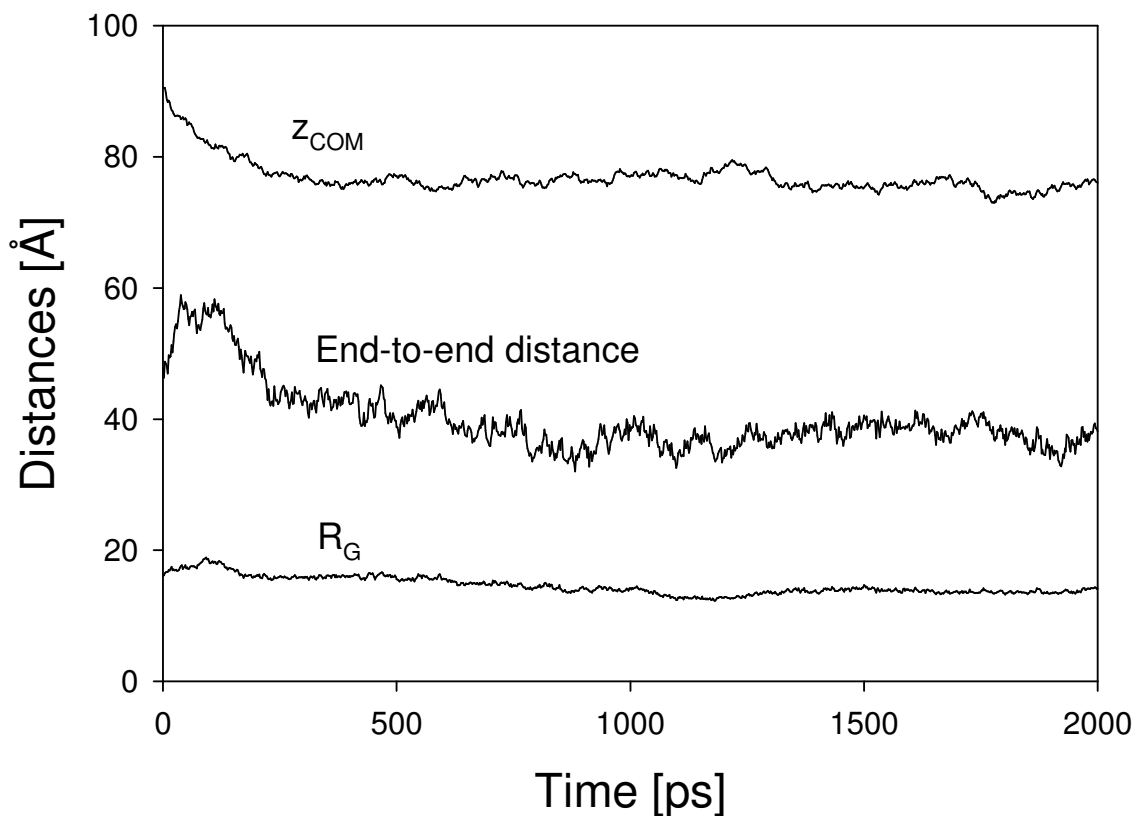


Figure V-30 Profiles of structural properties for A β (1-42) near hydrated lipids; A β -E case.

The profile of the number of hydrogen bonds, as described in Section 5.3, is drawn in Figure V-31. A sharp decrease in the number of H bonds was observed over the first 300 ps. The number of H bonds remains pretty much the same after 300 ps (~ 5), indicating that the protein doesn't change its structure very much compared to the initial change. The average number of H bonds for the last 500 ps was found to be 4.72.

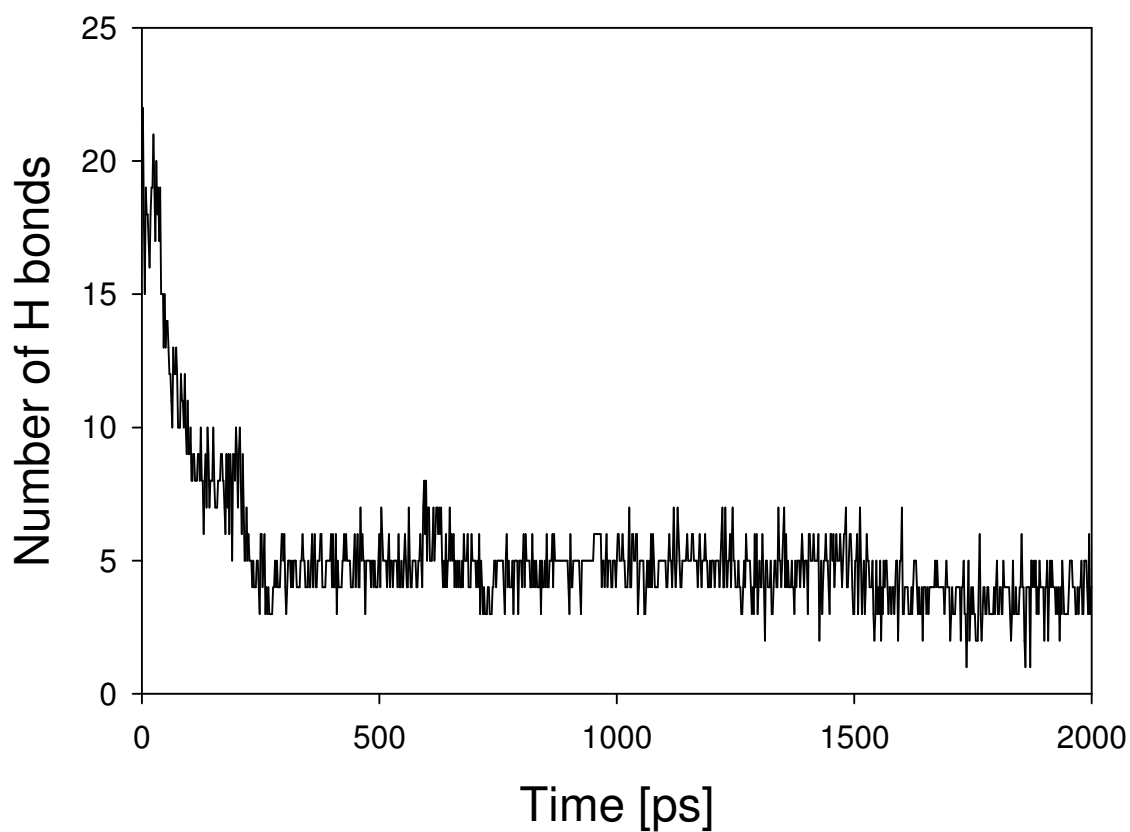


Figure V-31 Profile of the number of H bonds for A β (1-42) near hydrated lipids; A β -E case.

To identify the relationship between the protein structure change and the interaction between the protein and the interface of hydrated lipids, the distance D between the protein COM and the bilayer interface has been calculated and plotted in Figure V-32. As the COM of the protein varies, D also changes. The system undergoes sudden structural change initially, as confirmed by Figure V-31.

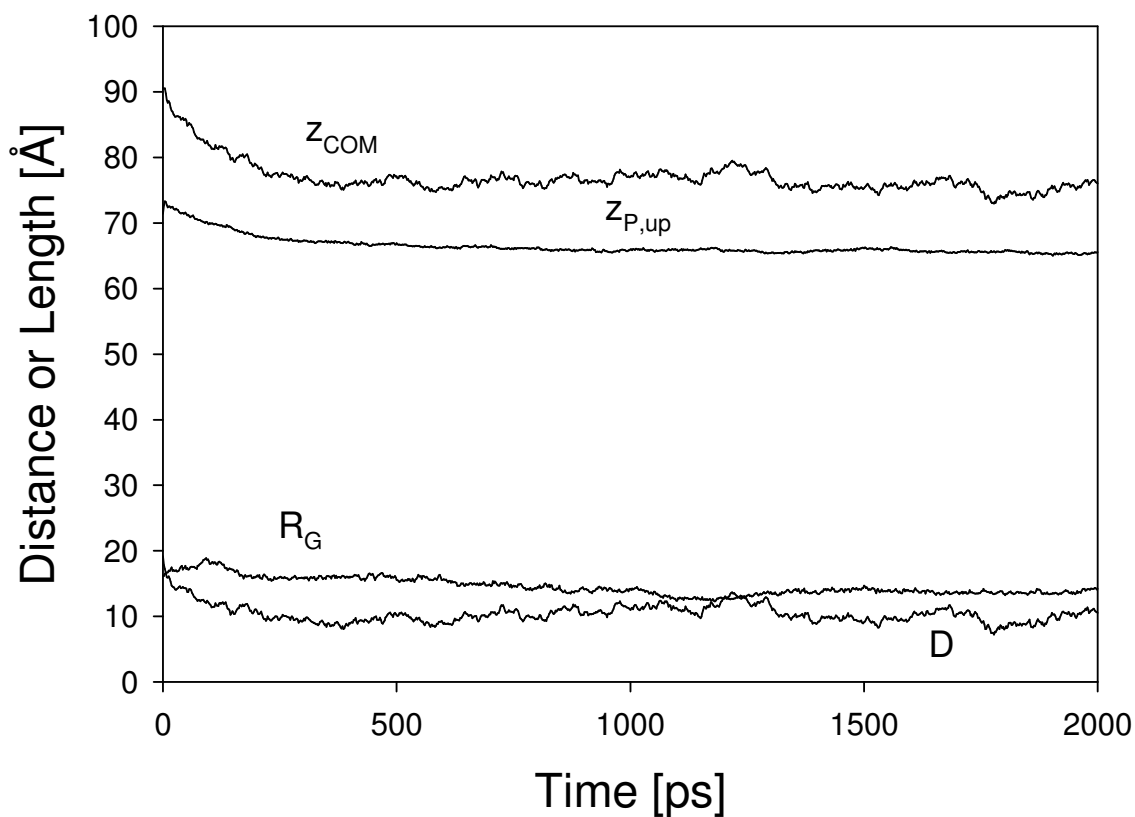


Figure V-32 Structural properties of A β (1-42) in hydrated lipids; A β -E case.

Structural changes are visualized in Figure V-33. We present the initial structure of the full protein (red ribbon) and its final structure after 2ns (cyan ribbon). It is observed that the protein lost its helical structure after 2ns simulation time compared to the initial structure, especially in the middle of the protein. It is not surprising that the final structure lost more portion of the helical structure compared to the case of the protein in water (A β _W-A case of section 5.3), since we performed longer simulation and the simulation box has changed greater than A β _W-A case.

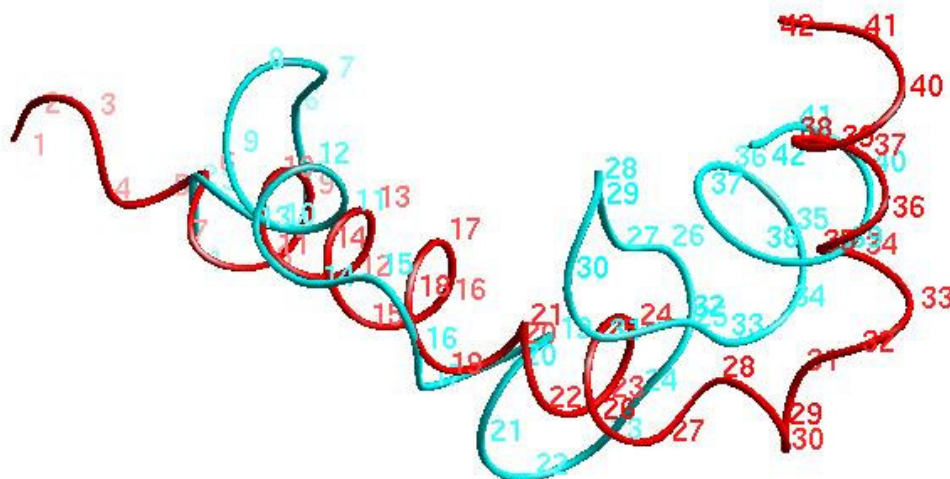


Figure V-33 Snapshots for $A\beta(1-42)$ near hydrated lipids; configurations of start and after 1000000 steps or 2ns, red ribbon represents the initial structure, cyan ribbon is the final structure, $A\beta$ -E case.

As a concluding remark on the study of $A\beta(1-42)$ near hydrated lipids with different parameters, specifically for the case of $A\beta$ -E, we observed that the protein exhibits structural change rapidly during the first 300 ps. This was confirmed from the profile of number of H bonds and snapshots of the starting and ending configurations of the protein. We could observe that the relative distance between the protein COM and the interface varies with simulation time, which tells us that the configurations generated from the simulation of $A\beta$ -E can be used for starting configurations of further studies ($A\beta$ -E series). The results of $A\beta$ -E series will be discussed in the following section.

5.5.2 Simulation of A β (1-42) – A β -E Series

From the case study of A β -E, we observed changes in the simulation box dimensions together with structural properties such as the number of hydrogen bonds. We expected that the protein is positioned at different locations relative to the interface with simulation time by setting the lateral pressure relatively low (-100 atm in A β -E case). Conceptual figure for showing the box dimension change and the structure and position change of A β (1-42) protein generating starting configurations for further simulations, A β -E series, is drawn in Figure V-34. As the simulation proceeds, the z -dimension box length decreases and accordingly the x - and y -dimension box lengths increase as confirmed by Figure V-29 in the previous section. Note that the protein structure for each simulation of this series is different and its location is also different from simulation to simulation. We use some of the snapshots or the restart files as our starting configurations from the simulation of A β -E case, for example, after each 100000 steps a restart file is generated and saved for further runs. We designate this series of case studies as A β -E series, since the starting configurations were generated from A β -E case.

As discussed in the previous section we used this fact to create different starting configurations with different positions of A β , by dilating the box in the x - and y -dimensions with a low pressure. The simulation conditions with the corresponding starting configurations are shown in Table V-13. The data files were created by saving instantaneous configurations every 100000 steps as described before. We applied a lateral pressure of 75 atm, since it has been found to be reasonable from the simulations of hydrated lipids with cvff force-field.

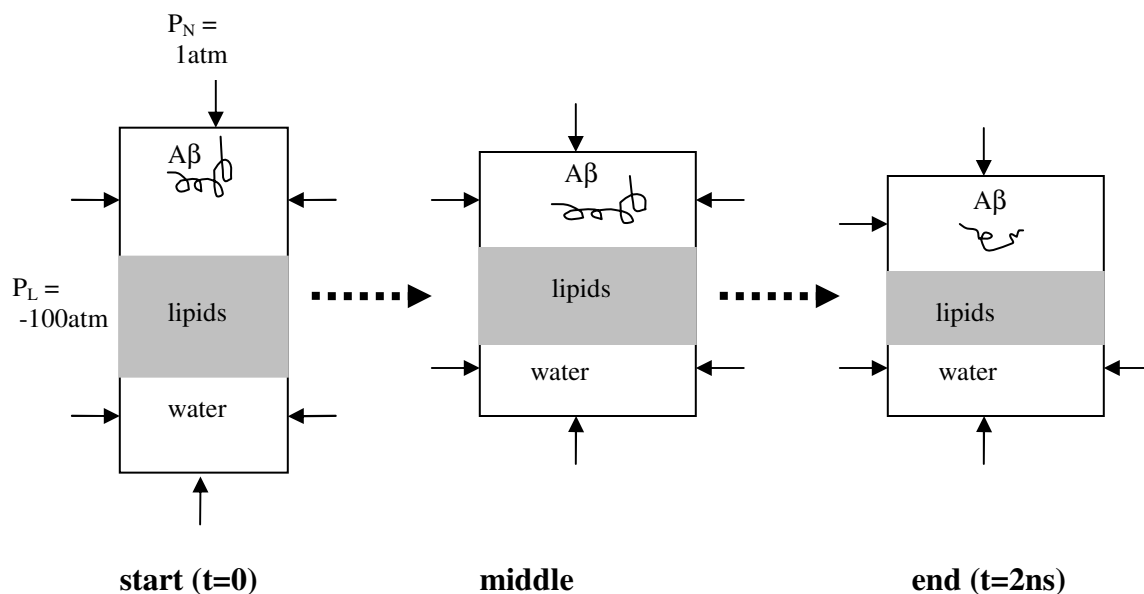


Figure V-34 Generating the starting configurations for A β -E series from the simulation of A β -E case.

It has to be mentioned that after creating animations, we could observe the formation of water pore through the lipid bilayer (approximately after 600000 steps or 1.2ns) for the case of A β -E, which is not realistic. The membrane rupture happened because of the low lateral pressure as was found in other literature (Leontiadou et al., 2004). For the case studies discussed in this dissertation (A β -E_01 to A β -E_06), however, we hardly have seen the transport of water molecules through the membrane.

The data file of A β -E_init case (data.last_mod_04) is quite similar to the data file of A β -E case. The A β -E case data file was obtained after further energy minimization of it and running 100 steps.

Table V-13 Summary of simulation parameters for A β (1-42) in hydrated lipids; A β -E series, CAT cluster with 8 cpus except A β -E_08_COS where COSMOS with 16 cpus used, the lateral pressure is set to 75 atm and the normal pressure is 1 atm, time span of 1ns used, and the last 500 ps data were used for analysis.

Index	Original Index	Data file
A β -E_init	Ab_H2O_DPPC_010506_1	data.last_mod_04
A β -E_01	Ab_H2O_DPPC_122005_1	npt_091805_1.100000
A β -E_02	Ab_H2O_DPPC_122005_2	npt_091805_1.200000
A β -E_03	Ab_H2O_DPPC_122005_3	npt_091805_1.300000
A β -E_04	Ab_H2O_DPPC_122005_4	npt_091805_1.400000
A β -E_05	Ab_H2O_DPPC_122005_5	npt_091805_1.500000
A β -E_06	Ab_H2O_DPPC_010606_1	npt_091805_1.600000
A β -E_07	Ab_H2O_DPPC_010606_2	npt_091805_1.700000
A β -E_08	Ab_H2O_DPPC_122005_8	npt_091805_1.800000
A β -E_08_COS	Ab_H2O_DPPC_122005_8_COSMOS	npt_091805_1.800000
A β -E_09	Ab_H2O_DPPC_010906_1	npt_091805_1.900000
A β -E_10	Ab_H2O_DPPC_010906_2	npt_091805_1.1000000
A β -E_10_data	Ab_H2O_DPPC_122105_1	data.npt_091805_1_1M

Potential energy profiles for several cases of the A β -E series are plotted in Figure V-35. The average potential energy profile shows that after 500 ps, the potential energy doesn't change much.

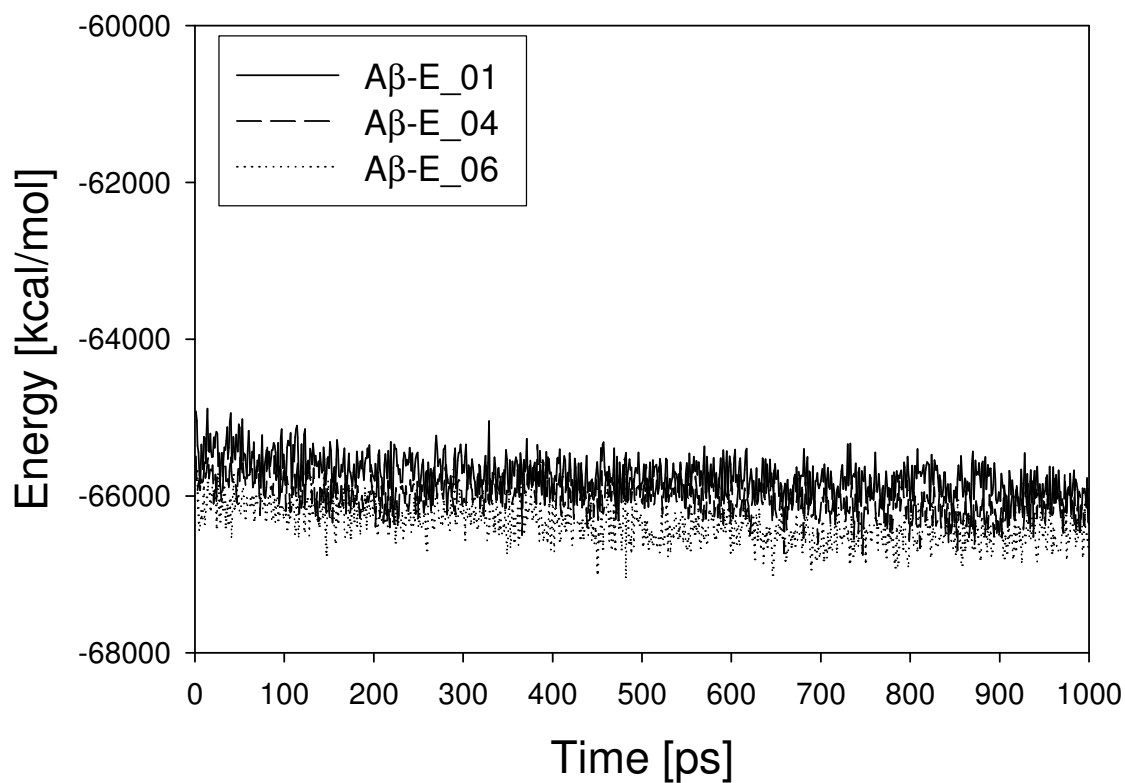


Figure V-35 Potential energy profiles for A β (1-42) near hydrated lipids; A β -E series.

Energy contributions are reported in Table V-14 for the A β -E series simulations. Potential energy differences of approximately 400 kcal/mol were found among the simulations with different protein locations, which mainly comes from nonbonding interactions.

Table V-14 Thermodynamic properties measured from simulations for A β (1-42) in hydrated lipids with different case studies; A β -E series, second row values are the standard deviations.

Index	Total E [kcal/mol]	KE [kcal/mol]	Temp [K]	PE [kcal/mol]	E_bond [kcal/mol]	E_anlge [kcal/mol]	E_dihed [kcal/mol]	E_impr [kcal/mol]	E_vdw [kcal/mol]	E_coul [kcal/mol]	E_long [kcal/mol]	Press [atm]	Volume [Å ³]
A β -E_init	-33657.7	33224.4	323.0	-66882.1	3306.6	15200.3	1680.7	102.7	8526.4	277551.0	-373249.8	45.3	451698.3
	88.6	5.7	0.1	91.2	5.3	31.1	12.4	0.5	62.6	49.9	1.8	8.5	590.9
A β -E_01	-33222.8	33219.4	323.0	-66442.2	3317.0	15239.9	1700.3	103.2	8714.8	285612.3	-381129.6	52.0	453270.0
	78.2	6.1	0.1	78.0	8.3	29.3	7.6	0.5	31.8	85.2	1.8	7.7	478.1
A β -E_02	-33256.7	33221.2	323.0	-66478.0	3313.7	15215.2	1694.2	103.2	8666.7	282117.7	-377588.7	46.4	452909.5
	132.7	6.4	0.1	132.9	9.6	29.4	21.8	0.6	53.5	88.1	2.4	8.7	629.2
A β -E_03	-33283.8	33219.5	323.0	-66503.4	3299.5	15166.3	1679.5	102.9	8621.8	275163.6	-370536.9	55.0	453181.2
	116.8	4.4	0.0	115.8	5.6	20.0	11.5	1.0	47.6	72.1	1.8	9.3	746.4
A β -E_04	-33400.2	33220.5	323.0	-66620.7	3304.8	15157.0	1668.4	102.7	8582.5	275577.9	-371013.9	46.0	452567.6
	69.3	4.4	0.0	68.5	7.9	28.6	8.6	0.7	60.5	78.9	1.1	10.6	508.9
A β -E_05	-33382.9	33221.0	323.0	-66603.9	3297.3	15146.7	1665.1	102.8	8549.5	275713.5	-371078.8	52.9	452534.2
	83.5	7.2	0.1	85.2	8.8	28.0	8.0	0.9	27.8	107.1	1.2	5.6	664.7
A β -E_06	-33570.1	33220.1	323.0	-66790.1	3303.2	15142.4	1650.6	102.9	8472.8	276233.1	-371695.2	50.2	451147.1
	77.0	6.2	0.1	79.8	5.2	19.8	5.7	0.8	16.5	104.4	1.6	8.4	364.9
A β -E_07	-33548.2	33222.2	323.0	-66770.3	3301.5	15147.3	1651.9	103.3	8470.8	276776.8	-372221.9	47.5	451338.1
	76.9	4.7	0.0	76.0	4.3	10.9	9.7	0.9	23.8	73.0	1.6	12.6	433.6
A β -E_08	-33545.8	33220.2	323.0	-66765.9	3296.8	15129.6	1643.1	103.1	8444.7	276878.4	-372261.6	52.9	451487.4
	98.9	8.1	0.1	101.7	6.9	14.0	14.3	0.7	28.8	75.5	3.4	9.3	492.7
A β -E_08_COS	-33579.6	33215.8	322.9	-66795.4	3303.1	15141.7	1648.6	102.9	8445.5	276826.3	-372263.6	56.1	451204.6
	60.8	6.3	0.1	61.2	10.5	32.3	9.8	0.8	27.9	72.0	0.9	9.2	367.1
A β -E_09	-33535.1	33222.6	323.0	-66757.6	3296.3	15137.0	1648.6	103.1	8413.3	277291.5	-372647.5	52.4	451127.8
	78.8	6.0	0.1	76.7	6.8	17.3	6.9	0.8	34.9	67.7	1.7	8.0	572.4
A β -E_10	-33484.7	33220.2	323.0	-66704.9	3304.4	15137.1	1639.1	102.9	8410.4	274264.2	-369563.0	53.0	451254.9
	44.7	4.2	0.0	47.0	6.7	19.1	4.6	0.9	32.0	56.0	1.6	6.0	325.0
A β -E_10_data	-33626.2	33222.1	323.0	-66848.3	3293.6	15116.9	1620.4	102.4	8341.1	274240.8	-369563.5	59.6	450197.6
	36.9	7.5	0.1	37.3	9.6	29.4	13.5	0.7	40.2	63.2	1.0	9.9	282.2

Some of the structural properties mentioned in section 2.3 can be obtained from the position data files saved during the simulations. After processing the raw data files we obtain various structural properties, such as the distance between the COM of the protein and the bilayer interface D , head group area, and the radius of gyration of the protein. Some of the structural properties are summarized in Table V-15.

Table V-15 Structural properties measured from simulations for A β (1-42) in hydrated lipids with different case studies; A β -E series, AVG(average) and STEDV(standard deviation) values are obtained from the last 500 ps data.

Index	D [Å]	A [Å ²]		D _z [Å]		R _G [Å]		<H bond> initial	<H bond> average
		AVG	STDEV	AVG	STDEV	AVG	STDEV		
A β -E_init	22.02	61.78	0.43	114.25	0.84	13.39	0.60	24	9.11
A β -E_01	10.95	81.90	0.30	86.48	0.40	12.44	0.30	9	8.57
A β -E_02	12.34	84.86	0.45	83.40	0.51	13.16	0.40	4	7.00
A β -E_03	17.23	87.30	1.65	81.15	1.40	13.46	0.39	5	4.73
A β -E_04	11.30	88.91	0.40	79.54	0.34	14.84	0.36	4	4.13
A β -E_05	16.96	89.20	0.46	79.27	0.39	11.50	0.53	4	4.11
A β -E_06	17.56	90.36	0.44	78.02	0.39	11.62	0.24	5	4.25

Figure V-36 shows an example figure of the structural properties for the A β -E_01 case. The protein stays 10 Å from the interface initially and slowly moves away from the interface as R_G of the protein slightly decreases. There is a monotonic decrease in the head group area due to the initially expanded simulation box (not shown in figure). The average value of A is 82 Å for the last 500 ps, which is 30% larger than that of A β -E_init case.

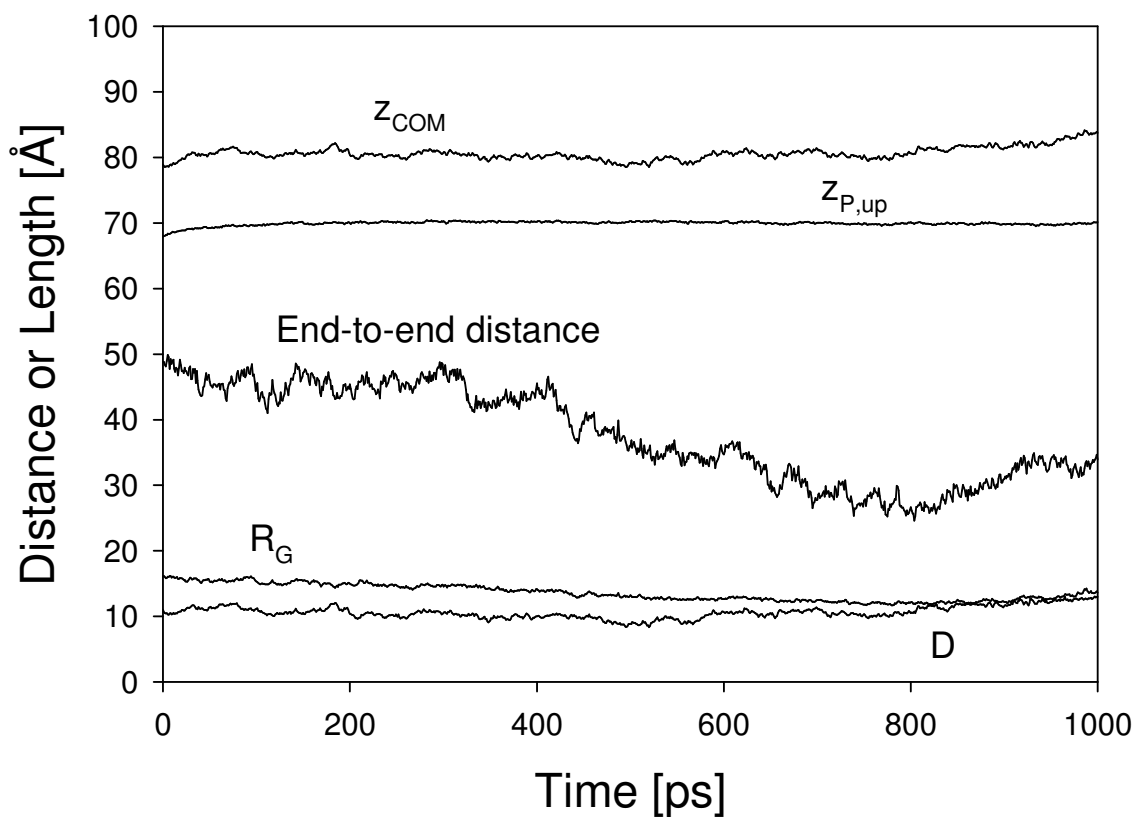


Figure V-36 Profiles of structural properties for A β (1-42) near hydrated lipids; A β -E_01 case.

To examine the relationship between the distance D and the structural properties such as the head group area A , the z -dimension box length D_z , and the radius of gyration R_G for different case studies plots are presented in Figure V-37. The data points were obtained using the average of last 500ps simulation, i.e. the variables are *not* instantaneous values. From the figure we found that the radius of gyration of the protein does not depend strongly on the distance between the protein COM and interface. This is probably because even though we start the simulations at different locations of the protein it translates and simultaneously experiences secondary structural changes as shown in Figure V-36. We found that it is very hard to make the entire protein move

near the lipids or enter the membrane by just dilating the simulation box within 1 ns of simulation. Another hypothesis is that R_G is not a very sensitive variable in general to describe the structural properties of the system. The correlations between D and A and between D and D_z are not clear from this figure. It seems to have a slightly decreasing tendency of A as D increase. The D_z shows reverse tendency. At distance of 22 Å ($A\beta$ -E_init case), the highest head group area was observed.

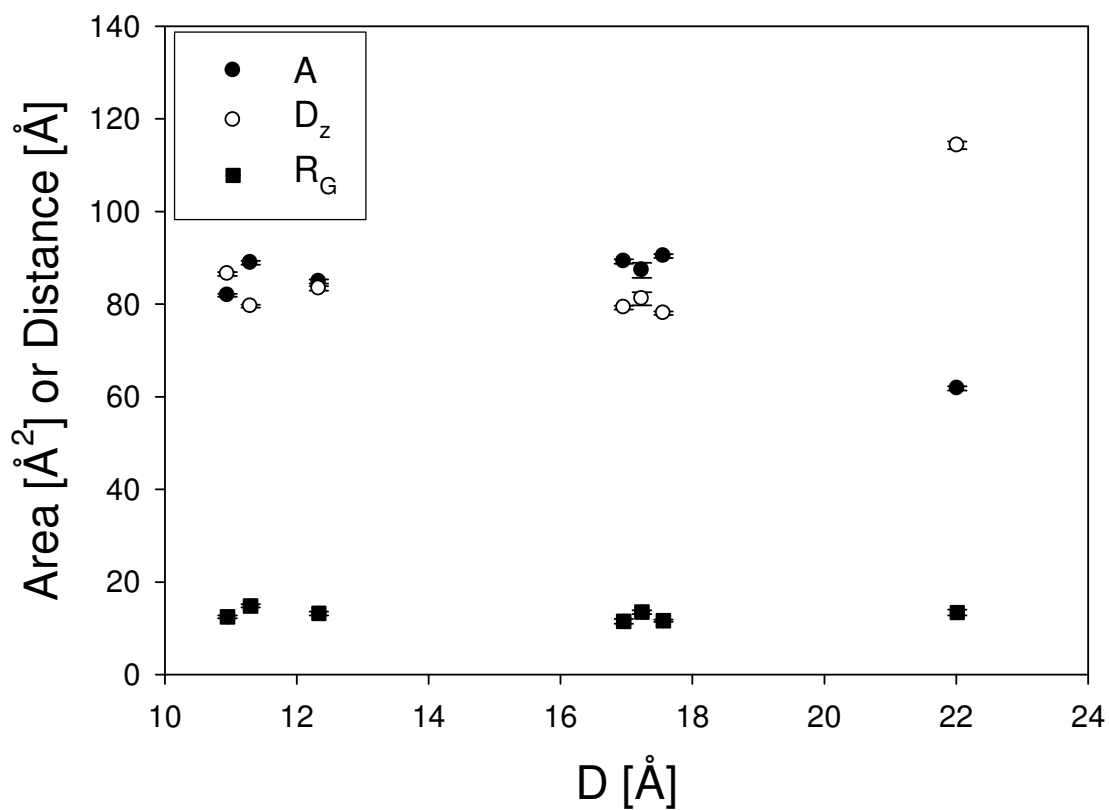


Figure V-37 Comparison of structural properties at different $A\beta(1-42)$ locations; $A\beta$ -E series.

To further investigate the relationship between the structural change and the distance between the protein and the interface we report a figure showing the number of hydrogen bonds with different protein locations as in Figure V-38. The general trend is that if we start the simulation using restart file after a longer simulation, the difference between the initial and final average numbers of H bonds becomes very close to each other ($A\beta$ -E_init vs the rest). Therefore, after a long run such as 2 ns we may expect a few hydrogen bonds remaining using our starting structure of α -helices with a kink.

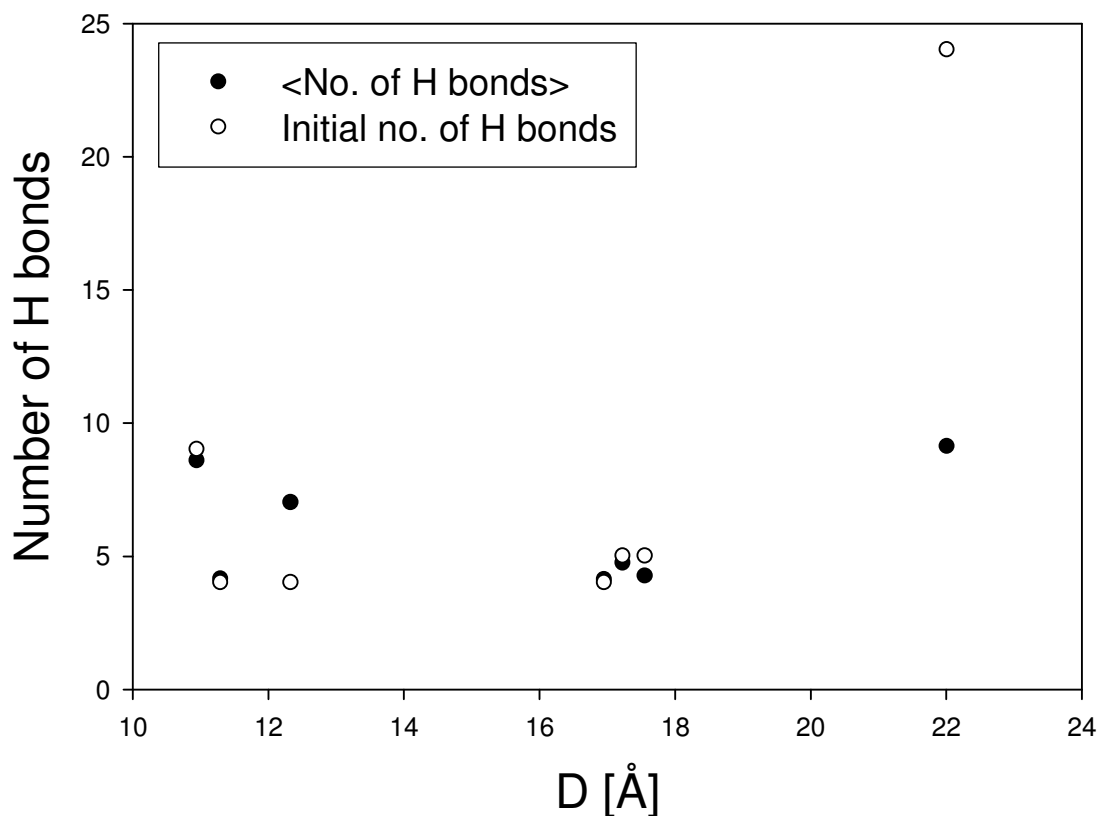


Figure V-38 Comparison of the number of H bonds at different $A\beta$ (1-42) locations; $A\beta$ -E series.

Based on the results of structural properties for the cases of A β -E series, weak correlations between D and R_G or A were observed. Combination of the structural property profiles and thermodynamic information seems to offer that the protein undergoes the structural change slowly due to the presence of the DPPC molecules. Discussion on the RMS deviation will clarify the above hypothesis, which appears later in this section. We speculate that the hydrogen bonds are formed to the water molecules and DPPC molecules, since we observe close contact of the protein with the DPPC molecules as seen in Figure V-39 and Figure V-40.

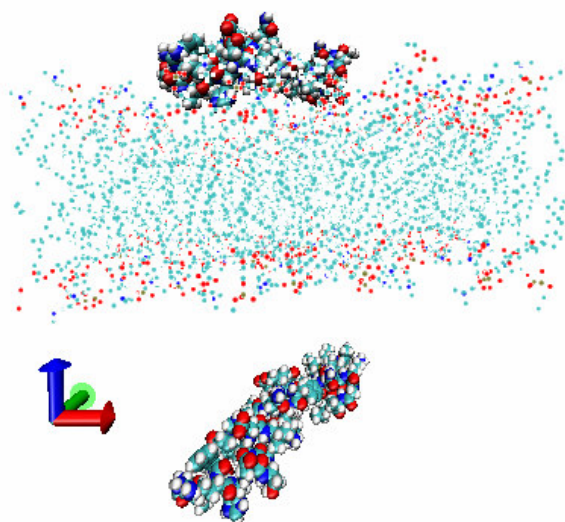


Figure V-39 A snapshot of initial configuration of A β (1-42) near hydrated lipids; A β -E_01 case.

Figure V-39 shows the initial snapshot of the A β -E_01 case, while Figure V-40 shows the snapshot after 1 ns of simulation time. To effectively visualize we applied the

periodic boundary condition for the protein. We observe that the protein in the last snapshot becomes more compact compared to the initial configuration, make a close contact to the DPPC surface.

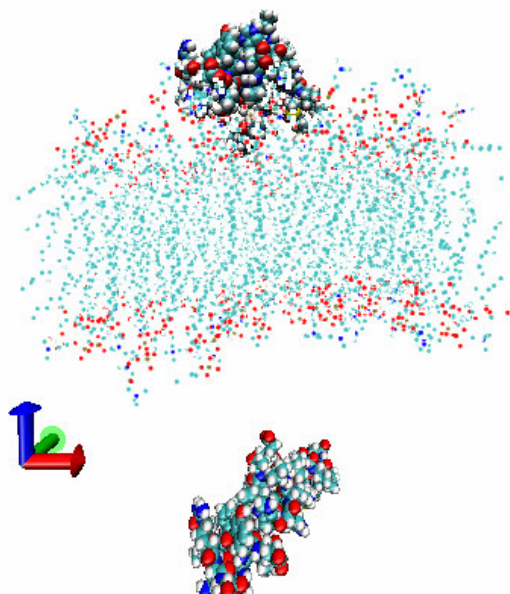


Figure V-40 A snapshot of final configuration of A β (1-42) near hydrated lipids; A β -E_01 case.

Since we found that the number of hydrogen bonds remains the same for the A β -E_01 case (Figure V-38), we analyzed the radius of gyration and the end-to-end distance as a function of D (End-to-end distance profiles are shown in Appendix C). It is not clear that there is a trend for the profile of R_G , but we notice that there is a significant change in the protein end-to-end distance at the protein-interface distances of 9 to 12 Å. At those distances we expect a structural change of the protein.

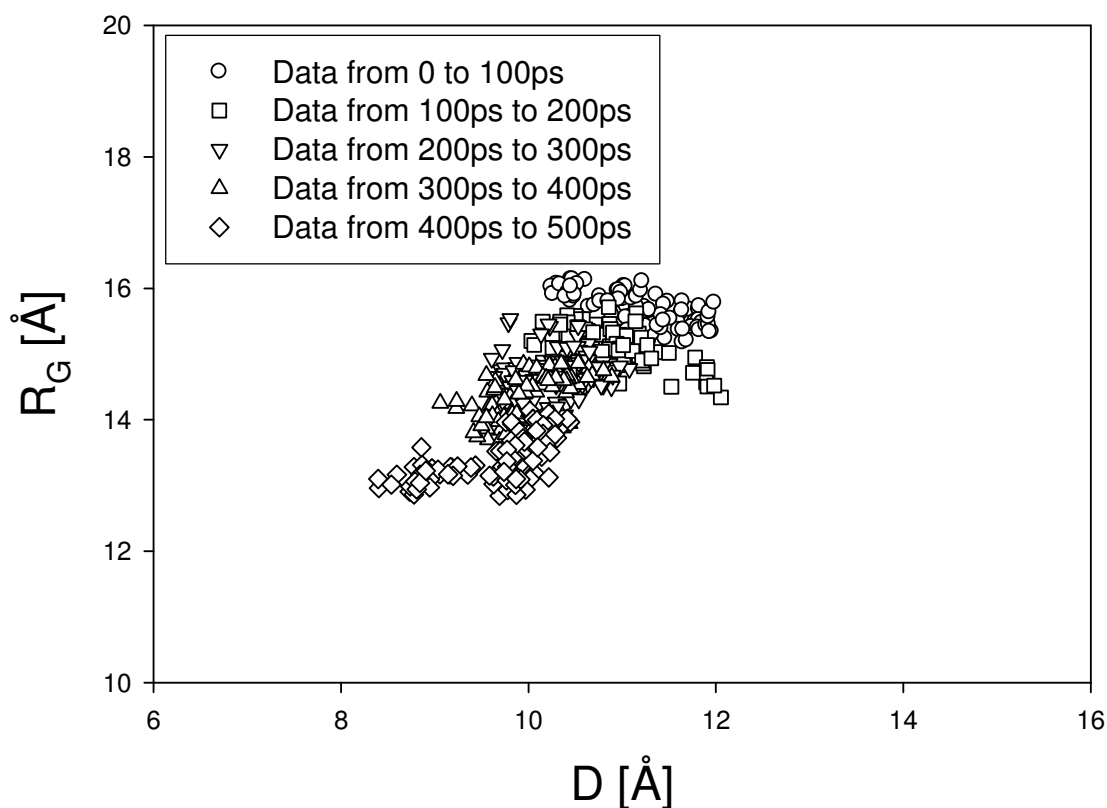


Figure V-41 R_G data as a function of instantaneous D ; A β -E_01 case, first 500ps.

From Figure V-41 we observe that the protein moves toward the lipid interface for the first 500 ps decreasing its size (R_G). During that simulation time of 500 ps the protein moved only about 4 \AA . The change in R_G is not significant for the last 500 ps as shown in Figure V-50. It is quite interesting to observe that the protein moves away from the lipid interface during this time period. Based on the radius of gyration profile as a function of the distance D excluding the effect of the simulation box change, we may say that the protein moves back and forth once during the simulation time of 1 ns with the moving distance of approximately 10 \AA .

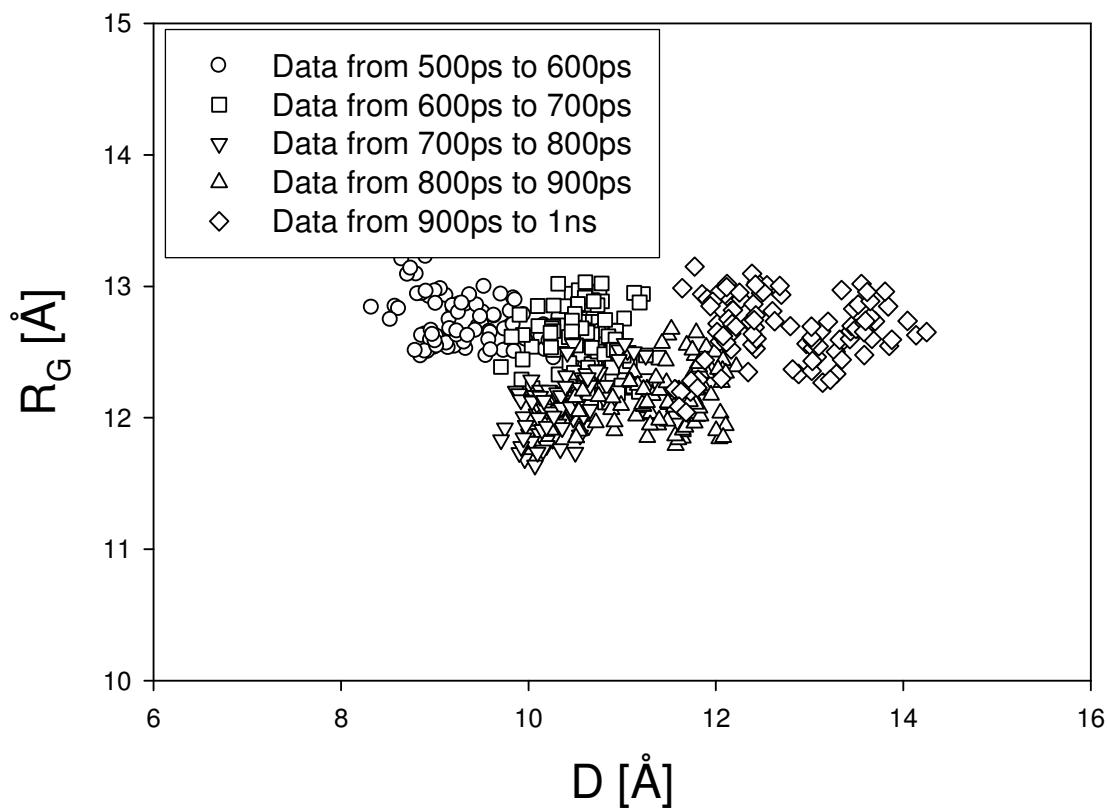


Figure V-42 R_G data as a function of instantaneous D ; A β -E_01 case, last 500ps.

We could observe that the protein makes a close contact with the lipid surface by looking at the animations and snapshots, however our method of defining the distance between the protein and lipid interface needs to be improved. We just employed the method of defining the interface as the average phosphorous atom positions in z -direction, which might be inappropriate to describe the interaction between the protein and the hydrated lipids due to the DPPC surface roughness and contact locations of atoms within the protein with DPPC molecules. To be more quantitative we may need to identify which atoms are in contact with which protein residues. Moreover, we will have

to investigate the hydrogen bonds which might be formed to the water molecules and DPPC molecules

The RMS deviation comparison profiles are shown in Figure V-43. Simulations from restart files, A β -E_04 and A β -E_06, exhibit smaller RMS deviation, which indicates that the starting configurations of those two simulations are structurally more stabilized than the other configurations (A β -E, A β -E_init, and A β -E_01). The RMS deviation profiles indicate that A β -E_init shows similar behaviour to A β _W-A where the protein is located in water only, which is quite reasonable since the distance D is large in A β -E_init case.

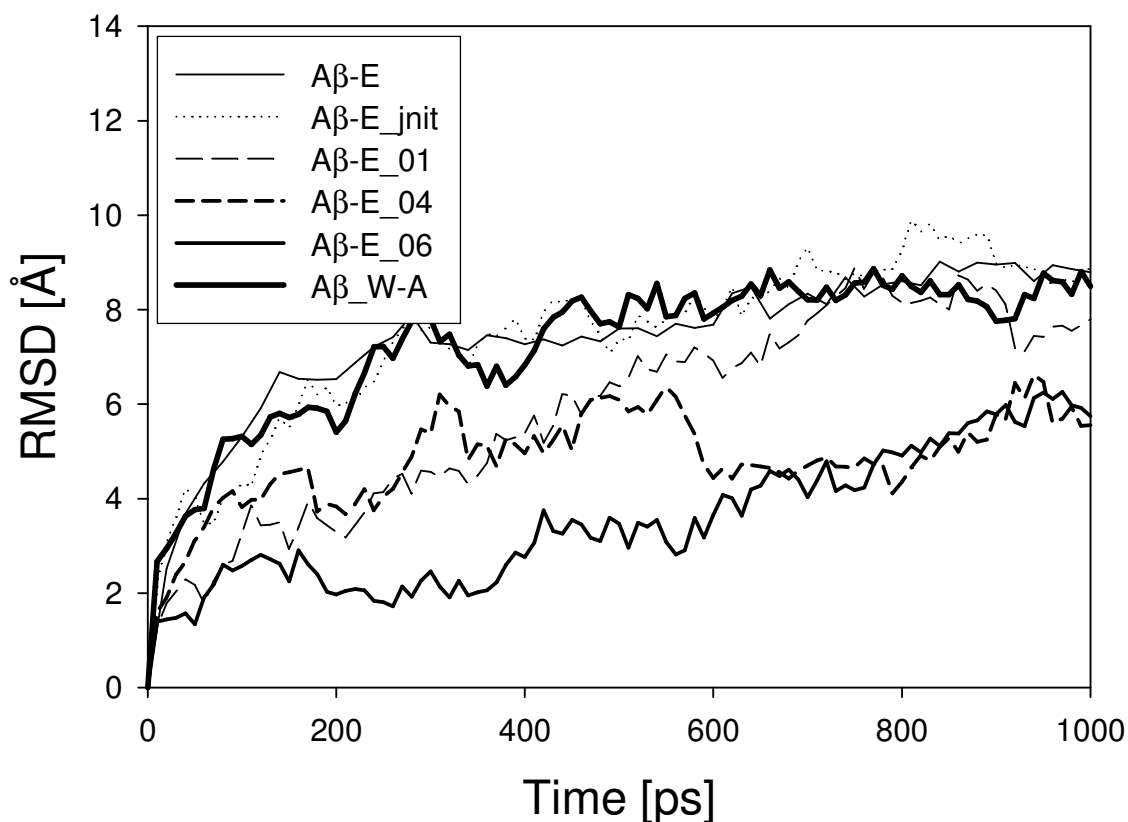


Figure V-43 Comparison of RMS deviation for various simulation case studies of A β (1-42) near hydrated lipids.

Since it is not clear whether the RMSD, more generally the structure, difference is more induced by the difference in the starting structure of the protein itself or by the distance between the protein and the interface by just examining the RMS deviations, we recommend supplementary simulations with the same starting structure maintaining the same distance as will be discussed in Chapter VI. To accomplish this, we believe that theoretical development of the method to define the distance D in a more realistic manner should accompany. However, it is noticeable to recall the MD study of alamethicin in a bilayer and in solution by Tieleman and colleagues (Tieleman et al., 1999). They observed little change in C_{α} RMSD in the POPC bilayer and in methanol (2 Å over 2 ns when inserted into a lipid, 2 Å over 1 ns in methanol), while there was substantial change in water environment (4 Å over 1 ns). Therefore, it is hypothesized to have different RMSD values from simulations with the same starting structure of the protein depending on the location of the protein, accordingly different final structure of the protein. It may be valuable to study the orientation of helical peptides together with its location, parallel to the bilayer surface vs. perpendicular to the bilayer surface, as Biggin and Sansom pointed out (Biggin and Sansom, 1999).

Structural change is visualized from the overlays of the protein structures represented by ribbons as shown in Figure V-44 (A β -E_init) and Figure V-45 (A β -E_04). In those figures, the red ribbon represents the initial configuration of the protein, while the cyan ribbon represents the last configuration. We measured the deviation from their respective initial structure, though the initial structures of the two are different.

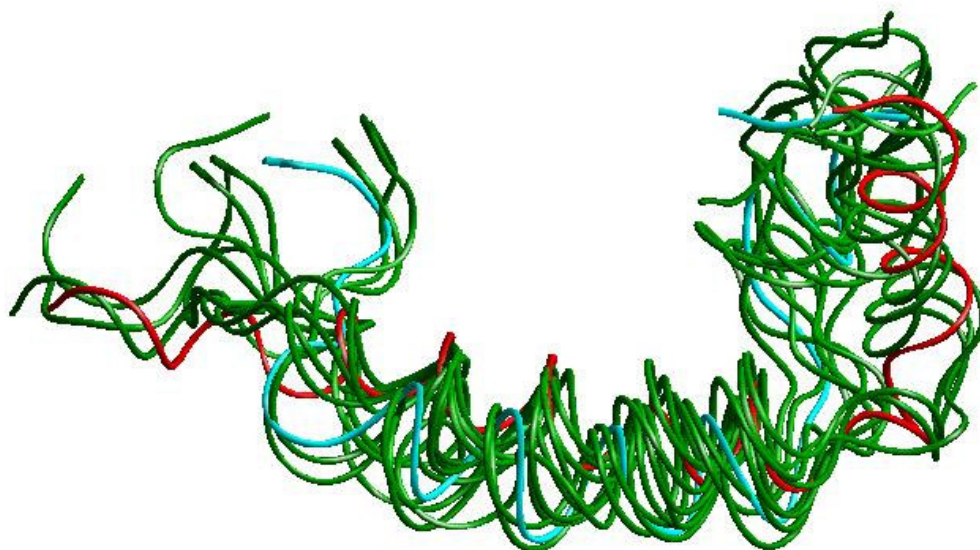


Figure V-44 Snapshots for A β (1-42) near hydrated lipids; 11 frames, red ribbon represents the initial structure, cyan ribbon is the last structure, A β -E_init case.

In the case of A β -E_init we observe that the starting and ending configurations of the N-terminal (left side of the figure) are quite different (8 Å) compared to the case of A β -E_04 (6 Å). From the snapshot it is obvious that the structural change is more significant in the case of A β -E_init ($D = 22$ Å), where the protein stays nearer than that of A β -E_04 ($D = 11$ Å). It was observed from the RMS deviation plots that A β -E_init reached the equilibrium structure more rapidly than that of A β -E_04, which in turn matches what we see from the two figures.

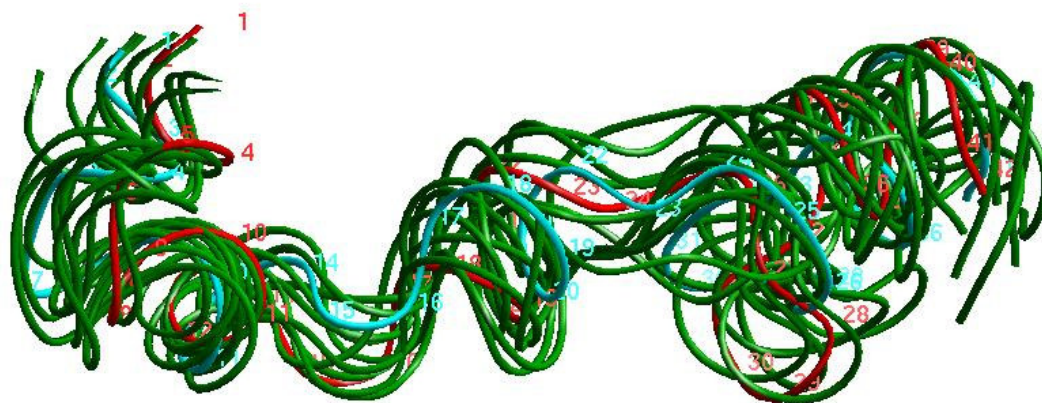


Figure V-45 Snapshots for A β (1-42) near hydrated lipids; 11 frames, red ribbon represents the initial structure, cyan ribbon is the last structure, A β -E_04 case.

As a summary of simulations of A β (1-42) near hydrated lipids, we could create different starting configurations with different locations of the A β (1-42) protein by applying a low lateral pressure of -100atm. Thus configurations generated during the preliminary simulation were used for further simulation studies (A β -E series). Structural properties such as the head group area, radius of gyration of the protein, and RMS deviation were obtained and the results were discussed. Based on the observations and analyses of A β -E series, it can be said that the structural change depends not only on the starting configuration of the system (relative location of the protein from the interface) but also the solution environment. From a representative case study of A β -E_01 case, it is observed that the protein moves back and forth from the lipid interface with the COM movement of approximately 10 Å during 1 ns of simulation time. It is hypothesized that

the radius of gyration for this system might not be sensitive to describe the structural properties appropriately.

5.6 Simulation of A β (31-42) β -Sheet Conformation near Hydrated Lipids

In this section of dissertation we will discuss the observations and results for the simulations of A β (31-42) near hydrated lipids. We have picked one representative case to explain the simulation result, A β -n_01 where the lateral pressure was set to 75 atm, and the system temperature was maintained at 323K. The readers can find other cases of simulation conditions and thermodynamic results in Appendix C. The simulation time was 1 ns, and the thermodynamic properties are measured for the last 500 ps. The starting data file (data.DPPC_B_frag_H2O_092705_2_min_100) is the same for all of the simulation cases discussed in this section.

5.6.1 Thermodynamic Properties

The simulation box was created with the same dimensions as described in section 3.2. Simulations were performed to obtain the thermodynamic and structural properties for the cases of A β (31-42) β -sheet conformation in hydrated lipids. Figure V-46 is the starting configuration of A β (31-42) β -conformation in the fully hydrated lipids without hydrogen atoms.

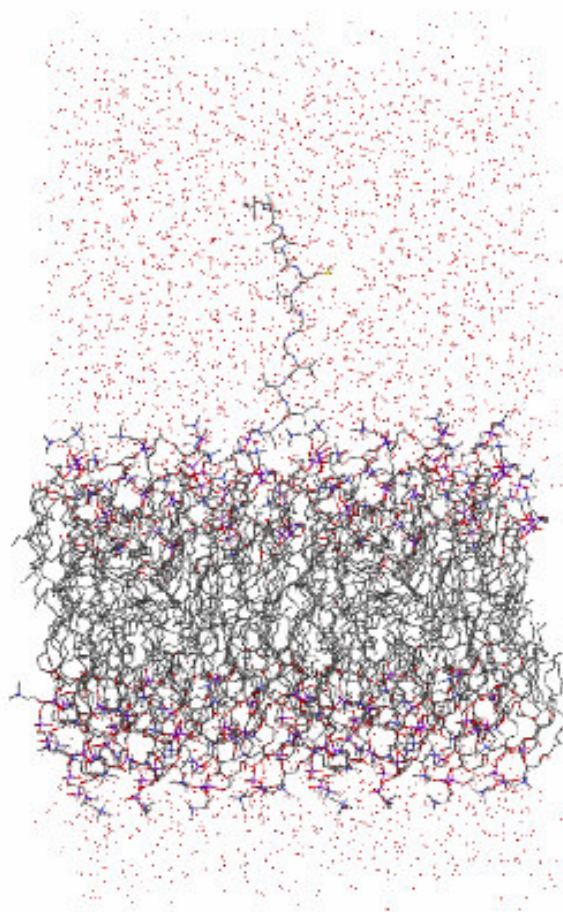


Figure V-46 A snapshot of A β (31-42) β -conformation near hydrated lipids; the protein is in close proximity to the interface, hydrogen atoms are intentionally hidden.

Total and potential energy profiles are shown in Figure V-47 for the A β -n_01. We see that there is slight energy drift even after 500 ps of simulation time, but we found that approximately 500 kcal/mol of the potential energy decrease was found for A β -n_01 case, where the average potential energy of the last 500 ps was approximately -68000

kcal/mol. The relative difference for this case was found to be less than 1%. We understand that longer simulations may be necessary to ensure the quality of simulations, but as a primary step toward the completion of the study of the system, we intend to discuss the results based on the simulation performed so far.

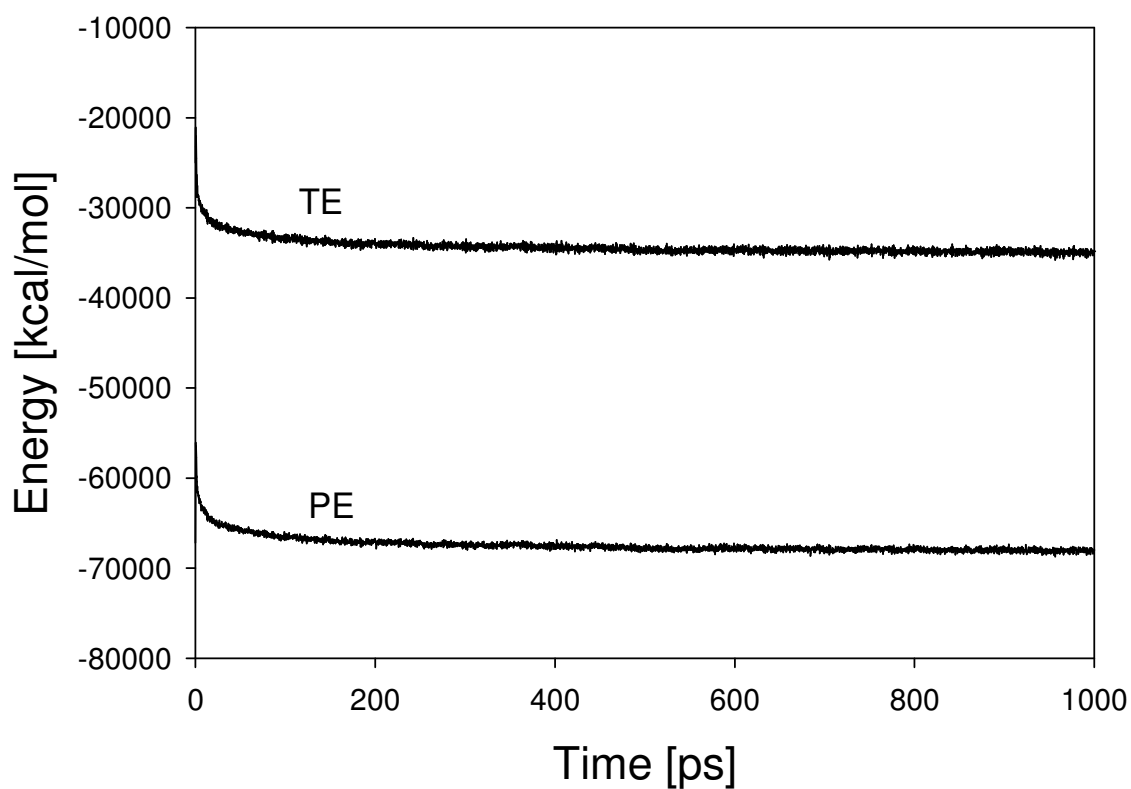


Figure V-47 Total and potential energy profiles for A β (31-42) β -sheet conformation in hydrated lipids; A β -n_01 case.

5.6.2 Structural Properties

We explain the results of the structural properties by picking one of our simulation cases, A β -n_01, where the lateral pressure was maintained at 75 atm. Figure V-48 shows some

of the structural properties during the simulation for the A β -n_01 case study. We observe a sudden drop in the end-to-end distance and the radius of gyration within 500 ps. The distance between the protein fragment and the lipid interface is larger than 15 Å during the simulation implying that it stays away from the interface.

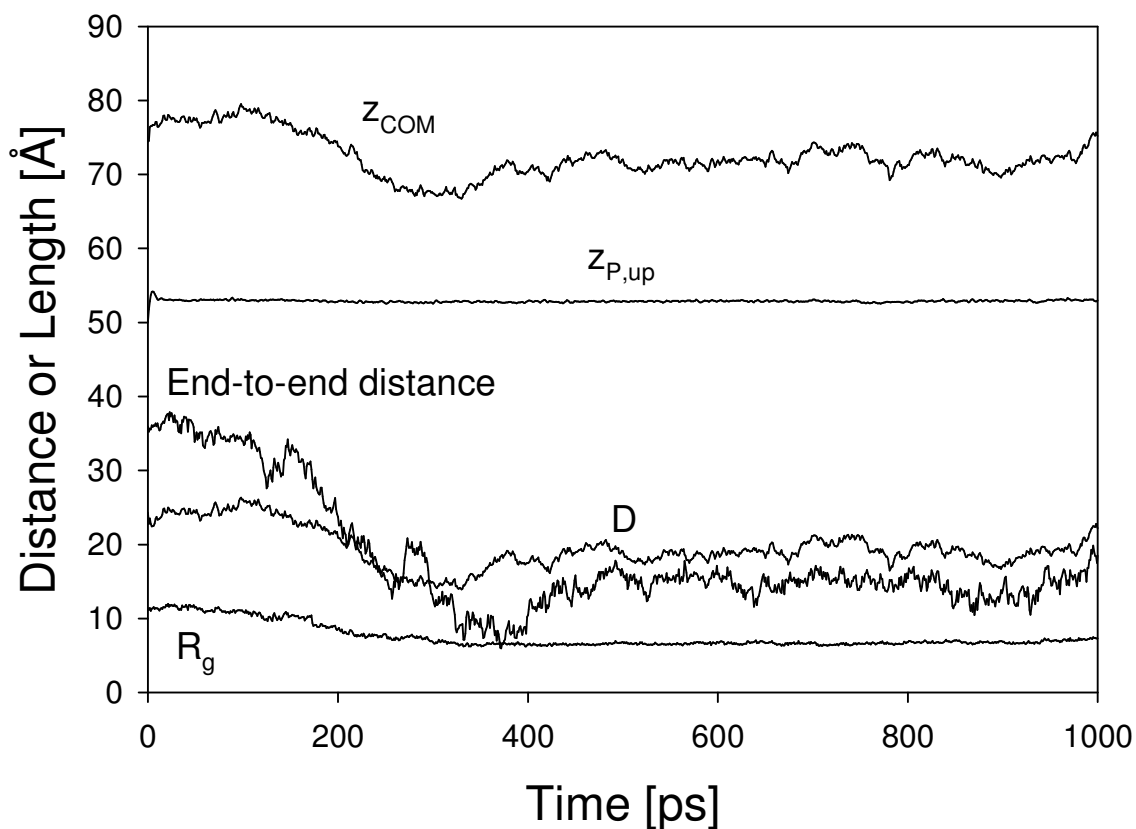


Figure V-48 Profiles of structural properties for A β (31-42) in hydrated lipids; A β -n_01 case.

Profiles of the radius of gyration as a function of instantaneous D are shown in Figure V-49 and Figure V-50 for A β -n_01. For the first 500ps of simulation time, R_G decreases rapidly indicating that the structural change occurs during that time span. Approximately 100% difference of R_G , which is a measure of size of the protein

fragment, was observed from the first 100ps and the fifth 100ps (400ps to 500ps) data. From the profile we observe that the protein moves toward the interface and moves back to the bulk water phase. While the protein stays near the surface (14 to 20 Å), R_G does not change much with the wide change of D and little correlation between D and R_G indicating that the structural change is not significant after 400 ps.

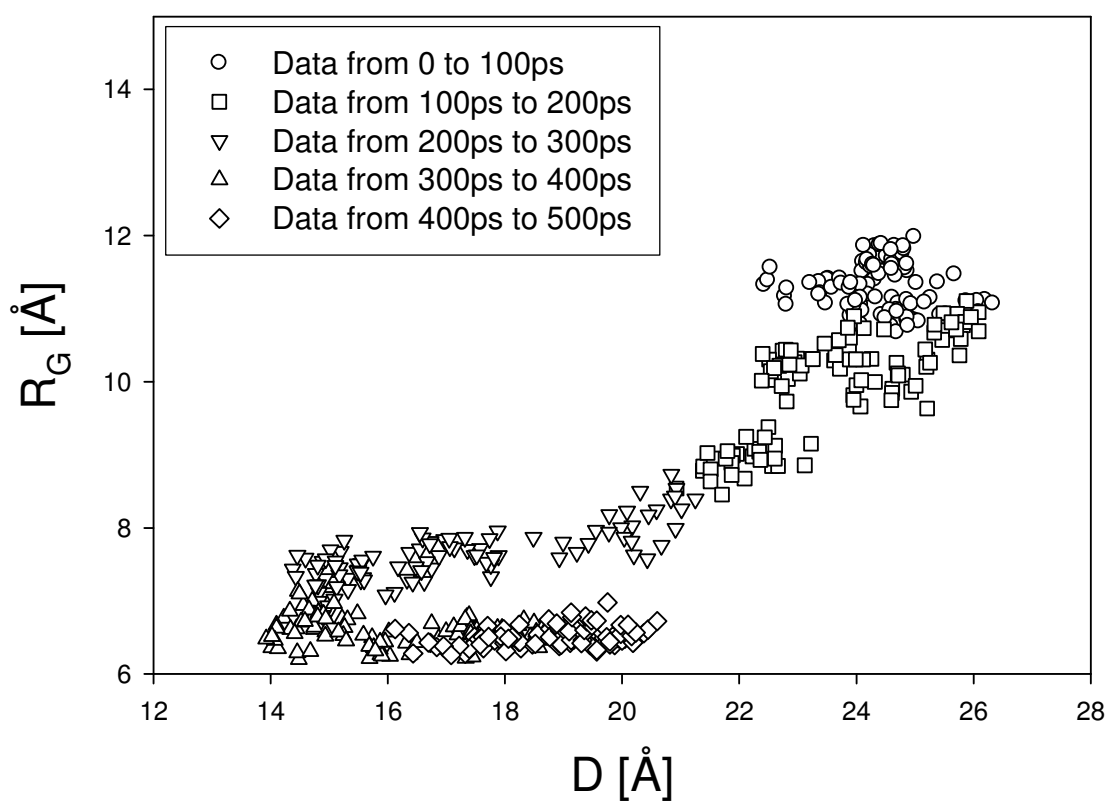


Figure V-49 R_G profile as a function of D ; 0 to 500ps, A β -n_01 case.

The profile of R_G for the last 500ps shows that both the values of D and R_G change little, which in turn implies that the protein fragment maintains its structure and stays

pretty much the same. The end-to-end distance profiles show the similar trend, which are drawn in Appendix C. Based on the R_G profiles, we reach the conclusion that the fragment undergoes structural change rapidly during the first 500ps, and molecular movement is relatively slow while staying the distance of 17 to 21 Å for the last 500 ps simulation. However, it is unclear from this 1 ns simulation if the fragment moves away from the interface.

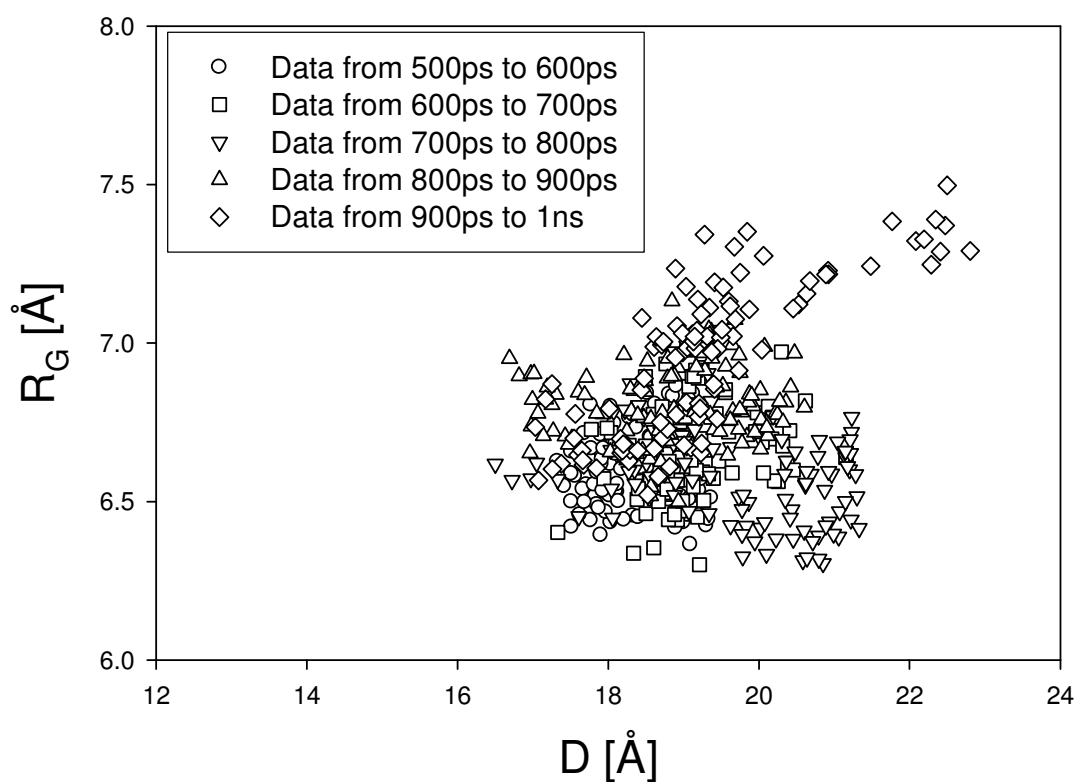


Figure V-50 R_G profile as a function of D ; 500ps to 1ns, A β -n_01 case.

We compare the RMS deviation of A β (31-42) in hydrated lipids with that of A β (31-42) in bulk water as shown in Figure V-51. We observe that RMS deviation of the protein fragment in bulk water is slower to increase compared to that near hydrated lipids. Consequently, the RMS deviation profile of A β -n_01 supports the fact that the A β (31-42) undergoes the structural change rapidly during the first 500 ps, which we have observed from the R_G profiles previously. It is interesting to compare this study with the study by Tieleman and colleagues (1998), since they observed quite different C_α RMSD values from the simulations of alamethicin in different solvent environment as discussed in section 5.5. There may be several reasons to the discrepancy: 1) different nature of peptides studied, 2) different starting structure of peptide (α -helix for alamethicin and β -sheet for A β (31-42)), 3) different solvent environment with lipids (alamethicin is inserted into a lipid, while A β (31-42) is not inserted into a lipid). It is also noteworthy to recall an MD study of A β (25-35) with α -helix in TFE/water (1:1, v/v) at 300K by Lee and Kim (Lee and Kim, 2004). They obtained relatively low heavy-atom RMSD (1 Å) during 1.5 ns simulation for the peptide compared to our results (~8 Å). We believe that the difference is mainly due to the different starting structure and the solvent environment, since TFE is known to stabilize α -helical structure as they pointed out.

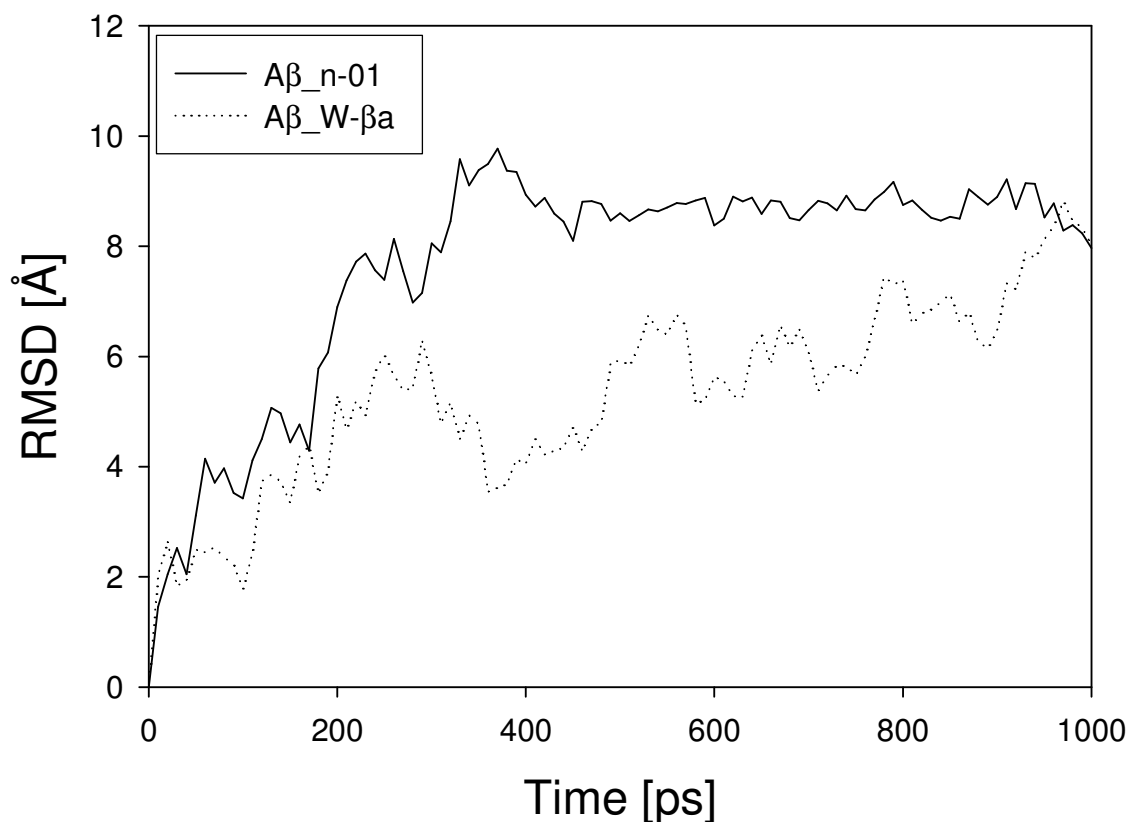


Figure V-51 Comparison of RMS deviation for A β (31-42) in water and near hydrated lipids; A β -n_01 and A β -W- β a cases.

The starting and ending configuration snapshots are presented in Figure V-52. As one can see in the figure the protein fragment has a starting configuration of β -sheet and finally forms a bent structure in the middle of the fragment. We notice that the bending part in the protein A β (31-42) near hydrated lipids is similar to the case of A β (31-42) in bulk water. The snapshots also confirm the fact that the R_G and end-to-end distance decrease compared to the initial and final structure of the protein fragment. To the best of authors' knowledge the study of A β (31-42) with β -sheet conformation has not been published, however, we compare the RMS deviation with an MD study of A β (12-36)

with α -helical structure in water at 450K (Suzuki et al., 2004). Suzuki and colleagues observed the unfolding process within 10 ns timescale and the RMSD values up to 8 Å.

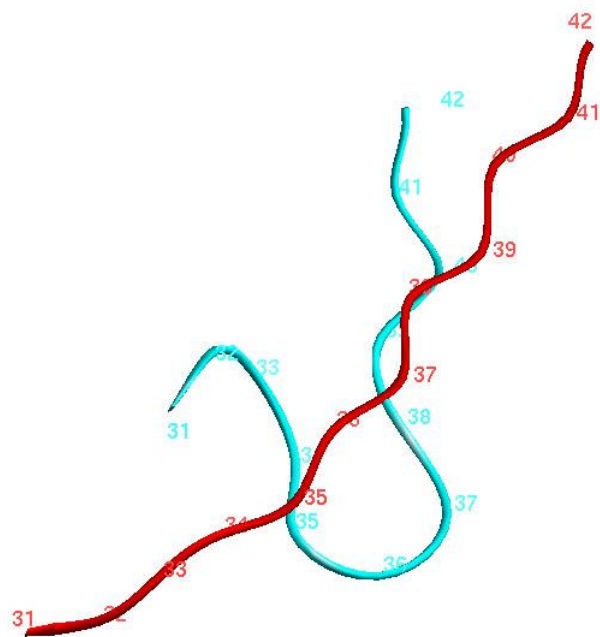


Figure V-52 Snapshots for A β (31-42) near hydrated lipids; 2 frames, red ribbon represents the initial structure, cyan ribbon is the last structure, A β _n-01 case.

Summarizing the simulation results on A β (31-42) with lateral pressure of 75 atm and at 323K we can say that protein undergoes the structural change rapidly within 500 ps of simulation time. We could hardly observe the formation α -helical structure from the starting β -sheet conformation within the simulation time scale of 1ns. Since we found

slight potential energy drift we may need to run longer simulation to ensure the quality of this work.

CHAPTER VI

SUMMARY AND CONCLUSIONS

6.1 Summary and Conclusions

6.1.1 Nano-Research

We examined the partitioning of single dendritic surfactants between clay galleries using canonical molecular dynamics simulations. The process is analyzed in terms of the confinement force and Helmholtz free energy A profiles. The magnitude and sign of confinement force varies in an oscillatory fashion along the layer separation for each molecule due to the possibility of changing configuration within each dendrimer molecule. This finding implies that there may exist several finite layer separation distances for the intercalation of each dendrimer molecule.

Free energy profiles were obtained from the numerical integration of the confinement force. From the free energy profiles analyses, it was found that the four different dendrimers are expected to intercalate. The general trend of forming intercalated structures for all the surfactants comes into good agreement with experimental results. We cannot easily quantify the difference between the types of intercalation, namely the frustrated and complete intercalations, from the simulation results only. However, we speculate that the smaller and linear surfactants (G1 and G2L) will form complete intercalation, while the two larger surfactants (G2 and G3) will form frustrated intercalation based on the location of free energy minimum(a) of approximately 18 Å, which is larger than that of bare clay interlayer spacing (14 Å). It turns out that the combined contribution of energetic and entropic factors affects the final outcome of the materials structure from intercalated to exfoliated ones. It can be concluded from this work and with the integration of corresponding experimental work that the partitioning process of dendrimer surfactant molecule into clay surfaces is strongly dependent on not only the molecular size but also the shape of each molecule.

6.1.2 Bio-Research

From the full atomistic molecular simulation study of A β (1-42) protein or A β (31-42) protein fragment in water and fully hydrated lipids, we could reach the following general conclusions. Large biomolecular systems with over 40000 atoms and with dimensions of several tens of Å in two dimensions and over 100 Å in z -dimension were successfully constructed with Cerius² and Insight II. Data files were converted into LAMMPS and LAMMPS can be efficiently used for such a big system, and produces reasonable results with multiple CPUs. The systems can be simulated with the NPT ensemble with constant pressure boundary condition at 323K. Long-range electrostatics can be accurately treated with the PPPM method combined with a cutoff radius of 10 to 15 Å. Tools were developed to calculate the structural properties for analyses. Considering the system size and slow dynamics of the protein, we found that a 1 ns simulation may be considered as a relatively short simulation time for such big biomolecular systems.

Specifically from the simulations of the biomolecular systems it can be concluded that

- 1) Simulations of bulk water using cvff and SPC resulted in slight different thermodynamic and structural properties, however, cvff can be used for bulk water simulations featuring similar isothermal compressibility, which is a key factor to simulate biological membranes.
- 2) Hydrated lipids using the cvff force-field were modeled with lateral pressures of 50 to 75 atm, which led to a similar head group area and membrane thickness compared with literature values.
- 3) From the simulations of A β (1-42) with α -helices in water, the protein lost some of the hydrogen bonds within the molecule indicating that it experiences secondary structural change within 1 ns of simulation time from a helical structure.
- 4) Based on the simulations of A β (31-42) with β -sheet conformation in water, we found that there is significant decrease in the end-to-end distance and R_G and we conclude that system undergoes a structural change from a sheet to a bent structure within 1 ns simulation time.

5) By applying relatively low lateral pressure such as -100 atm we could obtain starting configurations with different locations of A β (1-42) near lipid bilayer. From the observations and analyses of A β -E series, the protein undergoes structural change due to the different starting configurations (relative location of the protein from the interface) as well as the solution environment. The protein has close contacts with the membrane surface. It was impossible to observe the conformational change to β -sheet and protein entrance into the lipid bilayer within 1 ns simulations.

6) Relatively large structural changes from β -sheet to a bent structure were observed initially from the 1 ns simulation of A β (31-42) near hydrated lipids, even though the protein fragment stays approximately 15 Å from the interface.

6.2 Suggestions and Future Directions

6.2.1 Nano-Research

Uncertainty and discrepancy associated with this study are related to the following simulation deficiencies; excluded effects of water and retained solvents, ignored effect of tethering, the limited number of dendrimer molecules, exclusion of clay surface-surface interaction, and simplified model of clay layers, etc. For further studies we need to perform simulations taking into consideration of those effects as discussed in the text.

The long-term goal of this project will cover systems with clay and single freely-moving or untethered dendrimer, tethered dendrimers to multiple anchored or tethered dendrimers to the clay surface. Because of the limitation in the time and resources we restricted ourselves to the molecular simulations of single untethered dendrimers. However, it is highly suggested that the theoretical studies and molecular simulation studies on tethered dendrimers and multiple dendrimer interactions be studied in future.

6.2.2 Bio-Research

As short term tasks directly related to this work, we need to run longer simulations to investigate the long-time behaviour of the peptides in both bulk water and hydrated lipids such as α -helix to β -sheet conformational change. For the analysis of the simulation data, we will have to develop more analysis tools such as the Ramachandran plots.

Several technical problems should be dealt with in detail. To avoid the pore formation which we encountered during the simulations of A β (1-42) in hydrated lipids because of low lateral pressure, we may need to slowly dilate the simulation box. However, we found that it was not easy to move the whole protein into the bilayer by just expanding the simulation box, therefore it is required to develop more efficient way to simulate the system at different locations of the protein. We need to develop a method to make the protein fixed, for example by fixing the COM of the protein, and perform simulations. Since the lipid surface is rough, we need to define the lipid interface more realistically to improve the quality of this research, for instance we may calculate the interface by considering the closest DPPC molecules to the protein or fragment only. Accordingly, defining the normal vector to the lipid surface more appropriately for the calculation of order parameters is another necessary step.

As pointed out earlier in section 5.5, it is unclear whether the structural change is more induced by different location of the peptide or by different starting conformation. Therefore, we suggest performing simulations at different locations (with different orientations) but with the same starting structure, for instance a loop-like molecule as Mager suggested (Mager, 1998b), and vice versa to exclude the other effect. One way of obtaining different locations of the peptides is to locate the peptide manually by replacing some of DPPC molecules. This process may require much care to equilibrate and perform dynamics, since there might be bad overlap of atoms when the model construction is carried out. Putting aside the different location of peptides issue, it is possible to obtain different starting conformation of peptides by applying different lateral pressures and simulation times.

It is suggested that we need to optimize the system parameters such as the lateral pressure more precisely. It would be valuable to perform simulations using different force-fields as discussed in previous chapter for the improvement of our model systems. We may also need to apply different water model such as SPC water to compare and improve our quality of study. Moreover, to resemble the biological membrane more realistically, it is desirable to perform simulations with other membrane molecules such as cholesterol and gangliosides. Theoretically, we need to develop a method to effectively calculate the free energy profiles for such a big biomolecular system. Clearly, the simulation study of aggregation of oligomers is critical to the simulation of A β under biological conditions. It would be valuable to perform simulations with the solvent such as TFE to compare the structural changes due to the different solvent environment.

REFERENCES

- Abe, H., K. Kawasaki, and H. Nakanishi. 2002. pH-dependent aggregate forms and conformation of Alzheimer amyloid beta-peptide (12-24). *Journal of Biochemistry* 132(6):863-874.
- Acosta, E. J., Y. J. Deng, G. N. White, J. B. Dixon, K. J. McInnes, S. A. Senseman, A. S. Frantzen, and E. E. Simanek. 2003. Dendritic surfactants show evidence for frustrated intercalation: A new organoclay morphology. *Chemistry of Materials* 15(15):2903-2909.
- Albrecht, O., H. Gruler, and E. Sackmann. 1978. Polymorphism of phospholipid monolayers. *Journal de Physique* 39(3):301-313.
- Allen, M. P., and D. J. Tildesley. 1987. *Computer Simulation of Liquids*. Clarendon Press, Oxford.
- Ariga, T., and R. K. Yu. 1999. GM1 inhibits amyloid beta-protein-induced cytokine release. *Neurochemical Research* 24(2):219-226.
- Ayappa, K. G., and C. Ghatak. 2002. The structure of frozen phases in slit nanopores: a grand canonical Monte Carlo study. *Journal of Chemical Physics* 117(11):5373-5383.
- Berendsen, H. J. C., J. R. Grigera, and T. P. Straatsma. 1987. The missing term in effective pair potentials. *Journal of Physical Chemistry* 91(24):6269-6271.
- Biggin, P. C., and M. S. P. Sansom. 1999. Interactions of alpha-helices with lipid bilayers: a review of simulation studies. *Biophysical Chemistry* 76(3):161-183.
- Bitsanis, I. A., and C. M. Pan. 1993. The origin of glassy dynamics at solid oligomer interfaces. *Journal of Chemical Physics* 99(7):5520-5527.
- Braganza, L. F., and D. L. Worcester. 1986. Structural-changes in lipid bilayers and biological-membranes caused by hydrostatic-pressure. *Biochemistry* 25(23):7484-7488.
- Burnside, S. D., and E. P. Giannelis. 1995. Synthesis and properties of new poly(dimethylsiloxane) nanocomposites. *Chemistry of Materials* 7(9):1597-1600.

- Carrado, K. A. 2000. Synthetic organo- and polymer-clays: preparation, characterization, and materials applications. *Applied Clay Science* 17(1-2):1-23.
- Chan, D. Y. C., and R. G. Horn. 1985. The drainage of thin liquid films between solid surfaces. *Journal of Chemical Physics* 83(10):5311-5324.
- Chen, Z., and F. A. Escobedo. 2001. Conformational properties and entropic partitioning of topologically complex polymers under confinement. *Macromolecules* 34(25):8802-8810.
- Chen, Z., and F. A. Escobedo. 2004. Influence of polymer architecture and polymer-wall interaction on the adsorption of polymers into a slit-pore. *Phys. Rev. E* 69(2):021802.
- Chiu, S. W., M. Clark, V. Balaji, S. Subramaniam, H. L. Scott, and E. Jakobsson. 1995. Incorporation of surface tension into molecular dynamics simulation of an interface: a fluid phase lipid bilayer membrane. *Biophysical Journal* 69(4):1230-1245.
- Chiu, S. W., M. M. Clark, E. Jakobsson, S. Subramaniam, and H. L. Scott. 1999a. Application of combined Monte Carlo and molecular dynamics method to simulation of dipalmitoyl phosphatidylcholine lipid bilayer. *Journal of Computational Chemistry* 20(11):1153-1164.
- Chiu, S. W., E. Jakobsson, S. Subramaniam, and H. L. Scott. 1999b. Combined Monte Carlo and molecular dynamics simulation of fully hydrated dioleoyl and palmitoyloleoyl phosphatidylcholine lipid bilayers. *Biophysical Journal* 77(5):2462-2469.
- Choo-Smith, L. P., W. Garzon-Rodriguez, C. G. Glabe, and W. K. Surewicz. 1997. Acceleration of amyloid fibril formation by specific binding of A beta-(1-40) peptide to ganglioside-containing membrane vesicles. *Journal of Biological Chemistry* 272(37):22987-22990.
- Christenson, H. K. 1983. Experimental measurements of solvation forces in non-polar liquids. *Journal of Chemical Physics* 78(11):6906-6913.
- Damodaran, K. V., and K. M. Merz. 1994. A comparison of DMPC-based and DLPE-based lipid bilayers. *Biophysical Journal* 66(4):1076-1087.
- Dauber-Osguthorpe, P., V. A. Roberts, D. J. Osguthorpe, J. Wolff, M. Genest, and A. T. Hagler. 1988. Structure and energetics of ligand binding to proteins: *Escherichia coli*

- dihydrofolate reductase-trimethoprim, a drug-receptor system. *Proteins-Structure Function and Genetics* 4(1):31-47.
- de Joannis, J., J. Jimenez, R. Rajagopalan, and I. Bitsanis. 2000. A polymer chain trapped between athermal walls: concentration profile and confinement force. *Europhysics Letters* 51(1):41-47.
- de Young, L. R., and K. A. Dill. 1988. Solute partitioning into lipid bilayer-membranes. *Biochemistry* 27(14):5281-5289.
- Deserno, M., and C. Holm. 1998. How to mesh up Ewald sums. I. A theoretical and numerical comparison of various particle mesh routines. *Journal of Chemical Physics* 109(18):7678-7693.
- Douliez, J. P., A. Leonard, and E. J. Dufourc. 1995. Restatement of order parameters in biomembranes: calculation of C-C bond order parameters from C-D quadrupolar splittings. *Biophysical Journal* 68(5):1727-1739.
- Doxastakis, M., A. K. Sum, and J. J. de Pablo. 2005. Modulating membrane properties: the effect of trehalose and cholesterol on a phospholipid bilayer. *Journal of Physical Chemistry B* 109(50):24173-24181.
- Egberts, E., and H. J. C. Berendsen. 1988. Molecular dynamics simulation of a smectic liquid crystal with atomic detail. *Journal of Chemical Physics* 89(6):3718-3732.
- Egberts, E., S. J. Marrink, and H. J. C. Berendsen. 1994. Molecular dynamics simulation of a phospholipid membrane. *European Biophysics Journal with Biophysics Letters* 22(6):423-436.
- Essmann, U., L. Perera, and M. L. Berkowitz. 1995. The origin of the hydration interaction of lipid bilayers from MD simulation of dipalmitoylphosphatidylcholine membranes in gel and liquid-crystalline phases. *Langmuir* 11(11):4519-4531.
- Frenkel, D., and B. Smit. 2002. *Understanding Molecular Simulation - From Algorithms to Applications*. Academic Press, San Diego.
- Gee, M. L., P. M. McGuiggan, J. N. Israelachvili, and A. M. Homola. 1990. Liquid to solidlike transitions of molecularly thin films under shear. *Journal of Chemical Physics* 93(3):1895-1906.

- Ghatak, C., and K. G. Ayappa. 2001. Solid-solid transformations in a confined soft sphere fluid. *Phys. Rev. E* 6405(5).
- Ghatak, C., and K. G. Ayappa. 2004. Solvation force, structure and thermodynamics of fluids confined in geometrically rough pores. *Journal of Chemical Physics* 120(20):9703-9714.
- Gupta, S., D. C. Koopman, G. B. Westermann-Clark, and I. A. Bitsanis. 1994. Segmental dynamics and relaxation of n-octane at solid-liquid interfaces. *Journal of Chemical Physics* 100(11):8444-8453.
- Hackett, E., E. Manias, and E. P. Giannelis. 1998. Molecular dynamics simulations of organically modified layered silicates. *Journal of Chemical Physics* 108(17):7410-7415.
- Hackett, E., E. Manias, and E. P. Giannelis. 2000. Computer simulation studies of PEO/layer silicate nanocomposites. *Chemistry of Materials* 12(8):2161-2167.
- Hardy, B. J., and R. W. Pastor. 1994. Conformational sampling of hydrocarbon and lipid chains in an orienting potential. *Journal of Computational Chemistry* 15(2):208-226.
- Herrera-Valdez, M. A., 2/23/2006, Proteins,
<http://math.arizona.edu/~herrera/biochem/proteins.pdf>
- Hill, T. L. 1986. *An Introduction to Statistical Thermodynamics*. Dover Publications, Inc., New York.
- Hockney, R. W., and J. W. Eastwood. 1981. *Computer Simulation Using Particles*. McGraw-Hill Inc., New York.
- Horn, R. G., and J. N. Israelachvili. 1981. Direct measurement of structural forces between 2 surfaces in a non-polar liquid. *Journal of Chemical Physics* 75(3):1400-1411.
- Humphrey, W., A. Dalke, and K. Schulten. 1996. VMD: visual molecular dynamics. *J. Mol. Graph.* 14(1):33-38.
- Inoko, Y., and T. Mitsui. 1978. Structural parameters of dipalmitoyl phosphatidylcholine lamellar phases and bilayer phase transitions. *Journal of the Physical Society of Japan* 44(6):1918-1924.

- Israelachvili, J. N., and S. J. Kott. 1988. Liquid structuring at solid interfaces as probed by direct force measurements - the transition from simple to complex liquids and polymer fluids. *Journal of Chemical Physics* 88(11):7162-7166.
- Jacob, M. M. E., E. Hackett, and E. P. Giannelis. 2003. From nanocomposite to nanogel polymer electrolytes. *J. Mater. Chem.* 13(1):1-5.
- Jensen, M. O., O. G. Mouritsen, and G. H. Peters. 2004. Simulations of a membrane-anchored peptide: structure, dynamics, and influence on bilayer properties. *Biophysical Journal* 86(6):3556-3575.
- Kell, G. S. 1975. Density, thermal expansivity, and compressibility of liquid water from 0 degrees to 150 degrees C: correlations and tables for atmospheric pressure and saturation reviewed and expressed on 1968 temperature scale. *Journal of Chemical and Engineering Data* 20(1):97-105.
- Kirshenbaum, K., and V. Daggett. 1995. Ph-dependent conformations of the amyloid beta(1-28) peptide fragment explored using molecular dynamics. *Biochemistry* 34(23):7629-7639.
- Kojima, Y., A. Usuki, M. Kawasumi, A. Okada, Y. Fukushima, T. Kurauchi, and O. Kamigaito. 1993. Mechanical properties of nylon 6-clay hybrid. *J. Mater. Res.* 8(5):1185-1189.
- Krishnamoorti, R., R. A. Vaia, and E. P. Giannelis. 1996. Structure and dynamics of polymer-layered silicate nanocomposites. *Chemistry of Materials* 8(8):1728-1734.
- Krynicky, K., C. D. Green, and D. W. Sawyer. 1978. Pressure and temperature dependence of self-diffusion in water. *Faraday Discussions*(66):199-208.
- Lee, B. W., R. Faller, A. K. Sum, I. Vattulainen, M. Patra, and M. Karttunen. 2004. Structural effects of small molecules on phospholipid bilayers investigated by molecular simulations. *Fluid Phase Equilibria* 225(1-2):63-68.
- Lee, J. Y., A. R. C. Baljon, R. F. Loring, and A. Z. Panagiotopoulos. 1998. Simulation of polymer melt intercalation in layered nanocomposites. *Journal of Chemical Physics* 109(23):10321-10330.

- Lee, S., K. Carson, A. Rice-Ficht, and T. Good. 2005. Hsp20, a novel alpha-crystallin, prevents A beta fibril formation and toxicity. *Protein Science* 14(3):593-601.
- Lee, S., and Y. Kim. 2004. Molecular dynamics simulations on beta amyloid peptide (25-35) in aqueous trifluoroethanol solution. *Bulletin of the Korean Chemical Society* 25(6):838-842.
- Lee, S., Y. H. Suh, S. Kim, and Y. Kim. 1999. Comparison of the structures of beta amyloid peptide (25-35) and substance P in trifluoroethanol/water solution. *Journal of Biomolecular Structure & Dynamics* 17(2):381-391.
- Leontiadou, H., A. E. Mark, and S. J. Marrink. 2004. Molecular dynamics simulations of hydrophilic pores in lipid bilayers. *Biophysical Journal* 86(4):2156-2164.
- Levy, R., and C. W. Francis. 1975. Interlayer adsorption of polyvinylpyrrolidone on montmorillonite. *Journal of Colloid and Interface Science* 50(3):442-450.
- Lewis, B. A., and D. M. Engelman. 1983. Lipid bilayer thickness varies linearly with acyl chain length in fluid phosphatidylcholine vesicles. *Journal of Molecular Biology* 166(2):211-217.
- Lis, L. J., M. McAlister, N. Fuller, R. P. Rand, and V. A. Parsegian. 1982. Interactions between neutral phospholipid bilayer membranes. *Biophysical Journal* 37(3):657-665.
- Livadaru, L., and H. J. Kreuzer. 2003. Confinement of a polymer chain in a tube. *New Journal of Physics* 5:95.1-95.18.
- Mager, P. P. 1998a. Molecular simulation of the amyloid beta-peptide A beta-(1-40) of Alzheimer's disease. *Molecular Simulation* 20(4):201-222.
- Mager, P. P. 1998b. Molecular simulation of the primary and secondary structures of the A beta(1-42)-peptide of Alzheimer's disease. *Medicinal Research Reviews* 18(6):403-430.
- Mager, P. P. 2001. Molecular simulation of solution conformations of the amyloid beta-peptide A beta(1-42) by a backpropagation neural network model. *Molecular Simulation* 27(1):43-59.

- Mager, P. P., and K. Fischer. 2001. Simulation of the lipophilic and antigenic cores of the A beta(1-42) peptide of Alzheimer's disease. *Molecular Simulation* 27(4):237-242.
- Mager, P. P., B. Penke, R. Walter, T. Harkany, and W. Hartig. 2002. Pathological peptide folding in Alzheimer's disease and other conformational disorders. *Current Medicinal Chemistry* 9(19):1763-1780.
- Mager, P. P., R. Reinhardt, and K. Fischer. 2001. Molecular simulation to aid in the understanding of the A beta(1-42) peptide of Alzheimer's disease. *Molecular Simulation* 26(6):367-379.
- Manias, E., G. Hadziioannou, and G. tenBrinke. 1996. Inhomogeneities in sheared ultrathin lubricating films. *Langmuir* 12(19):4587-4593.
- Manias, E., A. Touny, L. Wu, K. Strawhecker, B. Lu, and T. C. Chung. 2001. Polypropylene/montmorillonite nanocomposites. Review of the synthetic routes and materials properties. *Chemistry of Materials* 13(10):3516-3523.
- Mansfield, S. L., D. A. Jayawickrama, J. S. Timmons, and C. K. Larive. 1998. Measurement of peptide aggregation with pulsed-field gradient nuclear magnetic resonance spectroscopy. *Biochimica et Biophysica Acta-Protein Structure and Molecular Enzymology* 1382(2):257-265.
- Marrink, S. J., M. Berkowitz, and H. J. C. Berendsen. 1993. Molecular dynamics simulation of a membrane/water interface: the ordering of water and its relation to the hydration force. *Langmuir* 9(11):3122-3131.
- Marrink, S. J., D. P. Tieleman, A. R. van Buuren, and H. J. C. Berendsen. 1996. Membranes and water: an interesting relationship. *Faraday Discussions*(103):191-201.
- Martyna, G. J., M. E. Tuckerman, D. J. Tobias, and M. L. Klein. 1996. Explicit reversible integrators for extended systems dynamics. *Molecular Physics* 87(5):1117-1157.

- Mashl, R. J., H. L. Scott, S. Subramaniam, and E. Jakobsson. 2001. Molecular simulation of dioleoylphosphatidylcholine lipid bilayers at differing levels of hydration. *Biophysical Journal* 81(6):3005-3015.
- Mason, R. P., J. D. Estermyer, J. F. Kelly, and P. E. Mason. 1996. Alzheimer's disease amyloid beta peptide 25-35 is localized in the membrane hydrocarbon core: X-ray diffraction analysis. *Biochemical and Biophysical Research Communications* 222(1):78-82.
- Massi, F., J. W. Peng, J. P. Lee, and J. E. Straub. 2001. Simulation study of the structure and dynamics of the Alzheimer's amyloid peptide congener in solution. *Biophysical Journal* 80(1):31-44.
- Massi, F., and J. E. Straub. 2003. Structural and dynamical analysis of the hydration of the Alzheimer's beta-amyloid peptide. *Journal of Computational Chemistry* 24(2):143-153.
- McLaurin, J., T. Franklin, P. E. Fraser, and A. Chakrabartty. 1998. Structural transitions associated with the interaction of Alzheimer beta-amyloid peptides with gangliosides. *Journal of Biological Chemistry* 273(8):4506-4515.
- McQuarrie, D. A. 2003. *Statistical Mechanics*. Viva Books Private Limited, New Delhi.
- Milchev, A., and K. Binder. 1998. A polymer chain trapped between two parallel repulsive walls: a Monte-Carlo test of scaling behavior. *European Physical Journal B* 3(4):477-484.
- Mobley, D. L., D. L. Cox, R. R. P. Singh, M. W. Maddox, and M. L. Longo. 2004. Modeling amyloid beta-peptide insertion into lipid bilayers. *Biophysical Journal* 86(6):3585-3597.
- Mori, K., M. Hata, S. Neya, and T. Hoshino. 2004. MD simulation of asymmetric phospholipid bilayers with ions and cholesterol. *Chem-Bio Informatics Journal* 4(1):15-26.
- Mouritsen, O. G. 1991. Theoretical models of phospholipid phase transitions. *Chemistry and Physics of Lipids* 57(2-3):179-194.

- Mouritsen, O. G., and K. Jorgensen. 1994. Dynamical order and disorder in lipid bilayers. *Chemistry and Physics of Lipids* 73(1-2):3-25.
- Nagle, J. F. 1993. Area/lipid of bilayers from NMR. *Biophysical Journal* 64(5):1476-1481.
- Nagle, J. F., R. T. Zhang, S. TristramNagle, W. J. Sun, H. I. Petrache, and R. M. Suter. 1996. X-ray structure determination of fully hydrated L(alpha) phase dipalmitoylphosphatidylcholine bilayers. *Biophysical Journal* 70(3):1419-1431.
- Nam, P. H., P. Maiti, M. Okamoto, T. Kotaka, T. Nakayama, M. Takada, M. Ohshima, A. Usuki, N. Hasegawa, and H. Okamoto. 2002. Foam processing and cellular structure of polypropylene/clay nanocomposites. *Poly. Eng. Sci.* 42(9):1907-1918.
- Narten, A. H., M. D. Danford, and H. A. Levy. 1967. X-ray diffraction study of liquid water in temperature range 4-200 degrees C. *Discussions of the Faraday Society*(43):97-107.
- Niemela, P., M. T. Hyvonen, and I. Vattulainen. 2004. Structure and dynamics of sphingomyelin bilayer: insight gained through systematic comparison to phosphatidylcholine. *Biophysical Journal* 87(5):2976-2989.
- NIMA Technology, 5/26/2006, Measuring surface pressure by the Wilhelmy technique, <http://www.nima.co.uk/equipment/ps/wilhelmy.htm>
- Ogata, N., S. Kawakage, and T. Ogihara. 1997. Poly(vinyl alcohol)-clay and poly(ethylene oxide)-clay blends prepared using water as solvent. *J. App. Poly. Sci.* 66(3):573-581.
- Pace, R. J., and S. I. Chan. 1982. Molecular motions in lipid bilayers. 1. Statistical mechanical model of acyl chain motion. *Journal of Chemical Physics* 76(8):4217-4227.
- Padilla, P., and S. Toxvaerd. 1994. Fluid alkanes in confined geometries. *Journal of Chemical Physics* 101(2):1490-1502.
- Pallitto, M. M., J. Ghanta, P. Heinzelman, L. L. Kiessling, and R. M. Murphy. 1999. Recognition sequence design for peptidyl modulators of beta-amyloid aggregation and toxicity. *Biochemistry* 38(12):3570-3578.

- Pasini, P., and C. Zannoni. 2000. *Advances in the Computer Simulations of Liquid Crystals*. Kluwer Academic Publishers, Boston.
- Patra, M., M. Karttunen, M. T. Hyvonen, E. Falck, P. Lindqvist, and I. Vattulainen. 2003. Molecular dynamics simulations of lipid bilayers: major artifacts due to truncating electrostatic interactions. *Biophysical Journal* 84(6):3636-3645.
- Patra, M., M. Karttunen, M. T. Hyvonen, E. Falck, and I. Vattulainen. 2004. Lipid bilayers driven to a wrong lane in molecular dynamics simulations by subtle changes in long-range electrostatic interactions. *Journal of Physical Chemistry B* 108(14):4485-4494.
- Peek M., 5/24/2006, Analysis of lysozyme structure, CHEM4581, Spring 2005, http://web.chemistry.gatech.edu/class/peek/4581/labs/pdb_tutorial.pdf
- Petrache, H. I., S. W. Dodd, and M. F. Brown. 2000. Area per lipid and acyl length distributions in fluid phosphatidylcholines determined by H-2 NMR spectroscopy. *Biophysical Journal* 79(6):3172-3192.
- Plimpton, S. 1995. Fast parallel algorithms for short-range molecular dynamics. *Journal of Computational Physics* 117(1):1-19.
- Plummer, C. J. G., L. Garamszegi, Y. Leterrier, M. Rodlert, and J. A. E. Manson. 2002. Hyperbranched polymer layered silicate nanocomposites. *Chemistry of Materials* 14(2):486-488.
- Pollock, E. L., and J. Glosli. 1996. Comments on P(3)M, FMM, and the Ewald method for large periodic coulombic systems. *Computer Physics Communications* 95(2-3):93-110.
- Quine, J. R., 5/18/2006, Torsion angles, PDB files, http://www.math.fsu.edu/~quine/IntroMathBio_04/torsion_pdb/torsion_pdb.pdf
- Ribarsky, M. W., and U. Landman. 1992. Structure and dynamics of normal-alkanes confined by solid surfaces. I. Stationary crystalline boundaries. *Journal of Chemical Physics* 97(3):1937-1949.

- Robello, D. R., N. Yamaguchi, T. Blanton, and C. Barnes. 2004. Spontaneous formation of an exfoliated polystyrene-clay nanocomposite using a star-shaped polymer. *J. Am. Chem. Soc.* 126(26):8118-8119.
- Robinson, A. J., W. G. Richards, P. J. Thomas, and M. M. Hann. 1994. Head group and chain behavior in biological membranes: a molecular dynamics computer simulation. *Biophysical Journal* 67(6):2345-2354.
- Ryckaert, J. P., G. Ciccotti, and H. J. C. Berendsen. 1977. Numerical integration of Cartesian equations of motion of a system with constraints: molecular dynamics of normal-alkanes. *Journal of Computational Physics* 23(3):327-341.
- Scarlata, S. F. 1991. Compression of lipid membranes as observed at varying membrane positions. *Biophysical Journal* 60(2):334-340.
- Schindler, H., and J. Seelig. 1975. Deuterium order parameters in relation to thermodynamic properties of a phospholipid bilayer. Statistical mechanical interpretation. *Biochemistry* 14(11):2283-2287.
- Seelig, A., and J. Seelig. 1974. Dynamic structure of fatty acyl chains in a phospholipid bilayer measured by deuterium magnetic resonance. *Biochemistry* 13(23):4839-4845.
- Seelig, J., and W. Niederbe. 1974. Deuterium-labeled lipids as structural probes in liquid crystalline bilayers. A deuterium magnetic resonance study. *J. Am. Chem. Soc.* 96(7):2069-2072.
- Serpell, L. C. 2000. Alzheimer's amyloid fibrils: structure and assembly. *Biochimica et Biophysica Acta-Molecular Basis of Disease* 1502(1):16-30.
- Shinoda, W., T. Fukada, S. Okazaki, and I. Okada. 1995. Molecular dynamics simulation of the dipalmitoylphosphatidylcholine (DPPC) lipid bilayer in the fluid phase using the Nose-Parrinello-Rahman NPT ensemble. *Chemical Physics Letters* 232(3):308-312.
- Shinoda, W., N. Namiki, and S. Okazaki. 1997. Molecular dynamics study of a lipid bilayer: convergence, structure, and long-time dynamics. *Journal of Chemical Physics* 106(13):5731-5743.

- Singh, C., and A. C. Balazs. 2000. Effect of polymer architecture on the miscibility of polymer/clay mixtures. *Polymer International* 49(5):469-471.
- Sisodia, S. S., and D. L. Price. 1995. Role of the beta-amyloid protein in Alzheimer's disease. *FASEB Journal* 9(5):366-370.
- Smondirev, A. M., and M. L. Berkowitz. 1999a. Molecular dynamics simulation of DPPC bilayer in DMSO. *Biophysical Journal* 76(5):2472-2478.
- Smondirev, A. M., and M. L. Berkowitz. 1999b. Structure of dipalmitoylphosphatidylcholine/cholesterol bilayer at low and high cholesterol concentrations: molecular dynamics simulation. *Biophysical Journal* 77(4):2075-2089.
- Sum, A. K. 2005. Molecular simulation study of the influence of small molecules on the dynamic and structural properties of phospholipid bilayers. *Chemistry & Biodiversity* 2(11):1503-1516.
- Suzuki, S., O. V. Galzitskaya, D. Mitomo, and J. Higo. 2004. General dynamic properties of A beta(12-36) amyloid peptide involved in Alzheimer's disease from unfolding simulation. *Journal of Biochemistry* 136(5):583-594.
- Takaoka, Y., H. Miyagawa, and K. Kitamura. 1998. Molecular dynamics simulation of phospholipid bilayer membrane. *Fluid Phase Equilibria* 144(1-2):387-393.
- Tanaka, G., and L. A. Goettler. 2002. Predicting the binding energy for nylon 6,6/clay nanocomposites by molecular modeling. *Polymer* 43(2):541-553.
- Teleman, O., B. Jonsson, and S. Engstrom. 1987. A molecular dynamics simulation of a water model with intramolecular degrees of freedom. *Molecular Physics* 60(1):193-203.
- Terzi, E., G. Holzemann, and J. Seelig. 1997. Interaction of Alzheimer beta-amyloid peptide(1-40) with lipid membranes. *Biochemistry* 36(48):14845-14852.
- Thurmond, R. L., S. W. Dodd, and M. F. Brown. 1991. Molecular areas of phospholipids as determined by 2-H NMR-spectroscopy: comparison of phosphatidylethanolamines and phosphatidylcholines. *Biophysical Journal* 59(1):108-113.

- Tieleman, D. P., and H. J. C. Berendsen. 1996. Molecular dynamics simulations of a fully hydrated dipalmitoyl phosphatidylcholine bilayer with different macroscopic boundary conditions and parameters. *Journal of Chemical Physics* 105(11):4871-4880.
- Tieleman, D. P., J. Breed, H. J. C. Berendsen, and M. S. P. Sansom. 1998. Alamethicin channels in a membrane: molecular dynamics simulations. *Faraday Discussions*(111):209-223.
- Tieleman, D. P., S. J. Marrink, and H. J. C. Berendsen. 1997. A computer perspective of membranes: molecular dynamics studies of lipid bilayer systems. *Biochimica et Biophysica Acta-Reviews on Biomembranes* 1331(3):235-270.
- Tieleman, D. P., M. S. P. Sansom, and H. J. C. Berendsen. 1999. Alamethicin helices in a bilayer and in solution: molecular dynamics simulations. *Biophysical Journal* 76(1):40-49.
- Tobias, D. J., K. C. Tu, and M. L. Klein. 1997. Atomic-scale molecular dynamics simulations of lipid membranes. *Current Opinion in Colloid & Interface Science* 2(1):15-26.
- Tu, K., M. L. Klein, and D. J. Tobias. 1998. Constant-pressure molecular dynamics investigation of cholesterol effects in a dipalmitoylphosphatidylcholine bilayer. *Biophysical Journal* 75(5):2147-2156.
- Tu, K., D. J. Tobias, J. K. Blasie, and M. L. Klein. 1996. Molecular dynamics investigation of the structure of a fully hydrated gel-phase dipalmitoylphosphatidylcholine bilayer. *Biophysical Journal* 70(2):595-608.
- Tu, K., D. J. Tobias, and M. L. Klein. 1995. Constant pressure and temperature molecular dynamics simulation of a fully hydrated liquid crystal phase dipalmitoylphosphatidylcholine bilayer. *Biophysical Journal* 69(6):2558-2562.
- Ulander, J., and A. D. J. Haymet. 2003. Permeation across hydrated DPPC lipid bilayers: simulation of the titrable amphiphilic drug valproic acid. *Biophysical Journal* 85(6):3475-3484.

- Vaia, R. A., and E. P. Giannelis. 1997a. Lattice model of polymer melt intercalation in organically-modified layered silicates. *Macromolecules* 30(25):7990-7999.
- Vaia, R. A., and E. P. Giannelis. 1997b. Polymer melt intercalation in organically-modified layered silicates: Model predictions and experiment. *Macromolecules* 30(25):8000-8009.
- Vaia, R. A., H. Ishii, and E. P. Giannelis. 1993. Synthesis and properties of 2-dimensional nanostructures by direct intercalation of polymer melts in layered silicates. *Chemistry of Materials* 5(12):1694-1696.
- Vaia, R. A., K. D. Jandt, E. J. Kramer, and E. P. Giannelis. 1995. Kinetics of polymer melt intercalation. *Macromolecules* 28(24):8080-8085.
- Vaia, R. A., K. D. Jandt, E. J. Kramer, and E. P. Giannelis. 1996. Microstructural evolution of melt intercalated polymer-organically modified layered silicates nanocomposites. *Chemistry of Materials* 8(11):2628-2635.
- van Buuren, A. R., S. J. Marrink, and H. J. C. Berendsen. 1995. Characterization of aqueous interfaces with different hydrophobicities by molecular dynamics. *Colloids and Surfaces A-Physicochemical and Engineering Aspects* 102:143-157.
- van der Ploeg, P., and H. J. C. Berendsen. 1982. Molecular dynamics simulation of a bilayer membrane. *Journal of Chemical Physics* 76(6):3271-3276.
- Wang, S. S. S., D. L. Rymer, and T. A. Good. 2001. Reduction in cholesterol and sialic acid content protects cells from the toxic effects of beta-amyloid peptides. *Journal of Biological Chemistry* 276(45):42027-42034.
- Wang, S. S. S., S. A. Tobler, T. A. Good, and E. J. Fernandez. 2003. Hydrogen exchange-mass spectrometry analysis of beta-amyloid peptide structure. *Biochemistry* 42(31):9507-9514.
- Woster, P. M., 2/23/2006, Protein structure and function - an overview, <http://wiz2.pharm.wayne.edu/biochem/prot.html>
- Xia, T. K., O. Y. Jian, M. W. Ribarsky, and U. Landman. 1992. Interfacial alkane films. *Physical Review Letters* 69(13):1967-1970.

Yoo, S. J. 2002. Exploration of the role of gangliosides and cholesterol in the mechanism of beta-amyloid neurotoxicity in Alzheimer's disease. Thesis. Texas A&M University, College Station.

Zhu, J., A. B. Morgan, F. J. Lamelas, and C. A. Wilkie. 2001. Fire properties of polystyrene-clay nanocomposites. *Chemistry of Materials* 13(10):3774-3780.

APPENDICES

APPENDIX A

ATOM INFORMATION FOR BIO-RESEARCH

Force-field information of the systems of protein (A β (1-42)) or protein fragment(A β (1-42)) in water or near hydrated lipids is tabulated below.

**Table A-1 Atom information for simulations of A β (1-42) in water;
data.Ab_H2O_100505_min_1_10k.**

atom number	atom type	atom	atomic mass	molecule
1	n4	N	14.0067	protein
2	ca	C	12.01115	protein
3	c'	C	12.01115	protein
4	o'	O	15.9994	protein
5	c2	C	12.01115	protein
6	c	C	12.01115	protein
7	o	O	15.9994	protein
8	hn	H	1.00797	protein
9	h	H	1.00797	protein
10	n4	N	14.0067	protein
11	c3	C	12.01115	protein
12	cp	C	12.01115	protein
13	n1	N	14.0067	protein
14	cr	C	12.01115	protein
15	n2	N	14.0067	protein
16	c5	C	12.01115	protein
17	np	N	14.0067	protein
18	oh	O	15.9994	protein
19	ho	H	1.00797	protein
20	cg	C	12.01115	protein
21	c1	C	12.01115	protein
22	s	S	32.064	protein
23	o*	O	15.9994	water
24	h*	H	1.00797	water

**Table A-2 Atom information for simulations of A β (31-42) in water;
data.beta_frag_water_min_091905_3 and data.alpha_frag_water_min_091905_3.**

atom number	atom type	atom	atomic mass	molecule
1	n4	N	14.0067	protein
2	ca	C	12.01115	protein
3	c'	C	12.01115	protein
4	o'	O	15.9994	protein
5	c1	C	12.01115	protein
6	c2	C	12.01115	protein
7	c3	C	12.01115	protein
8	hn	H	1.00797	protein
9	h	H	1.00797	protein
10	n	N	14.0067	protein
11	cg	C	12.01115	protein
12	s	S	32.064	protein
13	c-	C	12.01115	protein
14	o-	O	15.9994	protein
15	o*	O	15.9994	water
16	h*	H	12.01115	water

Table A-3 Atom information for simulations of A β (1-42) near hydrated lipids; data.last_mod(_04) and data.min_091405.

atom number	atom type	atom	atomic mass	molecule
1	c3	C	12.01115	DPPC/protein
2	n4	N	14.0067	DPPC/protein
3	c2	C	12.01115	DPPC/protein
4	o	O	15.9994	DPPC
5	p	P	30.973801	DPPC
6	o-	O	15.9994	DPPC/protein
7	c1	C	12.01115	DPPC/protein
8	c'	C	12.01115	DPPC/protein
9	o'	O	15.9994	DPPC/protein
10	h	H	1.00797	DPPC/protein
11	o*	O	15.9994	water
12	h*	H	1.00797	water
13	ca	C	12.01115	protein
14	c-	C	12.01115	protein
15	hn	H	1.00797	protein
16	n	N	14.0067	protein
17	cp	C	12.01115	protein
18	n1	N	14.0067	protein
19	cr	C	12.01115	protein
20	n2	N	14.0067	protein
21	ci	C	12.01115	protein
22	ni	N	14.0067	protein
23	oh	O	15.9994	protein
24	ho	H	1.00797	protein
25	cg	C	12.01115	protein
26	s	S	32.063999	protein

**Table A-4 Atom information for simulations of A β (31-42) near hydrated lipids;
data.DPPC_B_frag_092705_2_min_100.**

atom number	atom type	atom	atomic mass	molecule
1	c3	C	12.01115	DPPC/protein
2	n4	N	14.0067	DPPC/protein
3	c2	C	12.01115	DPPC/protein
4	o	O	15.9994	DPPC
5	p	P	30.973801	DPPC
6	o-	O	15.9994	DPPC/protein
7	c1	C	12.01115	DPPC/protein
8	c'	C	12.01115	DPPC/protein
9	o'	O	15.9994	DPPC/protein
10	h	H	1.00797	DPPC/protein
11	ca	C	12.01115	protein
12	hn	H	1.00797	protein
13	n	N	14.0067	protein
14	cg	C	12.01115	protein
15	s	S	32.064	protein
16	c-	C	12.01115	protein
17	o*	O	15.9994	water
18	h*	H	1.00797	water

APPENDIX B

PRELIMINARY STUDY FOR BIO-RESEARCH

Several preliminary tasks such as the machine reliability test, determination of damping parameters, and speedup test have been performed. Short discussions with corresponding simulation conditions and results are presented in this appendix.

B.1 Machine Reliability

Short simulations in NVT ensemble with α -helix and β -sheet conformations in water were performed to investigate the thermodynamic properties. The main purpose of this set of simulation is to check machine and # of cpus dependency. The simulation conditions are summarized in Table B-1. The data files for each simulation are data.alpha_frag_water and data.beta_frag_water for each conformation, respectively. Simulations were carried out with the time step of 0.5 fs and the simulation time was 5 ps. The cutoff radius of 10.0 Å was used for both of the nonbond interactions. The system was minimized using LAMMPS 2001, followed by production runs.

Table B-1 Summary of simulation parameters for A β (31-42) in water for machine dependency; NVT ensemble, $\Delta t = 0.5$ fs, LAMMPS 2001, minimization followed by 5 ps MD, last 2.5 statistics were used.

Index	Original Index	Machine	data file
A β _W- α _min_01	alpha_frag_water_091905_3	CAT/4cpus	alpha_frag_water
A β _W- β _min_01	beta_frag_water_091905_3	CAT/4cpus	beta_frag_water
A β _W- α _min_02	A_frag_H2O_101205_min	COSMOS/8cpus	alpha_frag_water
A β _W- α _min_03	A_frag_H2O_101405_min	COSMOS/4cpus	alpha_frag_water
A β _W- α _min_04	A_frag_H2O_101405_min_2p	COSMOS/2cpus	alpha_frag_water

Speedup of 1.57 for the 4 CPU job compared to 2 CPU job on COSMOS was found. The 8 CPU job showed 2.32 speedup compared to 4 CPU job (details not shown in this

Table B-2 Comparison of short MD results for A β (31-42) in water; NVT ensemble, $\Delta t = 0.5$ fs, cutoff = 10.0 Å for both nonbond interactions, 10000 steps or 5 ps of total time span, values are from the last 2.5 ps simulations.

Index	Total E [kcal/mol]	KE [kcal/mol]	Temp [K]	PE [kcal/mol]	E_bond [kcal/mol]	E_anlge [kcal/mol]	E_dihed [kcal/mol]	E_impr [kcal/mol]	E_vdw [kcal/mol]	E_coul [kcal/mol]	E_long [kcal/mol]	Press [atm]
A β _W- α _min_01	-50074.1 1366.8	26579.9 58.6	323.2 0.7	-76654.0 1346.9	7217.4 286.6	5777.8 38.6	15.2 1.0	5.1 0.5	12519.6 35.5	-102189.0 1629.1	0.0 0.0	-1576.9 290.2
A β _W- β _min_01	-45915.4 1797.4	26540.8 107.5	323.3 1.3	-72456.2 1737.3	7300.4 271.3	5734.6 16.9	17.0 1.7	4.2 0.2	12556.4 89.5	-98068.9 1562.3	0.0 0.0	-1234.2 224.1
A β _W- α _min_02	-49969.0 1886.8	26580.0 67.8	323.2 0.8	-76549.0 1837.2	7269.4 265.4	5774.3 21.9	14.1 1.0	4.0 0.3	12506.3 138.2	-102117.2 1609.0	0.0 0.0	-1622.3 259.4
A β _W- α _min_03	-46596.9 1232.8	26588.7 92.5	323.3 1.1	-73185.6 1308.7	7349.2 274.3	5769.5 9.6	15.3 0.7	4.1 0.2	12653.4 58.3	-98977.2 1272.1	0.0 0.0	-1239.5 146.0
A β _W- α _min_04	-48458.7 2926.4	26576.2 44.2	323.1 0.5	-75034.8 2919.0	7285.8 320.5	5755.9 18.4	15.7 0.3	4.6 0.2	12465.4 126.9	-100562.2 3330.5	0.0 0.0	-1532.2 352.1

dissertation). The corresponding table showing the thermodynamic properties is Table B-2. The potential energies on CAT with Myrinet interconnect and COSMOS were -76654 (A β _W- α _min_01) and -76549 kcal/mol (A β _W- α _min_02), which tells little difference between the two machines.

The potential energy of system with β -sheet conformation was -72456 kcal/mol, while that of α -helix was -76654 kcal/mol. The potential energy difference between the α -conformation and β -conformation is largely due to the Coulomb interaction or electrostatics as shown in the table. This result clearly implies that the energetic contribution to the free energy profile for different A β structure will be different.

B.2 Determination of Damping Parameters

The same size of simulation box as described in the previous section was constructed with A β (31-42) α -helix conformation. A set of test runs, 20 ps with the time step of 2 fs and PPPM option, with energy-minimized starting structures was performed. Summary table of short test simulation details to find the optimum damping parameters appears in Table B-3. The temperature and pressure damping parameters, T_{damp} and P_{damp} , vary from 0.1 ps to 10.0 ps.

Table B-3 Summary of simulation parameters for A β (31-42) α -conformation in water for damping parameters determination; the lateral pressure of -100 atm and the normal pressure is 1 atm, alpha_frag_water_min_091905_3 as the starting configuration.

Index	Original Index	Machine	T_{damp} [ps]	P_{damp} [ps]	Span [ps]	Average [ps]
A β _W- α _01	alpha_frag_water_092005_test01	CAT/2cpus	0.1	0.1	20	last 10
A β _W- α _02	alpha_frag_water_092005_test02	CAT/2cpus	0.1	1.0	20	last 10
A β _W- α _03	alpha_frag_water_092005_test03	CAT/2cpus	0.1	10.0	20	last 10
A β _W- α _04	alpha_frag_water_092005_test04	CAT/2cpus	1.0	0.1	20	last 10
A β _W- α _05	alpha_frag_water_092005_test05	CAT/2cpus	1.0	1.0	20	last 10
A β _W- α _06	alpha_frag_water_092005_test06	CAT/2cpus	1.0	10.0	20	last 10
A β _W- α _07	alpha_frag_water_092005_test07	CAT/2cpus	10.0	0.1	20	last 10
A β _W- α _08	alpha_frag_water_092005_test08	CAT/2cpus	10.0	1.0	20	last 10
A β _W- α _09	alpha_frag_water_092005_test09	CAT/2cpus	10.0	10.0	20	last 10

Simulation results of thermodynamic properties are shown in Table B-4. The temperature for cases A β _W- α _01, A β _W- α _02 and A β _W- α _03 were maintained at 323K, while others failed to keep the temperature 323K, though the deviation is small. The standard deviations of potential energy for the choice of pressure damping parameter of 1.0 ps were the smallest.

Note that the kinetic energy from this set of simulations is quite different from that of A β _W- α _min series due to the difference in the number of degrees of freedom. Recalling the definition of temperature we have

$$\langle KE \rangle = \frac{N_f kT}{2} \quad (\text{B-1})$$

where N_f is the total number of degrees of freedom, $k = 1.3807 \times 10^{-23}$ J/K is the Boltzmann constant. When applying SHAKE algorithm, we intrinsically constraints the bond length, which in turn reduces N_f from $3N$ to $3N - N_c$. N_c represents the number of constraints. An example calculation for simulations with data.alpha_frag_water tells that the total number of atoms is 27595 and the number of O-H bonds whose movement is constrained is 18280. For simplicity we ignored the constrained C-H bonds, since the number of bonds is quite small. So using $N_f = 3N - N_c = 64505$, we obtain $\langle KE \rangle = 20695$ kcal/mol, which is quite close to the measured kinetic energy.

Potential energy values with standard deviations are shown in Figure B-1 for different test cases. The potential energies for the four different case simulations are similar, but A β _W- α _02 case where the temperature and pressure damping parameters are 0.1 ps and 1.0 ps resulted in the smallest fluctuation. These values are the choice for other researchers' work, while they used united atom model for DPPC molecules with different force-field (Tieleman and Berendsen, 1996). The potential energy of the system varies from -76,461 to -76,584 kcal/mol for the nine test results.

Table B-4 Thermodynamic properties measured from simulations for A β (31-42) α -conformation in water for damping parameters determination; second row values are the standard deviations.

Index	Total E [kcal/mol]	KE [kcal/mol]	Temp [K]	PE [kcal/mol]	E_bond [kcal/mol]	E_anlge [kcal/mol]	E_dihed [kcal/mol]	E_impr [kcal/mol]	E_vdw [kcal/mol]	E_coul [kcal/mol]	E_long [kcal/mol]	Press [atm]	Volume [Å ³]
A β _W- α _01	-55781.1 70.9	20679.8 3.9	323.0 0.1	-76460.9 70.3	62.5 3.0	5320.2 22.8	16.4 0.3	4.8 0.1	10983.4 11.1	359139.8 102.8	-451988.1 2.0	-66.1 0.6	297693.5 558.4
A β _W- α _02	-55818.4 32.8	20678.3 4.4	323.0 0.1	-76496.7 32.2	62.1 0.8	5293.5 27.4	16.1 0.9	4.9 0.5	10980.9 38.8	359134.5 58.1	-451988.6 1.9	-68.9 13.1	297603.0 769.7
A β _W- α _03	-55355.9 1112.9	20679.9 4.1	323.0 0.1	-76035.7 1110.8	63.7 1.3	5282.7 26.8	16.1 1.3	5.3 0.3	10944.2 394.0	359630.5 1487.9	-451978.2 21.8	-150.4 609.6	304149.8 15549.0
A β _W- α _04	-55965.6 716.5	20618.5 241.0	322.1 3.8	-76584.1 475.7	61.3 0.9	5301.5 36.1	17.9 1.0	5.0 0.5	11020.7 120.5	358998.3 555.4	-451988.8 5.5	-66.2 1.6	297636.6 1194.8
A β _W- α _05	-55905.1 424.1	20648.7 149.6	322.5 2.3	-76553.7 280.1	61.2 0.9	5273.0 35.0	15.7 1.1	5.1 0.4	10972.8 53.6	359107.7 295.3	-451989.3 3.8	-67.9 9.7	297074.8 1051.5
A β _W- α _06	-55548.5 1717.9	20614.9 448.8	322.0 7.0	-76163.4 1376.6	59.5 0.3	5256.4 66.5	15.8 1.1	4.6 0.4	10977.2 413.2	359502.9 1732.4	-451979.9 23.9	-155.9 527.2	303871.6 14141.2
A β _W- α _07	-55582.2 148.6	20738.8 34.9	323.9 0.5	-76321.0 115.0	61.1 2.4	5275.5 13.0	16.7 0.5	4.9 0.5	10942.0 18.8	359364.2 120.5	-451985.5 2.5	-66.3 1.0	298303.0 837.6
A β _W- α _08	-55683.8 142.3	20731.3 44.9	323.8 0.7	-76415.1 99.1	62.2 0.8	5336.7 7.3	16.2 0.8	5.2 0.4	10980.8 16.6	359170.3 105.4	-451986.4 1.9	-68.6 6.4	297859.3 707.4
A β _W- α _09	-55701.4 47.1	20693.6 424.3	323.2 6.6	-76395.0 414.4	60.8 0.7	5260.1 95.4	16.3 0.9	4.9 0.4	11084.5 249.4	359164.1 731.3	-451985.8 14.8	76.0 715.1	299238.1 15185.2

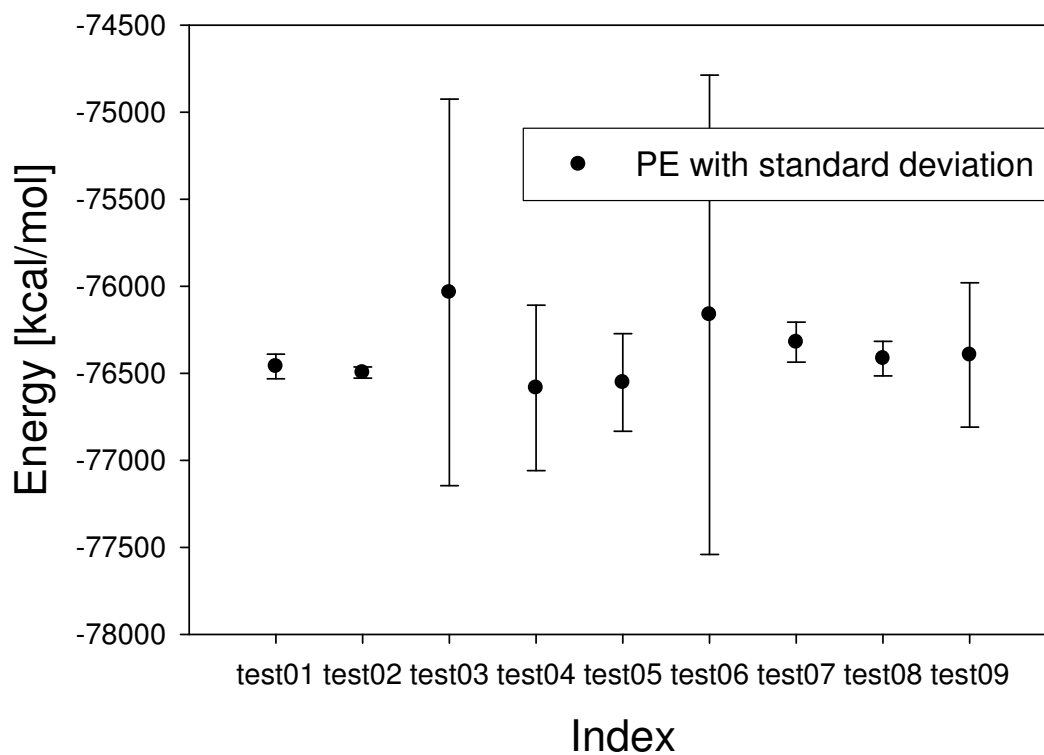


Figure B-1 Damping parameters determination from the simulations of $A\beta(31-42)$ α -conformation in water; testXX represents $A\beta_W-\alpha_XX$.

B.3 Speedup

Short MD simulations to test the speedup and machine dependency were performed and the simulation details are tabulated in Table B-5. The lateral pressure was maintained as -100 atm throughout the simulation time.

Table B-5 Summary of simulation parameters for A β (31-42) α -conformation in water for the effect of different number of cups on COSMOS; NPT ensemble with the lateral pressure of -100 atm and the normal pressure of 1 atm, data.alpha_frag_water_min_091905_3 as the starting configuration.

Index	Original Index	Machine	Span [ps]	Average [ps]
A β _W- α _01	alpha_frag_water_092005_test01	CAT/2cpus	20	last 10
A β _W- α _11	A_frag_H2O_100205_1p	COSMOS/1cpu	20	last 10
A β _W- α _12	A_frag_H2O_100205_2p	COSMOS/2cpus	20	last 10
A β _W- α _13	A_frag_H2O_100205_4p	COSMOS/4cpus	20	last 10
A β _W- α _14	A_frag_H2O_100205_8p	COSMOS/8cpus	20	last 10
A β _W- α _15	A_frag_H2O_100205_16p	COSMOS/16cpus	20	last 10

Table B-6 is the summary of simulation results for short MD runs with A β (31-42) α -helix conformation. The temperature is well maintained at 323 K and the energy terms in each column are the same within the statistical error regardless of the choice of machine and the number of CPUs. Therefore, we can conclude that LAMMPS produces statistically same results on those two machines.

Table B-6 Thermodynamic properties measured from simulations for A β (31-42) α -conformation in water for the effect of different number of cups on COSMOS; second row values are the standard deviations.

Index	Total E [kcal/mol]	KE [kcal/mol]	Temp [K]	PE [kcal/mol]	E_bond [kcal/mol]	E_anlge [kcal/mol]	E_dihed [kcal/mol]	E_impr [kcal/mol]	E_vdw [kcal/mol]	E_coul [kcal/mol]	E_long [kcal/mol]	Press [atm]	Volume [Å ³]
A β _W- α a_01	-55781.1 70.9	20679.8 3.9	323.0 0.1	-76460.9 70.3	62.5 3.0	5320.2 22.8	16.4 0.3	4.8 0.1	10983.4 11.1	359139.8 102.8	-451988.1 2.0	-66.1 0.6	297693.5 558.4
A β _W- α a_11	-55807.6 42.7	20679.1 1.7	323.0 0.0	-76486.8 42.5	63.0 1.2	5288.5 21.1	16.8 1.8	4.9 0.3	10988.0 32.2	359139.5 80.4	-451987.6 0.9	-66.3 0.9	297628.4 99.5
A β _W- α a_12	-55820.3 60.6	20679.3 6.6	323.0 0.1	-76499.7 59.4	60.8 0.7	5311.1 20.8	15.9 0.9	5.1 0.5	10987.0 19.4	359109.3 55.0	-451988.9 1.7	-66.4 0.7	297407.0 453.0
A β _W- α a_13	-55827.6 38.9	20679.4 6.0	323.0 0.1	-76507.0 36.4	63.7 0.4	5316.7 18.3	16.9 0.2	5.1 0.3	10991.7 41.8	359088.2 81.1	-451989.3 0.7	-66.5 1.0	297218.3 538.7
A β _W- α a_14	-55791.5 25.3	20677.9 2.6	323.0 0.0	-76469.3 24.2	60.5 2.9	5282.4 17.1	16.7 0.8	5.4 0.4	10973.2 18.0	359180.1 39.4	-451987.7 1.7	-66.0 1.5	297762.0 125.5
A β _W- α a_15	-55782.5 31.5	20681.1 9.5	323.0 0.1	-76463.7 29.3	63.6 1.1	5299.8 15.8	17.1 0.8	5.2 0.3	10971.0 25.2	359167.1 67.2	-451987.3 0.9	-66.6 1.3	297568.9 167.7

APPENDIX C

FURTHER SIMULATION RESULTS FOR BIO-RESEARCH

We present some of the simulations results which are not discussed in the main text in this appendix. Simulation conditions and results as tables of bulk water, A β (1-42) or A β (31-42) near hydrated lipids are presented in this appendix.

C.1 Simulation of Bulk Water

Supplementary simulations have been performed for bulk water. Table C-1 shows the simulation conditions and the corresponding thermodynamic results are shown in Table C-2. The simulations used different starting configurations discussed in the text section 5.1.

Table C-1 Summary of simulation conditions for bulk water; CAT cluster with 4 cpus.

Index	Original Index	Machine	P_tar [atm]	Span [ps]	Average [ps]	Data file
W-cvff_01	H2O_030606_7	cvff	-75.00	200	last 100	data.H2O_042206_min_cvff_100
W-cvff_02	H2O_030606_9	cvff	-50.00	200	last 100	data.H2O_042206_min_cvff_200
W-cvff_03	H2O_030606_6	cvff	1.00	200	last 100	data.H2O_042206_min_cvff_300
W-cvff_04	H2O_030606_10	cvff	50.00	200	last 100	data.H2O_042206_min_cvff_400
W-cvff_05	H2O_030606_8	cvff	75.00	200	last 100	data.H2O_042206_min_cvff_500
W-spc_01	H2O_042006_1	cvff	75.00	200	last 100	data.H2O_042206_min_spc_100
W-spc_02	H2O_030706_1	SPC	-75.00	200	last 100	data.H2O_042206_min_spc_200
W-spc_03	H2O_030706_4	SPC	-50.00	200	last 100	data.H2O_042206_min_spc_300
W-spc_04	H2O_030706_2	SPC	1.00	200	last 100	data.H2O_042206_min_spc_400
W-spc_05	H2O_030706_5	SPC	50.00	200	last 100	data.H2O_042206_min_spc_500

Table C-2 Thermodynamic properties from bulk water simulations; CAT cluster with 4 cpus.

Index	Total E [K]	KE [kcal/mol]	Temp [kcal/mol]	PE [kcal/mol]	E_anlge [kcal/mol]	E_vdw [kcal/mol]	E_coul [kcal/mol]	E_long [kcal/mol]	Press [atm]	Vol [Å ³]	D _x = D _y = D _z [Å]	Density [g/cm ³]
W-cvff_01	-3073.70	1122.08	322.94	-4195.78	282.66	600.26	15213.24	-20291.94	-72.65	16201.44	25.30	0.92
	5.42	0.68	0.20	5.80	3.09	2.23	8.73	0.09	11.42	62.60	0.00	
W-cvff_02	-3074.54	1122.23	322.98	-4196.77	282.52	600.01	15212.71	-20292.01	-48.19	16165.98	25.29	0.92
	7.93	1.02	0.29	7.89	3.68	3.15	13.04	0.12	8.39	55.33	0.00	
W-cvff_03	-3082.04	1121.57	322.79	-4203.61	282.72	601.99	15203.68	-20291.99	8.16	16078.94	25.24	0.93
	4.77	0.70	0.20	4.54	3.24	2.15	7.93	0.11	11.82	51.62	0.00	
W-cvff_04	-3081.68	1122.39	323.03	-4204.07	280.23	601.20	15206.51	-20292.01	50.41	16042.08	25.22	0.93
	5.96	0.88	0.25	5.59	3.24	1.90	8.22	0.13	11.68	51.56	0.00	
W-cvff_05	-3087.61	1122.44	323.04	-4210.05	282.40	603.34	15196.34	-20292.13	75.12	15982.85	25.19	0.94
	8.54	0.54	0.15	8.38	2.59	2.87	10.78	0.10	6.33	43.81	0.00	
W-spc_01	-3638.84	1122.29	323.00	-4761.13	306.22	850.65	14374.49	-20292.49	-73.38	15626.02	25.00	0.96
	5.70	1.47	0.42	6.35	2.61	4.38	9.01	0.09	14.70	73.09	0.00	
W-spc_02	-3635.77	1122.40	323.03	-4758.17	306.86	847.22	14380.29	-20292.54	-45.65	15583.90	24.98	0.96
	6.54	1.03	0.30	6.41	2.97	3.50	11.55	0.16	13.86	41.66	0.00	
W-spc_03	-3634.02	1122.24	322.98	-4756.27	305.38	848.88	14381.99	-20292.51	1.95	15567.14	24.97	0.96
	8.13	0.84	0.24	8.17	3.71	5.07	13.63	0.15	13.17	75.52	0.00	
W-spc_04	-3642.63	1122.68	323.11	-4765.30	306.76	848.72	14371.78	-20292.56	51.67	15448.97	24.91	0.97
	7.47	1.24	0.36	7.11	2.05	6.15	12.97	0.14	9.47	66.15	0.00	
W-spc_05	-3644.60	1122.09	322.94	-4766.69	307.35	852.81	14365.84	-20292.68	76.99	15477.18	24.92	0.97
	6.85	0.96	0.28	6.66	2.70	3.65	10.56	0.15	11.08	54.38	0.00	

C.2 Simulation of A β (1-42) near Hydrated Lipids – A β series

Table C-3 shows the parameters and major simulation variables for the preliminary task. We take into account systems with different options such as the ensemble, starting configuration, and different methods of long-range electrostatics treatment. Some simulations were not successful because of the configuration failure of CAT cluster.

Table C-3 Summary of simulation parameters for A β (1-42) in hydrated lipids; CAT cluster, the normal pressure is 1 atm for NPT simulations, PPPM was not used for A β -F.

Index	Original Index	# of cpus	P _x = P _y [atm]	Span [ps]	Average [ps]	Data file	Remark
A β -A	run_090905	16		140.4	last 80	whole_run01_070105.10000	NVT
A β -B	run_091205	2		630.4	last 400	data.last_mod_04	NVT
A β -C	npt_run_091205	2	-100.0	134.4	last 80	data.last_mod_04	$\epsilon=1.0\times 10^{-4}$
A β -D	npt_run_091305	16	-100.0	34.2	last 20	data.last_mod_04	$\epsilon=1.0\times 10^{-3}$
A β -E	npt_091805_1	8	-100.0	2000	last 1000	data.min_091405_04	$\epsilon=1.0\times 10^{-3}$
A β -F	npt_100605_1	4	1.0	22.8	last 12	data.last_mod_04	$r_c=15.0$
A β -G	npt_091505_2	2	-100.0	1800	last 800	data.last_mod_04	$\epsilon=1.0\times 10^{-3}$

The corresponding simulation results with energy terms are summarized in Table C-4. There was approximately 2% difference of potential energy between NVT and NPT simulations (A β -B vs. A β -G). The comparison between the two long runs of NPT simulation (A β -E vs. A β -G) with different starting structure exhibits similar MD statistics.

Table C-4 Thermodynamic properties measured from simulations for A β (1-42) in hydrated lipids with different case studies; second row values are the standard deviations.

Index	Total E [kcal/mol]	KE [kcal/mol]	Temp [K]	PE [kcal/mol]	E_bond [kcal/mol]	E_anlge [kcal/mol]	E_dihed [kcal/mol]	E_impr [kcal/mol]	E_vdw [kcal/mol]	E_coul [kcal/mol]	E_long [kcal/mol]	Press [atm]	Volume [Å ³]
A β -A	-34038.3 292.2	33219.0 168.7	323.0 1.6	-67257.3 218.4	3340.9 47.3	15735.0 105.1	1976.1 54.1	104.9 7.7	9044.4 175.9	371745.9 235.1	-469204.6 11.1	1154.0 177.8	
A β -B	-34550.5 268.2	33220.6 142.2	323.0 1.4	-67771.1 229.3	3307.1 53.7	15430.9 118.5	1790.9 37.1	103.9 8.3	9139.9 173.0	371663.1 216.0	-469206.8 11.0	1128.0 177.8	
A β -C	-31742.9 270.0	33208.4 134.6	322.9 1.3	-64951.3 241.2	3379.0 49.5	15525.4 121.4	1870.4 44.7	105.8 8.7	9223.5 157.6	374096.7 241.8	-469152.1 10.7	-58.7 163.2	461818.8 1313.3
A β -D	-30666.1 381.3	33221.8 168.2	323.0 1.6	-63887.9 334.6	3406.2 54.1	15666.3 118.2	2078.1 54.6	108.3 8.0	9514.8 216.7	279084.4 283.0	-373746.0 8.5	-52.2 182.9	467344.0 2700.3
A β -E	-32540.5 84.7	33218.8 5.9	323.0 0.1	-65759.3 85.8	3297.9 7.7	15142.4 31.7	1686.2 15.2	102.6 0.2	8666.2 87.6	278581.8 82.2	-373236.5 2.1	-61.5 11.0	458948.8 615.0
A β -F	-27233.2 5150.8	33224.2 167.5	323.0 1.6	-60457.4 5143.7	3056.7 53.2	14959.3 114.1	2354.2 61.9	106.2 8.0	8372.9 126.9	-89306.6 5136.1	0.0 0.0	-41.2 286.4	453641.2 1869.3
A β -G	-33127.4 248.3	33224.7 147.8	323.0 1.4	-66352.0 202.2	3267.5 51.7	14950.3 104.4	1721.3 27.8	101.1 7.9	9120.4 164.3	278245.2 250.8	-373757.8 8.3	-67.2 171.5	462090.1 1284.0

Figure C-1 shows the end-to-end distance profile for the A β -E_01 case. Approximately 15 Å of difference among the distances was observed during the first 500 ps simulation. The profile also indicates that the protein moves toward the bilayer interface decreasing the end-to-end distance.

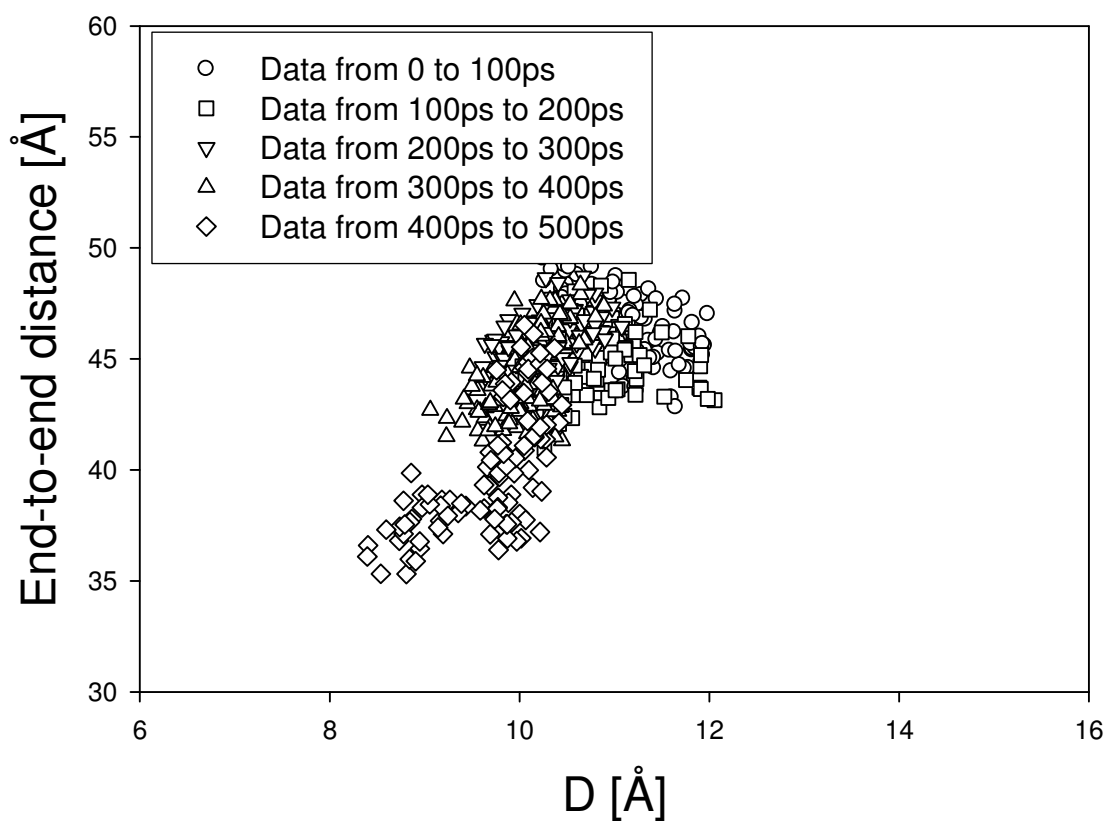


Figure C-1 End-to-end distance profile as a function of D ; 0 to 500ps, A β -E_01 case.

The end-to-end distance profile for the last 500 ps is plotted in Figure C-2 for the A β -E_01 case. It shows that the protein moves away from the interface during that time period changing its conformation simultaneously.

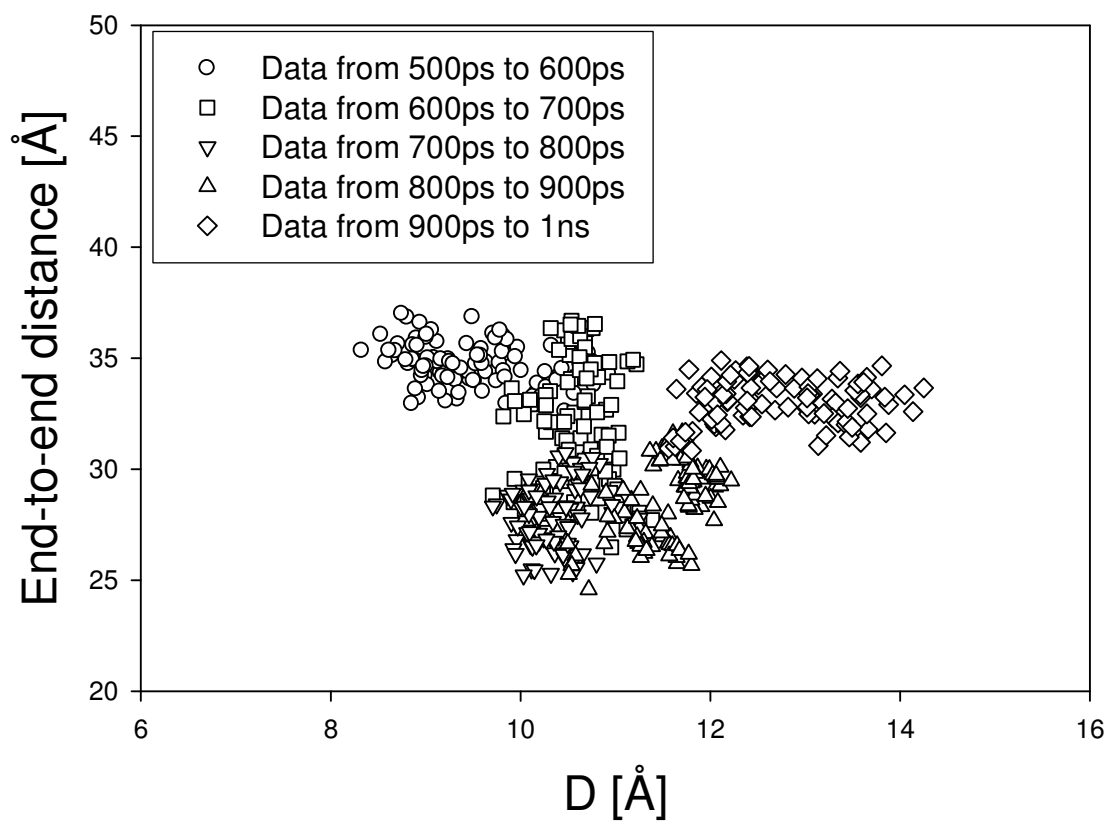


Figure C-2 End-to-end distance profile as a function of D; 500ps to 1ns, A β -E_01 case.

C.3 Simulation of A β (1-42) near Hydrated Lipids – A β -H series

Simulations with different starting configurations or different locations of the protein have been performed. The simulation details for A β -H series are shown in Table C-5,

where the starting configurations were generated by applying a highly negative lateral pressure ($P_L = -100$ atm) and a positive normal pressure ($P_N = 10$ atm) with data.last_mod_04. Saved restart files were used as starting configurations. The corresponding summary of thermodynamic properties is reported in Table C-6.

Table C-5 Summary of simulation parameters for A β (1-42) in hydrated lipids; A β -H series, CAT cluster with 8 cpusthe lateral pressure is set to 75 atm and the normal pressure is 10 atm, time span of 1ns used, and the last 500 ps data were used for analysis.

Index	Original Index	Data file
A β -H_01	Ab_H2O_DPPC_011606_1	Ab_H2O_DPPC_011506_1.50000
A β -H_02	Ab_H2O_DPPC_011606_2	Ab_H2O_DPPC_011506_1.100000
A β -H_03	Ab_H2O_DPPC_011606_3	Ab_H2O_DPPC_011506_1.150000
A β -H_04	Ab_H2O_DPPC_011606_4	Ab_H2O_DPPC_011506_1.200000
A β -H_05	Ab_H2O_DPPC_011606_5	Ab_H2O_DPPC_011506_1.250000
A β -H_06	Ab_H2O_DPPC_011606_6	Ab_H2O_DPPC_011506_1.300000
A β -H_07	Ab_H2O_DPPC_011606_7	Ab_H2O_DPPC_011506_1.350000

Table C-6 Thermodynamic properties measured from simulations for A β (1-42) in hydrated lipids with different case studies; A β -H series, second row values are the standard deviations.

Index	Total E [kcal/mol]	KE [kcal/mol]	Temp [K]	PE [kcal/mol]	E_bond [kcal/mol]	E_anlge [kcal/mol]	E_dihed [kcal/mol]	E_impr [kcal/mol]	E_vdw [kcal/mol]	E_coul [kcal/mol]	E_long [kcal/mol]	Press [atm]	Volume [Å ³]
A β -H_01	-33263.0 128.6	33223.2 5.2	323.0 0.1	-66486.2 129.1	3325.8 10.8	15248.3 20.2	1709.5 19.3	102.6 0.6	8746.4 75.2	277925.3 33.1	-373544.1 2.0	48.8 7.5	453264.6 709.4
A β -H_02	-33476.0 111.6	33219.5 5.7	323.0 0.1	-66695.5 110.7	3303.0 11.1	15177.8 25.0	1681.1 13.3	102.4 0.6	8605.3 73.7	269014.5 63.8	-364579.5 1.1	53.0 8.5	451912.6 904.2
A β -H_03	-33400.7 107.2	33221.9 3.2	323.0 0.0	-66622.6 107.8	3305.6 6.4	15187.6 16.2	1684.5 8.4	103.0 0.6	8576.9 41.4	279657.7 92.4	-375137.9 1.4	55.8 8.1	451989.1 598.2
A β -H_04	-33382.0 70.3	33220.4 4.2	323.0 0.0	-66602.3 68.4	3310.5 9.2	15173.4 28.8	1679.1 7.9	102.3 1.1	8623.5 30.8	282139.7 87.4	-377630.8 1.4	47.0 14.1	452613.4 538.7
A β -H_05	-33654.7 83.4	33218.7 5.3	323.0 0.1	-66873.4 83.0	3294.6 6.2	15132.8 22.1	1643.0 12.6	102.9 0.6	8473.1 56.0	275458.6 35.8	-370978.3 1.1	51.9 4.8	450806.2 527.4
A β -H_06	-33573.4 75.9	33221.9 6.4	323.0 0.1	-66795.2 78.1	3307.5 6.1	15153.2 28.4	1655.1 11.5	102.5 0.9	8494.5 61.8	276266.8 97.6	-371774.8 1.1	45.3 11.2	451184.6 511.8
A β -H_07	-33507.8 74.0	33217.8 7.6	323.0 0.1	-66725.6 76.5	3304.1 7.7	15134.7 23.8	1654.8 11.6	102.7 0.7	8499.1 60.0	276503.9 58.3	-371924.9 1.2	54.4 8.1	451684.9 331.0

C.4 A β (31-42) near Hydrated Lipids

Table C-7 is a summary of parameters and conditions of each simulation. One of the major variables, the lateral pressure, varied from -51.6 to -100. Other major variables are the cutoff radius change and the method of long-range electrostatics.

Table C-8 is the corresponding result summary table using the choices of Table C-7. First we will focus on the short simulation results. The cutoff radius change (10 Å vs 15 Å), comparison of A β -d with A β -e, shows approximately 2% difference in potential energy, which can be treated as the same output. To confirm this conclusion we need longer simulations, though. Potential energy of 10 ps to 20 ps run from A β -b (accuracy $1.0e^{-3}$) was found to be -65673 kcal/mol (not shown in the table), which is quite close to -64371 kcal/mol of A β -e (accuracy $1.0e^{-4}$). Again, our tentative conclusion will be verified using longer production runs.

Several production runs were done for longer simulation time, over 100 ps. The lateral pressure change doesn't affect the thermodynamic properties as can be seen from the comparison of A β -b and A β -h. This observation matches well with our physical intuition that the lipid bilayer has membrane fluidity and the system volume will not change much with the pressure change, since it is incompressible. We notice that the cutoff radius change in the electrostatic interactions will not affect the statistics much provided that the long-range electrostatics is treated with a proper method such as PPPM from the comparison between A β -a and A β -h. From the case simulation of A β -g, we found that the average head group area of DPPC is 72.55 \AA^2 , which is quite larger than the starting value of 62.9 \AA^2 . But, the result came out of very short simulation, therefore, we might see more reasonable value for longer runs. Controversy approximately the exact head group area has existed from both the simulations and experiments, still its value from our short simulation is close to the largest value of the literature (Chiu et al., 1995; Nagle et al., 1996; Tieleman and Berendsen, 1996).

Table C-7 Summary of simulation parameters for A β (31-42) in hydrated lipids; the normal pressure is 1 atm.

Index	Original Index	Machine	P _x = P _y [atm]	P _z [atm]	Span [ps]	Average [ps]	Remark
A β -a	npt_092905_2	CAT/8cpus	-100.0	1.0	400	last 200	
A β -b	B_frag_H2O_DPPC_100405_1	COSMOS/8cpus	-51.6	1.0	131.2	last 60	r _c =15Å
A β -c	B_frag_H2O_DPPC_100705_1	COSMOS/8cpus	-51.6	1.0	20	last 10	w/o PPPM
A β -d	B_frag_H2O_DPPC_100805_2	COSMOS/8cpus	-51.6	1.0	1000	last 500	PPPM $\epsilon=1.0\times 10^{-4}$
A β -e	B_frag_H2O_DPPC_101105_1	COSMOS/8cpus	-51.6	1.0	20	last 10	r _c =15Å, PPPM $\epsilon=1.0\times 10^{-4}$
A β -f	npt_101305_1	CAT/8cpus	-100.0	1.0	20	last 10	r _c =15Å
A β -g	npt_101405_test1	CAT/8cpus	-100.0	1.0	20	last 10	r _c =15Å
A β -h	npt_093005_1	CAT/8cpus	-100.0	1.0	2000	last 1000	r _c =15Å, PPPM n=3
A β -i	npt_092905_1	CAT/8cpus	-100.0	1.0	2000	last 1000	r _c =15Å
A β -j	npt_102805_1	CAT/8cpus	-51.6	1.0	1000	last 500	r _c =15Å
A β -k	npt_102805_2	CAT/8cpus	-10.0	1.0	1000	last 500	r _c =15Å
A β -l	npt_110805_1	CAT/8cpus	-2.0	1.0	1000	last 500	r _c =15Å
A β -m	npt_111205_1	CAT/8cpus	1.0	1.0	1000	last 500	r _c =15Å
A β -n_01	Ab_frag_B_H2O_DPPC_120905_1	CAT/16cpus	75.0	1.0	1000	last 500	
A β -n_02	Ab_frag_B_H2O_DPPC_121505_1	CAT/8cpus	75.0	1.0	1000	last 500	T=298K
A β -n_03	Ab_frag_B_H2O_DPPC_121605_1	CAT/8cpus	75.0	1.0	841.6	last 400	T=310K

Table C-8 Thermodynamic properties measured from simulations for A β (31-42) in hydrated lipids with different case studies; second row values are the standard deviations.

Index	Total E [kcal/mol]	KE [kcal/mol]	Temp [K]	PE [kcal/mol]	E_bond [kcal/mol]	E_anlge [kcal/mol]	E_dihed [kcal/mol]	E_impr [kcal/mol]	E_vdw [kcal/mol]	E_coul [kcal/mol]	E_long [kcal/mol]	Press [atm]	Volume [Å ³]
A β -a	-32979.8 99.6	33126.2 17.9	323.1 0.2	-66106.0 83.9	3108.2 16.1	15013.7 49.1	1724.7 21.6	90.3 0.8	9249.4 78.2	281697.0 78.4	-376989.4 1.7	-55.7 14.1	462819.9 538.2
A β -b	-34049.7 251.2	33117.3 146.5	323.0 1.4	-67167.0 204.9	3103.0 50.0	15134.1 104.8	1787.8 27.3	90.8 7.8	8573.0 160.8	152092.5 240.3	-247948.2 4.3	-31.4 164.1	462819.9 538.2
A β -c	-24172.8 1588.8	33114.9 11.2	323.0 0.1	-57287.7 1586.5	2365.9 24.8	13484.8 114.3	2036.1 29.2	78.1 1.8	8081.0 108.2	-83333.6 1806.1	0.0 0.0	-24.6 25.3	450600.9 3208.9
A β -d	-29952.4 615.1	33116.7 9.9	323.0 0.1	-63069.1 614.5	2844.7 42.4	14380.3 187.7	1970.2 60.6	88.1 1.4	9084.5 42.0	380012.2 781.3	-471449.1 15.5	-33.9 11.6	485586.2 7606.9
A β -e	-31255.0 652.6	33116.4 14.6	323.0 0.1	-64371.4 648.3	2837.1 56.7	14376.6 162.6	1985.6 48.8	88.4 2.5	8374.8 94.0	220700.1 731.8	-312734.0 4.8	-29.7 15.1	473275.9 7015.1
A β -f	-31858.8 318.7	33119.2 4.3	323.0 0.0	-64978.0 316.8	3064.9 11.2	15132.8 23.9	2109.7 43.3	95.3 1.4	8807.3 83.0	153753.4 223.2	-247941.5 1.3	-66.7 3.9	465100.8 1845.2
A β -g	-31912.8 309.0	33115.7 5.6	323.0 0.1	-65028.5 306.8	3065.6 12.4	15159.4 62.8	2095.1 62.7	95.6 2.3	8906.4 18.5	153591.4 326.6	-247941.9 2.3	-64.2 5.4	465767.3 1206.2
A β -h	-34576.5 86.5	33114.0 5.5	323.0 0.1	-67690.5 86.3	3096.7 7.0	14956.3 34.0	1661.4 16.6	89.9 0.5	8291.9 72.3	152158.3 58.4	-247945.0 0.5	-66.2 10.7	453601.0 643.5
A β -i	-34646.8 46.5	33124.0 5.9	323.1 0.1	-67770.8 51.5	3101.8 2.6	14977.7 20.3	1657.3 12.9	90.5 0.6	8338.4 31.3	149798.1 13.8	-245734.4 0.3	-68.1 4.8	453076.7 308.5
A β -j	-35087.1 122.2	33119.3 5.8	323.0 0.1	-68206.4 123.0	3101.5 11.4	14974.8 35.9	1638.7 20.5	90.9 0.6	8208.3 61.7	149515.1 78.1	-245735.8 0.6	-39.2 7.6	450637.6 480.2
A β -k	-35421.3 161.0	33115.5 5.7	323.0 0.1	-68536.8 163.4	3089.1 7.6	14951.4 24.9	1623.7 24.0	91.1 0.5	8080.3 90.5	149364.1 96.9	-245736.4 0.7	-7.1 5.9	448447.2 894.9
A β -l	-34977.5 267.2	33117.1 146.5	323.0 1.4	-68094.6 220.3	3097.7 51.4	15020.1 108.7	1672.8 29.7	91.0 7.7	8341.2 166.2	149418.6 249.7	-245736.0 4.1	1.8 173.4	451098.2 1216.0
A β -m	-35135.1 83.7	33117.0 8.9	323.0 0.1	-68252.1 81.4	3097.7 10.4	14983.7 45.1	1660.3 21.4	90.8 0.9	8280.0 100.5	149372.7 121.4	-245737.2 0.5	-5.2 10.4	450426.5 537.1
A β -n_01	-34814.1 83.6	33118.4 4.9	323.0 0.0	-67932.5 83.1	3076.5 7.4	14885.3 29.5	1606.2 14.1	90.3 0.4	8531.0 53.5	280881.8 45.3	-377003.6 1.5	53.3 10.2	451139.9 486.1
A β -n_02	-41740.6 178.1	30552.2 6.1	298.0 0.1	-72292.8 181.8	2890.1 4.5	14098.2 17.0	1504.4 19.9	84.1 0.6	9021.8 66.6	277131.5 94.9	-377022.9 2.2	49.1 8.7	441799.7 916.6
A β -n_03	-38333.7 261.4	31786.4 140.1	310.0 1.4	-70120.1 219.0	2984.2 48.1	14503.9 103.8	1559.1 29.1	86.7 7.4	8888.1 178.8	278875.0 253.6	-377017.0 7.3	52.1 173.1	447080.7 1173.1

Figure C-3 and Figure C-4 show the end-to-end distance profiles for the first and last 500 ps simulation for the A β -n_01 case. The biggest difference between the end-to-end distances is approximately 30 Å, indicating that the structural change is significant in this simulation case. We observe that the protein fragment moves toward the interface within 300 ps, then slightly moves away for the first 500 ps simulation.

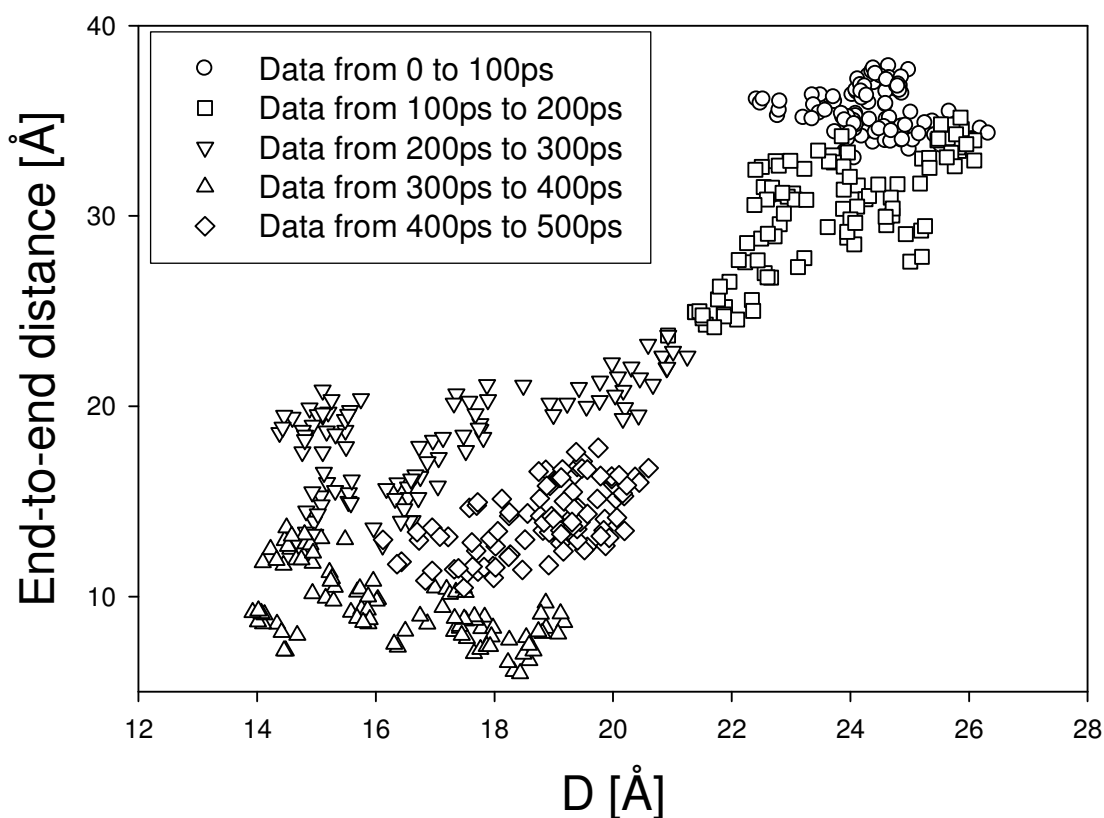


Figure C-3 End-to-end distance profile as a function of D ; 0 to 500ps, A β -n_01 case.

Relatively small difference (20 Å) in the end-to-end distance is observed for the last 500 ps simulation. The fragment seems to move away from the interface, however, it is

unclear from this profile whether it really translates away from the interface by examining this profile only.

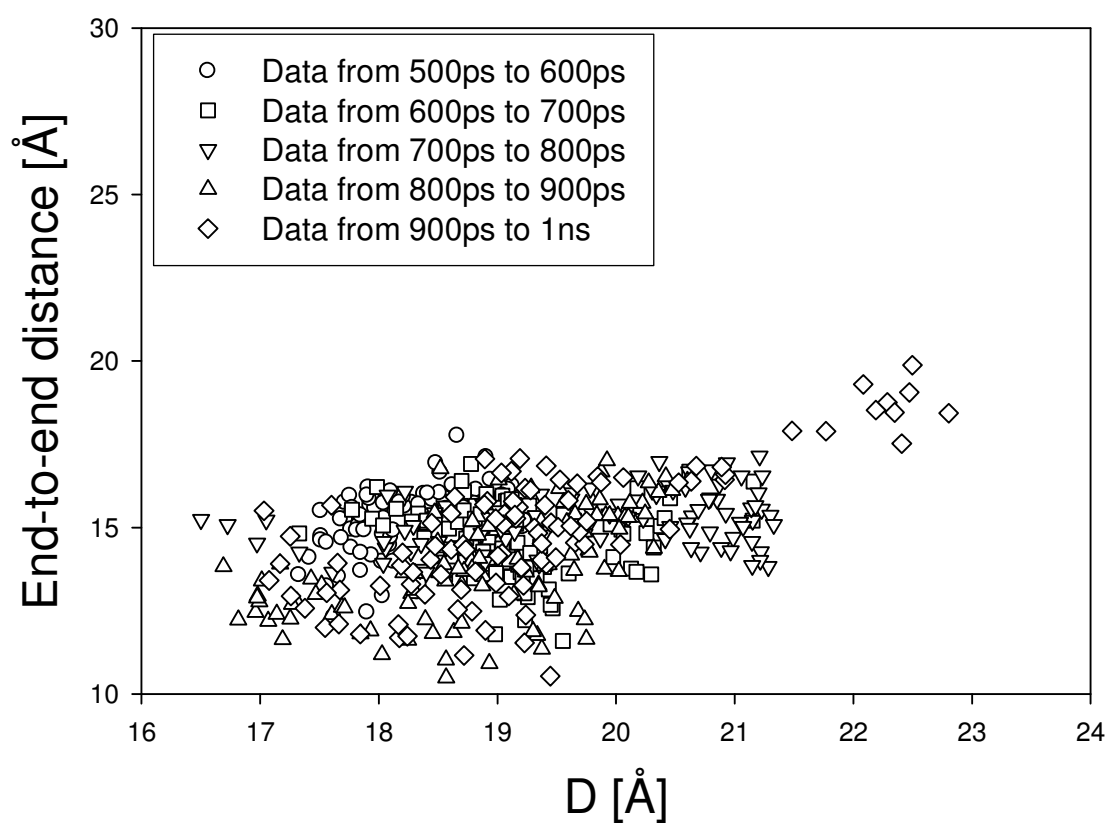


Figure C-4 End-to-end distance profile as a function of D ; 500ps to 1ns, A β -n_01 case.

VITA

Kunwoo Han was born to Songhag Han and Insoon Lee on August 7, 1970 in Jeonju, Republic of Korea. He received his Bachelor of Science and Master of Science degrees in chemical engineering from Pohang University of Science and Technology, R.O.K. He joined the Department of Chemical Engineering at Texas A&M University in August 2001 as a Ph.D. student and received his degree in 2006. His current research interests include molecular dynamics simulation and its applications to complex molecules at interfaces such as polymer/clay nano-composites and A β -protein behavior in hydrated lipids.

Kunwoo Han may be reached via e-mail at kunwoo.han@gmail.com or k0h6639@chemail.tamu.edu. His permanent address is 127-10 Geumam 2-Dong, Deokjin-Gu, Jeonju, 560-182, Republic of Korea.